Pathways Regulated by Glucocorticoids in Glioblastoma and Crosstalk with the Microenvironment

Hanadi Fuad Qashqari

Submitted in accordance with the requirements for the degree of Doctor of Philosophy

The University of Leeds

School of Medicine

November 2024

Copyright Declaration

Acknowledgements

Firstly, I would like to acknowledge my supervisor Laura Matthews, for her guidance on this project. I thank you for giving me the courage and confidence during my PhD journey. I am grateful for your endless support, and patience especially during the writing process. To my supervisor, Graham Cook, thank you for your valuable input on this project, support and proof-reading. A special gratitude for Fiona Errington-Mais and her group members for the great help and advice in the lab and weekly meetings, especially Victoria Jennings and Tyler Barr. Many thanks to Level 5 members, and flow cytometry staff for all the support and advice to complete my experiments. A special thanks to the Matthews group, past and present, Mengjiao Xia, Kathryn McGinnis, Fiona Leslie and Anna Nicholls. You have been a great support especially in my first year, and during quarantine, your kind and warm heart gave me a lot of encouragement and for that I thank you.

To my sponsor, the University of King Abdulaziz, Saudi Arabia. Thank you for giving me the opportunity to pursue my PhD abroad and special thanks to Dr. Mustafa Ziadi, thank you for supporting me during the hardest time completing my degree.

To my friends during this journey, Amani, Zharah, and Noura, thank you for all the beautiful moments we shared inside the lab, and outside. My dearest friend Hajer, you were the pillar support during my PhD journey. Thank you for being the friend I can rely on in my worst times, and for your encouraging words along the way. I wouldn't be able to do this without you.

Finally, to my family. I am grateful to my dear mom and dad, siblings, and nephews. Thank you all for the endless encouragement and support from abroad, and for believing in me. Being available to chat with me and listen to my smallest complaints. You gave me the strength to keep going and I am forever grateful for your support.

Abstract

Glioblastoma (GBM) is the most aggressive brain tumour in adults, with an average survival of just 18 months. Current treatment includes surgery in combination with radiotherapy and chemotherapy. Oncolytic viruses (OVs) are emerging to supplement standard cancer therapies as they kill tumour cells directly and activate immune surveillance. Most GBM patients are prescribed Dexamethasone (Dex), a synthetic glucocorticoid and potent anti-inflammatory drug that reduces brain inflammation, thereby limiting deleterious symptoms of GBM. While essential as part of standard therapy, it remains unclear how Dex might influence the efficacy of emerging immunotherapies such as OVs in GBM.

I*n silico* analysis of public RNA-seq data predicted potential crosstalk between glucocorticoids and reovirus in IL-6, AP-1 and TNF pathways. *In vitro* studies showed that Dex impairs direct GBM killing by reovirus. Dex did not influence virus entry or replication within GBM cells, suggesting that Dex alters GBM response to the virus. To elucidate the pathways involved, the effect of Dex on GBM cell infection by reovirus was explored by RNA-seq analysis. Gene ontology analysis demonstrated that Dex reduced pro-inflammatory signals, dysregulated activation of interferon response, and affected anti-apoptotic genes as well as cell cycle and ER stress response. A GBM-immune coculture model was used to investigate the effect of Dex on the ability of reovirus to activate immune cells and target GBM cells for destruction. Dex also impaired killing of GBM cells by immune cells. Dex altered expression of NK cell ligands on the surface of GBM cells which is predicted to reduce recruitment of NK cells. Dex significantly reduced NK cell number and activation in the presence of reovirus to reduce NK cells cytotoxic function. Consistent with this, the inhibitory effect of Dex was lost following NK cell depletion.

This study elucidates the potential pathways of Dex treatment during virus immunotherapy and emphasizes the importance of careful consideration for Dex management during immunotherapy to enhance treatment outcomes for GBM patients.

Abbreviation

5-ALA	5-aminolevulinic acid florescence dye
AC-like	Astrocyte
AP-1	Activator protein 1
ATRX	Alpha-thalassemia/mental retardation, X-linked
BBB	Blood brain barrier
BCR	B cell receptor
BEV	Bevacizumab
BF	Biological process
bFGF	Recombinant human basic fibroblast growth factor
CAR	Chimeric antigen receptors
CC	Cellular component
CDK4	Cyclin-dependent kinase 4
CDKN2A/B	Cyclin-dependent kinase inhibitor 2A/B
ChIP	chromatin immunoprecipitation
CIC	Capicua transcriptional repressor
CMC	Carboxymethyl-cellulose
CoA	Compound-A
CPE	Cytopathic effect
CPI	Checkpoint inhibitor
CSF1/2	Colony-stimulating factor
CTL	Cytotoxic T lymphocytes
CTLA-4	Cytotoxic T-lymphocyte protein 4
D-PBS	Dulbecco’s phosphate buffered saline
DAMP	Damage-associated molecular pattern
DBD	Exon 3-4 code the DNA-binding domain
DC	Dendritic cells
DCV	Dendritic cell vaccines
DEG	Differentially expressed genes
Dex	Dexamethasone
DMEM	Dulbecco’s modified eagle medium
DMSO	Dimethyl sulfoxide
DNA	Deoxyribonucleic acid
dsRNA	Double strand RNA
ECM	extracellular matrix
EDTA	Ethylenediaminetetraacetic acid
EGF	Epidermal growth factor
EGFR	Epidermal growth factor receptor
EIF2a	Eukaryotic translation initiation factor 2A
ELISA	Enzyme linked immunosorbent assay
EMT	Epithelial–mesenchymal transition
ER	Endoplasmic reticulum

f-MRI	Functional magnetic resonance imaging
FADD	Recruits Fas associated death domain
FCS	Foetal calf serum
FDA	Food and Drug Administration
FN1	Fibronectin
FOXP3	Forkhead box p3
FPKM	Fragments Per Kilobase of transcript per Million
FUBP1	Far upstream element-binding protein 1
GBM	Glioblastoma
GC	Glucocorticoids
GITR	Glucocorticoid-induced tumour- necrosis-factor-receptor-related protein
GM-CSF	Granulocyte-macrophage colony-stimulating factor
GO	Gene ontology
GR	Glucocorticoid receptor
GRE	Receptor response elements
GrzB	Granzyme B
GSC	Stem-like cells
H	hinge region
HBSS	Hanks' balanced saline solution
HDACi	Histone deacetylase inhibitors
HIF-1	hypoxia-inducible factor 1
HLA	histocompatibility antigen, class I
HPA	Hypothalamic–pituitary–adrenal axis
HSV-1	Herpes simplex virus 1
HVEM	Herpes virus entry mediator
ICAM1	Intracellular adhesion molecule 1
IDH	Isocitrate dehydrogenase
IDO1	Indoleamine 2,3-dioxygenase 1
IF	Immunofluorescent staining
IFI16	Interferon-gamma inducible protein 16
IFI6	Interferon-alpha inducible protein 6
IFN	Interferon
ISG	Interferon-stimulated gene
ISVP	Infectious subviral particles
JAM-1	Junctional adhesion molecule 1
LBD	Exon 5-9 code the C-ligand binding domain
LOH	Loss of heterozygosity
MAD5	Melanoma differentiation-associated protein 5
MDCS	Myeloid-derived suppressor cells
MDM2	Mouse double minute 2
MDSC	myeloid-derived suppressor cells
MES-like	Mesenchymal
MF	Molecular function
MFI	mean fluorescence intensity

MGMT	O6-Methylguanine-DNA methyltransferase
MHC	Histocompatibility complex
MIP	Macrophage inflammatory protein
MLKL	Mixed Lineage Kinase Domain Like Pseudokinase
MMP	Matrix metalloproteinase
MTT	3-[4,5-dimethylthiazol-2-yl]-2,5 diphenyl tetrazolium bromide
MOI	Multiply of infection
MYD88	Myeloid differentiation primary response 88
NARA	Neutralizing anti-reovirus antibody
NEAA	Non-essential amino acid
NF-κB	Nuclear factor kappa-light-chain-enhancer of activated B cells
NF1	Neurofibromatosis type I
NK	Natural killer
NPC-like	Neural progenitor
NR	Nuclear receptor
NR3C1	Nuclear receptor superfamily 3 group C member 1
NSC	Neural stem cells
NTD	N-terminal domain
OCT4	Octamer-binding transcription factor 4
OLIG2	Oligodendrocyte transcription factor 2
OPC-like	Oligodendrocyte
OS	Overall survival
OV	Oncolytic viruses
P2RY12	Purinergic Receptor P2Y12
PAMP	Pathogen-associated molecular pattern
PARP-1	Poly (ADP-ribose) polymerase-1
PBMC	Peripheral blood mononuclear cell
PD-1	Programmed cell death protein 1
PD-L1	Programmed cell death ligand 1
PDGFRA	Platelet-derived growth factor receptor alpha
PFA	Paraformaldehyde
PFS	Progression-free survival
PFU	Plaque forming units
PGE2	Prostaglandin E2
PKR	Protein kinase-R
PPI	Protein-protein interaction
PRR	Pattern recognition receptors
PTEN	Phosphatase and tensin homolog
PTGS2	Cyclooxygenase-2
QC	Quality control
Reo	Reovirus
RF1	Interferon Regulatory Factor 1
RIG-I	Retinoic acid inducible gene-I
RIN	Integrity number
RIPK3	Receptor Interacting Serine/Threonine Kinase 3

RNA	Ribonucleic acid
RNS	Reactive nitrogen species
ROS	Reactive oxygen species
RT	Room temperature
SDS	Sodium Deoxycholate
SOX2	SRY-box 2
STAT3	Signal transducer and activator of transcription 3
STS	Staurosporine
SVZ	Subventricular zone
T-VEC	Talimogene laherparepvec
T3D	Type 3 Dearing
TAA	Tumour associated antigen
TAA	Tumour-associated antigens
TAM	Tumour associated macrophage
TCGA	The Cancer Genome Atlas
TCR	T-cell receptor
TERT	Telomerase reverse transcriptase
TF	Transcription factor
TGF-β	Tumour growth factor-beta
TIGIT	T cell immunoreceptor with Ig and ITIM domains
TIL	Tumour infiltrating lymphocytes
TLR	Toll-like receptors
TME	Tumour microenvironment
TMEM119	Transmembrane Protein 119
TMZ	Temozolomide
TNF-a	Tumour- necrosis factor alpha
TRADD	TNF receptor type 1-associated death domain protein
TRAIL	TNF related apoptosis-inducing ligand
Treg	T-regulatory cells
Vam	Vamorolone
VEGF	Vascular endothelial growth factor
WHO	World Health Organization

Table of Contents

Table of figures

List of Tables

Chapter 1

Introduction

1.1 Glioblastoma (GBM)

Glioblastoma (GBM) is the most common and aggressive brain tumour in adults. It accounts 51% of all malignant brain tumours with annual incidence rate 4.41 cases per 100,000 population worldwide (Price *et al*., 2024), with a median survival of just 14.6 months (Stupp *et al.,* 2005). The symptoms of GBM are hard to recognize and include headache, nausea, seizures, change in personality, brain edema and increased intracranial pressure. The potential risk factors include older age (average of 60 years), ionizing radiation exposure and present more frequently in males than females. The first step for GBM diagnosis is brain imaging using computed tomography (CT) scan and magnetic imaging (MRI) to visualize the tumour size and location. A biopsy is also taken to examine the prognostic biomarkers and genetic characteristics that help the tumour classification (Thakkar *et al.,* 2014). The true cellular origin of GBM is debatable due to its heterogeneity. However, it is proposed that glial progenitor cells, astrocytes, or neural stem cells (NSC) are the cell of origin for GBM (Zong *et al*., 2012).

1.1.1 GBM Classification

The 2021 World Health Organization (WHO) classification system classifies adult diffused glioma based on isocitrate dehydrogenase (IDH) status into: IDH mutant including astrocytoma (Grade II, III, IV), oligodendrogliomas (Grade II, III) and IDH wildtype is classified as glioblastoma (Grade IV) as presented in Figure 1.1. The classification was refined based on defined molecular alterations and histologic features. Astrocytoma grade II and III were defined by alpha-thalassemia/mental retardation, X-linked (ATRX) mutations and TP53 mutations, whilst grade IV was defined by cyclin-dependent kinase inhibitor 2A/B (CDKN2A/B) homozygous deletion, vascular proliferation, and necrosis. Oligodendrogliomas was defined by 1p/19q codeletion, telomerase reverse transcriptase (TERT) mutations, capicua transcriptional repressor (CIC)

mutation, and far upstream element-binding protein 1 (FUBP1) mutation. Glioblastoma (GBM) grade IV was defined by IDH1/2 mutation, and at least one of the following criteria: TERT mutation, epidermal growth factor receptor (EGFR) amplification, or chromosome 7 gain and 10 loss (Louis *et al.,* 2021, Whitfield *et al.,* 2022).

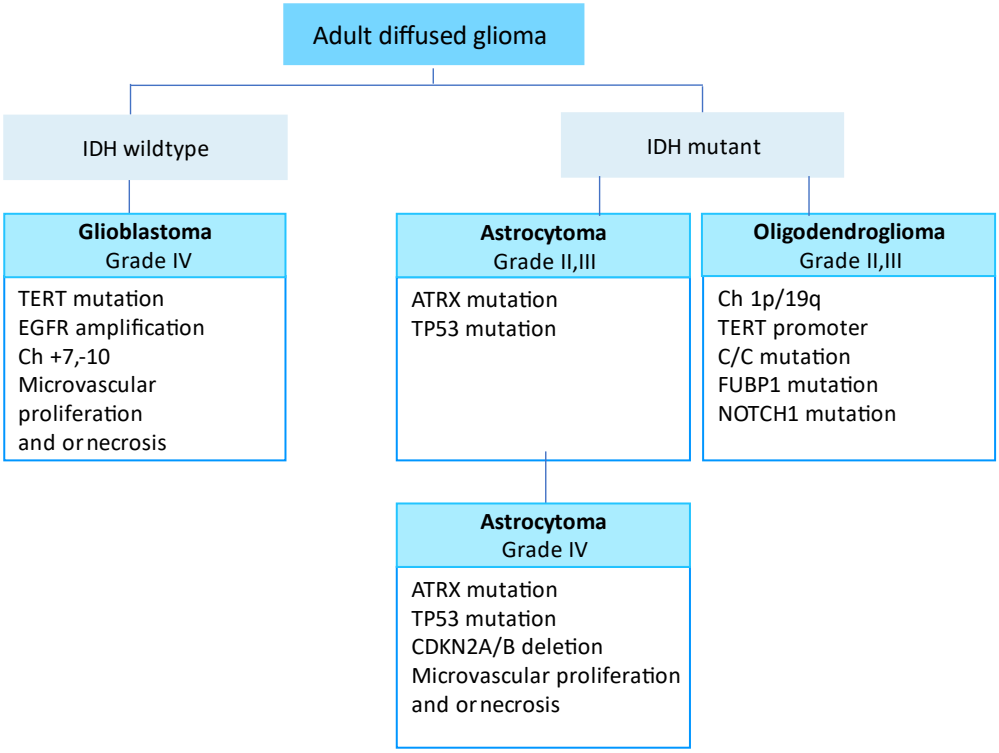

Figure 1-1 Adult diffuse glioma classification workflow.

Diffuse glioma initially classified based on IDH status. IDH-wildtype is divided into oligodendroglioma (Grade II, III) and astrocytoma (Grade II, III) based on 1p/19q and ATRX status. Astrocytoma (Grade IV) defined by CDKN2A and histologic evidence of microvascular proliferation/necrosis. IDH-wildtype is classified as GBM (Grade IV) with TERT promoter mutation, EGFR amplification, gain of chromosome 7 and loss of 10 with histologic evidence of microvascular proliferation/necrosis. The image was recreated using information from Whitfield *et al.,* 2021.

Previous studies have classified GBM tissues based on their molecular markers into three subclasses: classical, proneural, and mesenchymal (Wang *et al.,* 2017). Another study has classified GBM into six groups (clusters from M1 to M6) based on the DNA methylation profile (Brennan *et al.,* 2013). Later, a single-cell RNA sequencing study identified four GBM subtypes based on gene expression: oligodendrocyte (OPC-like) defined by platelet-derived growth factor receptor alpha (PDGFRA) high expression, astrocyte (AC-like) defined by EGFR

amplification, neural progenitor (NPC-like) defined by cyclin-dependent kinase 4 (CDK4) inhibition, and mesenchymal (MES-like) defined by neurofibromatosis type I (NF1) mutation and loss, showing plasticity and transition between these states, influenced by the cell cycle and the tumour microenvironment (Neftel *et al.,* 2019). Central to this plasticity is GBM stem-like cells (GSC) that are characterised by the ability to self-renew and differentiate into multiple tumour lineages and to evade treatment (Schiffer *at al.,* 2014). This key finding explains the molecular heterogeneity, invasiveness, and microvascular proliferation observed in GBM which in turn contributes to GBM recurrence (Boyrie *et al.,* 2019).

1.1.2 Current treatment

After diagnosis, GBM patients receive aggressive surgical resection guided by advanced surgical techniques, such as 5-aminolevulinic acid florescence dye (5-ALA), and resting-state functional magnetic resonance imaging (f-MRI) (Gerritsen *et al.,* 2022). Unfortunately, the invasiveness of the tumour makes it difficult to completely remove the mass and infiltrative cells often remain in the margin, leading to tumour recurrence. Following surgery, GBM patients are commonly treated with temozolomide (TMZ), a DNA alkylating chemotherapy agent (75 mg/m^2 per day for 6 weeks) and fractionated radiotherapy (60 Gy in 30 fractions over 6 weeks). This is then followed by adjuvant TMZ (150-200 mg/m^2 for 5 days every 28-day cycles) (Stupp *et al.,* 2005). Unfortunately, GBM cells eventually become resistant to TMZ which was reported to be associated with the induction of MGMT (O^6-Methylguanine-DNA methyltransferase) gene expression (Lee *et al.,* 2016).

Several therapeutic drugs are under investigation to overcome these challenges. One example is Poly (ADP-ribose) polymerase-1 (PARP-1), a nuclear protein involved in DNA repair pathway and found to be overexpressed in GBM (Murnyak *et al.,* 2017). The PARP inhibitor (olaparib) is approved for use in breast cancer treatment and is currently under phase I/IIa clinical trials for GBM patients in combination with radio/chemotherapy (Lesueur *et al.,* 2019). Other studies have focused on developing therapies which directly target pro-angiogenic mediators, including Bevacizumab (BEV), a monoclonal antibody that targets angiogenesis

via vascular endothelial growth factor (VEGF) pathway. A clinical trial of BEV in combination with the standard chemotherapy and radiotherapy in newly diagnosed GBM patients showed better progression-free survival (PFS) but not overall survival (OS) (Gilbert *et al.,* 2014). Several histone deacetylase inhibitors (HDACi) such as valproic acid, voristonat, and panobinostat have showed reductions in GBM stem cells and several clinical trials were conducted in GBM patients in combination with standard care of treatment (Reddy *et al.,* 2020).

1.1.3 The GBM tumour microenvironment (TME)

GBM is characterized by its complex microenvironment where tumour cells interact with immune cells to create a highly immunosuppressive microenvironment (Figure.1.2) that reduces the efficacy of current therapies and promotes GBM growth (Magaña-Maldonado *et al.,* 2016). The interaction between GBM cell and its TME promotes several signalling pathways contributing on GBM proliferation, angiogenesis and invasion.

1.1.3.1 Myeloid, Tumour associated macrophage and Microglia

Tumour associated macrophages (TAMs), and microglia are the most abundant component of the GBM mass, comprising ~50% of the microenvironment (Xuan *et al.,* 2021). A recent single-cell RNA-sequencing showed the heterogenicity of myeloid cells and microglial versus macrophage lineage in GBM (Yuan *et al.,* 2018). Thus, TAMs are heterogeneous and consist of a mixture of M2-like macrophages which mediate anti-inflammatory function, and M1-like macrophage mediating pro-inflammatory functions, alongside microglia, myeloid-derived suppressor cells (MDCSs) and dendritic cells (DCs). M1-like macrophages polarisation is induced by pro-inflammatory cytokines such as interferon gamma (IFN-γ), tumour- necrosis factor alpha (TNF-α), and granulocyte-macrophage colony-stimulating factor (GM-CSF) factors. The M1-like macrophages express surface markers such as CD80 and CD86, chemokines including CCL2, CCL4, CCL3L3, and cyclooxygenase-2 (PTGS2) (a key enzyme in the production of prostaglandin E2). M2-like macrophage polarisation is driven by anti-inflammatory cytokines such as interleukin-10 (IL-10) and transforming growth factor beta (TGF-β) and is characterized by the

expression of surface markers including CD136, CD206, CD204, CD163, LGMN and MSR1 (Zeiner *et al.,* 2019).

Macrophages interact with GBM cells through the CXCL12/CXCR4 axis (Würth *et al.,* 2014). TAM secrete TGF-β which induces matrix metalloproteinases (MMP)-2,9 and 14 which activate CX3CR1, leading to increased GBM adhesion/migration and invasion (Held-Feindt *et al.,* 2010). Macrophage colony-stimulating factor (CSF1) is highly expressed in the GBM and its secretion increased myeloid infiltration (Yuan *et al.,* 2018). Microglia express transmembrane protein 119 (TMEM119) and purinergic receptor P2Y12 (P2RY12) markers, but their function are similar to macrophages and can act as antigen presenting cells (APC) in GBM (Haage *et al.,* 2019).

MDSCs derived from the immature bone marrow cell reside in both GBM mass and in peripheral blood (Alban *et al.,* 2018). Monocyte activation and reprograming by TLRs, IL-10, LPS, and IFN-γ generate MDSCs (Millrud *et al.,* 2017). It has been found that GBM expressing VEGF and hypoxia-inducible factor-1 alpha (HIF1-α) besides other factors like CCL2, CCL20 and indoleamine 2,3-dioxygenase 1 (IDO1) also recruit MDSCs (Lakshmanachetty *et al.,* 2021). GBM cells secrete several immunosuppressive factors, including Interleukins (IL) IL-10, IL-6, and IL-4, tumour growth factor-beta (TGF-β), and prostaglandin E2 (PGE2). These secreted factors elevate circulating MDSCs (Raychaudhuri *et al.,* 2011), suppress microglial activation and skew macrophage into M2 phenotype (Hussain *et al.,* 2006; Humphries *et al.,* 2010). The TGF-β secreted by GBM induces Treg differentiation and infiltration and suppress cytotoxic T and NK cell activity (Djediai *et al.,* 2012).

1.1.3.2 T- regulatory cells (Treg)

Tregs are immunosuppressive T cells that express CD4, CD25 and forkhead box p3 (FOXP3). GBM cells and TAMs release factors like IL-10, TGF-β, IL-4, IL-6, CCL2, CCL20 to recruit Tregs to the tumour site (Humphries *et al*., 2010). Tregs promote immune escape by inhibiting T cell and NK cell activation using multiple mechanisms including IL-10 and TGF- β secretion as well as cell-cell contact based mechanisms (Smyth *et al.,* 2006).

1.1.3.3 Cytotoxic T cells and NK cells

Cytotoxic T lymphocytes (CD8+ T cells, called CTL) are important in controlling tumours. For example, they are very abundant in melanoma. However, the GBM TME is poorly populated by these T cells. In addition, TAMs and GBM cells express immune checkpoints like programmed cell death ligand 1 (PD-L1) that bind to program med cell death protein 1 (PD-1) on infiltrated T cells and inhibit their activation (Mirzaei *et al.,* 2017). In melanoma, the abundant T cell infiltrate allows immune checkpoint blockade (e.g. anti-PD1 or PD-L1 antibodies) to restore T cell function (Carlino *et al.,* 2021). However, the low T cell infiltrate in GBM makes this ineffective. The Cancer Genome Atlas (TCGA) analysis reported high PD-L1 and CTLA-4 expression (another T cell immune checkpoint) in mesenchymal GBM, indicating that high expression of immune checkpoint proteins correlates with the severity of GBM (Nduom *et al*., 2015). Previous studies have shown that the IDH-wt subtype shows high tumour infiltrating lymphocytes (TILs) and high PD-L1 expression (Berghoff *et al.,* 2017). In contrast, the IDH-mutant subtype is reduced in IFN-γ signature and TIL count (Pombo Antunes *et al.,* 2020). T cells binding to APC through the major histocompatibility complex (MHC) class-I, leading to activation and differentiation into cytotoxic T lymphocytes (CTL), which are required for mediating tumour killing (Raskov et al., 2021)

In addition, NK cells are important in innate immune response, including the identification and killing of tumour cells. Upon triggering by a tumour cell, NK cells release cytolytic granules containing pro-apoptotic granzymes (e.g. GrzB) and perforin which forms a pore to allow the granzymes to enter the target cell. Thus, NK cells are capable of mediating GBM killing (Paul *et al.,* 2017). However, due to the GBM immunosuppressive environment, GBM cells secrete multiple factors such as TGF-β, IL-6, IL-10 and IDO1 that suppress the cytotoxic activity of NK cells (Thomas *et al.,* 2006; Eisele *et al.,* 2006). GBM cells also express the histocompatibility antigen, class I (HLA)-G that binds to ILT2/4, and KIR2DL4 receptors on NK cells, suppressing their activity (Wiendl *et al.,* 2002; Lin *et al.,* 2015). This inhibition of NK cells is analogous to the immune checkpoints that operate on T cells.

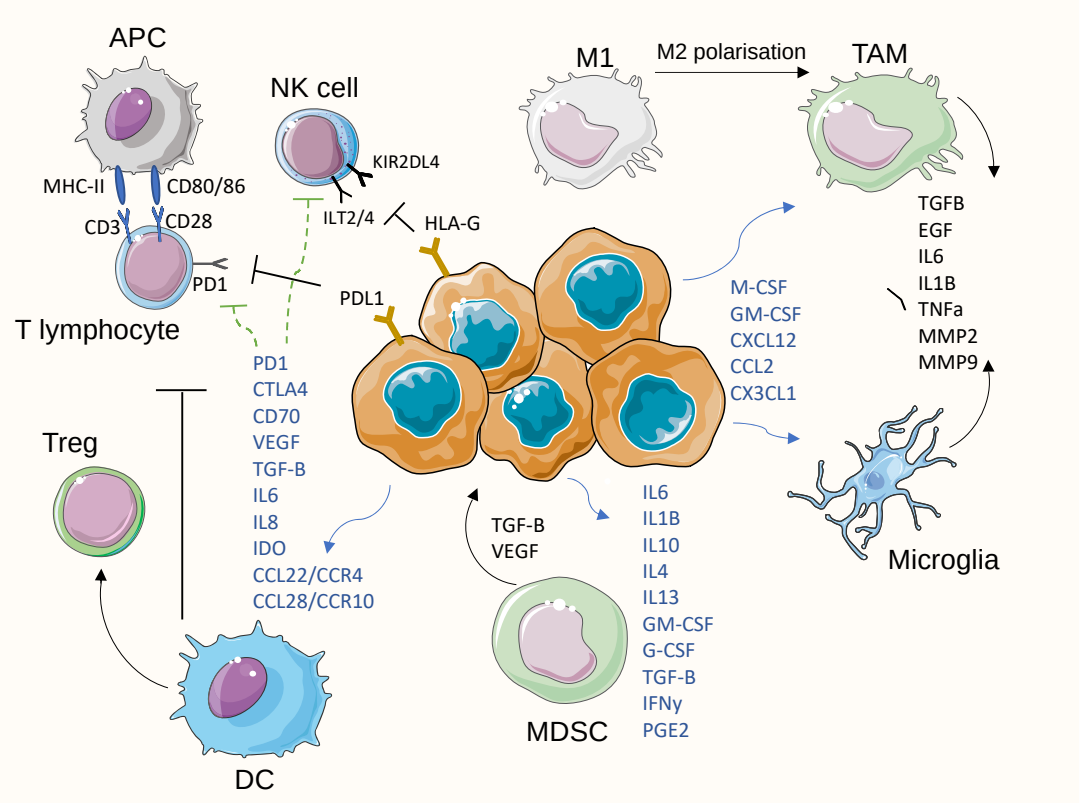

Figure 1-2. GBM immunosuppressive microenvironment.

GBM cells secrets immunosuppressive factors to recruit Treg cells and inhibit T cells and NK cells proliferation. M-CSF promote MDSC migration. GBM cells induce EGFR, MGMT, and IDO secretion. DCs downregulate IFN-γ expression. Immunosuppressive factors such as M-CSF, TGF-β, and IL-10 skew macrophages toward M2-like phenotype. M2 secretes MMPs and other GFs to increase microglia infiltration. The image was adapted using figure and information from papers (Magaña-Maldonado *et al.,* 2016) and (Codrici *et al.,* 2022).

1.1.3.4 Hypoxia

Lack of an adequate oxygen supply results in hypoxia in GBM, leading to accumulation of hypoxic niches which expand the GSC population (Colwell *et al.,* 2017). The GBM hypoxic environment modulates the GBM immunosuppressive microenvironment, enhancing recruitment of TAMs, MDSC's, and Tregs and upregulating PD-L1 expression in GBM cells as well as limiting the proliferation of T cells. Hypoxic responses are mediated by the hypoxia-inducible factor 1 (HIF-1), which triggers the expression of VEGF and promotes microvasculature formation to promote GBM angiogenesis. Furthermore, hypoxia activates oncogenic pathways including JAK1-2/STAT3 which induce GBM aggressiveness (Gray *et al.,* 2014). HIF-1 also promotes tumour migration and

invasion due to the enhancement of EMT, extracellular matrix (ECM) re-modelling, and vascular permeability (Joseph *et al.,* 2015).

1.1.3.5 The blood brain barrier (BBB)

One of the hallmarks in GBM is the dysfunction of the BBB, which is a physical barrier that protects the brain tissue from toxic pathogens and molecules greater than ~200-600 Daltons in size which allows transfer of small molecules, such as O_2/CO_2 but restricting access to other molecules such as cytokines, growth factors and antibodies (Fu *et al.,* 2018). The BBB thus also restricts drug delivery and immune cells such as T cell and NK cells are only allowed access under tightly controlled inflammatory conditions (Bhowmik *et al.,* 2015). GBM cells secrete VEGF which downregulates expression of endothelial tight junction molecules, leading to increased permeability of the BBB and vascular leakage. The leaky BBB allows influx of immune cells, including cells with anti-tumour activity (such as cytotoxic lymphocytes) but also those with immunosuppressive functions, such as MDSC and Treg (Abbott *et al.,* 2002).

1.1.3.6 Glioma Stem Cells (GSC)

GSC are a small population in GBM that have the ability to self-renew, proliferate, and migrate. GSC reported to arise from NSCs (neural stem cells) residing in the subventricular zone (SVZ) (Llaguno *et al.,* 2015). Previous studies have shown that GCSs localised near perivascular niches interact with the ECM which causes GSC migration and proliferation (Fidoamore *et al.,* 2016). A compilation of studies showed that GSC are characterised by the expression of the cell surface markers such as CD133 and CD44 and the intermediate filament protein nestin (Calabrese *et al.,* 2007; Brown *et al.,* 2017). GSC express stem cell markers such as SRY-box 2 (SOX2), Oligodendrocyte transcription factor 2 (OLIG2), and Octamer-binding transcription factor 4 (OCT4) (Trépant *et al.,* 2015). GSCs have high expression of the signal transducer and activator of transcription 3 (STAT3) transcriptional factor (Sherry *et al.,* 2009). The secretion of TGF-β and IL-10, IL-6 and PGE-2 by GBM cells favours the proliferation of GSC and simultaneously suppresses anti-tumour immunity, making the GBM TME favour tumour progression.

1.1.4 Current immunotherapies in GBM

Immunotherapy has emerged as a powerful strategy for the treatment of different types of tumours, including GBM. The aim of strategies involved in immunotherapies are based on re-educating immune cells in GBM patients, favouring an anti-tumour immune response. Several immunotherapeutic clinical trials are currently ongoing in the context of GBM.

1.1.4.1 Immune checkpoint inhibitors (CPIs)

Several clinical trials of immune checkpoint inhibitors (CPIs) are currently in progress in GBM. Monoclonal antibodies (MAbs) targeting PD-1 (nivolumab) showed the greatest effect in hypermutated GBM, suggested to be associated with DNA mismatch-repair machinery (Bouffet *et al.,* 2016). This is likely related to the increased abundance of neoantigen targets in DNA mismatch repair tumours which are more likely to induce T cell responses. Nivolumab and MAbs targeting CTLA-4 (ipilimumab) are currently under investigation in GBM patients in combination with radio-chemotherapy, reviewed in (Wang *et al.,* 2019). Several phase I clinical trials combining anti-PD-1 with co-inhibitory immune cell blockade (anti-TIM-3; NCT03961971) are being conducted by Curigliano *et al.,* 2021, the inhibitory T cell receptor blockade (anti-LAG3; NCT02658981) by Lim et al., 2019, and anti-TIGIT (NCT04656535) by Rotte *et al.,* 2021 are currently all under investigation. Importantly, TIGIT is expressed by both T cells and activated NK cells making this an attractive target in tumours where T cell infiltrates may be low.

1.1.4.2 Chimeric antigen receptors (CARs)

Chimeric antigen receptors (CARs) link the specificity of an antibody variable domain to the signalling activity of the T cell receptor. Expression of these CARs thus re-targets T cells from MHC-TCR restricted specificity to that defined by the antibody variable region component (Strohl *et al.,* 2019). A number of CARs have been developed to target GBM associated antigens, including anti-IL-13Rα2, anti-EGFRvIII, anti-HER2 and anti-CD70 (Bagley *et al.,* 2018). Though some CAR-T cells have demonstrated significant overall survival (OS) benefits in recurrent GBM patients, there are concerns of neurotoxicity during CAR T cell

infusion (Brown *et al.,* 2019). Furthermore, CAR-T cells work most effectively against haematological malignancies and were approved by FDA in 2017 for treatment of leukaemias and lymphomas (Haslauer *et al.,* 2022). For solid tumours, CAR-T cells appear to have many of the limitations of natural T cells in that the immunosuppressive TME inactivates CAR-T through multiple mechanisms, resulting in CAR-T exhaustion.

1.1.4.3 GBM vaccines

Therapeutic vaccines have also been developed to treat GBM. The main types of vaccination are peptide-based vaccines, and dendritic cell-based vaccines (DCV) that have recently been evaluated in GBM patients to promote adaptive anti-tumour immunity. A peptide vaccine (rindopepimut) targeting the EGFRvIII variant found in GBM showed some efficacy in 30% of GBM patients, with improved median OS in adults with newly diagnosed GBM (Swartz *et al.,* 2014). However, a phase III trial (ACT IV) did not show clinical benefit compared to the standard of care (TMZ) arm. However, humoral responses were observed in vaccinated patients, illustrating that inducing immune responses via this vaccination is possible (Weller *et al.,* 2017). Another phase II trial of combined EGFRvIII and BEV showed beneficial outcomes (Reardon *et al.,* 2020). A clinical trial investigating multi-targeting neonatigen (APVAC2) and unmutated peptides (APVAC1) vaccine showed an increase in T cell responses and increased patient survival (Hilf *et al.,* 2019). A neoantigen-specific T cell approach was recently evaluated for GBM with promising results (NCT02287428). Whole genome and RNA sequencing of GBM patients allows neoantigens to be predicted for production of personalized vaccines. A clinical trial found neoantigen-specific T cells can be generated and even infiltrate the tumour (Keskin *et al.,* 2019). SurVaxM vaccine (against survivin) showed promising results in a phase II trial (NCT012350470) as well as acceptable safety (Ahluwalia *et al.,* 2023). A 2019 phase I/II clinical trial study by Migliorini *et al.,* on IMA950 multi-peptide vaccine designed to activate T cells, was combined with poly-ICLC (NCT01920191) approved its safety and increased patient's survival.

The DCV approach uses antigen-presenting cells (APCs) capable of provoking immune responses. A clinical trial in ICT-107 vaccine (NCT01280552) which

target mixed antigens that are overexpressed in GSC showed increase in GBM patient OS (Wen *et al.,* 2019). Currently, a phase III study of lysate-loaded DCV (DCVax-L) is under investigation (NCT00045968) showing promising increase in patients OS (Liau *et al.,* 2018). However, whilst progress in immunotherapy is being made, there remains a great need to improve treatments and patient outcomes.

1.2 Glucocorticoids (GCs)

Glucocorticoids (GCs) are steroid hormones produced by the adrenal cortex and regulated by the hypothalamic–pituitary–adrenal *axis* (HPA) (Cenciarini *et al.,* 2019). GCs are used as anti-inflammatory drugs, broadly for the treatment of inflammatory disease and different types of cancer. It has been demonstrated that GC play a role in the regulation of circadian rhythms (Gibbs *et al.,* 2014), the cell cycle (Matthews *et al.,* 2011) and cell death (Distelhorst *et al.,* 2002). Dexamethasone (Dex) is a synthetic GCs that is commonly used for GBM patients to reduce cerebral oedema by reducing the permeability of the BBB (Salvador *et al.,* 2014).

1.2.1 GR structure and isoforms

The receptor for GC is the glucocorticoid receptor (GR), also called nuclear receptor superfamily 3 group C member 1 (NR3C1), a member of the nuclear receptor (NR) superfamily and a ligand-activated transcription factor. GR was cloned in the 1980s by Hollenberg *et al.,* (1985). The NR3C1 gene is located on chromosome 5 and consists of 9 exons. Figure 1.3 shows the organisation of the gene and GR protein; exon 1 is not translated, exon 2 encodes the N-terminal domain (NTD), exons 3-4 encode the DNA-binding domain (DBD), exon 5-9 encode the C-terminal ligand binding domain (LBD) with a hinge region (HR) separating DBD and LBD (Oakley *et al.,* 2013). The NTD domain contains the transcriptional activation function (AF-1) responsible for activating target genes via the TATA-binding protein. The LBD contains AF-2 regulated by ligand binding to allow interaction with coactivators or corepressors. The DBD contains two conserved zinc finger motifs which bind to DNA targets, known as the glucocorticoid response element or GRE (Yang *et al.,* 2012).

Alternative splicing of GR generates five different GR isoforms. GRα is the classic receptor that mediates GC action. GRα and GRβ share similar NTD and DBD but use exons 9α or 9β respectively which results in truncation of the LBD and the addition of 15 unique amino acids at the c-terminus of GRβ. As a consequence, GRβ does not bind GC, but acts as a negative inhibitor as it forms a heterodimer with GRα (Lewis-tuffin *et al.,* 2006). Additional alternative isoforms are generated from alternative splicing. This includes GRγ which includes 3 bases at the exon3/4boundary and contains arginine residue in the DBD domain compared with GRα (Ray., 1996). GRA is produced by alternative splicing that link exon 4 to 8 and delete half of the LBD (Ala-490-Ser-674). GRP is missing exon 8 and 9 (De Lange *et al.,* 2010). Isoforms GRβ, GRA, GRP are found to be linked to GC resistance (Figure 1.3).

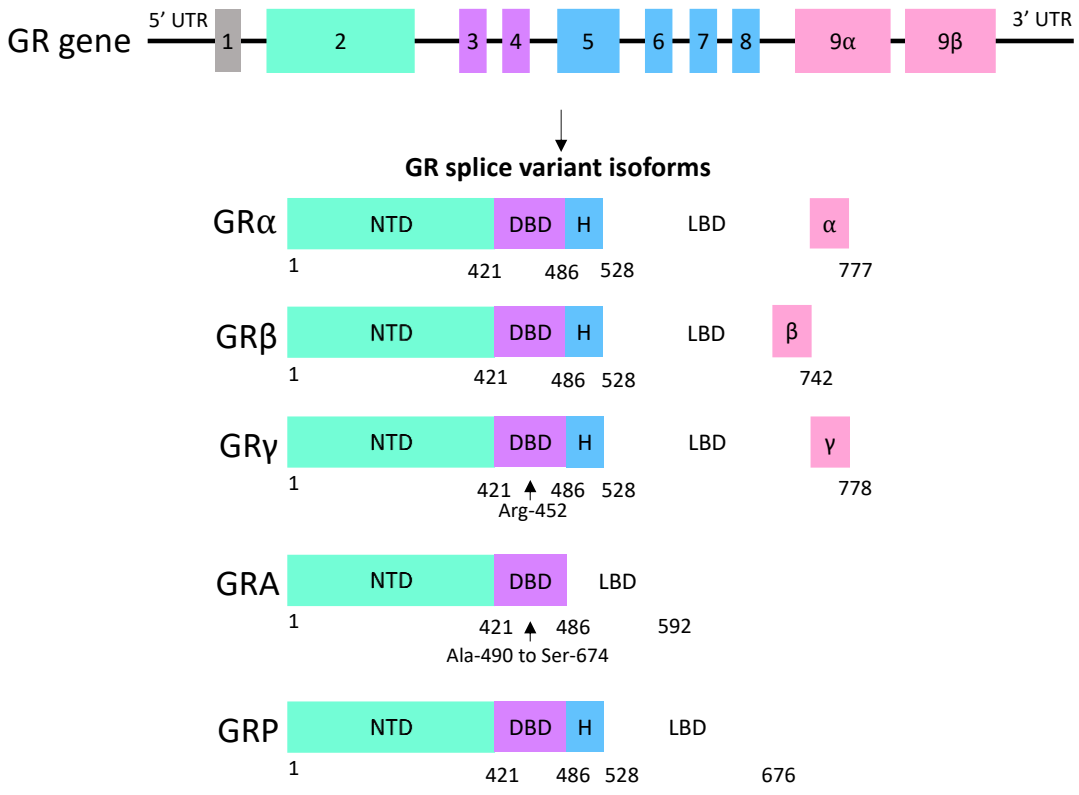

Figure 1-3 GR gene structure and its spliced variants resulted different isoforms.

GR gene structure (top) consists of N-terminal domain (NTD), DNA-binding domain (DBD), hinge region (H), and Ligand-binding domain (LBD). The alternative splice variants of the GR protein include GRα, GR β with different final amino acid than GRα, GRγ with additional arginine residue on the DBD. GRA with a shorter LBD and missing the hinge region, and GRP missing the 8 and 9 exons of the LBD. The image was recreated using information from Timmermans *et al.,* 2019 and Liu *et al.,* 2019.

1.2.2 GR mechanism of action

GR (NR3C1) in its inactive state resides in the cytoplasm in a complex with chaperones HSP70/HSP40 to form a chaperone complex that binds to the co-chaperone HSP90. In the presence of ATP, HSP40 and HSP70 are released from the complex. The co-chaperone HSP90 binds to HOP in the GR-chaperone complex and (catalysed by ATP) leads to the release of HSP40/70 which are replaced with p23 and FKBP51 to form the GR foldosome. When GC binds to GR, FKBP51 is replaced with FKBP52, allowing GR to translocate to the nucleus where it acts as a transcription factor (Timmermans *et al.,* 2019). In the cytoplasm, activated GR can regulate non-genomic pathways. These responses occur very early, within minutes of GC administration and prior to detectable GR translocation to the nucleus, and require no new transcription (Song *et al.,* 2006). GR is found to alter the activity of various kinase signalling cascades, for example activating c-src, and PI3K/AKT pathway (Leis *et al.,* 2004), inhibiting MAPK and SAPK pathways and increasing reactive oxygen species (ROS) and reactive nitrogen species (RNS) which increase DNA damage (Flaherty *et al.,* 2017).

Active GR translocated into the nucleus exerts genomic regulation and is categorised into three mechanisms (Figure 1.4). In the first mechanism, GR binds to DNA directly at glucocorticoid receptor response elements (GREs), leading to recruitment of co-regulators that bind to transcriptional activators and activate gene transcription. Alternatively, homodimers of GR can bind DNA at negative GREs (nGRE) to recruit co-repressors to repress gene transcription (Cain and Cidlowski, 2017). In the second mechanism, active GR tethers to another transcription factor via protein-protein interaction and, without direct DNA binding, mediates transcriptional activation or repression through the bound factor. Tethering mechanism mediates many GR immunosuppressive functions. For example, GR tethers with Nuclear factor kappa B (NF-kB), thus repressing the transcription of proinflammatory genes (such as TNF, IL-6 and IL-1β), or activates STAT3 which then drives immunosuppressive functions (Ratman *et al.,* 2013). In the third mechanism, GR binds to composite elements that comprise a GRE adjacent to the binding site for another transcription factor, leading to activation of gene transcription in the case of STAT5 or repression with AP-1 (Rogatsky *et al.,* 2006).

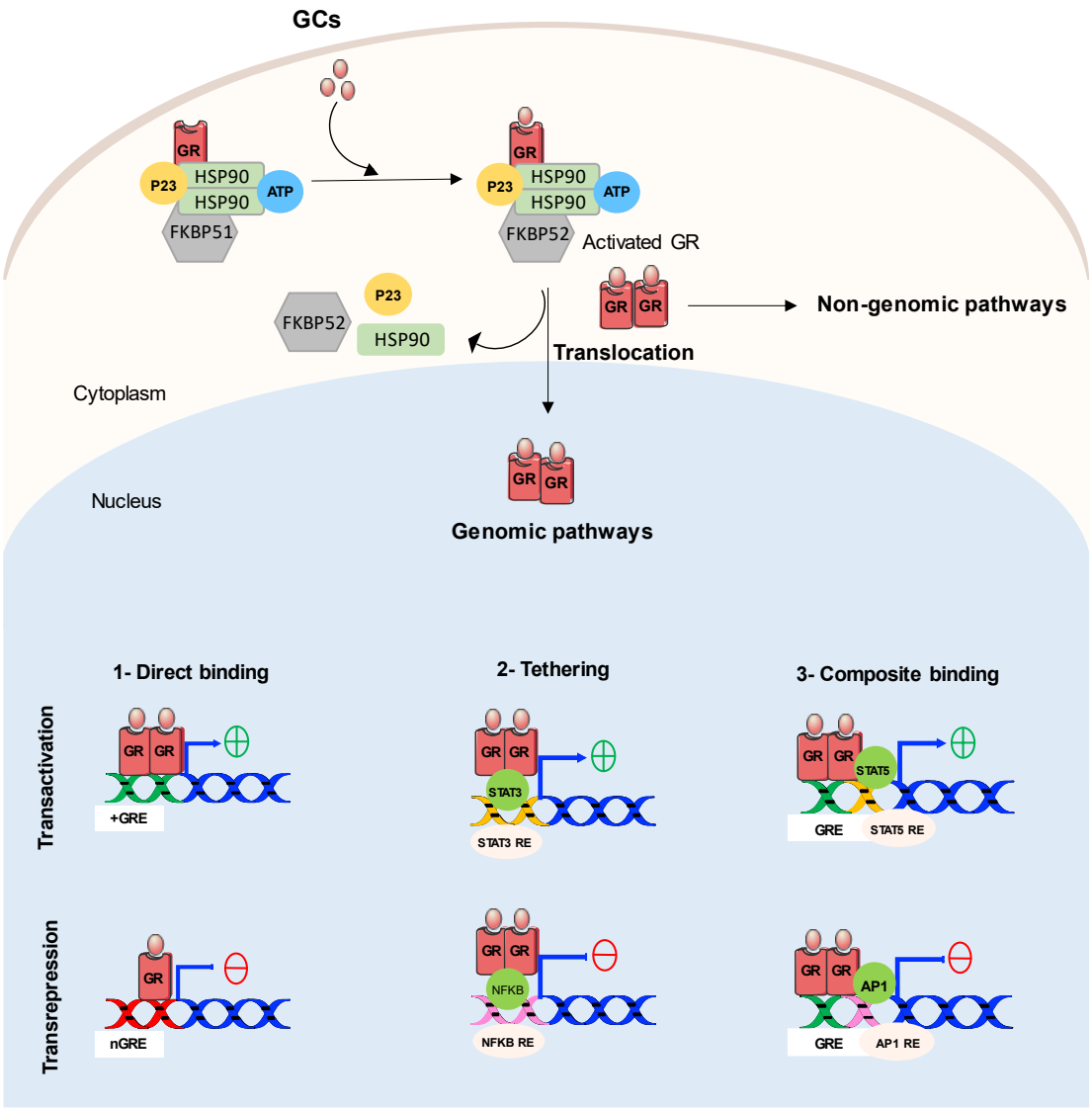

Figure 1-4 Glucocorticoid mechanism of action.

In the cytoplasm, GR bind to chaperone complex (heat chock proteins, FKBP, p23). When GC bind GR complex, GR undergoes confirmation changes between FKBP51 and FKBP52. This leads to the disassociation of the chaperone complex and the translocation of the active GR to the nucleus. The active GR can exert genomic pathways in three ways. GR will then activate or repress transcription of genes by directly binding to glucocorticoid-response element (GRE) or negative GRE, or by tethering to their transcription factor (TFs), or composite binding with DNA and GRE. The image was recreated using information from Cain and Cidlowski, 2017 and Kalfeist *et al.,* 2022.

1.2.3 Effects of GC on innate, adaptive, and anti-tumor immunity

During inflammation, stress increases the production of GC and this acts through GR to decrease the expression of inflammatory genes that influence innate, adaptive and anti-tumour immune responses. In this context, the natural production of GC is serving to provide a brake on the inflammatory process, to limit the damage done to healthy tissue by inflammation. GCs are used therapeutically to reduce inflammation and act as immunosuppressants, for example synthetic GC are used to limit inflammation in asthma and under more extreme circumstances to limit graft versus host responses in stem cell allografts. In innate immunity, GC influences the circulating monocyte phenotype (Gustafson *et al.,* 2010) to activate M2-Macrophage (anti-inflammatory) by inducing CD163 expression (Moyes *et al.,* 2018). These M2 macrophages in turn release the anti-inflammatory/ immunosuppressive cytokines TGF-β and IL-10. Macrophages express pattern recognition receptors such as Toll-like receptors (TLR) that sense infectious agents and activate the NF-kB pathway to induce expression of TNF and IL-1B genes as well as other proinflammatory cytokines. GC reduce the pro-inflammatory cytokines IL-6, and suppress IL-1B, IL-6, TNF-α, IFN-γ production (Ingawale *et al.,* 2020).

GC also stimulates adaptive immunity. GR can inhibit downstream TCR signalling by inhibiting the activity of downstream transcription factors AP-1, NF-kB, and NFAT, leading to a reduction in IL-2 secretion and T cell proliferation. T cells detect peptide antigen in complex with MHC-I or MHC-II; GC downregulate MHC-II, the co-stimulatory molecules CD80 and CD28, and decrease the pro-inflammatory cytokines IL-2, TNF-α and induce pro-inflammatory cytokine IL-10 (Cain and Cidlowski*,* 2017), thereby limiting T cell activation. Furthermore, GC influences Th polarisation toward Th2 and Treg and inhibit Th1 and Th17 lymphocytes, thereby favouring humoral reponses over cytotoxic and IL-17 mediated inflammation (Liberman *et al.,* 2018). In addition, GCs have potent cytotoxic action on lymphocytes and can induce the apoptosis of NK and T cells, limiting their ability to respond (Chen *et al.,* 2018).

GCs modulate anti-tumour immune responses by inhibiting both innate and adaptive immunity. It has been demonstrated that Dex treated NK cells can both enhance or repress NK cells proliferation, depending on cytokine provision

(Morgan and Davis., 2017). GC induces two genes: GITR, a glucocorticoid-induced TNFR family-related gene, and GILZ/TSC22D3, a glucocorticoid-induced leucine zipper which are both expressed in naïve T cells and NK cells (Riccardi *et al.,* 1999). GC also inhibits Treg numbers but did not activate T cells (Zappasodi *et al.,* 2019). The combination of anti-GITR and anti-PD-1 antibodies rescues CD8 T cells and maintains a memory T cells by increasing TIGIT expression on T and NK cells, leading to increased survival benefit (Chen *et al.,* 2022). GCs also mediate T cell exhaustion and dysfunction (Rudak *et al.,* 2019); Dex treatment inhibits the effector function of T cells by upregulating immune checkpoints PD-1, CTLA-4, and TIM-3 expression as well as causing apoptosis (Xing *et al.,* 2015).

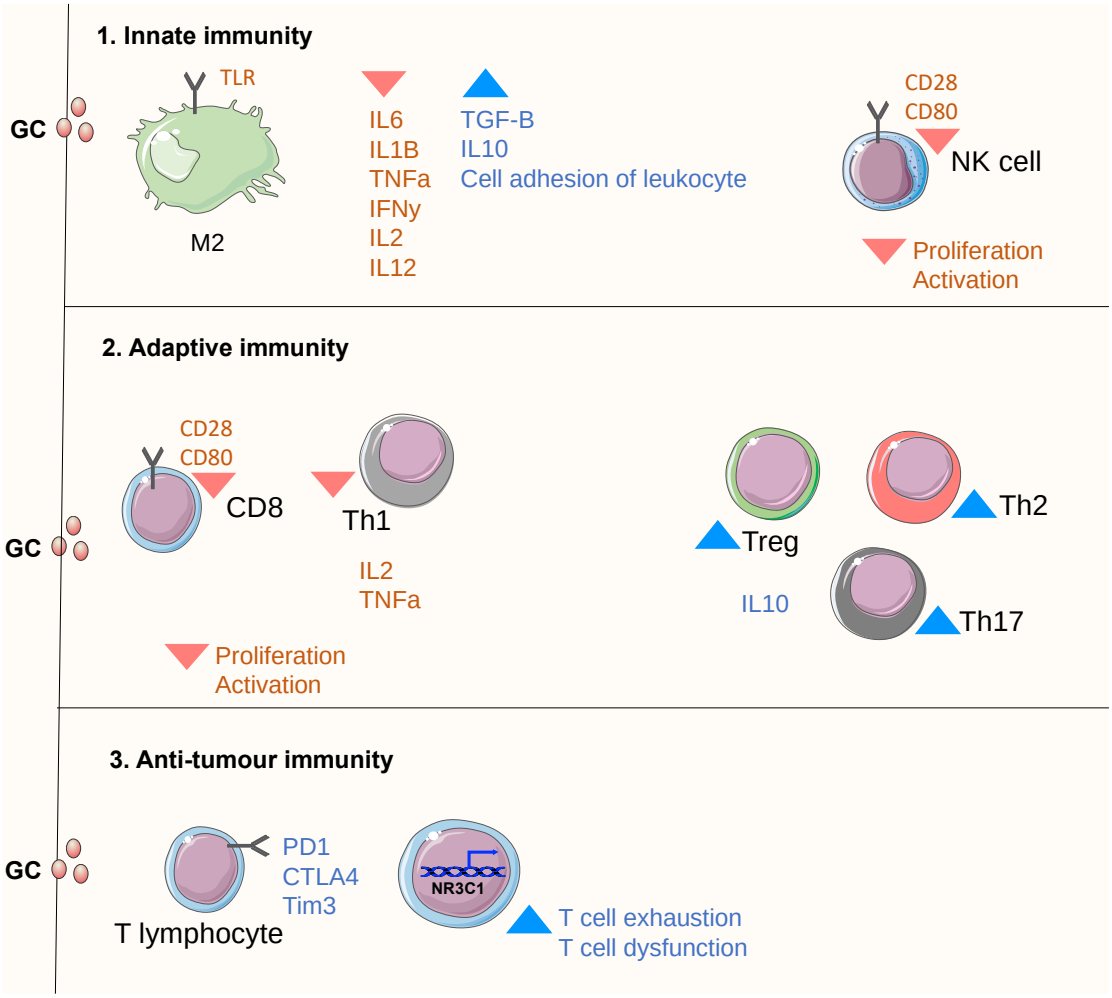

Figure 1-5 Glucocorticoids effect on immune cells.

GCs regulate 1. Innate immunity by reducing anti-inflammatory cytokines, and induce immunosuppressive factors. 2. Adaptive immunity by inhibiting the interaction between MHCII on APC with CD28, CD80 expression on T cells. 3. Anti-tumour immunity by increasing T cells exhaustion and increase GR expression and signalling and T cells dysfunction. The image was recreated using information from Kalfeist *et al.,* 2022

1.2.4 Effect of GC on GBM patient survival

The biological half-life of Dex is 36-52 hours, therefore GBM patients typically receive 10-16 mg per day for chronic neurologic symptoms such as headache, cerebral atrophy, and seizure, while patients with mild symptoms will receive 4-8 mg per day. Generally, once- or twice-a-day dosing is typically sufficient (Pitter *et al.,* 2023). GBM patients that receive Dex develop multiple adverse effect includes insomnia, anxiety, abnormal glucose metabolism, hyperglycaemia, cushingoid appearance and psychiatric symptoms that affect the patient's quality of life (Zhou *et al.,* 2021). Furthermore, Dex treatment causes lymphopenia in GBM patients (Gustafson *et al.,* 2010) which may restrict the action of immunotherapy.

Generally, the effect of Dex on GBM is controversial. GC showed inconsistent results on GBM cell proliferation, suggesting that sensitivity is linked to the time and dosage of Dex administration rather than solely due to tumour-intrinsic properties (Kaup *et al.,* 2001). Several studies demonstrated GC action on GBM patients, driving chemo-resistance and radio-resistance. Dex combined with TMZ and radiotherapy plus PD-1 blockade therapy in GBM patients showed reduction in overall survival (Iorgulescu *et al.,* 2021). GBM patients receiving high doses of GCs affect both tumour treating Fields (TTF) and reduce chemotherapy efficacy resulting in lower OS (Wong *et al.,* 2015). GBM patients under Dex treatment pre-radiotherapy treatment had a lower median PFS due to an increase in p21, a protein which induces cell cycle arrest and radio-resistance (Pitter *et al.,* 2016). Serum from GBM patients receiving GC showed altered cytokine secretion by GBM cells (Moyes *et al.,* 2018). Upregulation of GC-regulated genes associated with proliferation, cell death and cell movement were observed in GSC cells. CEBPB, a CCAAT Enhancer Binding Protein Beta gene, was upregulated in GC treated GSC cells, which indicates poor prognosis in GBM patients (Luedi *et al.,* 2017). GC induced GBM aggressiveness by enhancing invasion, proliferation, and angiogenesis in GBM cell line with mesenchymal GBM subtype cell line both *in vitro* and *in vivo* (Luedi *et al.,* 2018). GC induced the GSC phenotype in primary GBM cells by upregulating CD133 expression, a marker of multiple stem cell types (Kostopoulou *et al.,* 2018). GC is also reported to suppress MMP2/9 and IL-6 through E-cadherin induction leading to increased GBM invasion. It also showed that GCs suppress VEGF which inhibit angiogenesis (Martens *et al.,*

2019). Importantly, a phase I/IB study on GBM patients diagnosed with unmethylated MGMT promoters received neoantigen vaccination in the presence of Dex failed to generate neoantigen-specific $CD4^+$ and $CD8^+$ T cell responses (Keskin *et al.,* 2019), consistent with the effects on both innate and adaptive immunity.

The influence of Dex on immunotherapy and its possible effect on anti-tumour immune responses have been described in checkpoint inhibitor (CPI) therapies, and have shown variations in GC effects within tumours in general, including in GBM. A pre-clinical *in vivo* study by Giles *et al.* (2018) showed that Dex in combination with anti- CTLA-4 (ipilimumab) increased OS in a mouse model in comparison to ipilimumab alone and did not reduce T cell numbers in comparison to Dex alone. Dex combination treatment with anti-PD-1 in GBM animal model showed that Dex pre-treatment before anti-PD-1 administration did not influence mouse animal model survival. However, co-treatment of Dex with the anti-PD-1 showed increase in mouse animal model survival, reduced macrophages and reduced number of T cells in the tumour-draining lymph node (Iorgulescu *et al.,* 2021). Clinical studies of Dex combination treatment with CPI were conducted in GBM patients. GBM patients with IDH-wild type with anti-PD-1 or anti-PD-L1 showed negative correlation with patients OS. A recent phase II study on GBM patients showed that Dex reduced OS in patients receiving pembrolizumab plus bevacizumab (Nayak *et al.,* 2021). A phase III study in recurrent GBM showed that GCs in combination with bevacizumab or nivolumab is associated with shorter GBM survival (Reardon *et al.,* 2020). Overall, these studies fail to reach a consensus on the action of GCs in GBM in the context of immunotherapy.

While immunotherapies show promise, another option is to use oncolytic viruses. There are limited studies of GC in combination with oncolytic viruses (OV). It was reported in the Delta-24-RGD clinical study co-treatment with Dex depleted T cells and the OV effect was lost (Van Putten *et al.,* 2022). Overall, a little is known on GCs effect on OV, and reovirus in particular.

1.3 Viral immunotherapy

Oncolytic viruses (OVs) are naturally occurring or genetically engineered viruses that possess the ability to selectively infect and kill tumour cells without damaging normal cells (Figure 1.6). OV enter cells by binding to receptors on their surface and thus entry into both healthy and cells and tumour cells can occur. However, viral replication and lysis is restricted to tumour cells. This is poorly understood but is likely to be due to the inactivation of viral sensors and the lack of interferon induction pathways in tumour cells (Kaufman *et al.,* 2016). Furthermore, the sustained proliferation of tumour cells means that they compete very effectively for metabolic substrates (e.g. glucose, lipids etc) and can draw on large pools of metabolites to support biosynthesis of molecules required for cellular and viral replication. It was originally thought that the OV have anti-cancer properties because of their ability to lyse tumour cells. However, in addition, the OV stimulates innate and adaptive immune responses towards the tumour (Lichty *et al.,* 2014). Upon cell lysis, viral progeny is released with other several factors including virus associated pathogen-associated molecular patterns (PAMPs) as well as cellular factors such as damage-associated molecular patterns (DAMPs) and tumour-associated antigens (TAAs). These factors trigger immune cells and initiate anti-tumour immunity. TAAs processed by DC and other APC stimulate CD8 T cells, priming CTLs (Prestwich *et al.,* 2008). Both PAMPs and DAMPs stimulates innate immunity through Pathogen Recognition Receptors (PRRs) which induce type I interferon (IFN-I) production; IFN-I, including IFN-α and IFN-β induce the cytotoxic effects of NK cells, and promote anti-viral response (El-Sherbiny *et al.,* 2015).

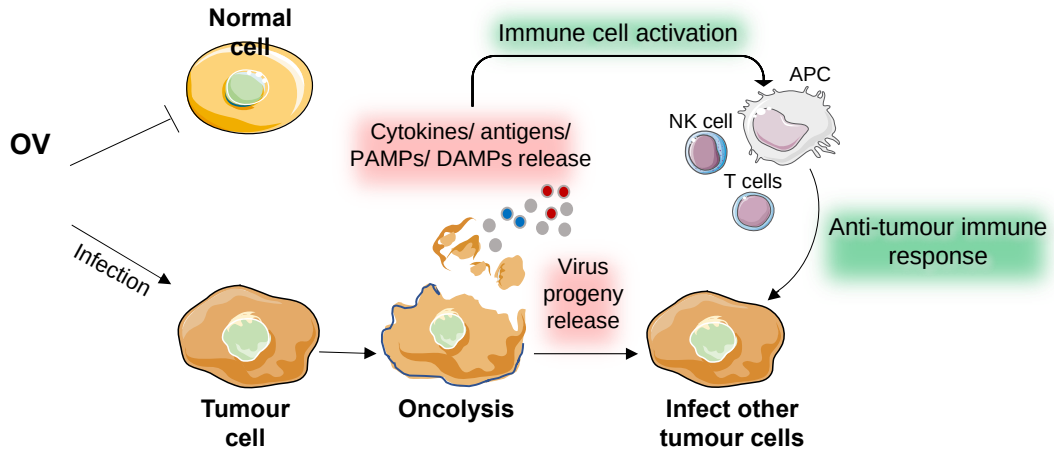

Figure 1-6 Overview of oncolytic virus (OV) mechanism of action.

The OV directly infects and kills tumour cells (oncolysis). Lysed cells release virus particles to infect and kill tumour cells nearby. Soluble tumour-associated antigens (TAA), viral pathogen-associated molecular pattern (PAMP), cell-derived damage-associated molecular pattern (DAMP), and type I IFNs recruit and activate antigen-presenting cells (APC). These factors resulted adaptive T cell responses against the tumour, recruitment of cytotoxic CD8 T-cells and NK cells. Activated cytotoxic T lymphocytes (CTL) recognise and kill neighbouring tumour cells. Both PAMP and DAMP stimulate immune cells by targeting toll-like receptors.

The first OV approved by the US Food and Drug Administration (FDA) was Talimogene laherparepvec (T-VEC), which is an attenuated herpes simplex virus type-1 (HSV-1) expressing GM-CSF for treating melanoma (Andtbacka *et al.,* 2019). In 2021, G47Δ HSV-1 (Teserpaturev) was approved in Japan for treating GBM (Todo *et al.,* 2022). Several OVs have been investigated for GBM with various success including HSV, reovirus (Reo), adenovirus, measles, parvovirus, poliovirus, retrovirus, and zika virus as reviewed in (Martikainen and Essand., 2019).

One of the promising OV candidates for GBM treatment is poliovirus (PVS-RIPO), an attenuated-live SABIN serotype contains heterologous internal ribosomal entry site (IRES), demonstrating favourable survival with tolerable level of toxicity. It has been demonstrated that PVS-RIPO can infect dendritic cells (DCs) and macrophages directly, resulting in an increase in IFN-I response and activation of pSTAT1 (Y701) leading to the expression of interferon-stimulated genes (ISGs), including IFIT1, ISG15, and PD-L1 (Brown *et al.,* 2017). A phase

I/Ib trial (NCT01491893) of PVS-RIPO in recurrent GBM patients is recruiting to evaluate virus safety and antitumor effect (Desjardins *et al.,* 2018). A more recent clinical II-trail (NCT02986178) of PVSRIPO alone or with anti-PD-1 (NCT04479241) is ongoing.

Another promising OV for GBM is adenovirus DNX-2401 (also known as Delta-24-RGD) with deletion of the Rb1-binding domain of E1A to enhance virus replication. The phase II clinical trial (NCT02798406) evaluated DNX-2401 in combination with anti-PD-1 (pembrolizumab) for recurrent GBM (Lang *et al.,* 2018), showing improved survival benefit (Nassiri *et al.,* 2023). DNX-2401 therapy in orthotopic glioma models with induced CD8+/CD4+ T cells, demonstrated the presence of protective immunological memory in treated animals, a shift towards an M1-like phenotype in the TME, and increased levels of IFN-γ and TNF-α in the CSF associated with T cells and NK cells. However, the therapeutic effect of the virus was lost following Dex treatment (Kleijn *et al.*, 2014; Kleijn *et al.,* 2017).

HSV-1 is a double-stranded DNA virus and a common human pathogen. Several oncolytic oHSV strains have been investigated in GBM. For example, HSV1716**,** which is a γ134.5 null mutant with an intact UL39 gene. A phase I trials of patients with recurrent glioma confirmed safety without adverse events, and with limited viral replication without showing toxicity (Harrow *et al.,* 2004). A preclinical study of oHSV in a neuroblastoma mouse model (a cancer of extracranial neural tissue distinct from GBM) demonstrated that Dex had no effect on the virus activity. However, Dex eliminated the antitumor immunotherapeutic effect in the long-term (Todo *et al.,* 1999). More recently, a phase I/II study (UMIN000015995) on G47Δ, an HSV-1 with ICP34.5, ICP6 and α47 triple deletion showed safety with 1-year OS for 84% of the patients (Todo *et al.,* 2022).

A recent clinical trial studied the efficacy of Reo T3D (Reolysin) for GBM patients and found that virus-mediated IFN stimulation can upregulate PD-L1 expression on tumour cells, with a small increase in T cell infiltration; no correlation was observed between immune cell infiltration and Dex treatment in patients in or outside the OV study (Samson *et al.,* 2018). The immunosuppressive effects of Dex observed with OVs are therefore not well described or at best, contradictory.

While only a small study, this is a surprising observation. In this thesis, HSV and Reo are investigated for their potential efficacy in the treatment of GBM in combination with GC, with the most detailed studies being performed with Reo (Table.1.1).

Table 1-1 Overview of selected OVs used in the thesis

Virus	**Herpes simplex virus (HSV-1)**	**Reovirus**
Stain	HSV-1718	Reolysin
Genome	dsDNA	dsRNA
Gene modification	1CP34.5 deletion	-
Receptor	Herpes virus entry meditor (HVEM)	Junctional adhesion molecule (JAM-1)
Virus entry	Nectin-1	Attachment protein sigma 1 (σ1)
Mechanism	PKR defects in tumour allow γ134.5 deleted HSV to receptor	Natural selectivity to activate Ras pathway
Clinical trial stage	NCT02031965 Phase I/II	NCT00528684 Phase 1

1.3.1 Reovirus structure and life cycle

Reovirus (Reo) is a non-enveloped double stranded RNA (dsRNA) virus, and its genome consists of 10 segments. Reo is composed of an outer capsid and inner core. The core is formed from the λ1, λ2 and σ2 proteins. The outer capsid is made up from σ1, σ3, and μ1 protein and is responsible for attachment and entry to host cells (Figure 1.7). Reo was first isolated in 1950s from paediatric stool samples termed Respiratory enteric orphan virus (Phillips *et al.,* 2018). Reo infects humans during childhood, typically with no clinical symptoms and the body rapidly clears the virus. There are four different serotypes (DeAntoneo and Balachandran, 2022) which are prototype strains Type 1 Lang (T1L), Type 2 Jones (T2J), Type 4 Ndelle (T4N), and Type 3 Dearing (T3D). In this study, the focus will be on Reo T3D strain (Reolysin).

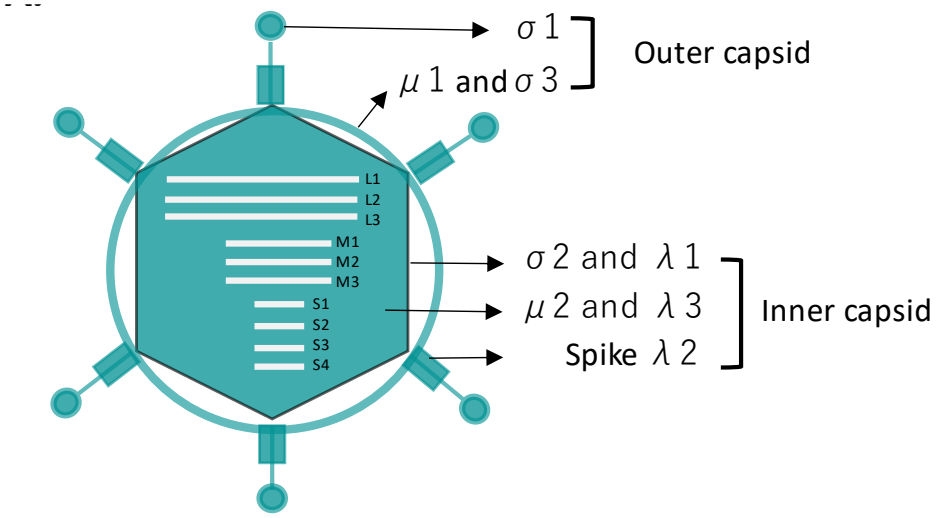

Figure 1-7 Reovirus structure.

Reo structure showing the outer capsid and inner core with 10 segments. Data was taken from Tenorio *et al.,* 2019.

The Reo life cycle starts with its attachment to the host cells through σ1 binding to cell surface sialic acid and the JAM-1 protein, leading to virus internalization via receptor β1-integrin mediated endocytosis (Barton *et al.,* 2001, Antar *et al.,* 2009). Upon virus entry, it is transported to endosomes where the capsid undergoes disassembly, leading to production of infectious subviral particles (ISVP), releasing virus core into the cytoplasm (Chandran *et al.,* 2001). The dsRNA genome is then transcribed (α3, μ1) leading to translation of virus proteins. The viral proteins (μ1, αNS, μNS) then create virus factories (Antczak *et al.,* 1992), allowing core virus assembly and replication which in turn release new virions particle (Figure 1.8).

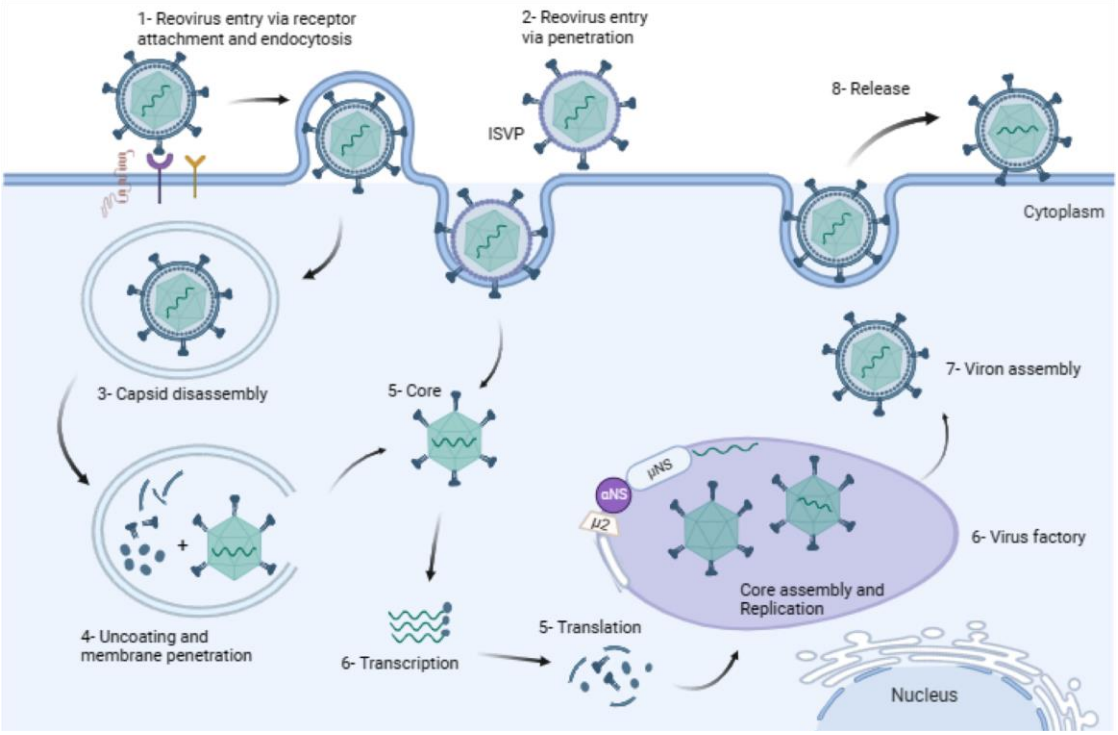

Figure 1-8 Reovirus life cycle.

Reo binds to cell surface receptor (JAM-1) facilitating membrane fusion. This allows the viral capsid and dsRNA genome transcription (a3, m1) to enter the host cell, where translation viral of proteins begin. Next steps include virus replication, viral assembly and genome packaging. The capsid undergoes conformational changes and traffics towards the ER. Finally, the fully mature virus is transported to the cell surface for release. Diagram created with BioRender.com. Data was taken from Tenorio *et al.,* 2019

1.3.2 Mechanism of oncolysis

Reo is naturally oncoselective to tumours due to its dsRNA genome interaction with the protein kinase R (PKR) pathway (a viral detection system), leading to apoptosis (Coffey *et al.,* 1998). In healthy cells, upon detection of dsRNA, PKR phosphorylates and inactivates the translation initiation factor eIF2. This causes a block in translation which prevents virus replication. However, in cancer cells, the activation of PKR by dsRNA is inefficient. In some cases, this has been attributed to constitutive signalling from Ras mutant or EGFR mutant molecules. The failure to activate PKR in cancer cells allows the virus to replicate and lyse the tumour cells (Gong *et al.,* 2014, Sadler *et al.,* 2008). The precise details of how Ras interferes with the PKR pathway are unclear. It has been shown that Ras transformed cells enhance Reo spread through MEK/ERK downstream signalling which inhibits IFN-β production and blocks expression of the dsRNA

detector RIG-1 (Shmulevitz *et al.,* 2010). Additionally, the Reo α3 protein was found to inhibit PKR activation which favours replication in cancer cells with otherwise intact PKR signalling pathways (Sharpe *et al.,* 1982).

Reo dsRNA is recognised by PRRs including Toll-like receptor (TLR), retinoic acid inducible gene-I (RIG-I), melanoma differentiation-associated protein 5 (MAD5), and PKR. In cancer cells, viral recognition activates transcription factors like NF-kB and IRF3 to induce the expression of IFN-α and IFN-β (Phillips *et al.,* 2018). Activation of NF-kB leads to secretion of the inflammatory cytokine TRAIL, which binds cell surface death receptors (DR4, DR5), recruits Fas associated death domain (FADD) proteins and leads to caspase 3 and 7 activation, causing apoptosis (Richardson-Burns *et al.,* 2020). Reo can also trigger apoptosis by activating other death ligands such as TNF-α and Fas ligand (FasL) which bind to cell surface receptors, initiating complex with FADD or TNF receptor type 1-associated death domain protein (TRADD) to activate caspase 8, 3, and 7 leading to apoptosis (O'Donnell *et al.,* 2003). Reo can also promote autophagy through acute ER stress. The autophagy protein, Beclin-1 interacts with BCL-2, inhibits BCL-2 expression and activated beclin-1 binds to myeloid differentiation primary response 88 (MYD88) and TIR-domain-containing adapter-inducing interferon-β (TRIF), leading to autophagy (Thirukkumaran *et al.,* 2013). Alternatively, Reo can induce cell death through necroptosis. Necroptosis is triggered by TNF- death receptor ligands (DR4/DR5) and PRRs which activates Receptor Interacting Serine/Threonine Kinase 3 (RIPK3) followed by Mixed Lineage Kinase Domain Like Pseudokinase (MLKL) phosphorylation, causing the cell membrane to rupture, causing cell death (Berger *et al.,* 2017). Cells undergoing necroptosis require IFN-β release and de novo synthesis of the Reo dsRNA. Mechanisms of cell death are illustrated in Figure 1.9.

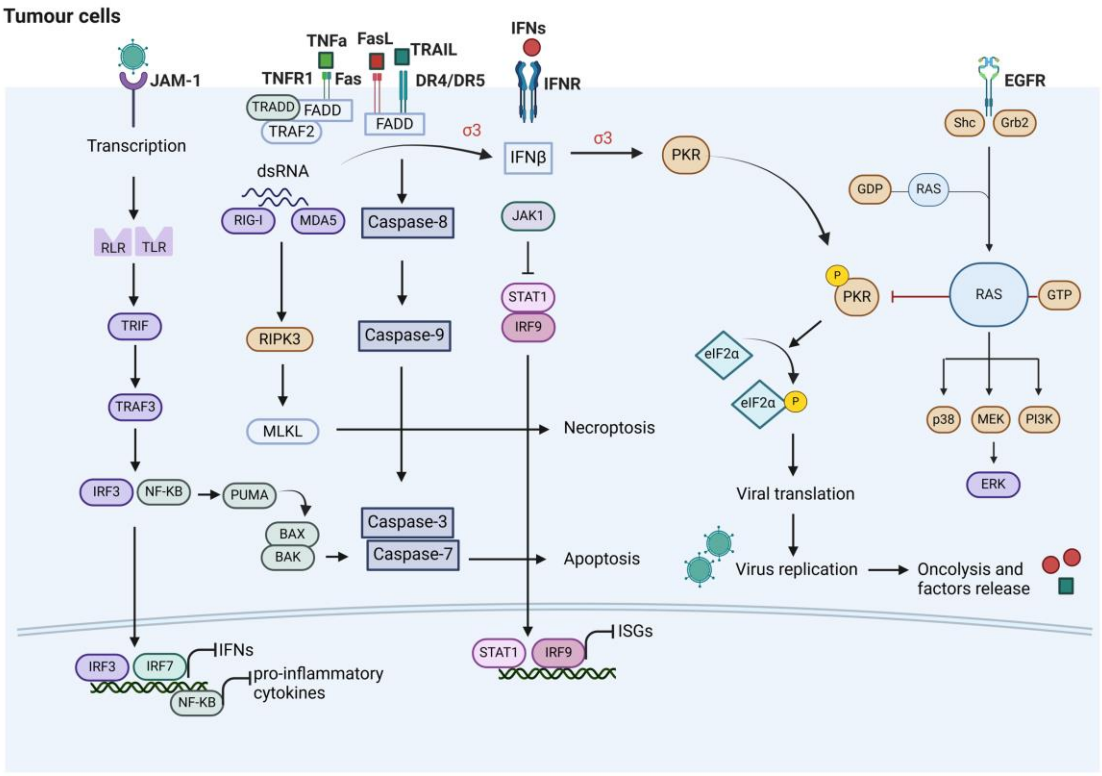

Figure 1-9 Reovirus death pathways.

In RAS-transformed cells, EGFR activates Ras, which inhibits PKR, allowing the cells to continue protein translation and proliferation leading to oncolysis. Reo is detected by toll-like receptor (TLRs), retinoic acid inducible gene-I (RIG-I), melanoma differentiation-associated protein 5 (MAD5), and PKR activates transcription factors of NF-kB, and IRF3 to induce the expression of IFN-α and IFN-β. NF-kB activation led to TRAIL secretion which binds to its receptors (DR4, DR5), recruits Fas associated death domain (FADD), lead to activate cleaved caspases 3 and 7 to induce apoptosis. Reo also triggers TNFa and Fas ligand (FasL) which bind to cell surface receptors, initiating a complex with FADD or TNF receptor type 1-associated death domain protein (TRADD) to activate caspase 8, 3, and 7 leading to apoptosis. Reo also trigger necroptosis by activating RIPK3 and phosphorylate MLKL. In addition, IFNs mediate JAK-STAT pathway, and activation of STAT1-IRF9 derives transcription of ISGs. Data was taken from DeAntoneo *et al.,* 2022; and Bourhill *et al.,* 2018

1.3.3 Reovirus anti-viral and anti-tumour immune responses

Tumour cells infected and lysed by Reo release PAMPs and DAMPs which stimulate innate immune cells to release pro-inflammatory cytokines. Theses cytokines include IL-6, IL-p70 and IFN-I from both tumour cells and immune cells. NK cells are recruited to the tumour site during OV infection, and become activated by IFN-I and via DC, leading to NK cell activation and the release of perforin and granzymes to initiate tumour cell apoptosis (Errington *et al.,* 2008).

In addition, Reo mediates adaptive immune responses; CTL activated following Reo infection can detect viral and tumour antigens and kill tumour cells. Reo release tumour associated antigens (TAAs) which are phagocytosed by antigen presenting cells (APC) such as DC and macrophage, and cross presented via MHC-I to T cells which activate CTL (Schulz *et al.,* 2005). DC and monocytes secrete IFN-α, TNF-α, IL-12, and IL-6. DC upregulating IFN-γ and IL-15 induce NK cells activation (Errington *et al.,* 2008). Importantly, Reo inhibits the immunosuppressive activity of MDSC through TLR3 and indirectly increases T cell responses (Katayama *et al.,* 2018).

A phase I study of patients with advanced cancer was treated with Reo to determine its safety showed upregulation of pro-inflammatory cytokines and IFN-I, leading to APC maturation, NK and T cell activation (White *et al.,* 2008). Furthermore, patients with colorectal cancer treated with Reo showed increased expression of NK surface marker (CD69) confirming NK cells activation (El-Sherbiny *et al.,* 2015).

OV can be delivered to GBM patients by surgical intratumoral injection (during tumour resection surgery). Challenges of delivering Reo systemically through IV injection include the BBB which reduces virus delivery to the GBM. However, a phase I clinical trial of Reo administrated intravenously (i.v) in GBM patients showed increased expression in chemokines macrophage inflammatory protein (MIP)-1α (CCL3), and 1β (CCL4) by tumour cells, increased intercellular adhesion molecule 1 (ICAM1) on T cells, increased M1-like marker (CD68), and a high percentage of CD8+ T cells in the tumour (Samson *et al.,* 2018). This study demonstrates that Reo infusion in GBM patients can reach the brain tumour.

1.3.4 Reovirus combination treatments to increase therapeutic efficacy

OVs such as Reo has shown evidence of therapeutic effects in various types of cancer. Generally, OVs are unlikely to ever be used as a sole therapy and will more likely be incorporated into existing standard therapies, such as surgery, chemotherapy and radiotherapy. There are two reasons behind this. First, clinical trials cannot be performed that take patients off a standard approved therapy to trial an experimental therapy. Second, different types of therapy frequently work best in combination. For example, surgery is a valuable approach to remove the

bulk of a tumour and then radiotherapy and/or chemotherapy can be used to kill remaining tumour cells. Therefore, several studies have assessed treatment options of OV in combination with chemotherapy and/or radiotherapy. These include Reo combined with cisplatin in melanoma (Pandha *et al.,* 2009), or with cisplatin plus paclitaxel in head and neck cancer (Roulstone *et al.,* 2013). Some combinations have been analysed at the molecular level, Reo combined with trastuzumab (anti-HER2 antibody) increases TRAIL expression in gastric tumour (Hamano *et al.,* 2015), while combination treatment with etoposide and actinomycin D increased p53-dependent expression of BAX and P21 in colorectal cancer (Hamano *et al.,* 2013). Reo and radiotherapy in melanoma increased apoptosis by reducing expression of anti-apoptotic genes (McEntee *et al.,* 2016). Reo induces neutralizing anti-reovirus antibody (NARA) but Reo effective responses remain when combining with chemotherapies in clinical trials (Maitra *et al.,* 2012). For instance, gemcitabine and Reo combination treatment in non-small lung cancer showed an attenuation in NARA response and successful induction of anti-tumour immune response (Villalona-Calero *et al.,* 2016). Such enhancements might be due to the chemotherapy acting on the immune system to reduce the production of neutralising antibodies.

One combination in particular show great promise, that of combining OV with immune checkpoint inhibition. As discussed, OV enhance anti-tumour immunity, and their use favours the infiltration of T cells into tumours. However, these T cells frequently have an exhausted phenotype due to induction of immune checkpoints. Thus, combination of OV with ICPs were investigated to increase therapeutic efficacy. A pre-clinical study in a murine model showed that Reo in combination with anti-PD1 increased survival rate, induced TNF-α production, reduced Tregs and induced T cells activity and the anti-tumour immune response (Rajani *et al.,* 2016). Another study investigated Reo intravenous administration in combination with anti-PD-1 to GBM patients. Surprisingly, histological samples showed that Reo RNA was detected in tumour cells, suggesting a promising administration method for Reo delivery, and RNA-seq data showed increase in cleaved caspase3 expression suggesting ongoing apoptosis (Samson *et al*., 2018). These types of studies suggest that combining OV with ICP and other modes of treatment has the potential to improve patient outcomes.

Thesis Aims and Objectives

GBM is aggressive and invasive with a median survival of ~18 months. New and improved therapies are desperately needed. Dex is part of standard care for many cancers due the potent anti-inflammatory effects. However, evidence suggests that Dex impairs the efficacy not only of current therapy but has potential to reduce the efficacy of emerging therapies. Understanding the underlying mechanisms will be critical not only to guide stratification of emerging treatments, but also provide a strategy to screen the efficacy of future treatments.

Aim1: Identify OV regulated gene sets in GBM and compare with Dex regulated gene sets to identify points of crosstalk and divergence: datasets will be identified using public data, and different web resources will be used to analyse and predict significant pathways regulated by GC and OV and determine their function.

Aim2: Investigate the effect of Dex on oncolytic virus mediated killing in panel of GBM cell lines. Complete RNA-seq on selected cell line treated with GC and Reo and analyse the transcriptome regulated by OV alone or in combination with GC.

Aim3: Develop a model to investigate crosstalk between human GBM and primary immune cells in response to Reo and Dex. Firstly, GC and Reo will be tested on GBM cells coculture model. Secondly, GC and Reo will be tested on immune cells in isolation. Finally, complete RNA-sequencing in coculture model and analyse the transcriptome regulated by OV alone or in combination with GC.

Aim4: Develop a model to investigate crosstalk between human GBM pre-treated with Dex and primary immune cells treated with Reo and Dex. Firstly, GC and Reo will be tested on GBM cells coculture model. Secondly, complete RNA-sequencing in coculture model in the pre-treated GBM cells and analyse the transcriptome regulated by OV alone or in combination with GC.

Chapter 2

Material and methods

2.1 Cell culture

Cell lines used in the thesis are listed in Table 2.1. All cells were cultured in an incubator at 37°C with 5%CO_2. Medium was changed every 3-4 days when needed, and routinely sub-cultured at 80% confluency.

Table 2-1 List of the cells used in the thesis.

Cells	Description	Sub-culture	Source
A172	Brain tissue of a patient with GBM	3-4 days 1:5 ratio	Cell line (ATCC) Cat. #CRL-1620
M059K	Brain tissue of a patient with malignant GBM. Useful model to study DNA protein kinase involving DNA damage recognition and repair	3-4 days 1:5 ratio	Cell line (ATCC) Cat. #CRL-2365
GBM1	Primary GBM (Classical/proneural subtype)	2-4 week 1:2 ratio	Dr. Heiko Wurdak, University of Leeds
GBM4	Primary GBM (Mesenchymal subtype)	2-4 week 1:2 ratio	Dr. Heiko Wurdak, University of Leeds
GBM11	Primary GBM (Mesenchymal subtype)	2-4 week 1:2 ratio	Dr. Heiko Wurdak, University of Leeds
GBM13	Primary GBM (Proneural subtype)	2-4 week 1:2 ratio	Dr. Heiko Wurdak, University of Leeds
GBM20	Recurrent GBM (Proneural/mesenchymal subtype)	1-2 week 1:2 ratio	Dr. Heiko Wurdak, University of Leeds
NP1	Normal brain progenitor cells	3-4 days 1:3 ratio	Dr. Heiko Wurdak, University of Leeds
Vero	African green monkey kidney cells	3-4 days 1:5 ratio	Cell line (ATCC) Cat. #CRL-2365
L929	Fibroblast cells	3-4 days 1:5 ratio	Cell line (ATCC) Cat. #CCL-1

2.1.1 Monolayer cell culture

The A172, Vero, L929 cell lines were grown in Dulbecco's modified eagle medium (DMEM; cat. #D6429, Sigma-Aldrich) supplemented with 10% foetal calf serum (FCS; cat. #10500064, Sigma Aldrich). Cell identity was verified by short tandom repeat (STR) profiling and lines were mycoplasma tested. MO59K cell line was grown in Dulbecco's modified eagle's medium: DMEM/F12 media (cat. #D8437, Sigma-Aldrich), supplemented with 10% FCS, 1mM sodium pyruvate (cat. #11360039, Thermo Fisher Scientific), and 1mM non-essential amino acid (NEAA; cat. #11140035, Thermo Fisher Scientific). For experiments, FCS was replaced with steroid free, charcoal stripped serum (CSS; cat. #12676029, Sigma-Aldrich). Cells were cultured in Corning flasks (Sigma Aldrich), and maintained at 37^{o}C, 5% CO_2 in a humidified atmosphere. Confluent cells were passaged by removing the media, and washed with sterile Dulbecco's phosphate buffered saline **(**D-PBS), and then incubated with trypsin-EDTA (Ethylenediaminetetraacetic acid; cat #T4174, Sigma-Aldrich) to detach cells from the flask surface. Media was added to stop the trypsin reaction and the cell suspension was centrifuged at 400xg for 5 minutes before being diluted in fresh growth media and divided into new flasks.

2.1.2 Patient-derived GBM cell culture

GBM1, GBM4, GBM11, GBM13 and GBM20 were kindly gifted from Dr. Heiko Wurdak's group (Polson *et al*, 2018; Wurdak *et al.,* 2010; Da Silva *et al.,* 2019). These cells were isolated from patient's tumour and are characterised as stem-cell like as they are poorly differentiated cells. These cells were grown in Neurobasal medium (cat. #21103-049, Thermo Fisher Scientific) supplemented with final dilution of B-27 (0.5x; cat. #17504-044, Thermo Fisher Scientific), N-2 (0.5x; cat. #17502-048, Thermo Fisher Scientific), recombinant human basic fibroblast growth factor (bFGF; 40ng/ml; cat. #PHG0026, Thermo Fisher Scientific), and epidermal growth factor (EGF; 40ng/ml; cat. #236-EG, Thermo Fisher Scientific). The cells are grown in flasks coated with poly-L-ornithine at a 1:2000 dilution in dH_2O (cat. #P3655, Merck) and laminin at a 1:500 dilution in PBS (cat. #23017-015, Thermo Fisher Scientific). The normal brain cell line (NP1) was used as a control and was grown in DMEM/F12 media supplemented with final dilution of B-27 (0.5x), N-2 (0.5x), GlutaMAX (1x), bFGF (20ng/ml), EGF

(20ng/ml), and FCS, 5% (v/v). All cells were maintained at 37^{o}C and 5% CO_2 in a humidified atmosphere.

2.1.3 Cryopreservation and revival of cells

To freeze cell lines for long-term storage, cell pellets were frozen in 90% FCS plus 10% DMSO (dimethyl sulfoxide) at a density of 1x10^{6} per cryovial, and stored in a Mr. Frosty container (cat. # 5100-0001, Thermo Fisher Scientific) at -80^{o}C for at least 24 hours before being transferred to vapour liquid nitrogen. To thaw cells, cryovials were warmed in 37^{o}C water bath for one minute and then transferred to a Falcon tube containing 9ml of growth media. Cells were then centrifuged at 400xg for 5 minutes, and cell pellets were resuspended in growth media and transferred to a new flask and incubated until cells reached 80-90% confluency. Media was replaced every 2-3 days as required.

2.1.4 Peripheral blood mononuclear cell (PBMC) isolation and culture

PBMC cones were obtained from the National Health Service Blood and Transplant (NHSBT) UK. The PBMC were isolated from healthy donor using Lymphoprep (cat.#07851, Stem Cell Technologies) and density gradient centrifugation. Briefly, whole blood was diluted with 20ml sterile Hanks' balanced saline solution (HBSS; cat.#37150, Stem Cell Technologies), and transferred carefully into 50ml falcon tube containing 15ml lymphoprep to form two layers. Samples were centrifuged at 800xg for 20 minutes with acceleration 3 and brake 0. The PBMC layer was transferred into a new falcon tube, washed with 40ml HBSS, centrifuged at 200xg for 20 minutes with acceleration 9 and brake 3, followed by another wash step centrifuged at 400xg for 10 minutes with acceleration 9 and brake 9. PBMC were then resuspended in 15ml RPMI media (cat.#R8758, Sigma-Aldrich) supplemented with 10% FCS, counted using a haemocytometer, and cultured at 2 x10^{6} cells/ml at 37^{o}C, 5% CO_2 in a humidified atmosphere.

2.2 Single culture preparation for RNA sequencing

MO59K cells ($2x10^5$ cells) per sample were grown overnight, and treated with Vehicle (DMSO diluted in PBS or media at final culture concentration 100nM), Reo at multiply of infection (MOI 1), or Reo (MOI 1) plus 100nM Dex (prepared in DMSO). Cells were incubated with treatment conditions for 24 hours, then gently washed with PBS and RNeasy mini kit (cat.#74104, QIAgen) was used for RNA extraction. Each treatment condition was prepared in triplicate.

2.3 Coculture models preparation for RNA sequencing

Two coculture models were prepared to isolate MO59K cells for RNA-seq. The first model is a direct coculture of MO59K cells with PBMCs and two isolation methods were used as described below. The second model is an indirect model using a cell insert preventing cell-cell contact. The purpose of using two models is to examine the different methods of isolation of GBM cells using PBMC donors to choose one model for further RNA-seq. Table 2.2 showed the treatment conditions used in the RNA-seq samples.

Table 2-2 Coculture treatment conditions

MO59K condition	PBMC condition	Coculture sample (MO59K_PBMC)
Veh	Veh	Veh_Veh
Veh	Reo MOI 1	Veh_ Reo
Veh	Reo MOI 1 + 100nM Dex	Veh_ ReoDex
100nM Dex	Reo MOI 1	Dex_ Reo

2.3.1 Direct coculture model

The first experiment plan to perform the coculture model was to isolate each of MO59K, macrophages and NK cells by using the cell sorter. Briefly, at day 0, MO59K cells were seeded in a 6-multi well plate. After cell attachment, 100nM Dex were added in the needed treatment conditions. In addition, multiple PBMC donors were also grown in T25 flasks (2x106 cells/ml), and treated with either vehicle, Reo (MOI 1), or Reo (MOI 1) plus 100nM Dex for hours. At day 1, treated

PBMC were cocultured with MO59K cells at 10:1 E:T ratio for 24 hours. Both attached cells and supernatant were collected and washed with PBS. Then, samples were prepared to isolate MO59K, NK cells, and macrophages by using the cell sorter (section 2.4). A second experiment was prepared to isolate MO59K cells only from the coculture model using negative fraction of CD14 microbeads (section 2.5).

2.3.2 Indirect coculture model using 0.4µm transwell

Similar coculture treatment conditions were replicated as previously described, but MO59K cells were grown on the lower chambers on day 0, and next day, the inserts (0.4µm pore size, cat.#PIHP03050, Sigma-Aldrich) were added on top of each well, and PBMC were seeded ($2x10^6$ cells/ml) at E:T ratio of 10:1 for 24 hours. Each treatment condition (Table 2.2) was repeated using three different donors for triplicate sampling. Both MO59K cells and PBMC were collected separately, washed with PBS and prepared for RNA extraction.

2.4 Cells isolation using cell sorter

Reo requires biological containment category II and therefore, a risk assessment was approved by the University of Leeds (CL2_nonGM_03_Melcher_Griffin) for using the virus in the cell sorter. Cells were trypsinised and washed with PBS twice, then incubated with the markers: APC human-anti-CD54 (cat.#304012, clone: HI30, Bio-Rad), pacific blue human-anti-CD3 (cat.#300330, clone: HIT3a, Bio-Rad), PE human-anti-CD56 (cat.#392404, clone: QA17A16, Bio-Rad), PE/Cynine7 human-anti-CD14 (cat.#367112, clone: RUO, Bio-Rad), and Live/dead stain for 30 minutes at 4°C in the dark. Cells were pelleted at 400xg for 5 minutes and washed twice with FACS buffer. Cells were suspended in FACS buffer with 0.1% EDTA to help maintain a single cell suspension. All samples were passed through a 70µm strainer to remove any clumped cells. All tubes were kept on ice, and safety procedures were taken in account to transfer the samples. Cell sorting was performed using a FACSAria III sorter at low pressure (100 µm nozzle) with the FACSDiva software V8.0.2 (BD Biosciences). Sorted cells were collected in 1.5ml Eppendorf tubes, and placed on ice, and purity was validated by re-acquisition of a small aliquot of sorted cells (~1000 cells). A

representative gating strategy for isolating each of MO59K cells (gated by size and CD45- to remove immune cells), Macrophage (gated by CD45+CD14+ markers), and NK cells (gated by CD45+CD3-CD56+ markers) was displayed in Figure 2.1. The sorted cells (MO59K cells, Macrophage, and NK cells) were directly lysed and processed for RNA extraction as described in section 2.14.1.

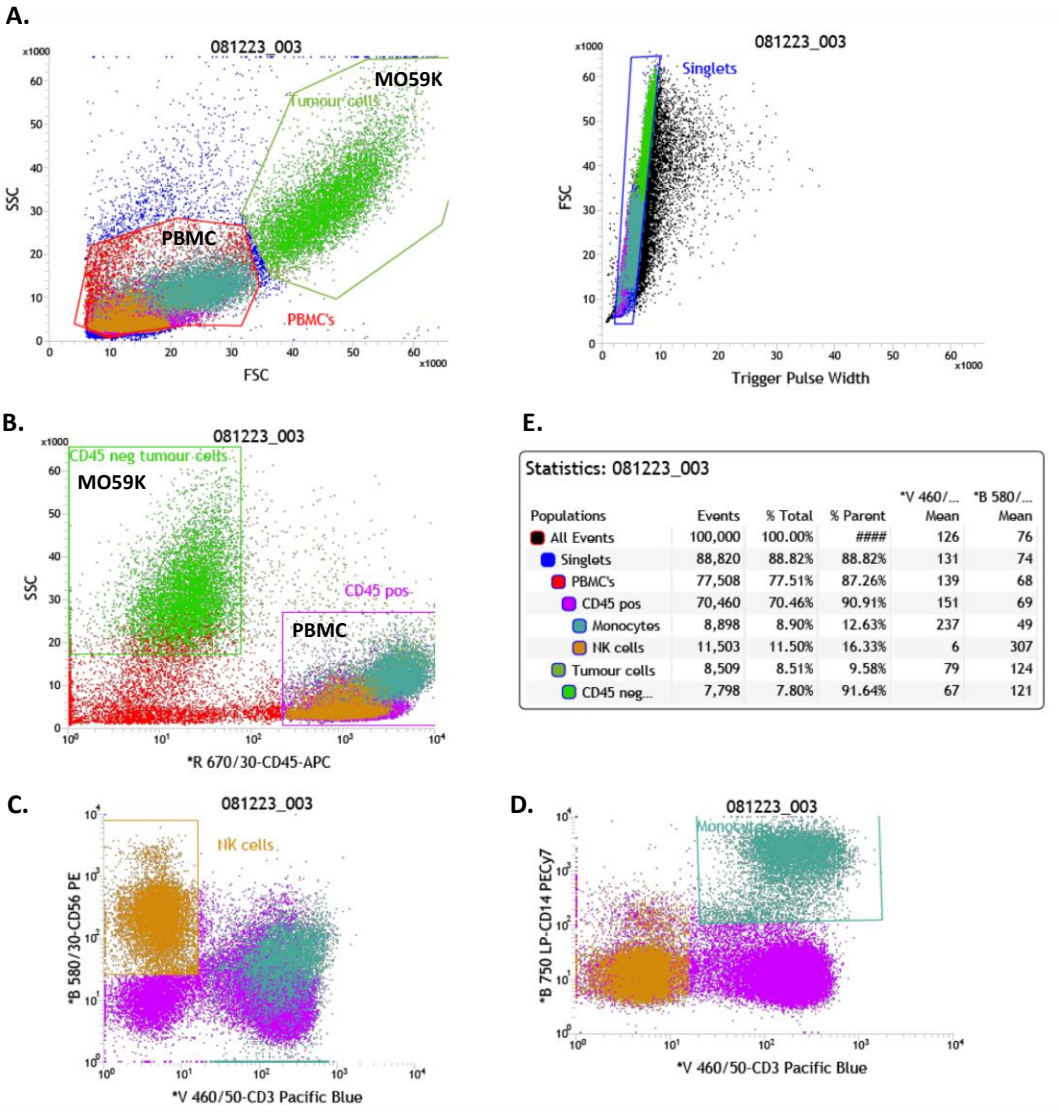

Figure 2-1 A representative strategy for isolating pure cell population using the cell sorter.

MO59K cells were cocultured with PBMC at 10:1 E:T ratio. After 24 hours, adhered cells were detached and collected alongside the suspension cells, washed with PBS. Cell sorter was used to isolate cells of interest. A. showing the distinct population of MO59K cells and PBMC identified on SSC:FSC plot. B. MO59K cells were then isolated using the markers CD45- and cell weight, C. Monocytes were isolated using the markers CD45+CD14+ and D. NK cells using the markers CD45-CD3-CD56+ E. Shows the percentage of each isolated cells.

2.5 Cells isolation using microbeads

MS or LS MACS columns and magnetic field MACS separator were used for the separation process. Generally, cells of interest were counted, centrifuged at 300xg for 10 minutes, and resuspended in 80µl MACS buffer (PBS, 0.5% BSA, 2mM EDTA) and 20µl of CD14 microbeads (cat.#130-050-201, Miltenyi Biotec, UK) or CD56 microbeads (cat.#130-050-401, Miltenyi Biotec, UK) per 10^7 total cells. Cells were incubated in the fridge for 15 minutes, then washed with 1ml MACS buffer, centrifuged at 300xg for 10 minutes, and resuspended in 500µl MACS buffer. MACS column was placed in the magnetic field separator and washed with MACS buffer once. A clean FACS tube was located under the column to collect cells that passed through (negative fraction). Cell suspensions were applied to the column, and the column was washed three times with 500µl MACS buffer. Finally, 1ml MACS buffer was added to the column to flush out the magnetically labelled cells using the plunger into a clean collection tube (positive fraction), washed two times with PBS, and suspended in appropriate media supplemented with 10% FCS. Cells were counted and split to the appropriate culture ware.

2.6 Drugs

Dexamethasone (Dex; cat.#D4902, Sigma-Aldrich) stock solution (20mM) was dissolved in 12.7ml Dimethylsulfoxide (DMSO). For experiment, Dex was diluted in PBS or media at working concentration (20µM) and the final culture concentration of 100nM. Staurosporine (STS; cat.#SM97-1, Cell Guidance Systems) stock solution (1mM) was dissolved in 2.14ml DMSO. For experiments, STS was diluted to a final concentration of 1nM. Selective steroids: Compound A (CoA; cat.#ab144525, Abcam) stock solution (10mM); AZD7594 (AZD; cat.#1196509-60-0, Medchemexpress) stock solution (10mM); and Vamorolone (Vam; cat.#HY-109017, Cambridge Bioscience) stock solution (10mM) were resuspended in DMSO. All drugs were reconstituted and aliquoted for long term at -20^{o}C.

2.7 Oncolytic viruses

2.7.1 Reovirus (Reo)

Type 3 Dearing strain (Reolysin) was a gift from Dr. Fiona Errington-Mais, University of Leeds, UK, with a stock titre of 2 x 10^9 PFU/ml.

2.7.2 Herpes simplex virus-1 (HSV-1)

HSV-1 (17+ 34.5- 47-) was a gift from Dr. Hardev Pandha, University of Surrey, UK. HSV was propagated following Simpson *et al.,* (2010) protocol with slight modification. Briefly, BHK cells (1x10^7) were plated in a T175 flask. The cells were infected with the virus stock at multiply of infection (MOI) of 0.01 and incubated at 37^{o}C until complete cytopathic effect (CPE) was observed. The flasks were then frozen at -80^{o}C for 1.5 hours, and thawed at room temperature (RT). Infected cells were scraped and pelleted by centrifugation at 1350xg for 30 minutes at 4^{o}C. The supernatant was subsequently passed through a 0.45μm filter. The virus particles were then pelleted by centrifugation at 21700xg for 2 hours at 4^{o}C. The supernatant was removed, and 1ml of this supernatant was used to resuspend the viral pellet by pipetting. The virus was aliquoted and stored in -80^{o}C. The titre of the resuspended virus was determined using the standard viral plaque assay on Vero cells (Simpson *et al.,* 2006). The titer of the newly propagated virus was 1.68 x 10^9 PFU/ml and is stored at -80C until use.

2.8 Plaque Assay

To measure virus replication, viruses were subjected to three cycles of freeze and thaw. Vero (for HSV-1; ATCC, cat. #CCL-81) or L929 (for Reovirus; ATCC, cat. #CCL-1) cell lines were plated at a concentration of 5x10^6 cells per well in a 6-well plate. A range of 10-fold dilutions of the virus was incubated on monolayers of Vero or L929 cells at 37°C for 1-2 hours. Supernatants were then aspirated, washed twice with PBS, and incubated with 2% carboxymethyl-cellulose (CMC) in 2% FCS-DMEM for 3-5 days at 37°C in a 5% CO^2 atmosphere to allow plaque formation. For plaque counting, the cells were fixed with 1% paraformaldehyde (PFA) for 30 minutes, followed by staining with 0.5% methylene blue for 10

minutes. Virus titres were calculated through plaque counting and expressed as a plaque-forming unit per *millilitre* (PFU/ml). The plaque count formula:

Virus count = plaque count x viral dilution x 10 = pfu/ml

2.9 MTT assay

For MTT (3-[4,5-dimethylthiazol-2-yl]-2,5 diphenyl tetrazolium bromide) assay, MO59K and A172 cells were seeded in 96 well plates at a density of $1x10^4$ cells/ml. Patients derived cell lines (GBM1, GBM4, GBM11, GBM13, GBM20) were seeded in 96 well plates at a density of $5x10^3$ cells/ml. Cells were treated with 100nM Dex alone, OV (HSV-1 or Reo) alone at MOI of 0.01, 0.1, 1, or 10, co-treatment of 100nM Dex plus OV, or pre-treatment with 100nM Dex overnight followed by OV. Diluted DMSO was used as vehicle control. Cells were left for 48-72 hours. Then, 20µL of MTT stock solution (5mg/ml; cat. #M6494, Thermo Fisher Scientific) was added per well and incubated for 3-4 hours. The media were carefully removed and 200µL DMSO were added per well. Absorbance at 405 nm was used for measurement using a microplate reader. Wells without cells, but incubated with MTT reagent were used as a background control.

2.10 Flow cytometry

The antibodies used in the flow cytometry experiments are listed in Table 2.3. and were analysed using the Cytoflex XL flow cytometer (Life Technologies), and the CytExpert software was used for results analysis.

Table 2-3 List of the antibodies used in flow cytometry experiments.

Antibody	Dilution	Company
Pacific Blue anti-human CD3	5µl per 1x10^6 cells	Biolegend; #300330
PE anti-human CD56	5µl per 1x10^6 cells	Biolegend; #355504
FITC anti-human CD69	5µl per 1x10^6 cells	Biolegend; #310904
APC Anti-human CD45	5µl per 1x10^6 cells	Biolegend; #304012
FITC anti-human CD14 PerCP anti-human CD14	5µl per 1x10^6 cells	Biolegend; #325603 Biolegend; #325632
FITC anti-human CD16	5µl per 1x10^6 cells	Biolegend; #360716
PE anti-human CD163	5µl per 1x10^6 cells	BD; #562670
BV421 anti-human CD206	5µl per 1x10^6 cells	BD; #566281
PE anti-human CD86	5µl per 1x10^6 cells	BD; #G71595L
BV421 anti-human HLA-DR DPDQ	5µl per 1x10^6 cells	BD; #564244
APC anti-human CD274 (PD-L1)	5µl per 1x10^6 cells	Biolegend; #329708
Herpes simplex entry mediator (HVEM) Anti-CD270	5µl per 1x10^6 cells	Biolegend #12-5969-80
Junction adhesion molecule 1 (JAM-1), Anti-CD321	5µl per 1x10^6 cells	Santa Cruz Biotech #J1414
gG1 Isotype	5µl per 1x10^6 cells	Miltenyi Biotec #130-113
IgG2a Isotype	5µl per 1x10^6 cells	Miltenyi Biotec #130-113

2.10.1 Live/dead assay

GBM cells were seeded in 24 well plates at a density of $1x10^5$ cells/ml and incubated overnight to adhere. Cells were treated with Dex alone, OV alone, co-treatment of Dex and OV, or pre-treatment of Dex for overnight and then treated with OV. Cells were also treated with selective steroids (CoA, Vam, AZD) alone or in combination with Reo MOI1 at indicated time points. A 20% of DMSO was used as positive control and complete growth medium as negative control. Media was removed and 1x trypsin/EDTA added to detach the cells. Cell pellets were washed with PBS and re-suspended in 1ml of LIVE/DEAD stain (1µl LIVE/DEAD yellow stain: 1ml PBS, cat. #L-34959, Thermo Fisher Scientific) solution per 1x 10^6 cells and incubated in the dark for 30 minutes. Cells were then washed with PBS and re-suspended in 1% PFA. Cells were analysed using the gating strategy depicted in Figure 2.2.

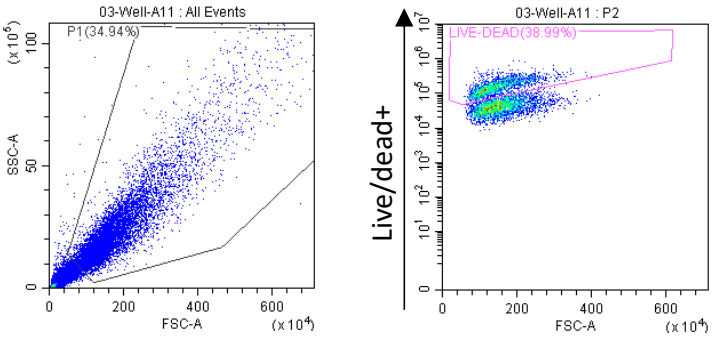

Figure 2-2 Gating strategy for cell viability assay by Live/ dead stain.

The figure shows gating GBM cell lines and debris were excluded based on SSC versus FSC (right), dead cells were gated with yellow florescent live/dead stain (left).

2.10.2 Cell line viral entry receptor expression

All GBM cells (1x10^5) were washed in FACS buffer (PBS + 10% FCS + 0.1% sodium azide) and fluorescently conjugated antibodies (JAM-1 and HVEM) or isotype controls diluted in FACS buffer were added (5µl per 1 x10^6 cells) for 30 minutes on ice, in the dark. Cells were then washed in FACS buffer, and re-suspended in 1% PFA. Cells were analysed using the Cytoflex XL flow cytometry (Life Technologies) and the mean fluorescence intensity (MFI) of bound antibody were determined in comparison to isotype control.

2.10.3 PD-L1 expression in GBM and PBMC cells

MO59K cells (1x10^5 cells/well) or healthy human PBMC (2x10^6 cells/ml) were treated with: Vehicle, 100nM Dex, Reo MOI 1, or 100nM Dex plus Reo MOI 1 for 24 hours. Cells were trypsinised and centrifuged at 400xg for 5 minutes, resuspended in 1ml media and transferred to FACS tubes. Cells were counted for total 1x10^5 cells/well, centrifuged at 400xg for 5 minutes, and washed in 1ml FACS buffer. Cells were stained with PD-L1 antibody (APC CD274; cat.#329707, Biolegend) or isotype control (APC mouse IgG2b; cat.#400322, Biolegend) and live/dead stain (cat. #L34968, Thermo Fisher Scientific) and incubated for 30 minutes on ice in the dark. Cells were washed in FACS buffer and resuspended in 1% PFA. Finally, cells were analysed using the Cytoflex XL flow cytometry and PD-L1 expression was determined as MFI of bound antibody normalized to IgG control.

2.10.4 PBMC mediated killing on GBM cells

GBM cells (MO59K, GBM20, GBM13) were seeded in a 12-well plate at a density of $1x10^5$ cells/ well and stained with 500nM MitoTracker green (cat.#M7514, Thermo Fisher Scientific) overnight. Cells were then either left untreated or treated with 100nM Dex cells after attachment with vehicle or 100nM Dex for 24 hours. PBMCs were grown in T25 flask ($2x10^6$ cells/ml) and treated with vehicle, 100nM Dex, Reo, or combined Dex plus Reo for 24 hours. GBM cells were cocultured with PBMC at E:T ratio of 10:1 ratio for another 5 hours. Cells were trypsinised and washed with PBS. To determine the percentage killing of GBM cells, anti-CD45 antibody and live/dead stain were used and incubate for 30 minutes on ice in the dark, washed with PBS and gated as (MitoTracker green+, CD45-, Live/dead+) to calculate the percentage of GBM cells death. In addition, NK cells were depleted from PBMC by negative fraction of CD56 microbeads (cat.#130-050-401, Miltenyi Biotec, UK). Figure 2.3 showed a representative gating strategy for the indirect killing assay in the coculture model.

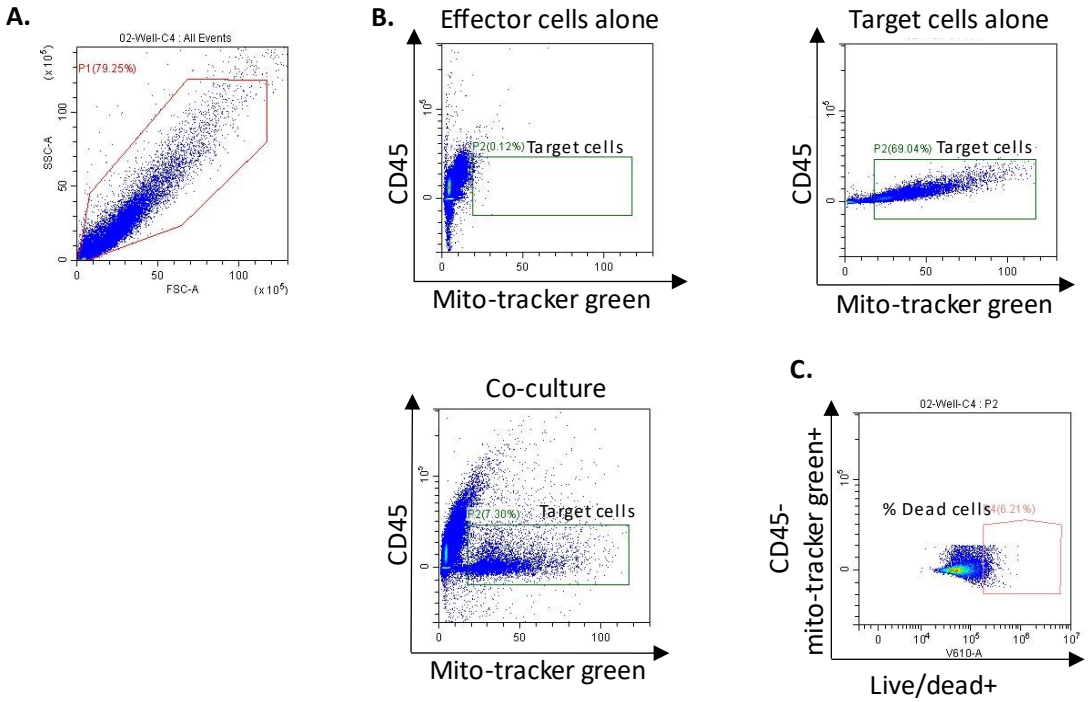

Figure 2-3 Gating strategy for the killing assay on GBM coculture system.

Effector cells **(**PBMC) isolated from healthy donors were treated for 24 hours and cocultured with target cells for 5 hours at indicated effector: target ratio (n=3). The figure shows the gating strategies **A.** Debris were excluded based on SSC versus FSC. **B.** Target cells were gated as CD45-/ MitoTracker green+, and **C.** dead target cells were gated as live/dead stain+.

2.10.5 Monocyte, T and NK cells phenotyping and viability assay

PBMC were seeded in 6-well plate at a density of $2x10^6$ cells/ml. Cells were then treated with either 100nM Dex, Reo (MOI 1) alone or in combination for 24 hours. For monocyte phenotyping and viability assays, live/dead stain, fluorescently conjugated anti-CD14, anti-CD16, anti-CD163, anti-CD206, anti-HLA-DR, anti-CD68 antibodies and corresponded isotype controls were added to the cells and incubated for 30 minutes on ice in the dark. For NK and T cells phenotyping and viability assays, live/dead stain, fluorescently conjugated anti-CD3, anti-CD56, anti-CD69 antibodies and corresponded isotype controls were added to the cells and incubated for 30 minutes on ice in the dark. Cells were then washed with FACS buffer and fixed in 1% PFA. Cells were analysed using the Cytoflex XL flow cytometer (Life Technologies), and the gating strategy is depicted in Figure 2.4. Experiment was repeated on PBMC to screen selective steroids (CoA, Vam, AZD) at 100nM alone or in combination with Reo for NK and T cells death percentage and activation.

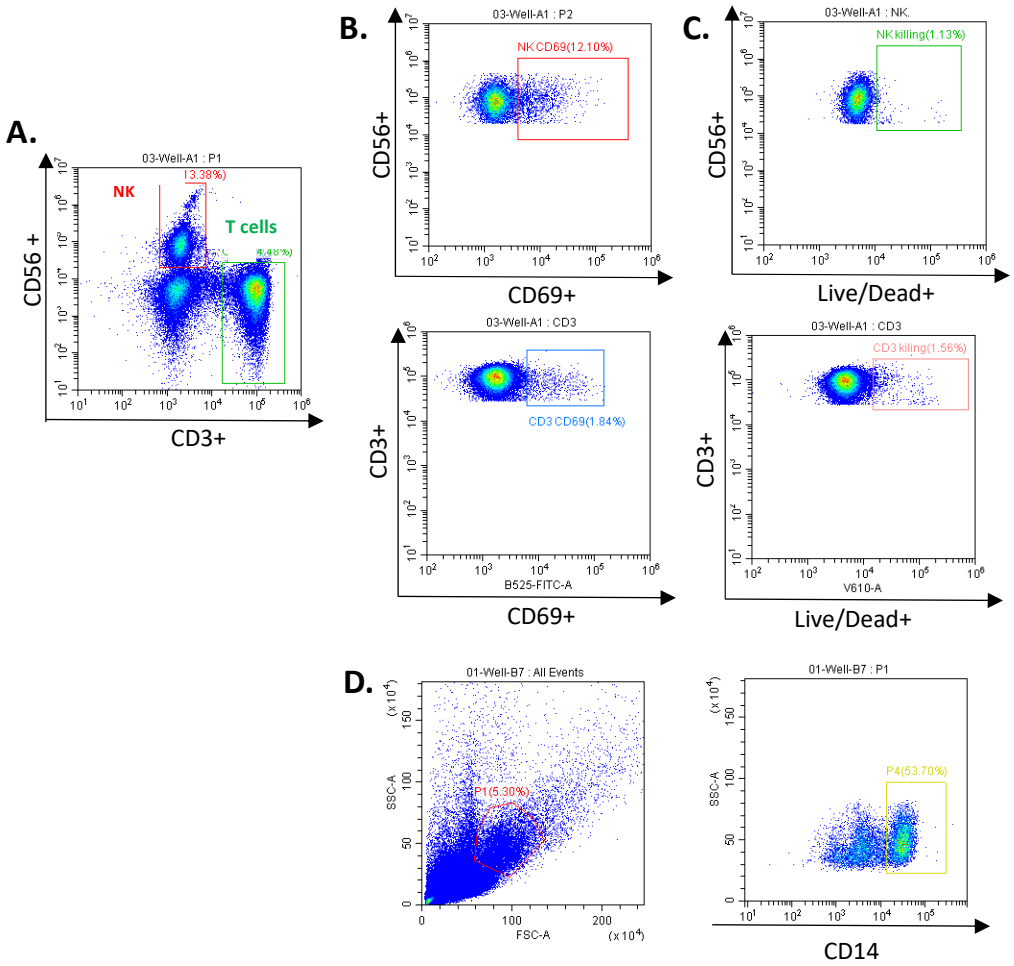

Figure 2-4 Gating strategy for T and NK cells, and monocyte from healthy PBMC donors.

PBMC isolated from the healthy PBMC donors, were treated for 24 hours with 100nM and or Reo MOI 1 for indicated time points and analyzed by flow cytometry. The figure is representative of one experiment showing the gating strategy used to identify **A.** Debris was excluded based on SSC versus FSC, **B.** T cells activation (CD3+ CD69+) and death percentage (CD3+ Live/dead+), **C.** NK cells activation (CD56+ CD69+) and death percentage (CD56+ Live/dead+). **D.** Monocytes were included based on SSC versus FSC, then gated as CD14+ monocyte.

2.10.6 Tumour associated- Macrophage (TAM) generation for phenotyping assay

TAMs were generated by coculturing GBM cells (MO59K, GBM20) with healthy donor-PBMC at effector to target cells (E:T ratio of 50:1) for 7 days in 50% DMEM/F12: 50% RPMI complete media. TAM cells were isolated using positive fraction of CD14 microbeads (cat.#130-050-201, Miltenyi Biotec, UK) according to the manufacture instruction (section 2.5). To confirm that TAMs has M2-like

phenotypic properties, cells were stained with antibodies against CD163, CD206, HLA-DR and CD86 as well as isotype controls for 30 minutes on ice in the dark. To examine Dex and OV effect on TAMs phenotype, treated TAMs only or treated cocultured GBM: TAM for 24 hours was stained with the same antibodies by flow cytometry. The gating strategy is depicted in Figure 2.5.

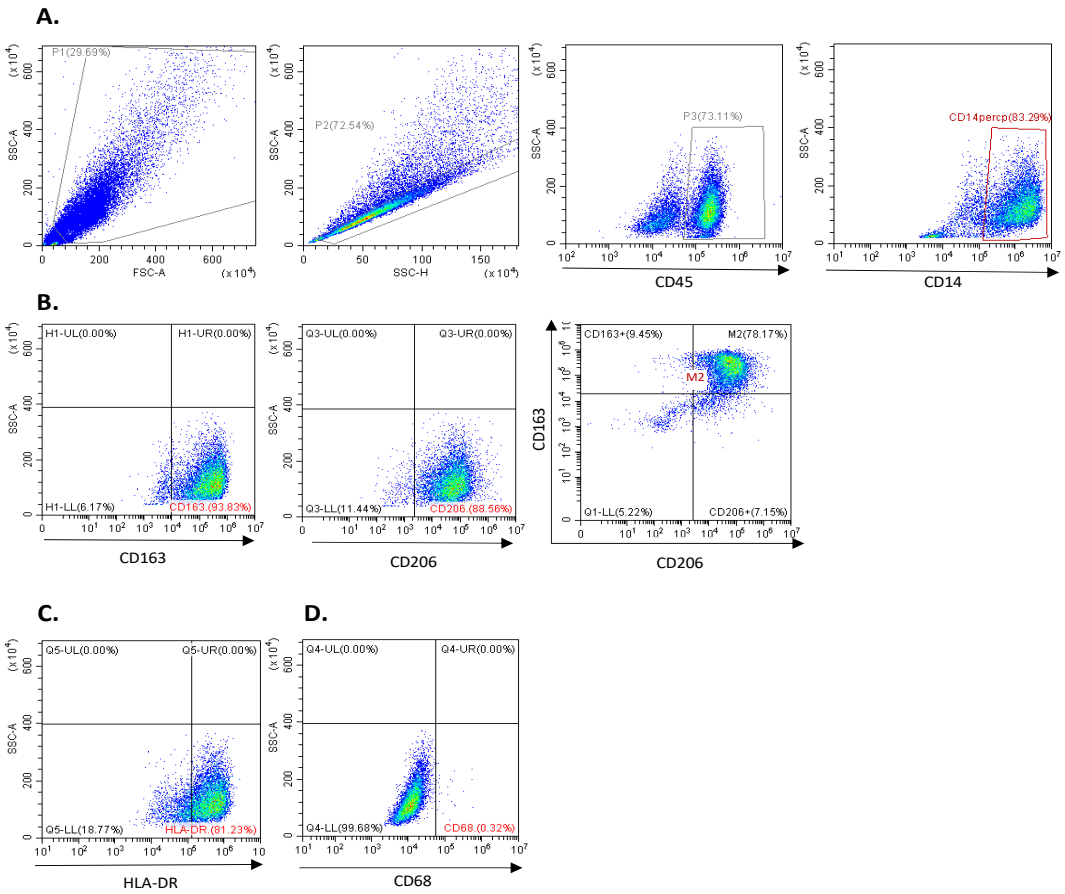

Figure 2-5 Gating strategy for TAM phenotype generated from GBM cells.

The figure is representative of one experiment showing the gating strategy used to identify TAMs isolated from coculture system by CD14 microbeads **A.** Debris was excluded based on SSC versus FSC. Doublets were excluded using a FSC-A and FSC-height (FSC-H). PBMCs were gated by using CD45+ cells followed by gating monocyte using CD14+ cells. **B.** CD163+ and CD206+ cells were used to identify the percentage M2 population. **C.** The percentage of HLA-DR+ and CD68+ of M2 population to show the shift between M2 and M1 phenotypes.

2.10.7 Reovirus σNS expression

Reo non-structural protein σNS expression was determined by flow cytometry after 24 hours of treatment. MO59K, GBM20, and GBM13 were seeded in 24 well plate ($5x10^4$). For intracellular staining, cells were fixed with 1% PFA, then re-suspend with primary Ab (2A9, cat.#2617402, DSHB) at 1:50 dilution in

permeabilization buffer for overnight, then washed in PBS-T buffer. Next, 2 drops/ml of 488 secondary anti-mouse antibody (cat.#R37120, Thermo Fisher Scientific) were added for 60 minutes, washed and resuspended in PBS. Unstained cells and secondary antibody alone were used as positive and negative control. Samples were analysed using flow cytometry and gated as FITC+ 2A9 positive cells (σNS). The gating strategy as represented in Figure 2.6.

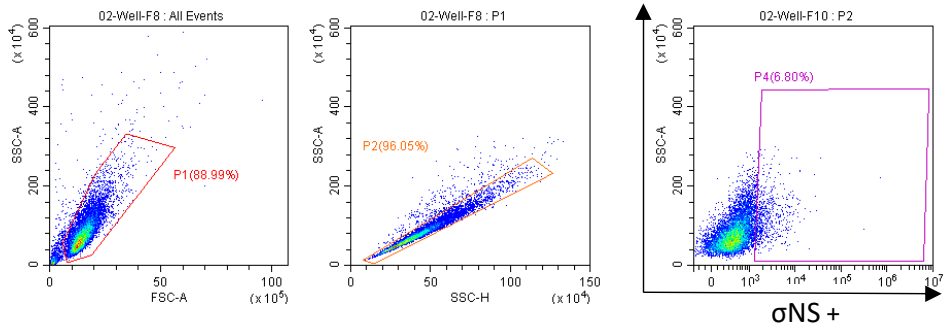

Figure 2-6 Gating strategy for reovirus σNS expression.

The figure shows gating GBM cell lines and debris were excluded based on SSC versus FSC (right). Debris was excluded based on SSC versus FSC. Doublets were excluded using a FSC-A and FSC-height (FSC-H). Cells with positive 2A9 expression were gated with FITC laser (left).

2.1 Enzyme linked immunosorbent assay (ELISA)

For cytokine production assays, supernatants were obtained 24 hours after treatment. Human-IL-6 and TNF-α were detected using corresponding antibodies (RD) according to the manufacturer's instructions. Briefly, 96-wells reaction plates (cat.#442404, Thermo Fisher Scientific) were coated with 100μl capture antibodies diluted in coating buffer for overnight in the fridge. Next, the plates were washed three times with PBS-T (29.4g PBS powder in 3L of dH_2O + 1500μl tween), then 200μl of block buffer (45ml PBS + 5ml FCS) was added per well and incubated for 2 hours, and washed three times with PBS-T. In triplicates, 100μl sample supernatants were added alongside with a serial dilution of corresponding cytokine standards, covered with foil and incubated overnight in the fridge. Next day, plates were washed six times with PBS-T, and a 100μl of diluted detection antibodies (IL-6, and TNF-α in block buffer) were added and incubated for additional 2 hours at the RT. Plates were washed six times with PBS-T, then 100μl of extravidin solution diluted in PBS-T was added and incubated for 90

minutes at the RT, and washed three times with PBS-T. Finally, 100μl of substrate solution (2 tablets + 40ml dH_2O + 2 tablets PNPP) was added in the plate, covered with foil, and incubated in the dark at RT for 5 minutes for IL-6 and 30-60 minutes for TNF-α. Absorbance at 405 nm was used for measurement using a microplate reader. IL-6 and TNF-α cytokines concentrations were determined using linear regression analysis on GraphPad Prism, using the standard curve. Table 2.4 details the list of the products used for the assay.

table 2-4 List of the products used for the ELISA assay

Antibody	Cat. number	Dilution	Company
IL-6 capture ab	14-7069-85	1:500 of stock in coating buffer	BD bioscience
IL-6 detection ab	14-7068-81	1:500 of stock in blocking buffer	BD bioscience
TNF-α capture ab	7117621	1:1000 of stock in coating buffer	BD bioscience
TNF-α detection ab	14-7349-81	1:1000 of stock in blocking buffer	BD bioscience
Extravidin solution	086M4786V	1:5000 of stock in PBS-T buffer	Sigma-Aldrich
PNPP tablets	34047	2 tablets in 40ml dH2O	Sigma-Aldrich

2.2 Luminex assay

Samples supernatants were obtained 24 hours after treatment, centrifuged and stored at -80°C until use. Luminex multiplex screening assay was designed by Biorad Laboratories Ltd. The kit included human Interleukin-6 (IL-6), interleukin -8 (IL-8), interleukin -1B (IL-1B), macrophage inflammatory protein-1 α, (MIP-1α, CCL3), macrophage inflammatory protein-1β (MIP-1β, CCL4), Interferon-α (IFN-α), interferon- y (IFN-γ), and Tumour necrosis factor-α (TNF-α) as they listed in Table 2.5. The assay was performed according to the manufacturer's recommendations, and was carried out by Miss. Caitllin Smalley from Dr. Orsi's lab at University of Leeds.

Table 2-5 List of cytokines tested by Luminex assay

Item	cat. number	Company
Bio-Plex Pro Human Cytokine IFN-γ Set	171B5019M	Bio-Rad Laboratories Ltd
Bio-Plex Pro Human Cytokine IL-1β Set	171B5001M	Bio-Rad Laboratories Ltd
Bio-Plex Pro Human Cytokine lL-6 Set	171B5006M	Bio-Rad Laboratories Ltd
Bio-Plex Pro Human Cytokine IFN-α2 Set	171B6010M	Bio-Rad Laboratories Ltd
Bio-Plex Pro Human Cytokine MIP-1α Set	171B5022M	Bio-Rad Laboratories Ltd
Bio-Plex Pro Human Cytokine MIP-1β Set	171B5023M	Bio-Rad Laboratories Ltd
Bio-Plex Pro Human Cytokine TNF-α Set	171B5026M	Bio-Rad Laboratories Ltd
Bio-Plex Pro Human Cytokine IL-8 Set	171B5008M	Bio-Rad Laboratories Ltd
Bio-Plex Pro Reagent Kit III with Flat Bottom Plate	171304090M	Bio-Rad Laboratories Ltd
Bio-Plex Pro Human Cytokine Screening Panel Standards	12007919	Bio-Rad Laboratories Ltd

2.11 Immunofluorescent imaging

Treated cells grown in a 12-well plates ($5x10^4$) containing 0.5μm glass coverslips for MO59K. GBM13 and GBM20 cells were grown in a coated coverslip (poly-L-ornithine and laminin). Wells washed with PBS, fixed with 4% PFA for 1 hours, then washed with PBS, and blocked in IF blocking buffer (50ml PBS, 50μl TritonX-100, 500μl FCS) for 4 hours at RT. The primary antibody was diluted in blocking buffer (2A9,1:200) and incubated overnight on a rocker at RT. Coverslips were then washed with PBS, and stained with secondary antibody in diluted in blocking buffer (Alexa488 anti-mouse,1:500; cat.#R37120, Thermo Fisher Scientific). For actin staining, Alexa conjugated phalloidin, was diluted in blocking buffer (cat. #A22287, Invitrogen, 1:200) for 2 hours in a rocker in the dark. Coverslips were washes with PBS, and Hoechst (cat. #B2261, Sigma) was added at 1:10,000 dilution with PBS for 10 minutes. Coverslips were finally washed three times for 5 minutes with PBS, and mounted with 2 drops of Vectamount (Vectashield) for each slide. Slides were stored at 4°C in the dark until imaging. For quantification, cells were imaged using EVOS upright fluorescent microscope at 10x magnification. Four fields were randomly captured for each condition using the GFP channel for the infected cells (2A9) and DAPI channel for the total cells (nuclei). The number of infected cells (2A9, green) was quantified for each

position and plotted as percent normalised by the total number of cells per field (nuclei, DAPI) cells.

2.12 Caspase-3/7 activation assay

Cells were plated ($5x10^4$ cells/ well) in a 24-well plate and treated with 100nM Dex, Reo (MOI 1) alone or in combination at different time points (24,48,72 hours). The caspase 3/7 (Staurosporine; STS; 1nM) and the pan-caspase inhibitor (Z-VAD-FMK; 50nM) were used as controls for the assay. Cells were incubated with 2 drops of CellEvent Caspase-3/7 Green Ready Probes (cat. #R37111; Thermo Fisher Scientific) at 37°C and 5% CO_2 for 1 hour. Cells were then imaged using EVOS upright fluorescent microscope at 10X magnification (Three positions per well) using the GFP and brightfield filters. The number of cleaved caspase-3/7 positive cells was quantified for each position and the average of three independent experiments were plotted in a dot plot.

2.13 Protein extraction and quantification

2.13.1 Protein extraction

Treated cells ($3x10^5$ cells/well) were washed with PBS and then lysed in RIPA buffer (50mM Tris-HCl pH 7.4, 1% NP40, 0.25% Sodium Deoxycholate, 150mM Sodium chloride, 1mM Ethylenediaminetetraacetic acid) containing protease (cat. #539134, Merck) and phosphatase inhibitors (cat. #P5726 and P0044, Sigma), centrifuged at 21700xg for 20 minutes at 4°C to remove insoluble cellular components. Lysates were then quantified by using the bicinchonic acid (BCA) kit (cat. #23227, Thermo Fisher Scientific). Briefly, 10μL of protein samples or 5μL of standard were added into 96 well plate and mixed with up to 200μL/well of BCA working reagent. The reaction was incubated for 30 minutes at 37°C, and lysates were quantified by using the plate reader at 540nm wavelength. Protein lysates were diluted with 5x loading dye and RIPA buffer to give a final concentration of 1μg/μl for all samples, and then boiled for 5 minutes on heat block at 95°C.

2.13.2 Western blot

Protein samples and protein ladder (cat. #1610374, Bio-Rad) were loaded into 4-15% pre-cast gels (cat. #4561098, Bio-Rad) and run initially at 120V for 1 hour in 1x of SDS page running buffer (cat. #1610772, Bio-Rad) in a BioRad system on ice. The gel was then transferred to 0.45μm nitrocellulose membranes (cat. #GE10600003, Merck) in a transfer system at 90V for 2 hours on ice. Membranes were blocked (1% skimmed milk powder, 4.39g sodium chloride, and 0.1% Tween-20), then immunoblotted in primary antibodies (listed in Table 2.6) diluted 1:1000 in blocking buffer for overnight in a rocker at 4°C. Next, membranes were washed three times (3g Tris Base, 7.5g Tris HCl, 3g skimmed milk powder, 1ml Tween 20 per 1L buffer) and incubated with HRP-conjugated secondary antibodies diluted 1:5000 in washing buffer for 1 hour. After three further washes, the immunoreactive bands were detected using SuperSignal West Femto (cat.#34095, Thermo Fisher Scientific). Signal intensity was quantified using ImageJ software and normalized to B-actin as housekeeping control. Table 2.6 lists the antibodies used in the experiment.

Table 2-6 List of antibodies used for western blot.

Target	Supplier	Cat number	Dilution	Band size
B-actin	Sigma-Aldrich	A5441	1:5,000	45
Glucocorticoid receptor (D8H2)	Cell signalling	3660T	1:1,000	90, 94
Phospho- GR (ser211)	Cell signalling	4161S	1:1,000	90, 94
Anti-rabbit HRPlinked	GE Healthcare	NA934	1:5,000	-
Anti-mouse HRPlinked	GE Healthcare	NA934	1:5,000	-

2.14 RT-PCR, and qRT-PCR

2.14.1 RNA extraction

Treated cells were lysed by using RNeasy mini kit (cat.#74104, QIAgen) according to the manufacturer's instructions. Briefly, media was removed from the cells, washed with PBS, and lysed with RLT buffer supplemented with 1% β-mercaptoethanol. Cell lysate were then transferred to QIAshredder (cat.#79654,

QIAgen). An equal amount of 70% ethanol was added and mixed, then transferred into RNeasy columns. Columns were centrifuged at 8000xg for 20 seconds, and supernatants were discarded. RW1 buffer was then added to the column and centrifuged at 8000xg for 20 seconds, and supernatant was discarded. RNase free DNase (cat. #79254, QIAgen) was added to the column, and left at RT for 15 minutes. RW1 buffer was added to each column, and centrifuged at 8000xg for 20 seconds, and supernatant was discarded. RPE buffer was added to each column, and centrifuged at 8000xg for 20 seconds, and supernatant was discarded. Columns were placed into new collection tubes, and centrifuged in full speed for 1 minute to dry the membrane. Columns were placed into a new Eppendorf tube, RNA was eluted using 30µl of RNase free water, and centrifuged in highest speed for 1 minute. The eluted RNA was quantified using a nanodrop spectrophotometer (Thermo Fisher), using RNase free water as a blank.

2.14.2 cDNA synthesis

Using 0.4µg to 1µg RNA per 20µl reaction, cDNA synthesis was performed with high-capacity RNA-to-cDNA kit (cat.#4387406, Applied Biosystems) according to the manufacturer's instructions. RT reaction mix was prepared in PCR tubes (2x RT buffer mix, 20x RT enzyme mix, nuclease free H_2O, and RNA samples), and centrifuged shortly to remove air pebbles. Samples were then incubated in a thermal cycler for 37°C for 1 hour, stopped by heating to 95°C for 5 minutes and held at 4°C. cDNA samples were diluted and stored at -20°C until use.

2.14.3 RT-PCR

RT-PCR reaction was executed using Taqman Fast Advanced Master Mix (cat. #4444557, Thermo Fisher Scientific) according to the manufacturer's instructions. A 13.5µl of reaction mix (10µl of 2x Taqman fast advanced master mix, and 1µl of 20x Taqman assays) (Table 2.7) were added to 96-well plate. A 1.5µl of cDNA samples were then added to each well for a total of 15µl reaction mix, and then centrifuged for 2 minutes at 400xg. RT-PCR reaction plates were run on a QuantStudio 5 Real-Time PCR System machine (Applied Biosystems). The PCR condition to detect gene expression includes: 2 minutes incubation at

50°C, 20 seconds at 95°C, 40 cycles of 1 second at 95°C, followed by 20 seconds at 60°C. 2-ΔΔCT method was used to quantify the relative gene expression of targeted gene with respect to B-Actin as housekeeping gene. Samples were then normalised to the vehicle control.

Table 2-7 List of PCR probes used for RT-PCR.

Target gene	Supplier	Cat number
IL-6	Thermo Fisher Scientific	Hs00174131_m1
TNFa	Thermo Fisher Scientific	Hs00174128_m1
IFN-B	Thermo Fisher Scientific	Hs01077958_s1
IFTIM3	Thermo Fisher Scientific	Hs03057129_s1
GILZ	Thermo Fisher Scientific	Hs00608272_m1
RIG-1	Thermo Fisher Scientific	Hs00223636_m1
B-ACTIN	Thermo Fisher Scientific	Hs01060665_g1
NFKBIA	Thermo Fisher Scientific	Hs00355671_g1
DUSP1	Thermo Fisher Scientific	Hs00610256_g1
FST	Thermo Fisher Scientific	Hs01121165_g1
ID1	Thermo Fisher Scientific	Hs00357821_g1
IFI6	Thermo Fisher Scientific	Hs00242571_m1
IFI16	Thermo Fisher Scientific	Hs00194261_m1

2.14.4 Quantification of Reo genomic copies by quantitative RT-qPCR

RNA was extracted from GBM cells treated for 8 and 24 hours, and cDNA synthesis was performed as described previously. RT-qPCR was performed using SYBR Green PCR Master Mix (cat. #6625270; Quantabio) and primers specific to the Reo σ3 gene primers and 18S rRNA primers were served as cellular RNA controls. Standards dilutions were prepared between 10^{-2} to 10^{-9}, and 10^{-6}, 10^{-7}, 10^{-8}, 10^{-9} were used as a negative control. Briefly, 3µl sample or standard were transferred into 348 well plate. Master mix (5µl SYBR green, 4µl RNase free water, 0.15 primer mix) was added to the plate. RT-qPCR reaction plates were run on a QuantStudio 7-Flex PCR System machine (Applied Biosystems). The PCR conditions were 50°C for 30 minutes (for reverse transcription); 95°C for 15 minutes; and 25 (or 35) cycles of 95°C for 30 seconds, 62°C for 45 seconds, and 72°C for 45 seconds followed by 72°C for 7 minutes. The copy numbers fold increase was calculated using 2-ΔΔCT method of σ3 gene

with respect to 18S as housekeeping gene. The samples were then normalised to the vehicle control. Table 2.8 shows the primers used in the experiment.

Table 2-8 List of genes of interest for RT-qPCR

Gene	Sequence	Product size (BP)
18S	F: GACTCAACACGGAAACCTC R: TAACCAGACAAATCGCTCCAC	124
REO σ3	F: GATGGTGATACTGTGGTTCCTGT R: AATCCTTTGAGTCCGTCGTCT	291

2.15 Novogene RNA sequencing

For single culture experiment, MO59K cells were treated with Veh, Reo MOI 1 alone or in combination with 100nM Dex. 24 hours later, cells were lysed for RNA extraction. For coculture experiment, MO59K cells (Veh or pre-treated with Dex for 24 hours) and PBMCs (Veh, Dex, or ReoDex treated for 24 hours) were cocultured at 10:1 ratio for 24 hours. All samples were prepared in triplicates. The concentration and the purity of the extracted RNA from MO59K cells from the direct single culture (section 2.2) and isolated from coculture model (section 2.3.1) using the negative fraction CD14 microbeads were tested by nanodrop, with OD260/280 and OD260/230, ranged between 1.8 - 2.3. All samples were sent to Novogene company on a dry ice for sequencing. Samples were evaluated for quality control (QC) prior sequencing by the company, and samples with RNA integrity number (RIN) score above 9 based on the QC test and ready for sequencing.

Figure 2.7 shows the summary of the cDNA library construction workflow, and the purified messenger RNA (mRNA) from total RNA using poly-T oligo attached magnetic beads. Following fragmentation, the cDNA strand was synthesized using dTTP for non-directional library preparation. After the end repair, the library underwent A-tailing, adapter ligation, size selection, amplification, and purification. Next, qubit and real-time PCR were used to check the library. Bioanalyzer was used to detect the size distribution. The libraries were then pooled and sequenced using the Illumina platform based on the library concentration and data amount. Figure 2.7 shows the workflow summary and

cDNA library construction and the RNA-seq project workflow. Raw reads on fastq format were cleaned by removing reads containing adaptor, poly-N and low-quality reads. The paired-end clean reads were mapped to the reference genome using Hisat2 software. FeatureCounts was used to count the reads mapped to each gene, and the fragments Per Kilobase of transcript per Million mapped reads (FPKM) for each gene was calculated according to the gene length and read count mapped for each gene. The differential expression analysis was performed using the DESeq2 R package. P-value was adjusted using the Benjamini & Hochberg method (Robinson *et al*., 2010). Adjusted P-value < 0.05 was set as the threshold for significantly differentially expressed genes.

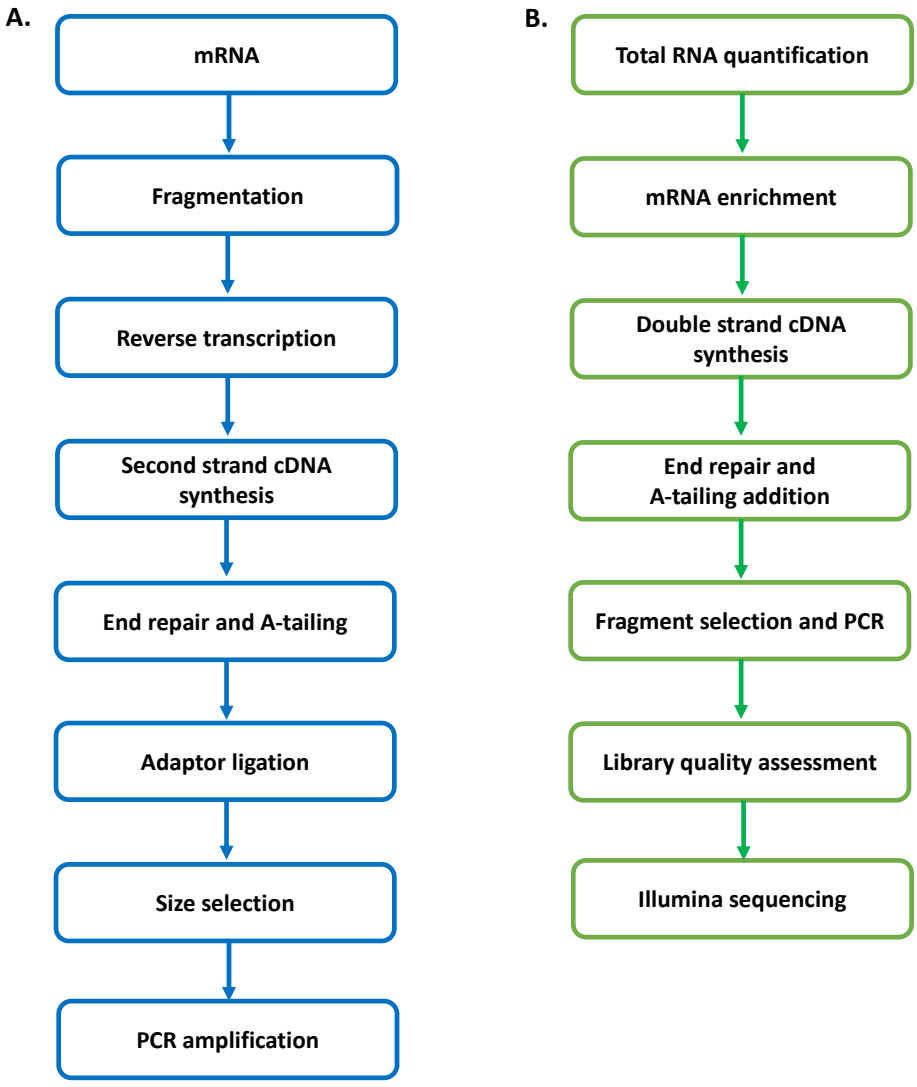

Figure 2-7. Novogene RNA sequencing.

A. shows the workflow of cDNA library construction. **B.** shows the summary of the RNA-seq project workflow.

2.16 Secondary transcriptome data analysis

2.16.1 Data mining

RNA-sequencing or microarray datasets were compiled. Search engines were used, inputting the terms “RNA-sequencing”, “microarray”, “glioblastoma”, “reovirus”, “HSV”, “oncolytic virus”, “glucocorticoids”, and “dexamethasone”. A total of five databases were publicly available for analysis as listed in Table 2.9.

Table 2-9 List of databases for secondary transcriptome analysis

Reference	Sample	Treatment	Technique	Data source
Dr.McGinnis	MO59K cells	Dex(100nM) for 4 hours	RNA Sequencing	Unpublished lab group data
Samson *et al.,* 2018	GBM patients	Reovirus, single, i.v. Surgery was undertaken 3 to 17 days after reovirus infusion	RNA Sequencing	Supplementary
Reyes *et al., 2019*	Human CD4 T cells & Monocyte	Dex (100nM) or IFN-a (250U/ml) for 24 hours	RNA Sequencing	Supplementary
Goujon *et al., 2013*	U87-MG	IFN-a (500U/ml) for 24 hours	Microarray	GSE46599
Berkeley *et al., 2018*	Human Monocyte	Reovirus vs. Ab vs. Reovirus-Nab 24 hours	RNA Sequencing	Requested from author

2.16.2 Data processing

For the secondary transcriptome analysis in chapter 3, the datasets were re-analyzed and filtered by log2FC < -0.5 or > 0.5 and p. value <0.05, while the transcriptome datasets of immune cells were filtered by log2FC < -0.5 or >0.5 and adjusted p-value <0.1. For the RNA-seq samples prepared in the lab by Dr. McGinnis, were filtered by Log2Fold Change of ≥1 or ≤ -1 and p.adj of ≤ 0.05. The usage of different cut-off criteria for different datasets is for the purpose of comparing datasets with differences in experiments conditions such as comparing a cell line to patient’s tissue samples. In addition, the purpose of the secondary transcriptome analysis was for exploratory studies to detect any overlaying genes which were more critical than stringent statistical significance. The selected overlaying genes were validated by biological methos such as RT-PCR.

2.16.3 Data overlays

A Venn diagram online tool (https://bioinformatics.psb.ugent.be/webtools/Venn/) was used to compare multiple datasets. The overlapping genes lists were then exported in excel sheet. The Venn diagram was redrawn in PowerPoint.

2.16.4 Pathways enrichment and TF analysis

For chapter 3, the DEG list were uploaded to Enrichr tool (https://maayanlab.cloud/Enrichr/, Chen *et al.,* 2013) to predict pathways involved by theses DEGs. The adjusted p-value <0.05 was used to determine significance. Lists of the candidate genes symbols were input into the Enrichr webpage and pathways and transcriptions taps were used. The significance of each pathway was then exported as an Excel file and visualized as histograms using GraphPad. Clustergram figures of the pathways were also exported to visualize the gene list for the top identified terms. In chapter 5, the KEGG pathway of the coculture data were re-drawn as a bubble plot by using SRplot website tool (http://www.bioinformatics.com.cn/srplot; Tang *et al.,* 2023) with a cutoff of adj.p-value <0.05.

2.16.5 Pathway visualization using Cytoscape

Pathways network group of the DEGs were visualized by using the ClueGO/CluePedia based enrichment. Gene symbols were input into the software with FDR 0.05 as a cut-off criterion and grouped based shared genes (kappa score >0.3) and shown with different colors.

2.16.6 Protein-protein interaction (PPI) analysis using STRING

STRING database (v11) was used to visualize protein-protein interaction networks and determine associations, or important nodes among genes in a given dataset (Szklarczyk *et al.,* 2023). The analysis tab was used to select specific ontologies such as Reactome, gene ontology (GO) and the node was re-colored based on the selected terms.

2.16.7 Gene ontology analysis

In chapter 3, the biological process of GO enrichment analysis was generated using SRplot online tool and selected terms were graphed using chord plot to show the relationship between GO terms and genes.

2.16.8 Human GBM analysis using gepia2

Gepia2 website tool (http://gepia2.cancer-pku.cn/#index) was used to compare genes of interest level in comparison to normal brain tissue and graphed as boxplot using the database based The Cancer Genome Atlas (TCGA). Kaplan-Meier survival analysis for GBM patients was also obtained from Gepia2 tool. The OS of genes of interest stratified into high and low gene expression and comparison between the 2 groups using log-rank test with hazard ratio (HR) and 95% confidence interval (CI) displayed. A p.value < 0.05 and HR> 1.5 was considered statistically significant.

2.16.9 Transcription factor (TF) analysis using cistrome

Cistrome online database was used to visualise gene tracks from chromatin immunoprecipitation (ChIP)-seq analysis of GR/NR3C1. GR (NR3C1) was searched under Homo sapiens selection. Individual samples were checked for pass of quality control, and selected if there were more 5000 peaks, and the percentage of reads uniquely mapped was above 60%. The peak profile was also visualised. Dataset for A549 (64333) and MCF-7 (74155) visualised using the UCSC gene browser, alongside histone ChIP-seq from the ENCODE genome project.

2.17 Statistical tests

All statistical analysis were performed using GraphPad prism. For grouped datasets with multiple variables, a two-way ANOVA test was used with Tukey's *post hoc* analysis for multiple analysis. All data were presented with error bars indicate standard error of the mean (± SEM). All experiments were performed in triplicates unless otherwise stated. For experiments with n=2 and non-normally distributed (Shapiro-wilk tested), a nonparametric one-way ANOVA (Friedman

test) with multiple comparison (Dunn's) was used. The significance level used were ns $p>0.05$, *$p\leq0.05$, **$p\leq0.01$, and ***$p\leq0.001$.

Chapter 3

Pathways regulated by GCs and OV in human GBM and immune cells

3.1 Introduction

GCs are widely used as anti-inflammatory drugs to reduce brain inflammation in GBM patients. However, little is known on their mode of action and how they might alter responses to immunotherapy, with OV. Computational methods and transcriptome analysis allow characterization of the influence of GCs on OV treatment in GBM. A previous PhD student undertook RNA-seq of Dex treated MO59K cells (a human GBM cell line), identified pathways regulated by Dex. These included genes related to anti-inflammation, DNA repair, and stemness; SOX4, KLF4-6, NR2F2, FOXO1, SNAI2, HOXC11-13, SOX9, MAF, CEBPD, CEBPB, GLIS1, RUNX2. Here this dataset will be re-analyzed to compare it with OV regulated gene datasets in GBM patients and immune cells to identify potential points of crosstalk and divergent pathways. I use web resources to predict significant pathways, transcription factors and genes regulated by GCs and OV in an attempt to determine their functions.

The aims of this chapter are:

1. Identify OV regulated gene sets in GBM and compare them with Dex regulated gene sets to identify potential points of crosstalk
2. Identify OV regulated gene sets in immune cells and compare them with Dex regulated gene sets to identify potential points of crosstalk
3. Validate candidate genes using different techniques including RT-PCR, Luminex assay, and flow cytometry.

3.2 Results

3.2.1 Analysis of GBM cells

3.2.1.1 Genes regulated by GC

The McGinnis dataset of MO59K cells treated with Dex (100nM) for 4 hours was re-analysed. This identified 266 differentially expressed genes (DEGs) with threshold cut-off >1.5 fold change and < 0.05 FDR. A volcano plot was created to visualize these DEGs showing 74.4% upregulated genes and 25.6% downregulated genes (Figure 3.1.A and B). The DEGs were then inputs into Enrichr platform to enable Gene Set Enrichment Analysis (GSEA). The top ranked terms in the Elsevier pathway were cortisol (the naturally occurring glucocorticoid) and the NF-κB signalling pathway. Genes within this ontology included IL-1B, CXCL8, and NFKBIA, all known to be regulated by Dex. The NCI-Nature database highlighted two major GC target pathways, IL-6 and the AP-1 transcription factor network, which are evidenced by regulation of IL-6 and the AP-1 component JUN (Figure 3.1.C). Cytoscape was used to visualise the genes network and identify potential crosstalk between the networks. For the Wikipathway, the Nuclear Receptor (NR) meta-pathway links to neural crest differentiation, STAT3 signalling, IL-18 and TGF-β pathways with GC target genes KLF5, CEBPB, CEBPD and TWIST1, while transcription misregulation in cancer (RUNX2, FOXO1 and CEBPB) in the KEGG pathway links to FOXO1, Wnt and NF-κB signalling (Figure 3.1.D).

A

Cell type	Treatment	Platform	Total DE genes	Genes Increased (%)	Genes Decreased (%)	Reference
MO59K GBM	100nM Dex	RNA-Seq	266	198 (74.43%)	68 (25.65%)	Not published

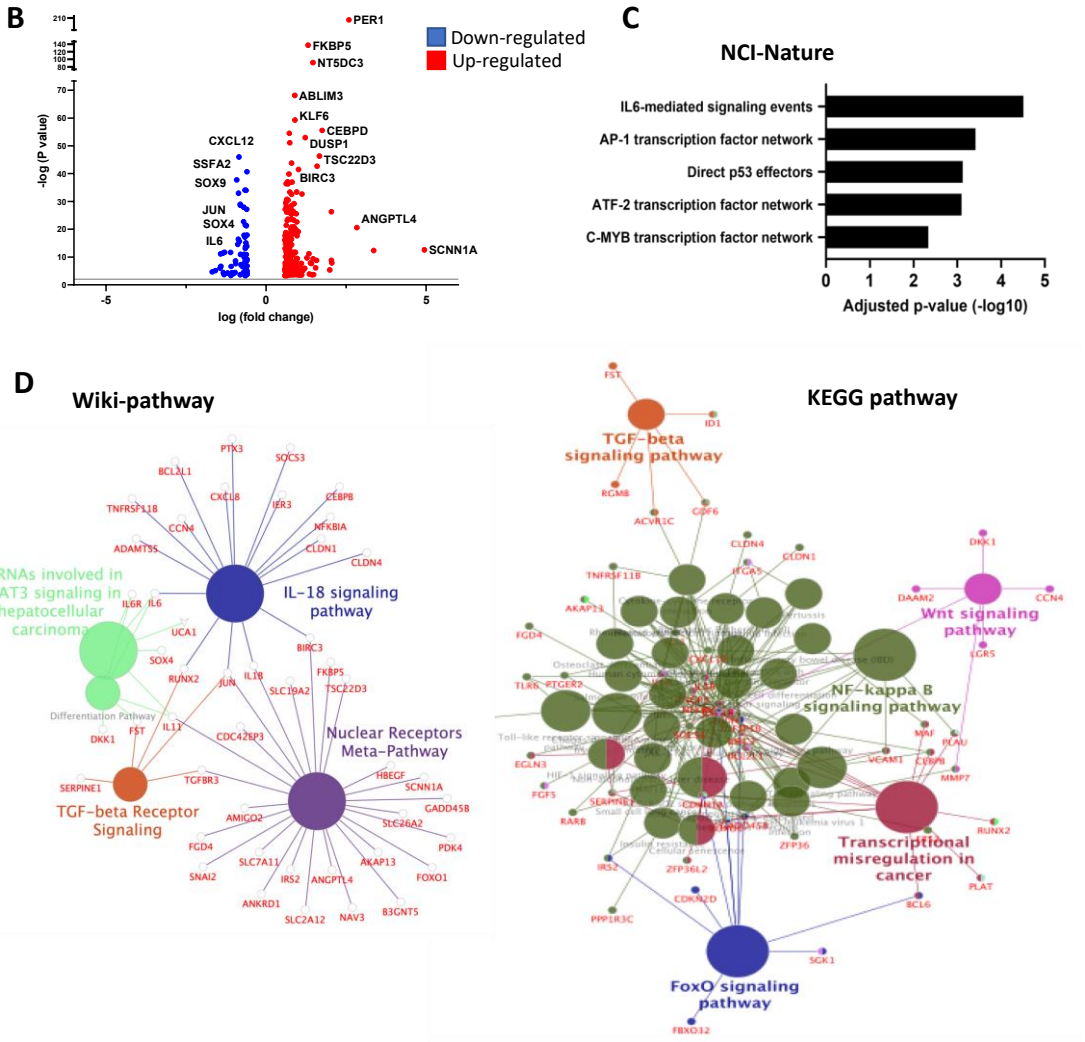

Figure 3-1 Genes regulated by Dex in GBM are enriched in Cortisol, IL-6, AP-1, and NF-κB signalling.

A. The table represents GBM cell line treated with Dex, identifying 266 DEGs (74.4% up-regulated; 25.6% down-regulated). **B.** Volcano plot of the DEGs, up-and downregulated genes are marked as blue and red dots, respectively. The x-axis shows adj. p-value (log10) and the y-axis the log-FC. Vertical grey line represents log2-FC in expression. **C, D.** Pathways enrichment analysis by NCI-Nature displayed in a bar graph and analysis was performed on "Enrichr" tool. KEGG and Wiki-pathway identifies nuclear receptor meta-analysis, TGFB, FoxO, and Wnt signalling pathways (P <0.05) by Cytoscape-ClueGo/CluePedia.

In addition to looking at downstream effects using the pathways tool, upstream predictions were also made by using the transcription factor tool in Enrichr. Comparison of the GC regulated genes with Encode ChIP-seq libraries identified NR3C1, the gene symbol for the GR as the best correlated transcription factor (Figure 3.2.A, left). Interestingly two other NRs (NR4A3 and NR4A2) were predicted to regulate 58 of the genes (Fig 3.2.A, right). The 58 DEGs predicted to be regulated by GR, NR4A2 and NR4A3 were therefore compared **(**Figure 3.2.B). There was a greater overlap between GR and NR4A2, and 19 genes were commonly regulated by all three transcription factors. These 19 genes are shown in a string network, and identifies CDKN1A as overlapping between GBM and response to GCs (Figure 3.2.C).

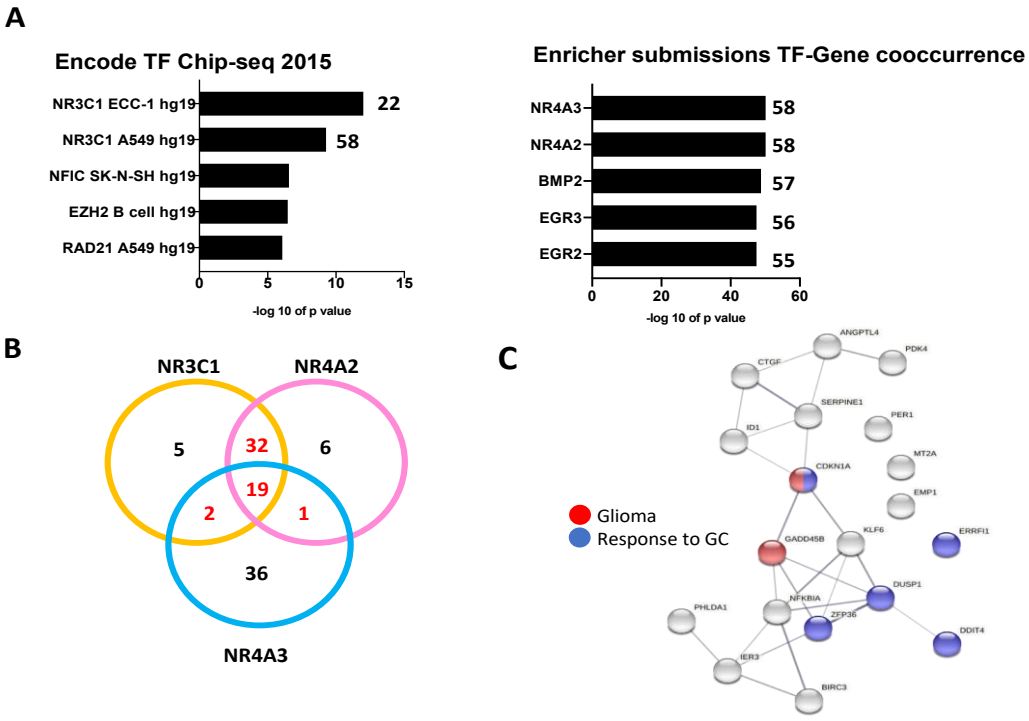

Figure 3-2 Genes specifying TF identifies nuclear receptors.

A. List of the top TFs in Enrichr submissions TF-Gene cooccurrence and Encode TF Chip-seq 2015. Values next bars indicate number of regulate genes. **B.** Venn diagram shows the overpulling between the nuclear receptors. **C.** STRING interaction network of all 19 overlaying genes. Analysis from biological process and KEGG shows response to GC and glioma (CDKN1A), respectively.

3.2.1.2 Genes regulated by OV

I then performed a similar analysis to define OV regulated genes in GBM. We identified a dataset of RNA-seq for the small clinical trial performed by Samson *et al.*, of GBM patients treated with single dose of Reovirus (iv) comparing to control GBM tumours. Surgery was performed between day three and seventeen post infection and the tumour tissues were collected for RNA seq (Samson *et al.*, 2018). The dataset was re-analysed and filtered by different cut-off methods, and we decided to use log2 FC of 0.5 and p.value of < 0.05 for analysis. 939 DEGs were identified with 77.7% upregulated genes, and 22.3% downregulated genes (Figure 3.3.A, B). NCI-Nature database highlights HIF-1/2 alpha (eg. EDN1, JUN, SERPINE1, AKT1), Integrins in angiogenesis (COL1A1, AKT1, VEGFA) and AP-1 (EGR1, IL-6, DUSP1, BCL2L11) (Figure 3.3.C). Cytospace was used to visualize KEGG gene network and identified pathways in cancer, TGF-β signaling, viral protein interaction with cytokines and cytokines receptor, transcription misregulation in cancer, and IL-17 signaling (Figure 3.3.D).

A

Cell type	Treatment	Platform	Total DE genes	Genes Increased (%)	Genes Decreased (%)	Reference
GBM tissue	REO	RNA-Seq	939	730 (77.7%)	209 (22.3%)	Samson 2018

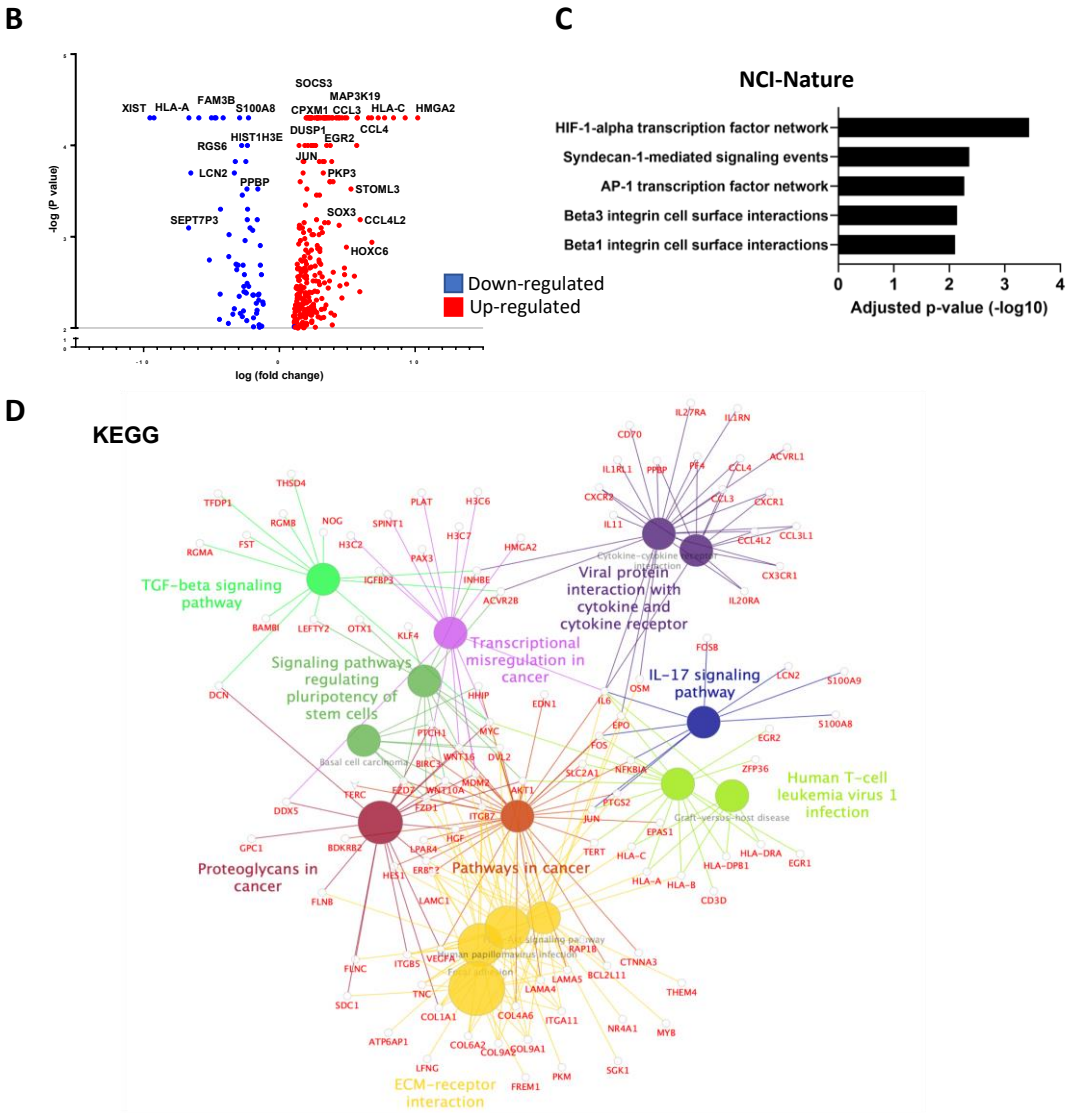

Figure 3-3 Genes regulated by OV in GBM patients are enriched in HIF-1, AP-1, WNT signalling, and viral protein interaction with cytokines.

A. Table represents GBM patients treated with Reo has identified 939 DEGs (77.7% up-regulated; 22.3% down-regulated). **B.** Volcano plot of the DEGs, up-and downregulated genes are marked as blue and red dots, respectively. The x-axis shows log2-FC in expression and the y-axis the -logFC of a gene being differentially expressed. Vertical grey line represents 2-logFC in expression. **C.** NCI-Nature pathway displayed in a bar graph, analysis performed on the "Enrichr" platform. D. KEGG pathway network view proteins and their related signalling pathways identified viral protein interaction with cytokines and transcriptional mis-regulation in cancer was performed by Cytoscape-ClueGo with P <0.05.

3.2.1.3 Potential crosstalk pathways between genes regulated by GC and OV

A Venn-diagram was produced to show the overlap between the DEGs in GC treated GBM (unpublished data) and OV treated GBM (Figure 3.4.A) and 27 DEGs were overlapping with 62.9% upregulated genes in both datasets, and 37.1% differentially expressed (RGMB, SOX4, FST, IL-6, CLDN1, IL-11, JUN, CYP24A1, S1PR3, BIRC3) (Figure 3.4.B), and Table 7.1. Both S1PR3 and BIRC3 were upregulated under GC regulation and downregulated under OV regulation, whereas IL-6 and IL-11 were downregulated under GC regulation and upregulated under OV regulation. In addition, HOXC11 was 5 times higher under OV regulation compared to GC regulation in GBM. The 27 overlapping genes were then input into the Enrichr platform. This highlighted the top ranked pathways in TNF, IL-6, AP-1, TGF-β and GR regulatory network. Genes involved in these ontologies includes NFKBIA; SOCS3; JUN; IL-6; BIRC3; CEBPD; DUSP1; TGFBR3; FST; SERPINE; and SGK1 (Figure 3.4.C). The Reactome network in cytoscape identified TNF and IL-6 signalling (Figure 3.4.D). Finally, upstream predictions of TFs analysed in Enrichr submissions (the TFGene cooccurrence library) identified NR4A3, NR4A2, EGR1, and EGR2 and was predicted to regulate 19, 18, 17 and 17 genes respectively out of the 27 DEGs (Figure 3.4.E).

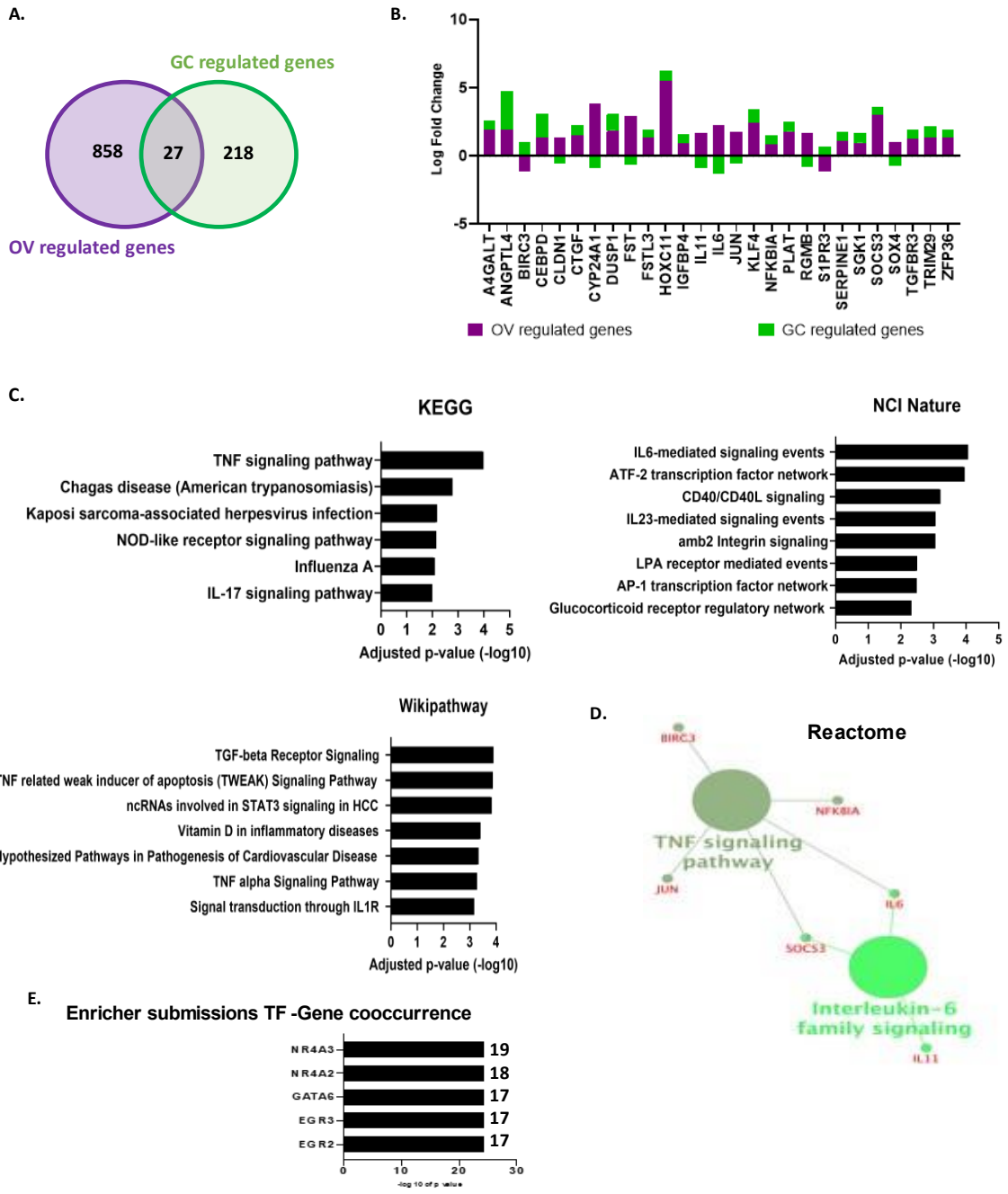

Figure 3-4 Overlaying genes under OV and GC regulation are enriched in IL-6, TGF-β, and TNF signalling and NR enriched TFs.

A. The Venn diagram identified 27 overlaying genes between OV-treated GBM patients and GC-treated GBM cells RNAseq datasets. **B.** Bar plot of log2-FC between the OV and GC overlaying genes. **C.** Pathways enrichment analysis displayed the top enriched terms in a bar graph, and the analysis was performed on the "Enrichr" platform. **D.** Network view for Reactome was performed by Cytoscape-ClueGo/CluePedia ($P < 0.05$). **E.** Genes specifying TF identified NR as the top TFs in Enrichr submissions TF-Gene cooccurrence and Encode TF Chip-seq 2015.

3.2.1.4 Potential crosstalk pathways between genes regulated by OV and interferons in GBM

Type 1 interferons (IFN-I) are antiviral cytokines induced during virus infection. These aid virus elimination but are also important in anti-tumour immune responses. Due to the lack of publicly available OV datasets, we analyzed an IFN-α dataset in a GBM cell line (Goujon *et al.*, 2013) and compared it to OV treated GBM patients. A total of 53 DEGs overlapped between OV and IFN regulation. 33.9% were differentially expressed, 5.6% similarly downregulated (AKT1, LCN15, C12orf56), and 60.3% similarly upregulated (Figure 3.5.A, B), and Table 7.2. The Elsevier database identified MHC-1, and genes within mutation in cancer immune escape as the top enriched terms (Figure 3.5.C). The Cytoscape of Reactome network were visualized and identified cytokine signalling and immune response (eg. IFI6, HLA-A/B/C, AKT1, CCL3). (Figure 3.5.D).

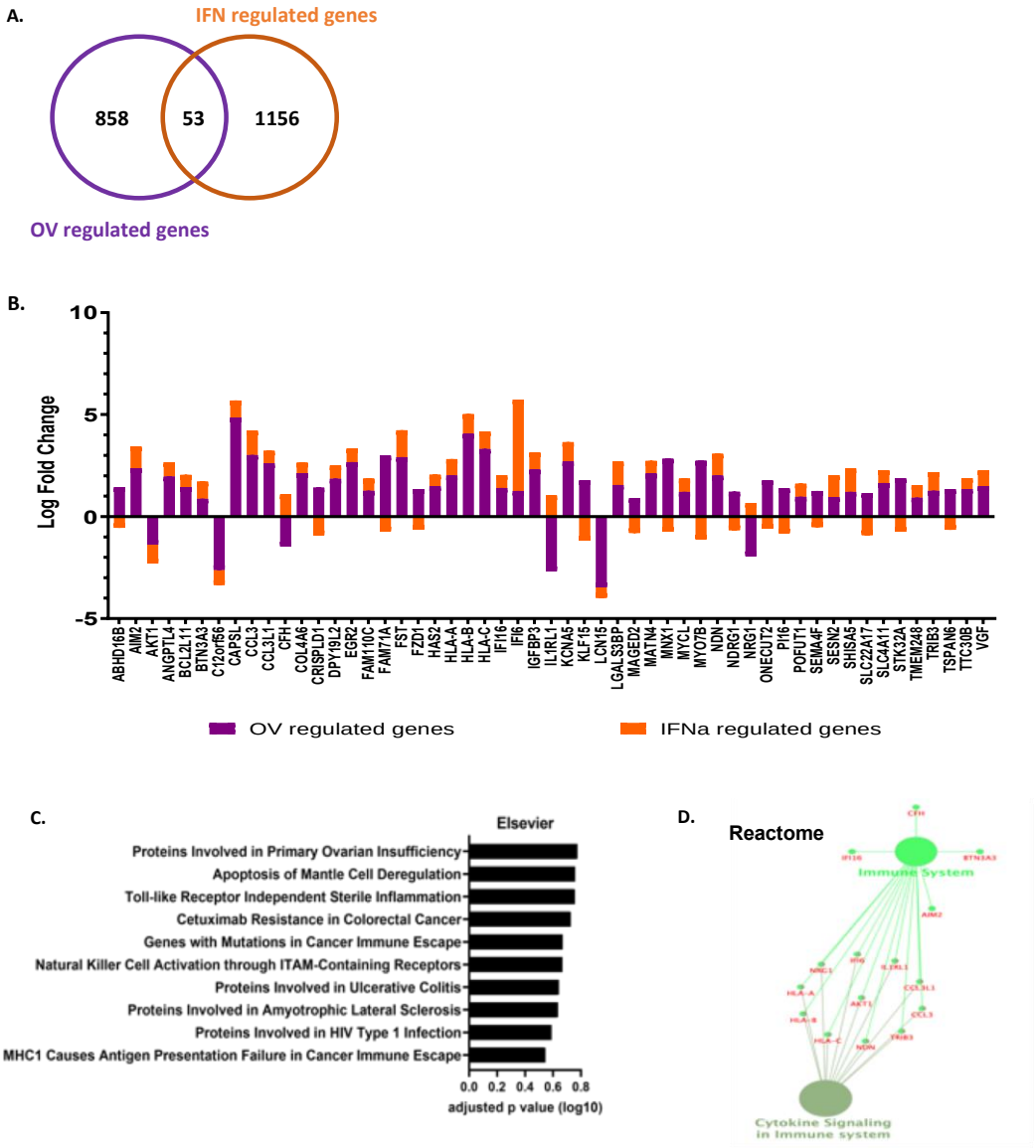

Figure 3-5 Overlaying genes under OV and IFN regulation are enriched in antigen presentation, immune system, and cytokines signalling.

A. Venn diagram identified common genes between OV-treated GBM patients and IFN-treated GBM cells datasets. **B.** Bar-plot of log2-FC between the common OV and IFN regulated genes. **C.** Pathways enrichment analysis displayed the top enriched terms in a bar graph, and the analysis was performed on the “Enrichr” platform. D. Network view for Reactome performed by Cytoscape-ClueGo/CluePedia (P <0.05).

3.2.2 CD4 T cells

3.2.2.1 Genes regulated by GC in human CD4+ T cells

To identify GC regulated genes in CD4+ T cells, RNA-seq data generated by Reyes *et al.*, 2019 were reanalysed. CD4+ T cells treated with 100nM Dex for 24 hours were re-analysed using a cutoff method of log FC > 1, and p-value < 0.05 (Figure 3.6.A). 948 DEGs were identified, 66.24% upregulated genes and 33.75% downregulated genes (Figure 3.6.B). Notably, CCL2, which is expressed in monocytes and activated T cells, was downregulated by GC. Pathway analysis based Reactome database was enriched in the terms, immune system and MHC-I presentation, while Wikipathway database identified T-cell receptor (TCR) signalling (MAP4K1, CD83, NFTC1, CD3E, CD3D, MAP3K8) and mRNA involved in immune response (IL-10; TRAF6; IRF1; CCL4; CCL3; REL; IRAK4) (Figure 3.6.C).

A

Cell type	Treatment	Platform	Total DE genes	Genes Increased (%)	Genes Decreased (%)	Reference
Human CD4 T cells	100nM Dex 24 hrs	RNA-Seq	948	628 (66.24%)	320 (33.75%)	Reyes et al., 2019

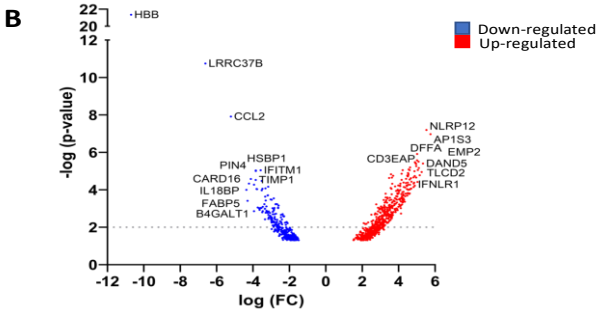

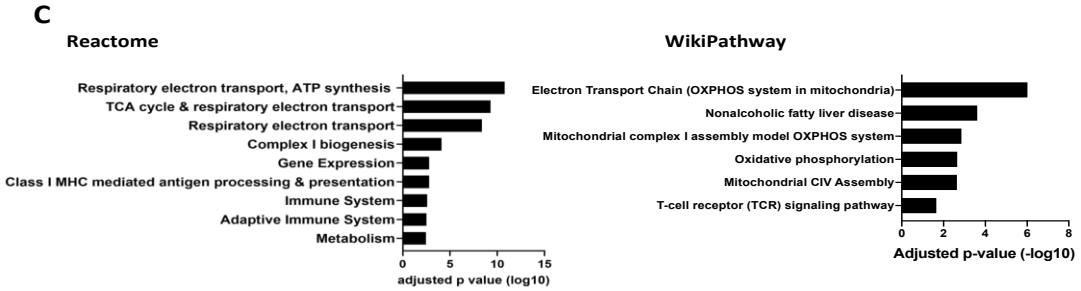

Figure 3-6 Dex regulated genes in human CD4 T-cells are enriched in antigen presentation and immune system signalling.

A. The table represents primary human CD4 T cell treated with Dex for 24 hours. **B.** A Volcano plot of the DEG. The up-and downregulated genes are marked as blue and red dots, respectively. The x-axis shows log2FC in expression and the y-axis the –log (p-value) of a gene being differentially expressed. Vertical grey line represents 2-FC in expression. **C.** Reactome and Wikipathway analysis displaying in a bar graph.

3.2.2.2 Potential crosstalk pathways between genes regulated by GC and OV

Additionally, a comparison between GC treated CD4+ T cells and OV treated GBM patient datasets identified 27 overlapping genes, 55.5 % were differentially expressed, and mostly upregulated by OV and downregulated by GC (Figure 3.7.A, B) and Table 7.3. Wikipathway analysis showed significance enrichment in chemokines expressed during T cell polarization (CCL3, CCL4).

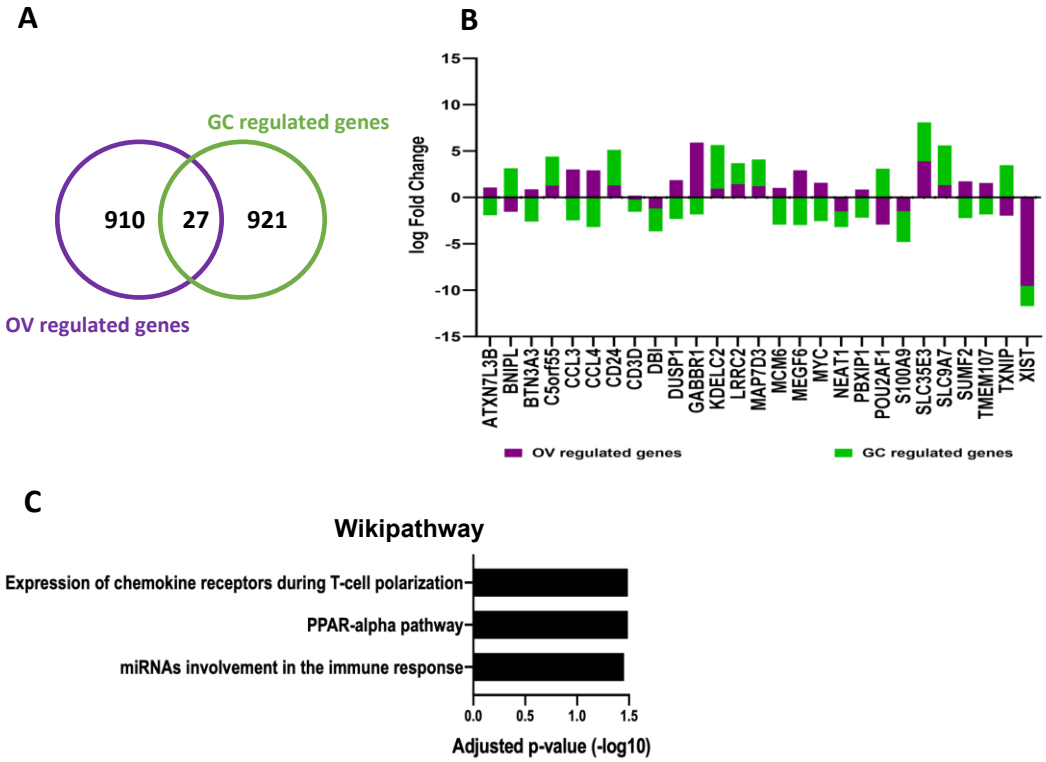

Figure 3-7 Overlaying genes under OV and GC regulation in CD4 T-cells are enriched in chemokines receptor during T cell polarization.

A. A Venn diagram identified overlapped genes between GC-treated GBM cells and IFN-treated GBM cells. **B.** Bar-plot of log2-FC between the common OV and IFN regulated genes. **C.** Wikipathway analysis displayed in a bar graph, and analysis performed on the "Enrichr" platform.

3.2.3 Monocytes

3.2.3.1 Genes regulated by GC and OV in human Monocyte

To identify GC regulated genes in human monocytes, RNA-seq datasets generated by Reyes *et al*, 2019 were reanalysed, where monocytes were treated with 100nM Dex for 24 hours (Figure 3.8.A). We used a cut-off of Log2FC 1 and p-val 0.05, and 790 DEGs were identified and 33.8% were up-regulated while 66.2% were down-regulated (Figure 3.8.B). Notably, the top expressed genes are CD163, which is an M2-like Macrophage marker, and GR target genes (TSC22D3, FKBP5). The DEGs were input in Enrichr platform for pathways analysis, and the top enriched pathway terms-based NCI- Nature included Notch signalling, AP-1, and BCR signalling. Genes within these ontologies include ERG2, CTNNB1, CCL2, IL-10 and MAF. While Wikipathway database was enriched in term TYROBP network in microglia (eg. CD84; RBM47; GPX1; PLEK; SAMSN1; MAF; ADAP2; RGS1; SH2B3), cholesterol metabolism (eg. ABCA1; CYP27A1; EBP; HMGCS1; ACSL1; CYP51A1; ACSL3; HSD17B7), Macrophage markers (CD163; CD83; CD14), and GR Pathway (PRRG4; FGD4; RGS2; HSP90AA1; TSC22D3; ALOX5AP; TNFAIP3; CCL2; NR3C1; BIRC2) were also identified (Figure 3.8.C).

A

Cell type	Treatment	Platform	Total DE genes	Genes Increased (%)	Genes Decreased (%)	Reference
Human Monocyte	100nM Dex 24 hrs	RNA-Seq	790	267 (33.8%)	523 (66.2%)	Reyes et al., 2019

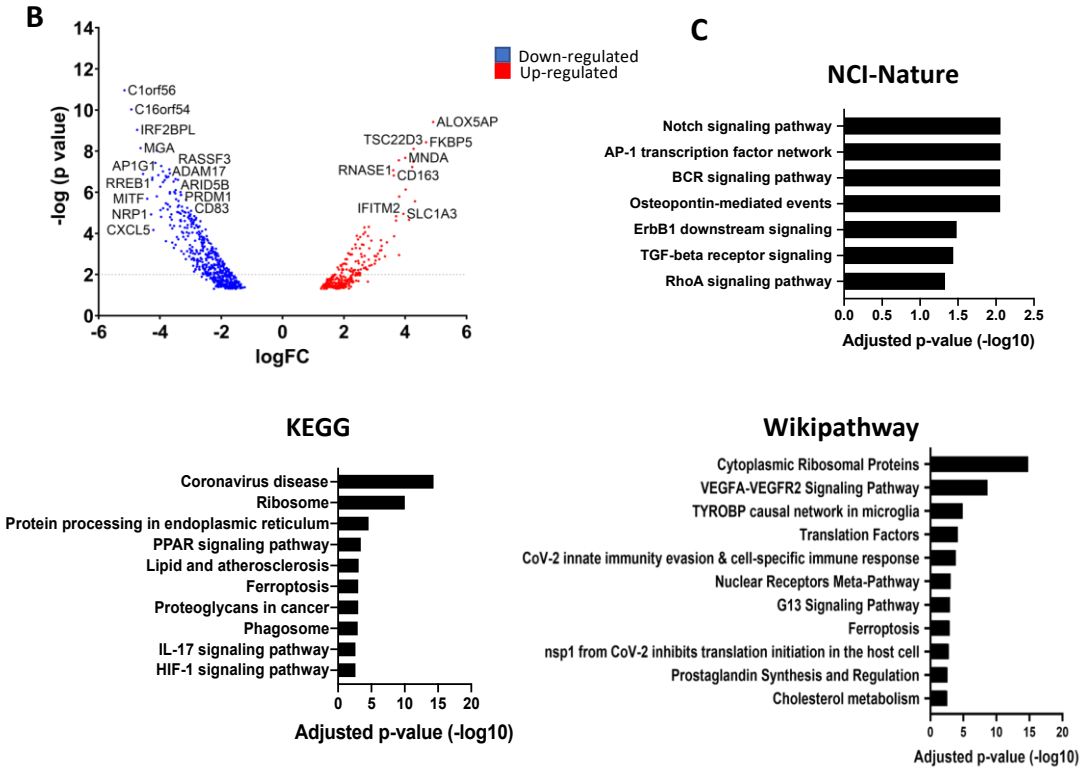

Figure 3-8 Dex regulated genes in human monocyte cells are enriched in AP-1, BCR signalling, and NR meta pathway.

A. Table represents primary human CD4 T cell treated with GCs. **B.** Volcano plot of the DEGs, up-and downregulated genes are marked as blue and red dots, respectively. The x-axis shows log2-FC in expression and the y-axis the -logFC of a gene being differentially expressed. Vertical grey line represents 2-FC in expression. **C.** Pathway enrichment analysis for the GC-treated CD4 displaying the top enriched terms in a bar graph.

Furthermore, monocytes treated with Reo for 24 hours by Berkeley *et al*., 2018 was reanalysed and cut off method used is Log2FC>1.5, <0.01 FDR was used (Figure 3.9.A). There were 3345 DEGs in Monocyte, 52.9% were upregulated and 47.1% downregulated (Figure 3.9.B). Pathway analysis of the DEGs showed enrichment in immune system and interferons (Reactome), Cytosolic DNA-sensing, TLR signalling, and apoptosis (WikiPathway), p53 and p38 MAPK signalling (NCI-Nature), RIG-1 like receptor, and TNF-α signalling (KEGG). Genes within these ontologies include IFNA1; IFNA2; IFI6; IFIT3; SOCS1; EGR1; STAT1; HLA-A; ISG15; ISG20; IRF1; IRF7, and CCL4 (Figure 3.9.C).

A

Cell type	Treatment	Platform	Total DE genes	Genes Increased (%)	Genes Decreased (%)	Reference
Human Monocyte	Reovirus vs. Ab vs. Reo-NAb	RNA-Seq	3345	1769 (52.9%)	1576 (47.1%)	Berkeley et al., 2018

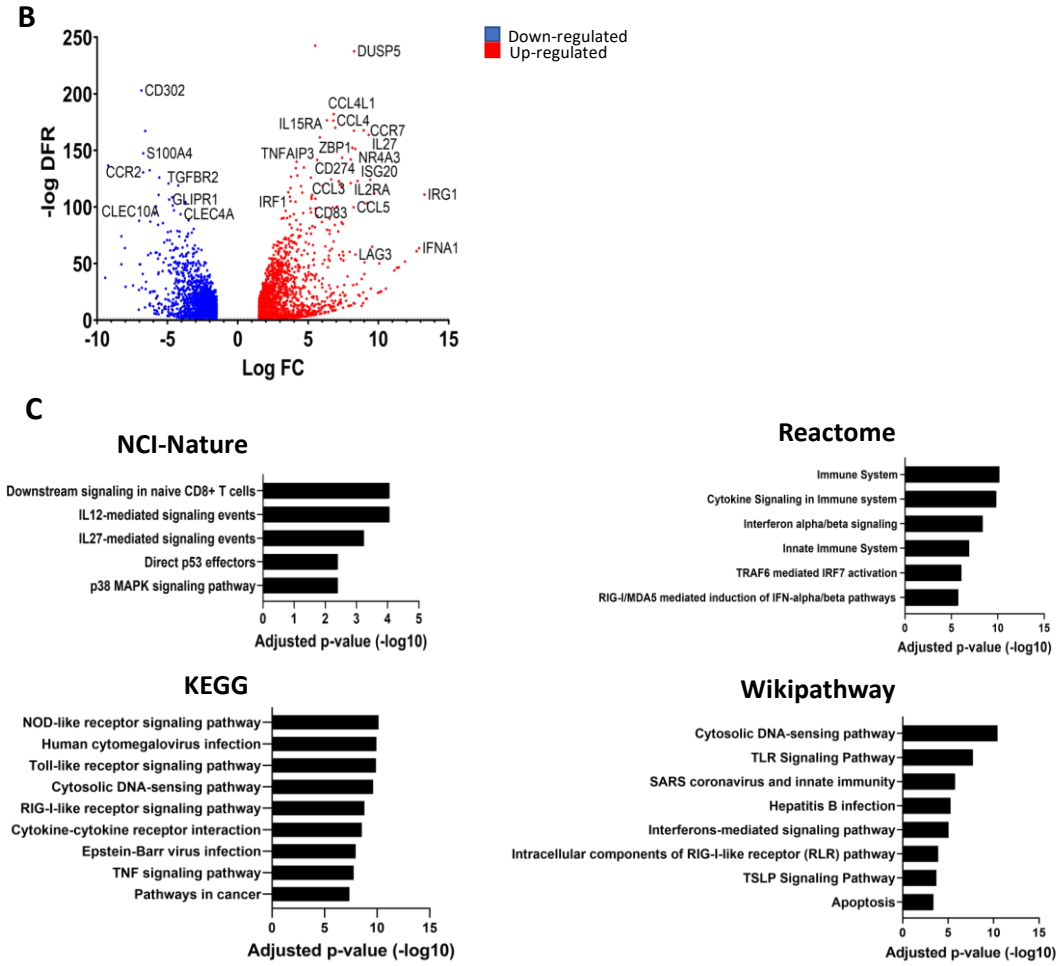

Figure 3-9 Reo regulated genes in human monocytes are enriched in RPR receptors, immune system, Interferon, and cytokines.

A. A table represents primary human CD4 T cell treated with OV for 24 hours. **B.** Volcano plot of the DEGs, up-and downregulated genes are marked as blue and red dots, respectively. The x-axis shows log2-FC in expression and the y-axis the -logFDR of a gene being differentially expressed. Vertical grey line represents 2-FC in expression. **C.** Pathway enrichment analysis for the OV-treated monocyte displaying the top enriched terms in a bar graph.

3.2.3.2 Potential crosstalk between genes regulated by GC and OV in human Monocyte.

The next step is to identify the common genes between the GC and OV datasets in monocytes (Reyes *et al*., 2019 versus Berkeley *et al*., 2018) and compare it with Samson *et al*., 2018 dataset. Interestingly, there were 12 overlaying genes between the three datasets (Figure 3.10.A). Four genes were similarly expressed (CCL3L1, HLA-A, HLA-B, HLA-C) while the rest were differentially expressed (EGR1, FOS, LGMN, PCMTD2, POGLUT1, RGS18, S100A8, and SERPINE1). LGMN and POGLUT1 were down-regulated by GC and up-regulated by OV while RGS18 and S100A8 were upregulated by GC and downregulated by OV (Figure 3.10.B). Pathway analysis identified antigen presentation (HLA-A, HLA-B, HLA-C, LGMN) and TGF-β receptor signalling (SERPINE1, FOS) as the top enriched terms (Figure 3.10.C). Also, see tables 7.4, 7.5 and 7.6.

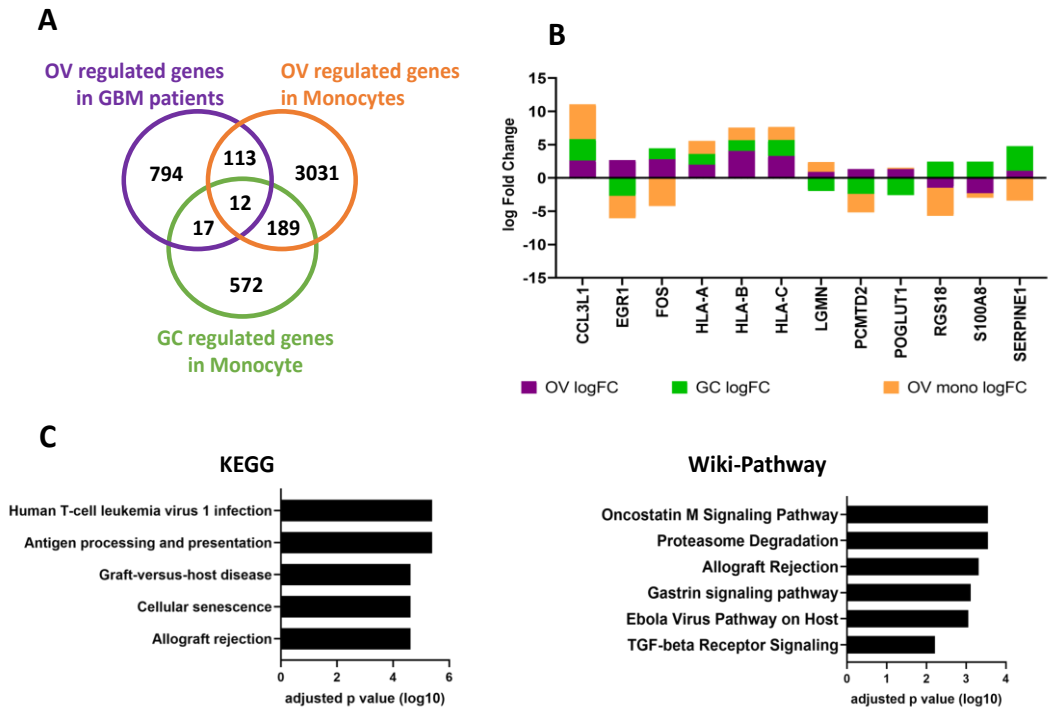

Figure 3-10 overlaying genes between OV and GC in Monocyte and OV regulation in GBM patients are enriched in antigen presentation, and TGF-B signalling.

A. Venn diagram identified overlaying genes between GC-treated monocytes, OV-treated monocyte, and OV-treated GBM patients. **B.** Bar-plot of log2-FC of the 12 common genes between the three datasets. **C.** Pathway enrichment analysis of the 12 overlaying genes displayed in bar graph, and analysis performed on the "Enrichr" platform

OV regulation in monocytes from healthy donor PBMC were then compared with GBM patients and found 125 overlaying genes (Figure 3.11). Pathways analysis identified AP-1, HIF-1 and GR regulatory network by NCI-Nature. Genes within these ontologies included ERG1, EDN1, IL-6, MYC, FOS, HLA-A, SERPINE1, VEGFA; and MDM2. KEGG pathway identified TLR, cytosolic-DNA sensor and viral protein interaction in cytokines, and genes included CXCR1, CCL3L1, CCL4CL2, CCL3, CCL4, NFKBIA, AIM2).

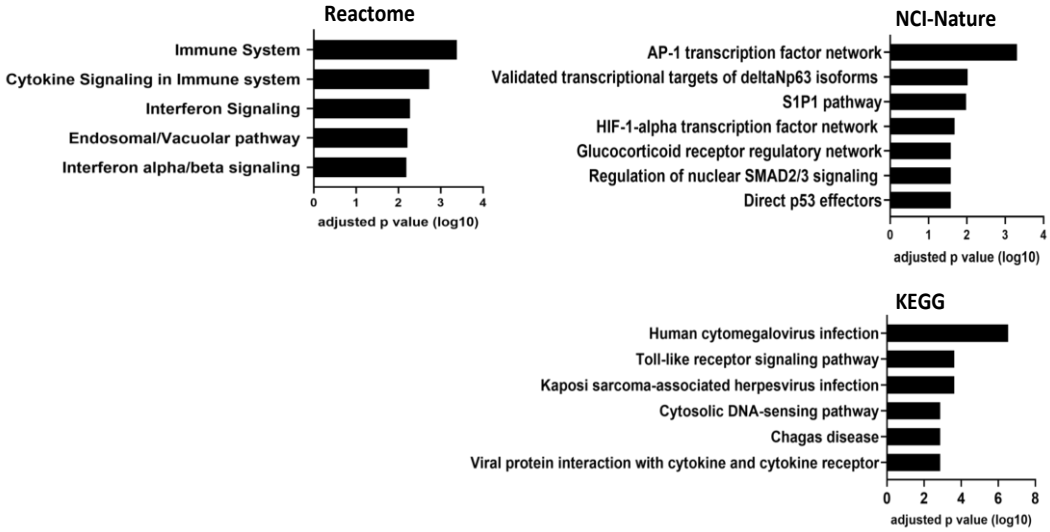

Figure 3-11 Overlaying genes between OV-treated Monocyte and OV-treated GBM patients are enriched in AP-1 TF, GR, immune system, interferons, and cytokines pathways.

Enriched pathways displayed in bar graph, and analysis performed on the “Enrichr” platform.

29 overlaying genes were observed between monocytes treated with GCs and GBM patient treated with Reo. Pathways analysis identified AP-1, S1P1, HIF1, GR, and effector p53 by NCI database. KEGG identified TLR, DNA-sensing and viral interaction with cytokines and Reactome immune system and interferons (Figure 3.12). LGMN, and EGR1/2 were downregulated by GC and upregulated by Reo, while SERPINE were similarly upregulated.

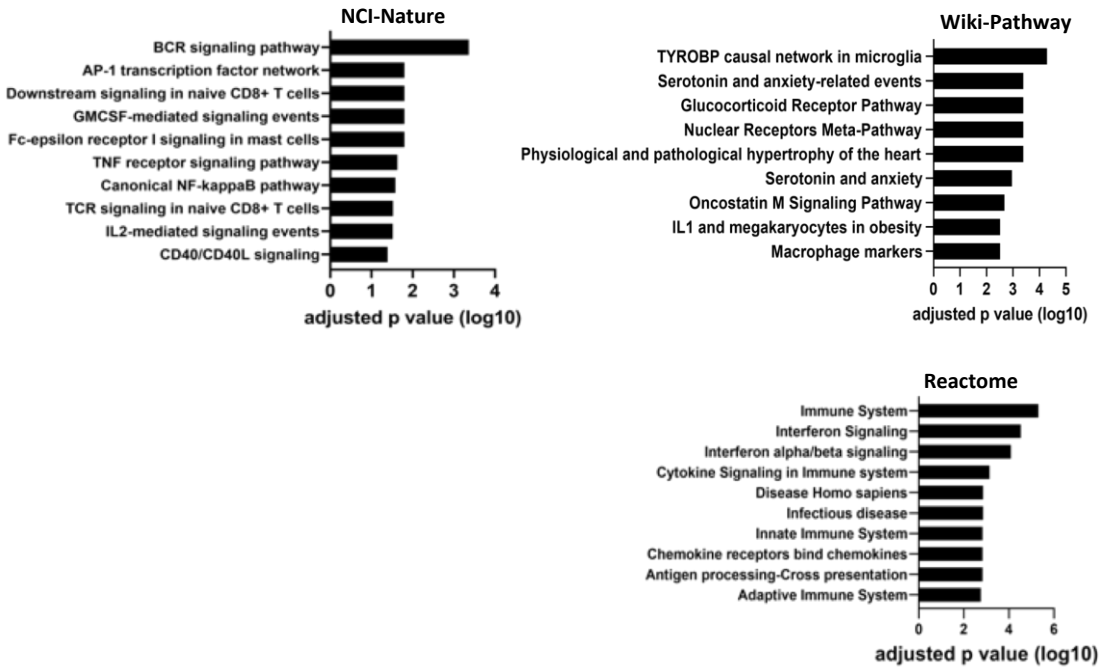

Figure 3-12 Overlaying genes regulated by OV and GC in Monocyte identified macrophage markers, BCR, immune system, interferons, APC, GR pathways.

Enriched pathways displayed in bar graph, and analysis performed on the "Enrichr" platform

3.2.4 Validation

3.2.4.1 Identifying crosstalk between GC and Reovirus in GBM cells and immune cells population

To confirm the results seen in the transcriptome data analysis, validation of selected candidate genes (Table 3.1) regulated by GCs, Reo or both treatments were investigated. These genes were identified in pathways related NF-kB, AP-1, interferons, and the immune system.

Table 3-1 List of the candidate genes regulated by GCs and/or Reo in the transcriptome datasets (log2FC)

Gene name	Related pathway	GBM patients treated Reo	GBM cells treated GCs	CD4 cells treated GCs	Monocyte treated GCs	Monocyte treated Reo
DUSP1	Inflammation	1.8729	1.2217	-2.3047	-	1.0731
NFKBIA	NF-kB	0.8397	0.6622	-	-	2.2511
IFI16	Interferons	1.4026	-	-	-	-
IFI6	Interferons	1.2561	-	-	-	3.2219
FST	Activin	2.9175	-0.0659	-	-	2.5516
ID1	TGF-β	-	0.6989	-	-	-1.5796
CD274	PD-L1	0.9703	-0.7447	-	-	5.6376
IL-6	Anti-inflammatory	2.2213	-1.2967	-	-	8.124
IL-1B	Anti-inflammatory	-	-1.3114	-	-	0.8137
IL-8	Inflammation	-	-1.3463	-	-1.2332	1.7545
CCL3	Inflammation	3.0180	-	-2.4629		5.2856
CCL4	Inflammation	2.9353	-	-3.1954	-	6.8064

Firstly, RT-PCR was completed in MO59K cells and healthy donor PBMC treated with Reo or HSV-1 in the presence or absence of Dex for 24 hours. RNA was extracted and RT-PCR was performed on the selected target genes, normalized to Beta-Actin (ACT-B) expression and displayed in a bar graph as a relative gene expression. The results showed a significant increase in DUSP1 expression by Dex (*p=02) and Reo (*p=0.01). The expression was significantly higher in combined treatment than single treatment in both MO59K cells and PBMC (Fig 3-13.A, B). NFKBIA expression was not significantly increased in MO59K but was significant in PBMC. In MO59K cells, FST expression was not significantly downregulated by Dex but significantly upregulated by Reo. However, the increase in FST expression was shown by Dex treated PBMC, but not by Reo. ID1 expression did not change among the treatment groups in MO59K but had minimal increases in Dex treated PBMC. Both IFI16 and IF16 expression were upregulated by Reo in MO59K, and Dex downregulated these gene expressions when combined with Reo in MO59K cells only. Overall, these results show that several genes identified in the bioinformatics analysis are indeed regulated by both Dex and Reo.

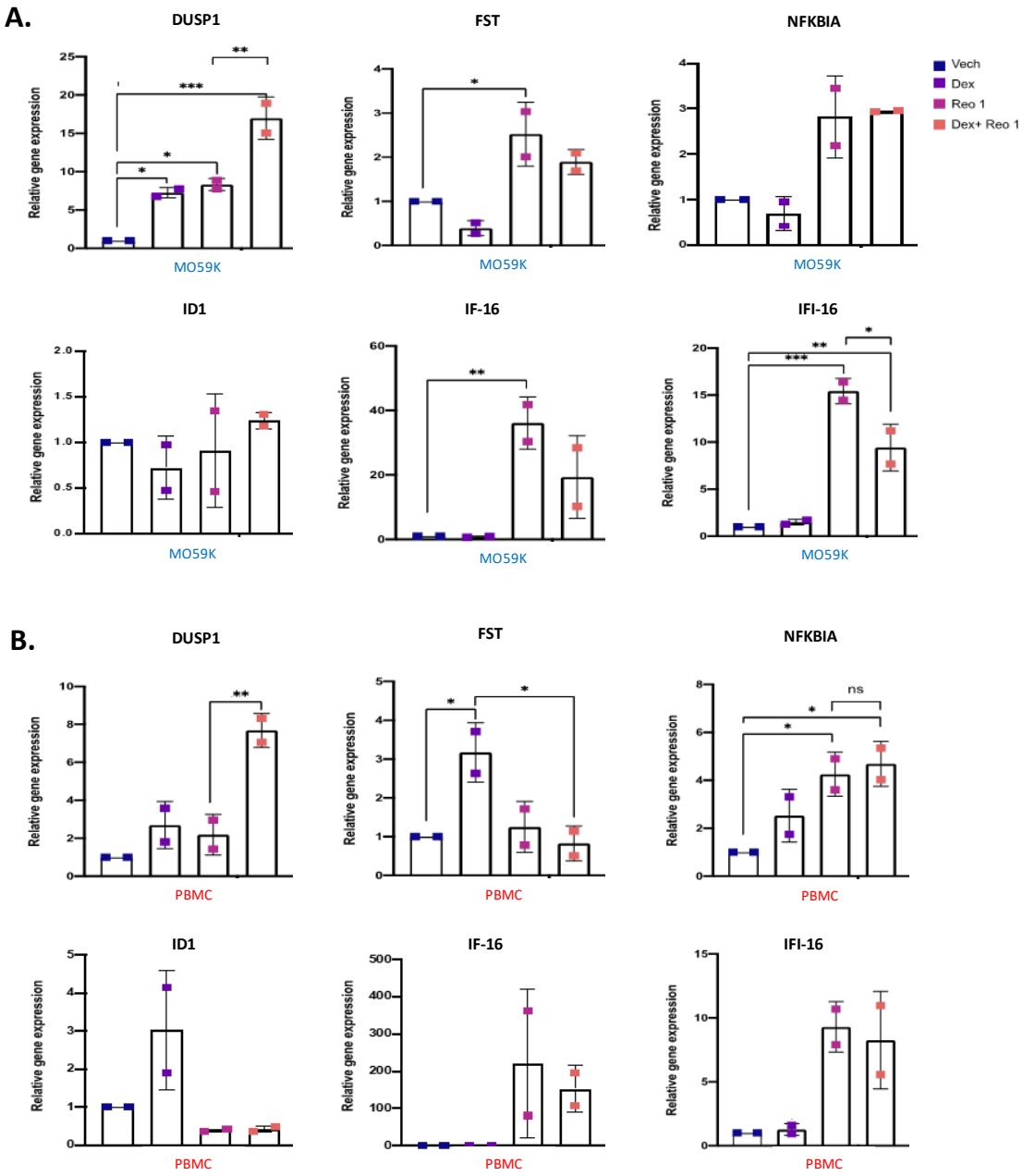

Figure 3-13 Candidate differentially expressed genes regulated by GC and OV in GBM cells and PBMC.

A. MO59K cells and **B.** PBMC from healthy donors were treated with Veh, Dex, OV (Reo or HSV-1), or combination for 24 hours. RNA was extracted from the samples for RT-PCR to validate the expression of the genes of interest. Graphs show the mean ± SEM for n=2 independent experiments, each in triplicates, and significance was tested with nonparametric one-way ANOVA with Dunn's multiple comparison test, where *= p≤0.05, **= p≤0.01, and ***= p≤0.001.

Next, Luminex assays were performed on supernatants collected from MO59K cells and PBMCs treated for 24 hours to evaluate secretion of selected pro-inflammatory cytokines and chemokines (IL-6, IL-8, IL-1B, and TNF, CCL3, CCL4). Results were plotted in a line graph (Figure 3.14.A and B). Results show that Reo significantly induced the production of IL-6 in GBM cells and PBMCs, and Dex reduces Reo-mediated IL-6 production in both GBM cells (significant) and PBMCs (non-significant). Elevated IL-8 level was detected in reovirus group while Dex alone or combined with Reo has lower level. Both CCL3 and CCL4 have similar trends to IL-8 in GBM cells. In the context of PBMC, IL-8 was significantly upregulated by Reo and combining it with Dex lead to reduce the level of IL-8. Although CCL3 was not detectable in samples, CCL4 showed significant increase level. Unexpectedly, combining Dex with Reo showed a higher IL-8 level than Reo alone. Unfortunately, IL-1B levels were almost non-detected. These results were consistent with what we observed on the transcriptome analysis.

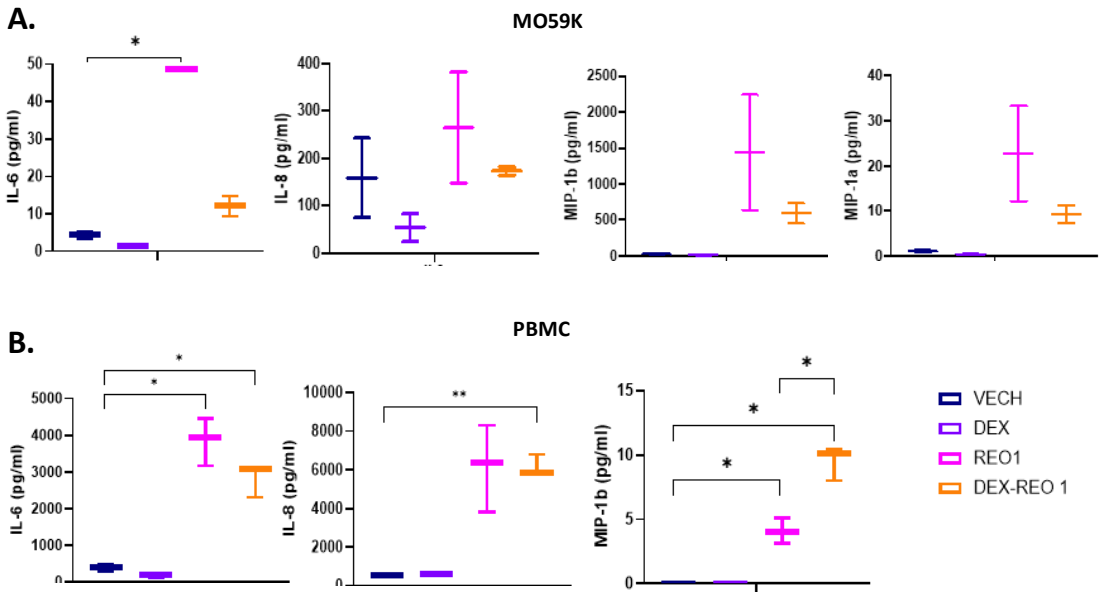

Figure 3-14 Cytokines and chemokines are differentially expressed in GBM and PBMC treated with Dex and Reo.

The candidate cytokines and chemokines in response to the treatment of Dex and Reo were validated by Luminex assay for IL-6, IL-8, IL-1B, CCL3, and CCL4 for supernatant collected 24 hours post treatment in **A.** MO59K (n=2 independent samples, each in duplicate) and significance was tested with nonparametric one-way ANOVA (Friedman) with Dunn's multiple comparison test. **B.** PBMC (n=3 independent samples), and significance was tested with one-way ANOVA with Tukey multiple comparison test. ns>0.05, *p≤0.05, **p≤0.01, ***p≤0.0001, and ****p≤0.0001.

3.2.4.2 PD-L1 expression was differentially regulated by Dex and Reo in GBM cells and monocytes

Bioinformatics analysis also defined PD-L1 (programmed death-ligand 1; also known as CD274 or B7-H1) to be upregulated by Reo and downregulated by GCs (Figure 3.15.A). Close *et al.,* (2020) identified immunomodulatory cell surface molecules in GBM stem-like cell lines. We compared these genes signature to datasets of GBM, monocytes and CD4+ T cells treated GCs (Figure 3.15.B), and found PD-L1 differentially expressed between GBM patients samples and GBM cells treated with GCs (Figure 3.15.C). Next, PD-L1 expression was validated on MO59K and PBMC treated with Veh, Dex, Reo or combined Dex with Reo for indicated time points and analysis completed by flow cytometry. Results showed that MO59K treated with Reo has significantly higher PD-L1 expression than Veh and Dex groups after 48 and 72 hours, and combining Dex with Reo reduced PD-L1 expression after 48 and 72 hours. In term of monocytes, significant PD-L1 reduction was observed in Dex treated group, while expression was enhanced by Reo treated group after 72 hours (Figure 3.15.D).

A.

Gene	Signaling pathway	GBM patients treated Reovirus	GBM cells treated GCs	PBMC treated GCs
CD274	PD-L1	Up-regulated	Down-regulated	Down-regulated

B.

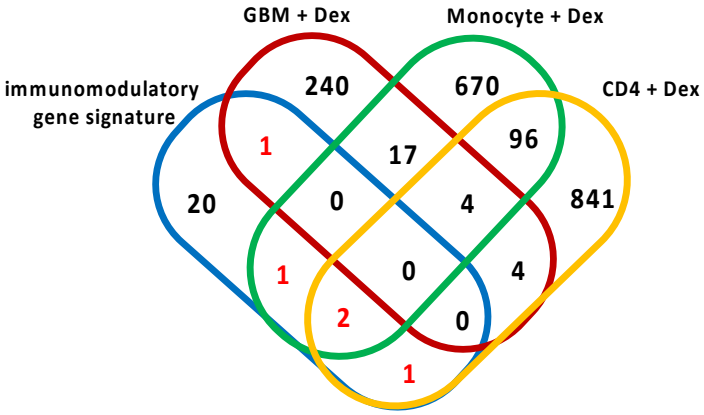

C.

Gene	GC regulated Log FC	immunomodulatory signature LogFC
CD274	-0.744737	0.51400421
HAVCR2	2.9672662	3.41450792
IDO1	3.4741951	0.02544588
IL10	2.4641759	0.63197718
GAPDH	1.8935384	11.1961103
IDO1	1.9216391	0.02544588
IL10	2.2193988	0.63197718

D.

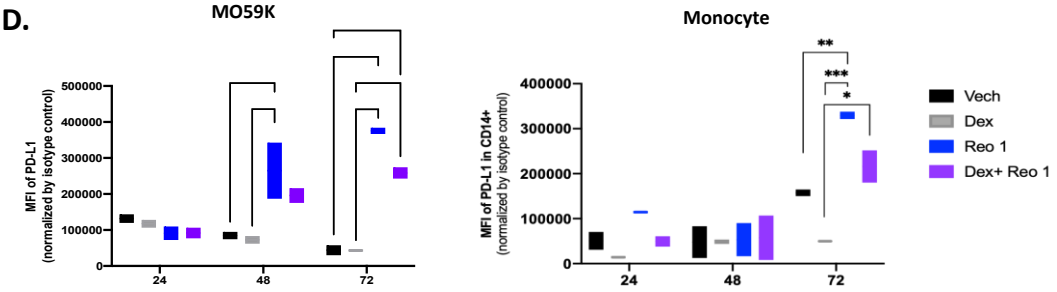

Figure 3-15 Immunoregulatory gene signature correlation with GC regulated cells in RNA-seq datasets.

A. CD4 T cells, and GAPDH, IDO, IL-10 in monocyte cells. **B.** Table of the genes with log2FC to represent gene expression. **C.** Data analysis shows that PD-L1 is differentially expressed in response to each treatment. **D.** Results were validated by Flow cytometry for PD-L1 expression on MO59K cells treated with Veh, Dex, Reo, or combination. Results presented as MFI fold change compared to isotype control, The data presented as mean ± SEM, for n=3 independent experiments and significance was tested using 2-way ANOVA with Tukey's multiple comparison (ns>0.05, *p≤0.05, **p≤0.01, and ***p≤0.001).

3.3 Discussion

Most GBM patients receive GCs, a potent anti-inflammatory drug that is used as a standard therapy to control brain oedema. While GCs are highly effective in patients, little is known about their mechanism of action directly on GBM cells and how this might be modified by the tumour microenvironment. New immunotherapies that harness the immune system have shown promising results for many cancers, including GBM. OV, an immuno-virotherapy, act directly to drive oncolysis of tumour cells, and activate the immune system to induce cytotoxic killing, and anti-tumour immune response. Consequently, the effect of GC on OV action in GBM is not clear, and requires investigation. This chapter re-analyzed relevant datasets to identify potential points of crosstalk between GC and OV in order to begin to understand how these two treatments might interact. Overall, results in this chapter show that Reo tends to stimulate the production of pro-inflammatory molecules, but this is reduced in the presence of Dex. This agrees with current models of Dex action, but this is the first time that such studies have been performed in the context of GBM.

The transcriptional response of GBM cells to GC was first examined using the MO59K cell line treated with Dex, and 266 DEGs were detected in comparison to control. Pathways analysis for the dataset has identified the nuclear receptor (NR) meta pathway, which GR is a member of the NR superfamily (Kumar and Thompson, 2005). It also identified cortisol, the natural GC known to regulate various processes including metabolism, inflammation, and stress (Marques *et al.,* 2009). Another top enriched pathway is AP-1 transcription factor, which is well known to bind to GR, repressing inflammatory genes such as IL-6 (Atsaves *et al*., 2019). Results showed down-reregulation of the pro-inflammatory genes IL-6, IL-1B, IL-11, and CXCL8 in response to GCs treatment. Additionally, the Enrichr platform was used to analyse the TFs predicted to regulate the DEGs, and identified NR3C1 (the gene symbol for GR), NR4A2, and NR4A3. NR4A2 is pro-oncogenic in GBM and thus considered as a potential therapeutic target for patients with tumours expressing this receptor (Karki *et al.*, 2020). It was reported that NR4A family receptors were expressed in cancers including GBM, and affecting apoptosis, DNA repair, proliferation, migration, inflammation,

metabolism and angiogenesis (Mohan *et al.*, 2012). Overall, these analysis shows that the dataset is robust and that the ontology has identified relevant terms.

Genes regulated in response to Reo in patients with GBM were next explored. Pathways analysis of the DEGs were enriched for NF-kB, AP-1, HIF-1, and TGF-β signalling. It is not clear how some gene such as DUSP1, MYC, or BCL2L11 influence Reo efficacy. However, in term of GBM, DUSP1 expression is high in GBM cells (Yu *et al*., 2012), while MYC is overexpressed in GBM and correlates with poor survival (Wang *et al.,* 2008), while BCL2L11 (Bcl-2 like protein 11; also known as BIM) plays a key role regulating apoptosis. EDN1, Jun and Fos are components of AP-1 transcription factor complex. It was reported that c-Jun is phosphorylated by Reo, leading to AP-1 activation (Berard *et al.,* 2015). Interestingly, Jun expression in GBM patients treated with Reo dataset was also upregulated, suggesting AP-1 activation upon Reo treatment. Additionally, AKT1 was found to be upregulated in GBM and associated with poor prognosis (Wang *et al*., 2021). The phosphoinositide 3-kinase (PI3K)/ AKT signalling pathway is a hallmark of cancer, promoting cell survival and proliferation. AKT1 expression leads to increased susceptibility of tumour cells to Reo-induced apoptosis via PI3K/Akt/mTOR signalling (Thirukkumaran *et al.*, 2017). Here, the dataset analysis found that AKT1 is downregulated upon Reo treatment in GBM patients. KEGG analysis was also enriched for viral protein interaction with cytokine and cytokines receptors including: CCL3, CCL3L1, CCL4, CXCR2, CD70, and SERPINE1. CCL3 and CCL4 are pro-inflammatory chemokines secreted by macrophages. It has been shown that Reo increases the level of CCL3, CCL4 which are involved in leukocyte infiltration, leading to an enhanced anti-tumour immune response (Wang *et al*., 2016).

To examine the potential crosstalk pathways between genes regulated by GC and OV, I identified 27 overlapping DEGs between OV-regulation and GC regulation in GBM. The expression of BIRC3 (anti-apoptotic gene) and S1PR3 (inflammation activated S1P receptor) were upregulated under GC regulation in comparison to OV. A previous study demonstrated the differential expression of BIRC3 in GBM patients, and that downregulated BIRC3 expression correlates with enhanced GBM overall survival (Giles *et al.*, 2018). This indicated that GC

protects GBM cells from apoptosis. In addition, although S1PR1, S1P2, and S1P3 were expressed in GBM patients, but only S1PR1 and S1PR2 were critical for patient survival (Mahajan-Thakur *et al.,* 2017). It was reported that S1PR3 is expressed in astrocytes, thereby modulating the blood tumour barrier (BTB) in brain metastases (Gril *et al.*, 2018). Reo activates DCs through PKR signalling, leading to the secretion of pro-inflammatory cytokines such as IFN-α, IL-12, TNF-α and IL-6. Transcriptional re-analysis showed that IL-6 and IL-11 were upregulated under OV regulation while downregulated under GC regulation. Although IL-6 secretion increases GBM invasion and angiogenesis. Nonetheless, IL-6 secretion by immune cells such as monocytes could be beneficial under OV treatment, by promoting CD8+ T cell differentiation to cytotoxic T cells (Pol *et al.*, 2020).

It was noticed that the dataset did not include pathways related to virus activity such as interferon pathways. This could be due to the end timepoint where the tissue samples were taken from patient surgery (between 3-17 days post Reo infusion). Reo commonly induces type 1 Interferons (IFN-α and IFN-β) to activate innate immune responses by stimulating NK cells, promote antigen presentation, and activated CTL. Due to the lack of transcriptome datasets in OV treated group, a comparison of dataset for GBM cells treated with IFN-a and OV-treated GBM was analysed. 53 overlapping gene between OV regulation and IFN regulation in GBM cells were identified and 66% were similarly expressed. Pathways analysis showed enrichment in immune system and cytokines pathways. IFI6 (interferon-alpha inducible protein 6) and IFI16 (interferon-gamma inducible protein 16) were upregulated in both datasets. IFI16 can detect viral DNA in the nucleus, activate IFN signalling through the STING-TBK1 axis (Yang *et al.,* 2019). Previous study showed that IFI16 can directly sence PAMPs to trigger canonical pyroptosis in Reo (DeAntoneo *et al*., 2022). Taken together, both OV and IFN datasets showed similarity in gene expression pattern.

Genes regulated in response to GCs in immune cells were next evaluated. Firstly, CD4+ T cells treated with Dex for 24 hours were re-analysed, and the volcano plot of DEGs shows downregulation in CCL2 expression. GBM cells express CCL2 that recruits Treg to inhibit immune response and promotes GBM progression. Pathways analysis identified T cell receptor (TCR) signalling

including CD3E, CD3D, and CD27, which were downregulated under GC regulation, indicating T cell inhibition as a result of GC treatment. GC is known to induce apoptosis of lymphocytes. TSC22D3/GILZ is also upregulated under Dex treatment, which showed to mediates immunosuppression by blocking interferon response in DC, and T cell activation (Yang *et al*., 2019). GBM patients treated with Reo might activate T cells to induce anti-tumour immune response. Therefore, Samson *et al.* 2018 dataset was compared to GC treated CD4 T cells. 27 overlaying genes were displayed. CCL3, CCL4 were differentially expressed in addition to DUSP1, MCM6, TXNIP and MYC (regulation of cell division) and pathways analysis identified expression of chemokine receptor during T cells polarization (CCL3, CCL4), PPAR-alpha pathway, and mRNA involved in immune response.

Next, monocytes were analysed, and the volcano plot showed upregulation of CD163 (macrophage marker) as one of the top enriched genes. It has been reported that high CD163 expression in GBM correlates with worse patient survival. Pathways analysis identified AP-1 TF, TGF-β. IFNs, antigen presentation, HIF-1 signalling, NR as top enriched terms. Genes involved in AP-1 and GR ontologies such as CCL2 and NR3CA were downregulated while TSC22D3/GILZ which is a direct transcriptional target of GR and IL-10 (M2 marker) were upregulated. CCL2 is required for macrophage recruitment to the tumour and inflammation. It has been reported that human GBM contains mixed polarized TAMs (Ma *et al*., 2021). A recent study characterised macrophage within GBM and categorized cells expressing CCL2, CCL3, CCL4 and PTGS2 as anti-tumoral macrophage markers, while CD68, MRC1, LGMN, CD163, IL-10 and MSR1 as pro-tumoral macrophages marker (Zeiner *et al.,* 2019). In conclusion, our analysis of human monocyte identified a robust induction of anti-inflammatory genes which is an important mechanism of GC action. Pathways analysis from monocyte treated with OV dataset identifies RIG and IRF7, NOD-like receptor, which are pattern recognition receptors (PRR) that recognise viruses to activate innate and adaptive immune responses. It also identified immune cells and interferons as top enriched pathway, revealing upregulation in IFN-associated genes (eg. IRG1, IFNA1, ISG20, IFITM1, IRF7), cytokines and chemokines, antiviral defence proteins such as ISG15 and ISG20. Finally, immune checkpoints (eg. CD274, LAG3) were downregulated by GCs suggesting re-

education of M2 phenotype into M1 phenotype. A volcano plot was created to analyse common genes between monocyte treated with GCs, OV and compare it with GBM patients treated with OV, and 12 genes between the three datasets were identified. LGMN was downregulated under GC regulation while S100A8 were upregulated by Reo. It is well known that S100A8/9 are highly expressed in GBM patients and are upregulated in monocytes treated with GC. LGMN is associated with M2 Macrophages (Ma *et al.*, 2021) within the GBM microenvironment. SERPINE1 correlates with poor GBM survival, and is a mesenchymal signature (Seker *et al.,* 2019). 201 genes were also identified between monocyte datasets treated with OV or GC. Pathways analysis identified AP-1, BCR, GMCSF-mediated signalling, TNF receptor, canonical NF-kB, GR, NR, and macrophage markers. Canonical NF-kB involve TLR, TNFR, BCR, TCR which are pathways mentioned earlier, suggesting the importance of this pathway in monocytes. Cytokines and chemokines like CCL2, CCL3L1, CCL7, CXCL3, IL-8 were upregulated under OV regulation. M2 markers CD163, MRC1 and IL-10 were downregulated by OV and upregulated by GC while LGMN, MSR1 were upregulated by OV and downregulated by GC. This suggests that OV drives macrophages toward the M1 phenotype while GC drives them toward the M2-phenotype. Multiple S100 proteins such as S100A4, S100A6, and S100A8 are downregulated in OV and up in GC. S100 proteins are main regulators of macrophage, and GC increased the expression of S100AA8 and S100A9 in human monocytes. Notably, SYK was downregulated in OV dataset and upregulated in GC dataset. SYK gene plays a role as oncogenic gene in different type of cancers. It is reported to be expressed in monocyte and mediates inflammatory response (Yi *et al.*, 2014). SYK is also expressed in samples of GBM patients, and it has been shown that targeting SYK inhibited tumour proliferation and migration and might play a role in the GBM microenvironment (Moncayo *et al.,* 2018). A compression between OV-treated GBM patients and monocytes treated with GC or OV was conducted to investigate the marker patterns expressed by monocytes within the GBM microenvironment. 125 genes were common between OV treated monocytes and OV treated GBM patients, which were enriched in pathways involving viral protein interaction with cytokines, DNA sensors and IFNs signalling. This suggests a role of OV in modulating interferon signalling in both immune cells like monocytes and GBM. Additionally, it highlighted the crosstalk to activate innate and adaptive immune responses

within the TME. While 29 DEGs were common between GC-treated monocyte and OV-treated GBM patients. The result showed that BTG2, EGR1, EGR2, LGMN were downregulated under GC regulation while S100A8 was upregulated. Both EGR1 and EGR2 were inhibited by GC on monocyte and were listed under enriched AP-1 signalling. This suggests the role of EGR pathway in monocyte differentiation and activation is affected by GC treatment. BTG2 is an apoptosis gene that has been shown to be downregulated in microglia within the GBM mass. Pathways analysis showed enrichment in IFNs, antigen presentation, AP-1 signalling, and p53 effector pathways. In parallel to inflammatory responses, these genes reported to be involved in GBM angiogenesis, cell proliferation, migration, invasion, and immune response.

Throughout the Enrichr pathways analysis of different transcriptome datasets, a list of genes was identified that is known to be GC mediated via GR network (DUSP1, NFKBIA), reovirus mediated via interferon pathway (IFI16, IFI6), and genes mediated by both GC and reovirus (FST, IL-6, IL-1B, CXCL8, CCL3, CCL4, PD-L1). These genes identified under AP-1 transcription factor, IL-6 signaling, TNF signaling and TGF-β signaling, as the most significant terms by both GCs and reovirus. Different methods were used to validate these genes in mRNA level (qPCR), cytokines/chemokines release (Luminex assay) and flow cytometry to correlate between genes of interest in and cell surface protein expression.

The mRNA results confirm that Dex alone or in combination with OV significantly increases DUSP1 expression in both MO59K cells and PBMC, suggesting that DUSP1 might regulate tumour growth. Interestingly, it seems that OV alone upregulates DUSP1 expression. DUSP1 function in cancer is complex as it has been reported to act as a tumour suppressor or promoter. Several studies showed DUSP1 overexpression is regulated through p38, MAPK, and JNK dephosphorylation (Dedobbeleer *et al*, 2017), which induced apoptosis and suppresses tumour growth. In other cases, reduced DUSP1 expression, led to MAPK induction and cancer survival. In context of GBM, it has been reported that DUSP1 expression is higher in GBM cells than in normal brain cells and been associated with increased tumour proliferation (Bermudez *et al.,* 2010). DUSP1 could contribute in chemoresistance by inhibiting apoptotic pathways via p38, MAPK, and JNK (Yu *et al*., 2012), and the gene expression is induced by hypoxia,

Dex and chemotherapeutic agent's treatment, and maintain the stem cells population In GBM (Milles *et al*., 2017). Dex is known to upregulate DUSP1 expression, leading to decrease the pro-inflammatory cytokines (Jiang *et al*., 2016, Abraham *et al*., 2006). In immune cells, Dex-induced DUSP1 expression in THP-1 cells, which promote macrophage polarization toward the M2 phenotype (Gauthier *et al.*, 2017). DUSP1 expression by RT-PCR analysis showed upregulated gene expression on GBM cell line (Figure 3.13), suggesting that Dex alone or in combination to OV might affect the MAPK pathway, alter apoptosis pathways which could impact tumour survival. However, upregulation of gene expression was observed on PBMC treated with either Dex, OV or combination treatment in comparison to vehicle group. This might influence the immune landscape negatively within the TME and impacting GBM progression.

Dex does not seem to play a role in reducing NFKBIA mRNA level in GBM cells, while OV alone or in combination with Dex showed increased in NFKBIA expression. On other hand, Dex induced NFKBIA expression in all groups compared to vehicle, though OV alone and combination treatment has higher expression that Dex alone when compared with Vehicle (Figure 3.13). The results suggest that Dex treatment did not significantly increase gene expression in GBM cells, however in PBMC, a significant increase was observed with the combination treatment compared to single treatment. NFKBIA might be an early Dex-induced gene and results observation might be due to the time of treatment where mRNA level was evaluated after 24 hours of treatment instead of 4 hours. Previous studies indicated NFKBIA phosphorylation, led to NF-kB translocation to nucleus and NFKB activation (Cahill *et al.,* 2015). Deletion or decrease expression of NFKBIA is associated with shorter survival in GBM patients (Miyar *et al.*, 2016) (Bredel *et al.,* 2011). Generally, Dex is known to upregulate NFKBIA expression (Desmet *et al.,* 2017). NFKBIA is reported as an IFN/RIG-1 independent gene induced by Reo in melanoma, mediating the innate immune response, impacting cells death, and influencing virus spread (Mohamed *et al.,* 2020).

FST, Follistatin, is reported to inhibit TGF-β, a key signalling involved in tumour progression. It binds Activin and BMP (TGF-β members), and the isoform FST288 is demonstrated to have inhibitory effects on tumorigenesis, metastasis and

angiogenesis (Thirukkumaran *et al.*, 2017; Shi *et al*., 2016). Little is known about FST role in GBM. Data analysis in GBM showed Dex downregulated FST expression and upregulated in Reo treaded GBM patients. Analysis of mRNA confirmed that FST is downregulated by Dex, up-regulated by OV and a degree of reduction in combined group of Dex plus HSV-1 when compared to HSV-1 treatment alone (Figure 3.13), suggesting the selective effect of Dex in OV efficacy based on the OV strain. In addition, FSTL1 (Follistatin Like 1) was reported to be highly expressed in GBM and is correlated with poor GBM progression (Reddy *et al.*, 2009). Interestingly, opposite results were found in the context of immune cells, where PBMC treated with Dex showed significant increase in FST expression, while OV and combined treatment has lower expression than Dex alone, suggesting that FST might play role in immune cells function when treated with Dex but not OV.

IF16 and IFI16 are members of interferon-inducible gene family, that act as antiviral factor mediates innate immune response. IFI16 induced IFN-1 production following detecting viral DNA in the nucleus (Lee, Chathuranga and Lee, 2019). It was reported to bind RNA viruses such as Influenza via RIG-1 signalling and correlates with the viral load (Jiang *et al.,* 2021). IFI16 also interacts with STING signalling in response to RNA viral infection. The results from the RT-PCR showed that IF16 and IFI16 are scientifically upregulated by reovirus and expression was reduced when combined with Dex in GBM cells (Figure 3.13). Similar results were observed in PBMCs, except that gene expression in combination treatment is similar to OV alone, suggesting that Dex response is restricted to tumour cells.

We next sought to investigate selected cytokines and chemokines level mediated by Dex and OV using a Luminex assay (Figure 3.14). Both IL-6 and IL-8 level were induced in Reo group while the combined group has lower level in GBM cells and PBMC. IL-6 and IL-8 are pro-inflammatory cytokines/chemokines that play a key role in the TME of GBM. It has been reported that increased IL-6 expression correlates with poor GBM survival (West *et al.*, 2018) and associated with increased macrophage activation in GBM (Wang *et al.*, 2018) by upregulating in M1-phenotype and downregulating in M2-phenotype, deriving myeloid immunosuppression activity, and inducing PD-L1 expression through

STAT3, leading to induction of immune-mediated antitumor response in GBM (Lamano *et al.,* 2019). Likewise, IL-8 is reported to be highly expressed in GBM patients which correlates with poor survival, and promotes cell proliferation and angiogenesis (Sharma *et al*., 2018). Previous studies demonstrated that GCs inhibit IL-6 and IL-8 production which limit cell proliferation (Laberage *et al*., 2012). A coculture of macrophage: GBM cells treated with Dex was shown to decrease IL-8 expression at mRNA level (Hong *et al.,* 2009), and that IL-8 production is mediated by NF-kB activation (Mukaida *et al*., 1994).

A previous study found that CCL4-CCR5 axis was increased in macrophages to promote GBM invasion (Wang *et al.,* 2016). This suggests that GCs limit the effect of Reo to produce CCL3/4 in GBM cells. More studies in coculture models are needed to understand the interaction between tumour cells and the TME in the presence of both GCs and Reovirus and how this affects the production of CCL3 and CCL4. Reo induced IFN-α and IFN-β, IL-6 expression in MDSC, which reported to induce MDSCs immunosuppressive activities (Yuki *et al.,* 2018). Reovirus infected melanoma cells secrete IL-8, CCL3, CCL4, and IFN-β, which induce innate and adaptive anti-tumour response (Steele *et al.,* 2011). Validation of CCL3 (MIP-1a) level were detected in GBM cells but not PBMC. The Reo group showed the highest level, while Dex plus Reo showed reduction in CCL3 level. Similar results were detected in CCL4 (MIP-1b) level in GBM cells. However, PBMC showed increased CCL4 level in combination group over reovirus group, while Dex group has lower CCL4 level (Figure 3.14). CCL3 and CCL4 impact the tumour microenvironment and immune response. It would be interesting to investigate cytokines/chemokines in a coculture system at the cellular and transcriptional level to understand the complex interaction of immune cells such as macrophage in GBM progression and in the presence of GCs and OV therapy.

PD-L1 is an immune checkpoint ligand that highly expressed by GBM cells and monocytes. Upregulated PD-L1 expression contributes to the immunosuppressive microenvironment by binding to PD-1 on T cells leading to T cells inhibition, promoting tumour immune escape and tumour progression. It has been reported that Dex-mediated PD-L1 downregulation and reduce tumour cells ability to evade immune surveillance. Recent studies indicated an association between GCs and poor GBM patient survival when treated with checkpoint

inhibitors, and pre-clinical studies of Dex downregulating the pro-inflammatory cytokines led to reducing T cells, macrophage, and DC proliferation and function (Kyra *et al.,* 2022). Flow cytometry analysis of treated GBM cells and PBMC (Figure 3.15.D) showed that Dex significantly reduce effects of OV efficacy by reducing PD-L1 expression in GBM cells impacting its ability to promote anti-tumour immune responses, as well as reducing PD-L1 in human monocytes and consequently to inhibit T cells proliferation and toxicity. In summary, GCs negatively affects GBM patients receiving immunotherapy, such as OV, by exerting immunosuppressive effects. Clinicians are advised to consider the timing and dose of Dex when combined with CPIs to the treatment plan.

Overall, this chapter highlighted some insight into how GC influences Reo efficacy in GBM cells and immune cells at a transcriptional level. One of the limitations in the transcriptome analysis in this chapter is the limited publicly available datasets of OV treated- GBM. We had access to a small pilot clinical trial of GBM patients treated Reo (n=3) and the time-point of collecting tissue after reovirus infusion plus the treatment regime before admitting or during the trail such as the timepoints and dose of Dex before and after surgery could cause variation between samples. Further in vitro assays will be performed in the next the chapter to understand the combination effect of GCs and Reovirus on GBM cells and immune cells population within TME.

Chapter 4

The effect of GCs on OV mediated killing in GBM

4.1 Introduction

Despite their benefits, GCs immunosuppressive properties might negatively impact the efficacy of OV therapy. In the previous chapter, I analysed public datasets to identify points of crosstalk between OV and GC. However, as the datasets were from different sources, it is difficult to draw conclusions from the analysis. Understanding the complex interplay between GCs and OV is essential for optimizing GBM treatment protocol and improve patients outcome. Recent preclinical studies suggested that the immunosuppressive effect of GCs is detrimental to the response to immunotherapy (Kalfeist *et al.*, 2022), and some reported GCs reduce the efficacy of checkpoint inhibitor and CAR-T cells therapy (Poiret *et al*., 2024). The complex effects of GCs on tumours and the immune system and a lack of specific information on GBM response to GCs or in combination treatment with OV suggests the need to study this in more depth.

<u>The aim of this chapter are therefore two-fold:</u>

1. To determine the effect of GCs on efficacy of OV direct killing in a panel of GBM cell lines
2. To complete RNA-seq on GBM to examine the interplay between Dex and oncolytic virus at the transcriptional level

4.2 Results

4.2.1 GCs impairs OV direct killing effect on GBM cell lines

To investigate the effect of GCs treatment on OV efficacy, I pre-treated the GBM cell lines MO59K and A172 with or without the synthetic GC dexamethasone (Dex; 100nM) overnight. Reo or HSV-1 was then added to these cultures (MOI 0.1, 1, 10) and cell viability assayed using an MTT assay, a colorimetric assay of metabolic activity at 48 or 72 hours post-infection. The A172 cells showed strong resistance to Reo infection up to 72 hours post-infection, with no significant effect of Dex (Figure 4.1.A, B). In contrast, MO59K were susceptible to lysis by Reo; Dex pre-treatment provided a modest protective effect against Reo-mediated lysis though this was not statistically significant (Figure 4.1.C). However, the protective effect of Dex was significant when Dex and Reo were added to MO59K cells simultaneously (Figure 4.1.D). This reveals that Dex treatment reduces the susceptibility of MO59K cells to Reo.

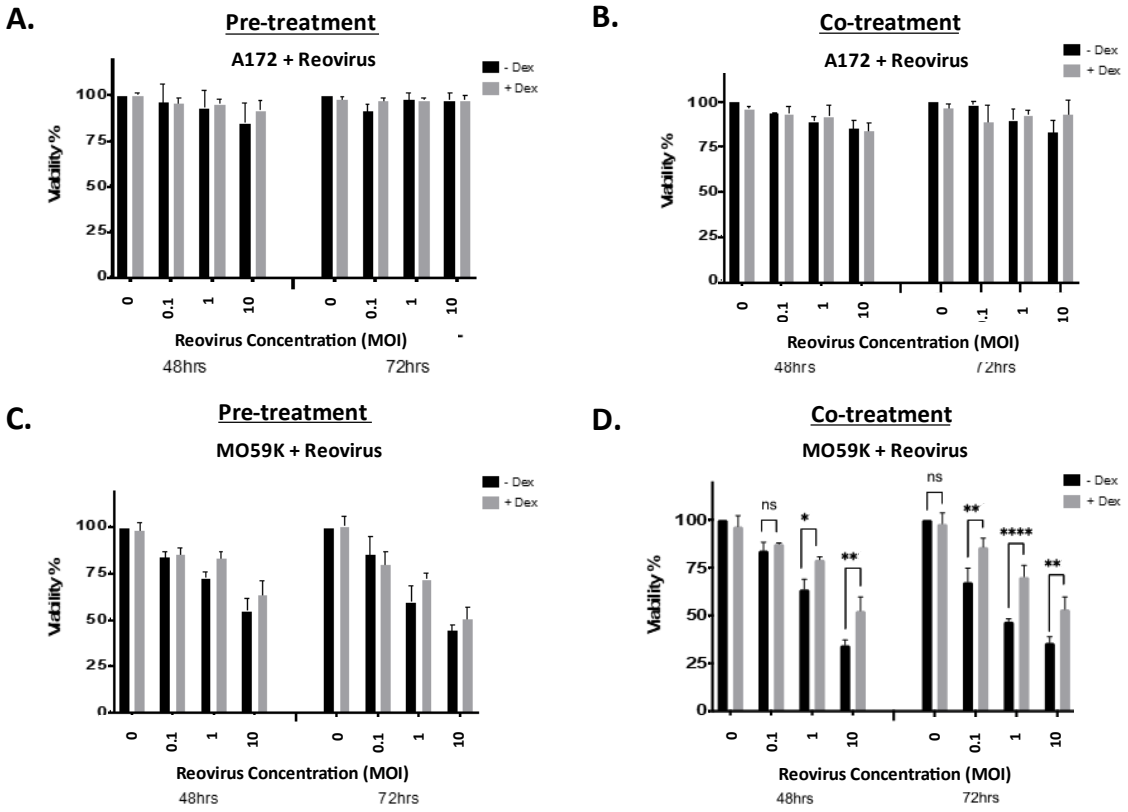

Figure 4-1 Dex impairs Reo mediated killing of GBM cell lines.

A. A172 cell line was pre or **B.** co-treated with/without 100nM Dex, and combined with Reo at MOI of 0, 0.1, 1, and 10. C. MO59K cell line was also either Dex pre-treated or **C.** co-treated with the previous treatment conditions. Percentage cell viability was determined using MTT assay 48 and 72 hours post-infection (p.i). Graphs show the mean ± SEM for n=3 independent experiments and significance was tested using a 2-way

ANOVA with Bonferroni's multiple comparison test (ns p>0.05, *p≤0.05, **p≤0.01, ***p≤0.001, and ****p≤0.001).

In contrast, both A172 and MO59K cells were susceptible to HSV-1, as shown by the dose-dependent reduction in cell viability and the MOI of HSV-1 increased. However, Dex treatment did not alter susceptibility of either cell line to HSV-1 when given as a pre-treatment or as co-treatment (Figure 4.2.A-D). These data show that the protective effect of Dex is specific to Reo (a dsRNA virus) and MO59K cells and that susceptibility to HSV-1 (a dsDNA virus) is unaffected by Dex treatment.

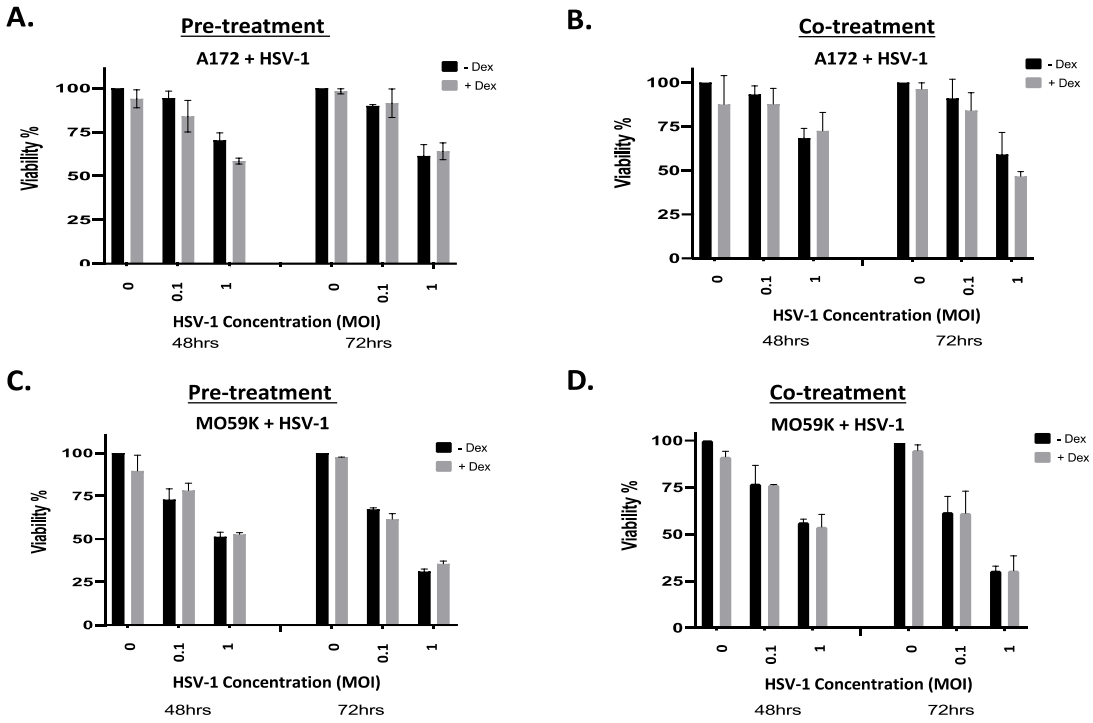

Figure 4-2 Dex does not affect HSV-1 mediated killing of GBM cell lines.

A. A172 cell line was either pre or **B.** co-treated with/without 100nM Dex, and combined with HSV-1 at MOI of 0, 0.1, 1, and 10. **C.** MO59K cell line was also either pre or **D.** co-treated with the same previous treatment conditions. Percentage cell viability was determined using MTT assay 48 and 72 hours post-infection (p.i). Graphs show the mean ± SEM for n=3 independent experiments and significance was tested using a 2-way ANOVA with Bonferroni's multiple comparison test (ns p>0.05, *p≤0.05, **p≤0.01, ***p≤0.001, and ****p≤0.001).

I speculated that the differential susceptibility of A172 and MO59K cells to Reo (Figure 4.1) could be due to differences in the cell surface expression of the Reo entry receptor, junctional adhesion molecule-1 (JAM-1). I therefore analysed expression of JAM-1, as well as the HSV-1 entry receptor HVEM on A172 and MO59K cell lines using flow cytometry. Additional GBM patient-derived cells (GBM1, GBM4, GBM11, GBM13, GBM20), along with the neural progenitor cell line (NP1), a non-malignant brain-derived cell line (PMID: 20129251), were also assessed for viral entry receptor expression. Representative flow cytometry histograms are shown in Figure 4.3.A, and data from multiple replicates is shown in Figure 4.3.B. Expression of JAM-1 was lower on A172 cells than MO59K cells, but was detectable, suggesting that differential expression of this entry receptor was not the reason behind the resistance of A172 cells to Reo. With the exception of GBM4, all cell types tested showed evidence of JAM-1 expression, albeit at varying levels. Expression of HVEM was more restricted, with only low levels of HVEM detected in some cell lines, in particular MO59K cells.

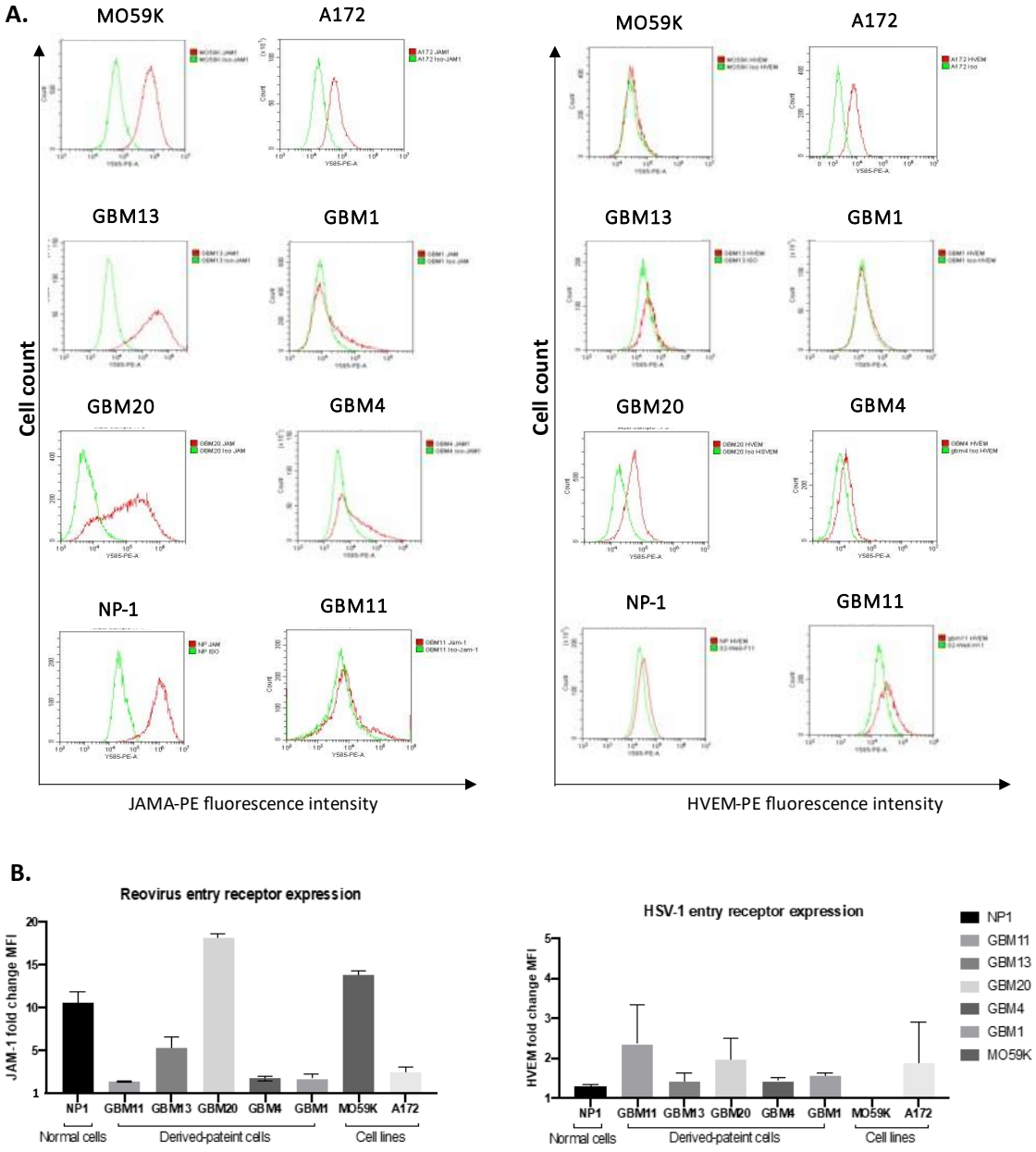

Figure 4-3 Screening of viral entry receptors expression on panel of GBM cells.

Normal brain cell line (NP1), GBM-derived patient cells (GBM1, GBM4, GBM11, GBM13, GBM20), and GBM cell lines (MO59K, A172) were tested for the expression of viral entry receptors (JAM-1 for Reo, HVEM for HSV-1) using flow cytometry. **A.** Representative histograms of JAM-1 and HVEM expression (red line) and isotype control (gray line) on GBM cells. **B.** Graph of MFI fold change JAM-1 and HVEM expression in comparison to isotype control. The data is presented as mean ± SEM, for n=2 independent experiments, and significance was tested with nonparametric one-way ANOVA with Dunn's multiple comparison test.

Results in Figure 4.1 show that Dex can alter the susceptibility of the GBM cell line MO59K to Reo oncolysis, but Dex does not alter susceptibility of A172 to MO59K to HSV-1. However, both A172 and MO59K are long established cell lines and it was important to determine whether Dex altered susceptibility of GBM derived cells that are more representative of patient tumour cells. I therefore tested the susceptibility of GBM13, GBM20 and NP1 to both Reo and HSV-1 when the cells were co-treated with Dex and virus (as Figures 4.1 and 4.2).

The non-malignant cell line NP1 was highly resistant to Reo and only showed limited susceptibility to HSV-1 (Figure 4.4.A,B). This confirms the selectivity of OVs to kill tumour cells, but not normal cells. The GBM20 cell line showed that Dex co-treatment was protective against both Reo and HSV-1, whereas Dex made no difference in susceptibility to either virus in GBM13 (Figure 4.4.C-F).

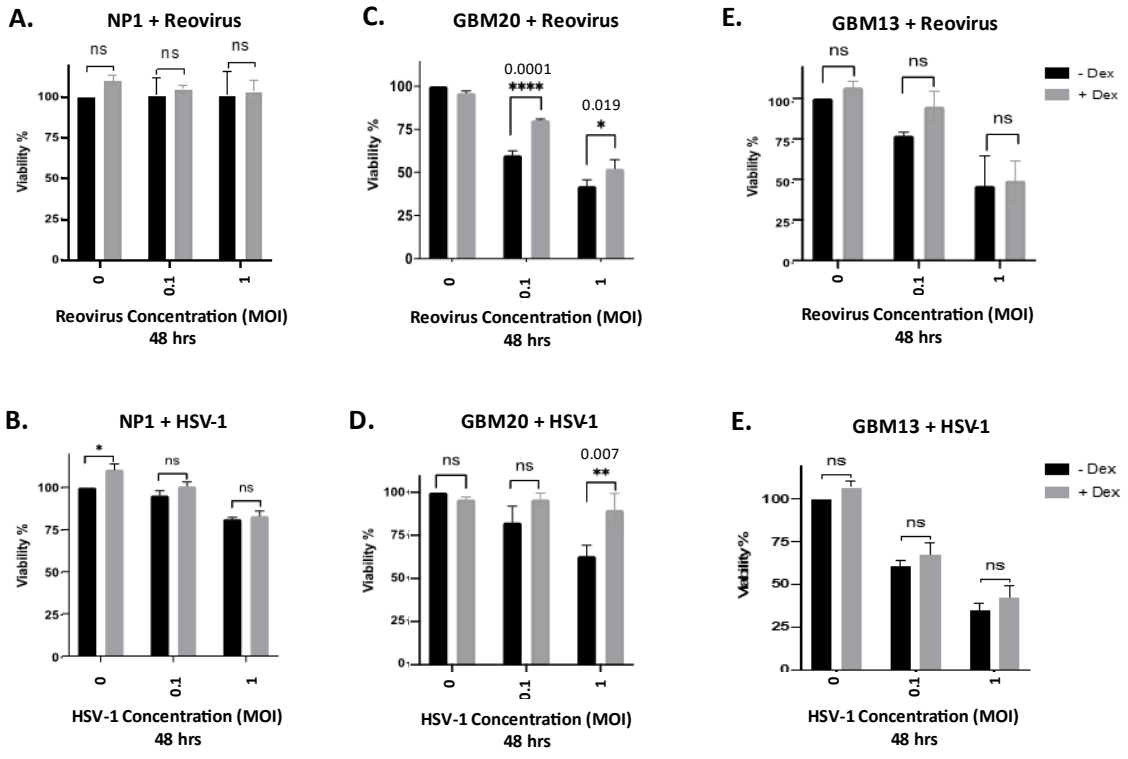

Figure 4-4 Dex impairs OV direct killing on GBM derived patient cells.

Normal brain cell line (NP1) treated with **A.** Reo or **B.** HSV-1, GBM20 treated with **C.** Reo or **D.** HSV-1 and GBM13 treated with **E.** Reo or **F.** HSV-1 were co-treated with 100nM Dex and different MOIs of OV. The viability % was determined by MTT assay 48 hours post-infection. The data presented as mean ± SEM for n=3 independent experiments and significance was tested using 2-way ANOVA with Tukey's multiple comparison test (ns $p>0.05$, *$p\leq0.05$, **$p\leq0.01$, ***$p\leq0.001$, and ****$p\leq0.001$).

As an alternative to the MTT assay (which measures cellular NADPH levels, a surrogate for viability), I repeated the Reo experiments using a flow cytometry based live/dead stain where dead cells show greater permeability and retention of a fluorescent dye. In addition, I extended the analysis time from 48 hours to include both a 48hr and 72hr timepoint. This assay confirmed that NP1 cells were highly resistant to Reo and that Dex reduced killing by Reo in MO59K and GBM20 cells. Extending the assay time to 72 hours showed that this protective effect was also detected in GBM13 cell line. Furthermore, NP1 cells did show some evidence of Reo-mediated oncolysis at 72 hours and again, Dex showed a protective effect. Taken together, these results show that Dex can protect against Reo mediated killing (Figure 4.5.A-D).

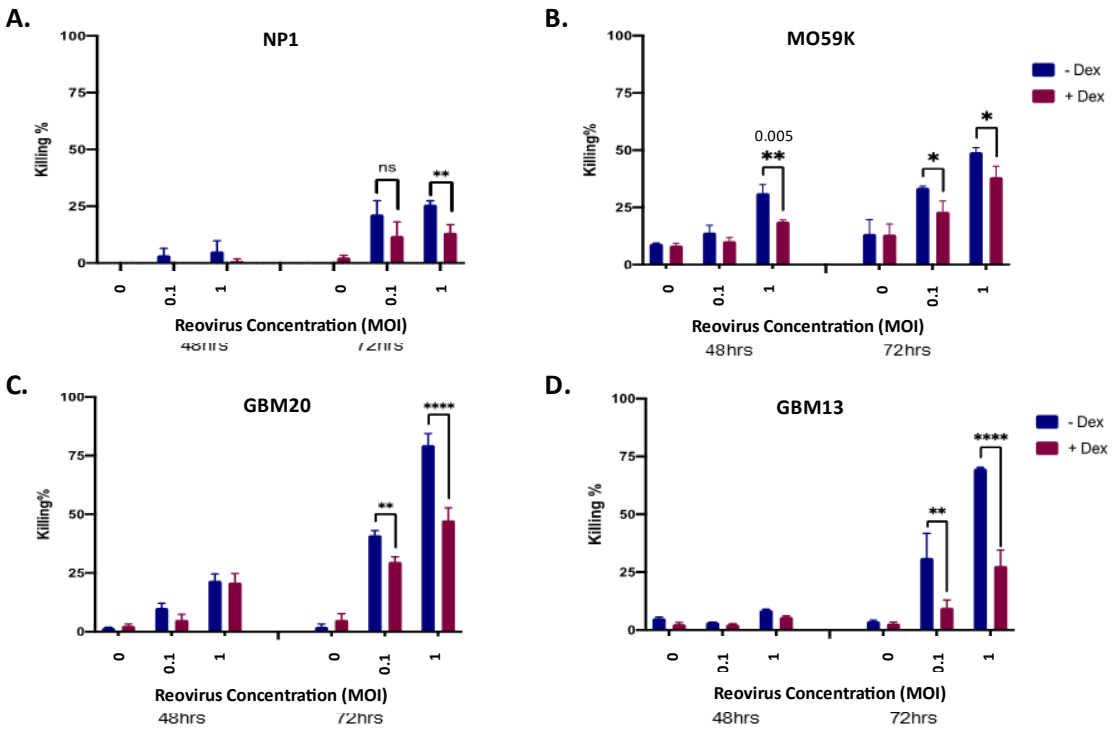

Figure 4-5 Dex impairs Reo mediated killing of GBM cells.

A. Normal brain cell line (NP1) and **B.** MO59K cell line **C.** GBM20 and **D.** GBM13 derived patient's cells were co-treated with 100nM Dex and Reo at MOI 1. The killing % by LIVE/DEAD stain was analyzed by flow cytometry 48 and 72 hours post reovirus-infection. The data presented as mean ± SEM for n=3 independent experiments and significance was tested using 2-way ANOVA with Tukey's multiple comparison test (ns $p>0.05$, * $p\leq0.05$, ** $p\leq0.01$, *** $p\leq0.001$, and **** $p\leq0.001$).

4.2.2 Dex does not regulate Reo entry or virus replication in GBM cells

Generally, OV replicate specifically in tumour cells, generating tumour specific oncolysis, and release of virions from dying cells to infect neighbouring tumour cells. The ability of Reo to replicate in the presence or absence of Dex was investigated. GBM cell lines were treated with 1 MOI of Reo alone or combined with Dex at various time points.

The reduction in Reo-mediated oncolysis seen in the presence of Dex might be due to Dex-mediated reductions in cell surface expression of JAM-1, limiting Reo entry. However, Dex did not alter the expression of JAM-1 suggesting this is not the case (Figure 4.6.A). The possibility that Dex impairs Reo replication was also explored. Reo replication was analysed using a plaque assay, which demonstrated substantial replication in the cell lines tested, but there was with no significant change in viral titre in the presence of Dex (Figure 4.6.B). Lastly, GBM cells were collected at early and late time points (8 and 24 hours p.i) followed by RNA extraction to measure the copy number of the σ3 Reo RNA using real time (RT-qPCR). An increase of viral σ3 gene copy number was observed 24 hours p.i compared to 8 hours p.i (control group). However, no significant changes in the copy number of viral σ3 gene were observed between Reo alone and co-treated with Dex (Figure 4.6.C). Overall, these results show that Dex does not regulate virus entry or replication in GBM.

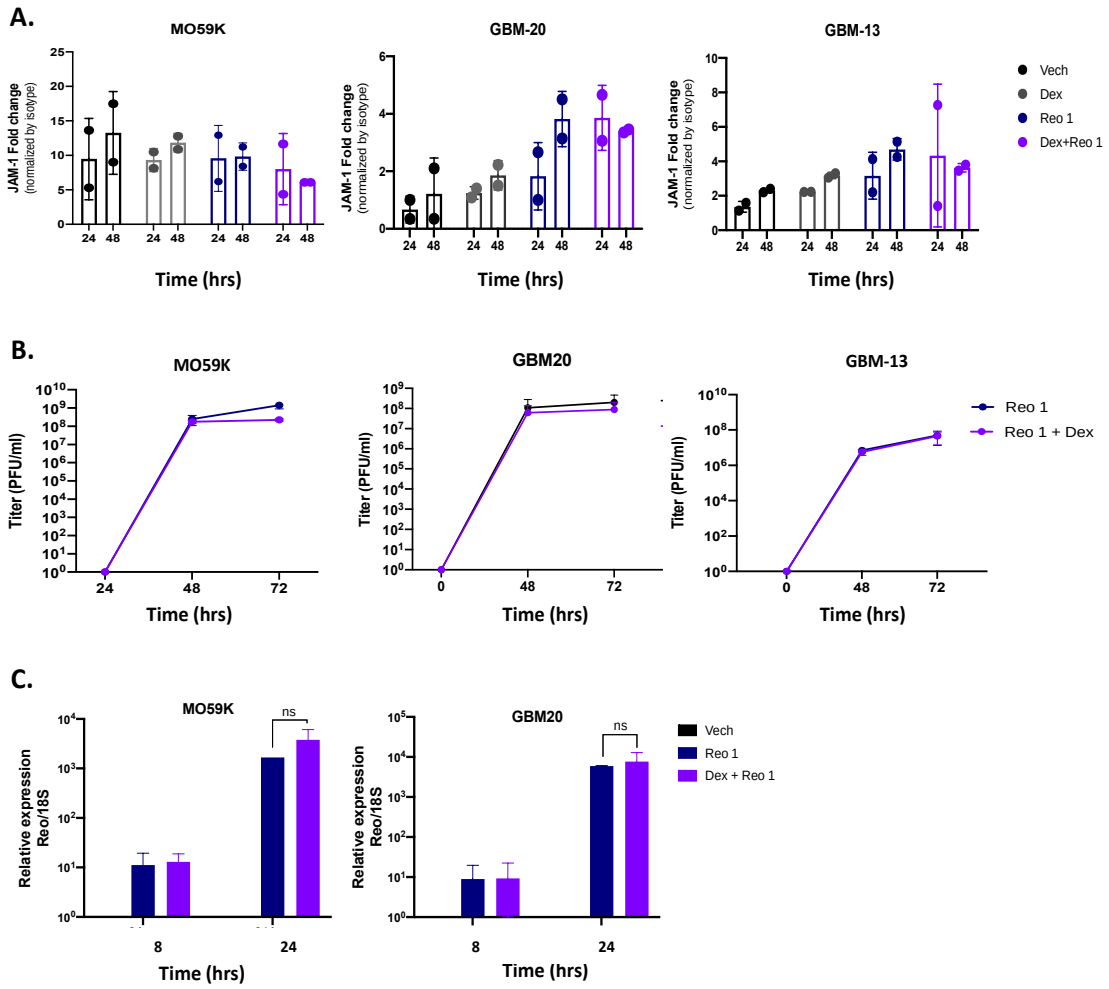

Figure 4-6 Dex does not regulate Reo entry or replication.

A. GBM cells (MO59K, GBM20, GBM13) were treated with Veh, 100nM Dex, Reo MOI1, Dex+ Reo MOI1 and the expression of the Reo entry receptor (JAM-1) was determined by flow cytometry at 24 and 48 hours post-treatment. **B.** Treated GBM cells with Reo MOI1 or Dex+ Reo MOI1 were collected to perform plaque assay on L929 cells at different time points to measure Reo cytopathic effects. **C.** RNA was extracted from treated cells at 8 and 24 hours post-treatment and the relative RNA level of Reo S4 genome segment (σ3) was determined by RT-qPCR normalized to 18S. Results graphed in **A**. and **C**. are for n=2 independent experiments and significance was tested with nonparametric one-way ANOVA with Dunn's multiple comparison test, while **B.** from n=3 independent experiments, and significance were tested using 2-way ANOVA with Tukey's multiple comparison test (ns $p>0.05$, *$p\leq0.05$, **$p\leq0.01$, ***$p\leq0.001$, and ****$p\leq0.001$).

Like many other viruses, Reo replicates in virus factories in infected cells (Antczak *et al.,* 1992). I visualized these replication factories in GBM cells in the presence or absence of Dex using the 2A9 antibody specific for the virus non-structural protein σNS. GBM cells (MO59K, GBM20, GBM13) were either untreated, treated with Reo alone at MOI of 1, or co-treated with Dex for 24 hours. Cells were fixed and co-stained with anti-σNS antibody (2A9) and DAPI to highlight nuclei. Images were taken on EVOS for random fields. The percentage of infected cells (2A9, green) compared to the total number of cells (nuclear, DAPI) ratio were calculated and plotted as percentage number of σNS positive cells using imageJ software to quantify the signal intensity. The results show that the percentage of σNS positive cells was not significantly different between cells infected with Reo alone or co-treated with Reo and Dex (Figure 4.7.A). Higher resolution images of MO59K cells were also taken using the TiE Eclipse microscope (Figure 4.7.B) which demonstrated the presence of discrete areas of σNS expression, consistent with previous reports identifying Reo replication factories (Kniert *et al.,* 2022). To confirm the observation that Dex did not alter σNS expression, the percentage of σNS positive cells was assessed by flow cytometry. Again, the results showed no significance difference between Reo infected GBM cells and those co-treated cells with Reo and Dex (Figure 4.7.C). In summary, these results show that Dex does not modulate the production of Reo σNS non-structural protein or the formation of viral factories for viral replication.

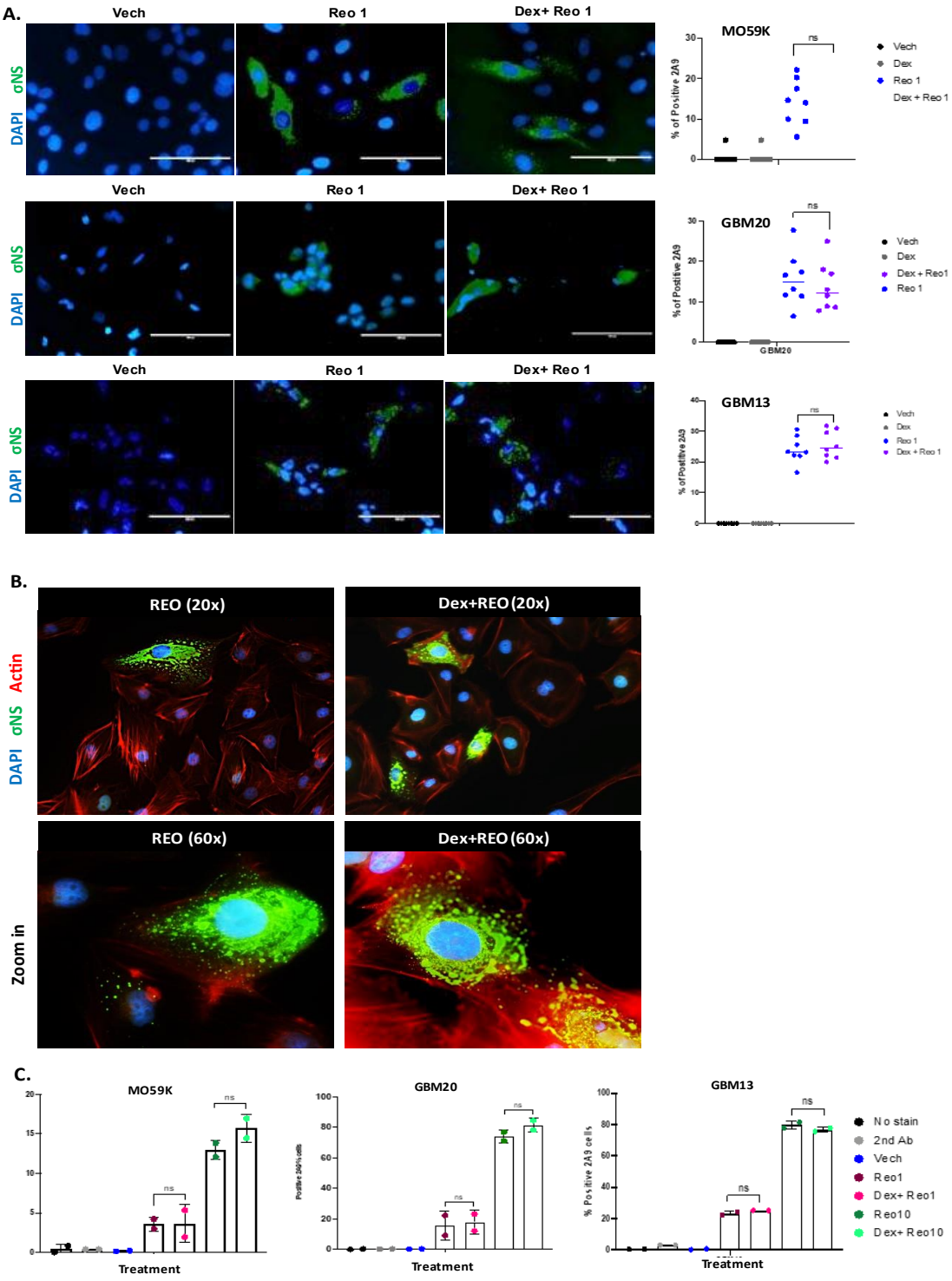

Figure 4-7 Dex don't regulate Reo σNS protein to form viral factories.

A. Treated GBM cells were for 24 hours were fixed and labeled with the monoclonal mouse σNS (2A9, green) and nucleus (DAPI, blue). The number of co-stained cells were quantified on EVOS and plotted as a percentage of the total number of positive 2A9 cells. A representative Image of GBM cells were taken by EVOS at power of 10x and **B.** MO59K cells stained with σNS (2A9, green), actin (red), and nucleus (DAPI, blue) were imaged by TiE Eclipse at power of 20X and 40X. Cells were treated with Reo (MOI 1, 10) alone or with 100nM Dex for 24 hours. **C.** Cells were also fixed for intracellular staining of 2A9 protein and measured by flow cytometry. All data were evaluated from n=2 independent experiments, and significant was tested with one-way ANOVA with multiple comparison test (ns>0.05, * p≤0.05, **p≤0.01, ***p≤001, and ****p≤0001).

4.2.3 Combination treatment of Dex and Reo on GBM cells is not mediated through apoptosis pathway

The results above show that Dex reduces Reo-mediated lysis of GBM cells. However, this reduction was not due to Dex-mediated inhibition of viral entry or replication. I hypothesised that Dex might reduce Reo-mediated oncolysis by interfering with cell death pathways. Previous studies have indicated that Reo induces cell death via several mechanisms, including caspase-mediated death (DeAntoneo *et al.,* 2022) and Dex was reported to reduce TMZ-induced apoptosis in GBM (Das A., *et al.,* 2004). Therefore, I analysed caspases 3, 7 on MO59K cells treated with Dex and Reo (alone or in combination) for 24 and 48 hours. Staurosporine (STS; a chemical stimulator of caspase activation) was used as a positive control for caspase cleavage. I examined different concentrations of STS and observed ~90% of cells had detached from the wells at high concentrations under the light microscope. Cells were stained with CellEvent Caspase-3/7 Green Ready Probes after 48 hours and images were taken by EVOS to count positive active caspase3/7 signals. The CellEvent reagent consists of a four-amino acid peptide (sequence DEVD) that is labelled with a green dye. When caspase 3/7 is activated in apoptotic cells, the DEVD peptide is cleaved, enabling the dye to bind to DNA and produce a fluorescent green signal. The number of cells positive for cleaved caspase3/7 activity were counted and plotted for three independent experiments. I used STS as a positive control for apoptosis induction and included the pan-caspase inhibitor Z-VAD in some experiments. Untreated cells, or cells treated with Dex or Z-VAD alone had low numbers of apoptotic cells compared to other groups. Reo alone induced significantly more caspase induction than control ($p=<0.0001$), and this effect was lost when combined with the caspase inhibitor (Z-VAD; $p=<0.0001$). Though STS combined with Dex showed higher apoptosis effect than STS alone, it could be due to the low STS concentration used in the experiment. Most importantly, there was no significant difference in caspase activation in Dex plus Reo treated cells compared to Reo alone, suggesting that the mechanism used by Dex to impair Reo mediated killing of GBM cells is caspase-independent (Figure 4.8).

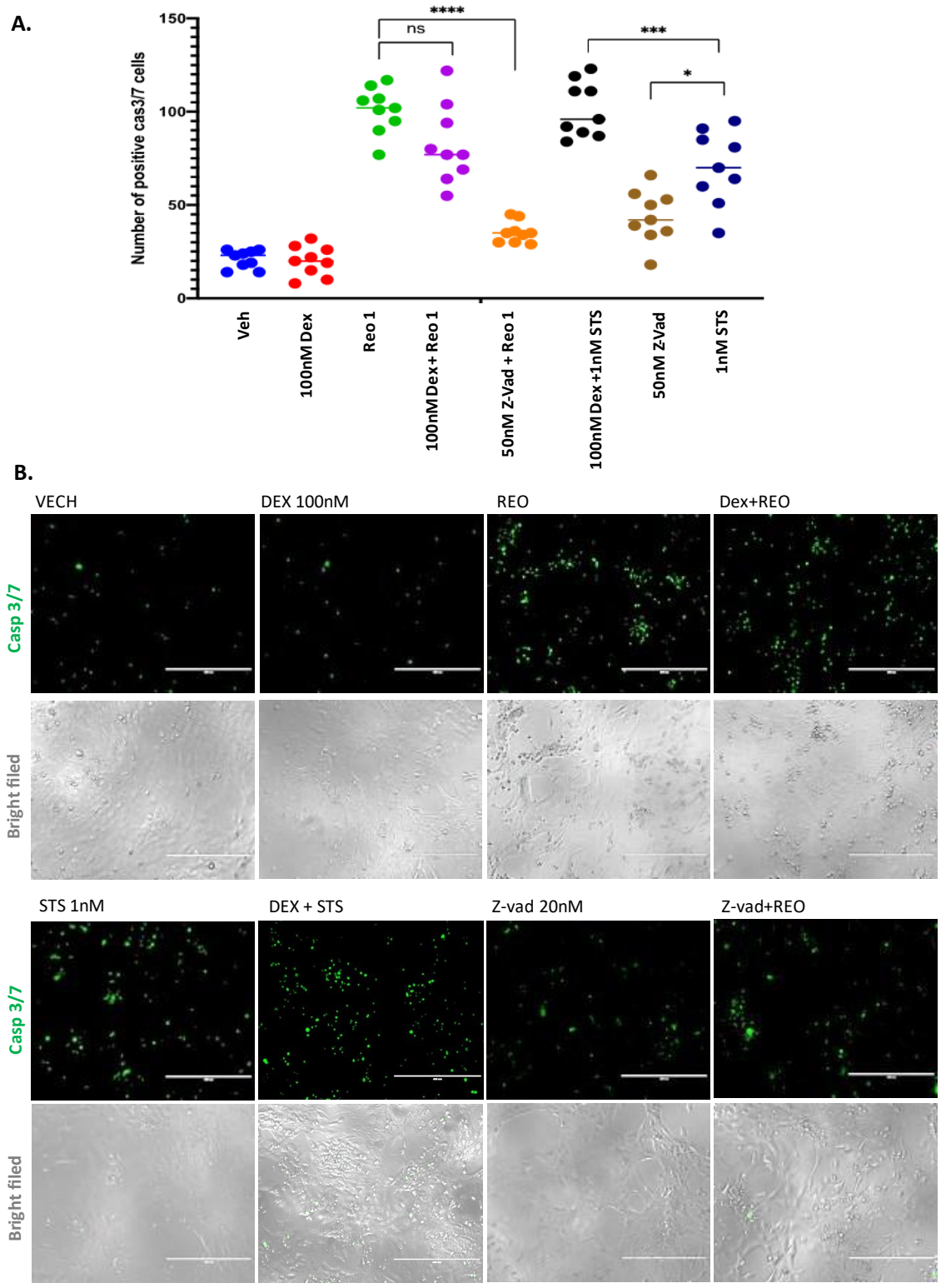

Figure 4-8 Apoptosis pathway on MO59K cells.

A. MO59K cells was treated with Veh, 100nM Dex, Reo MOI 1, or combination and caspase 3/7 was determined using cellevent readybrobe caspase3/7 in indicated groups, cells were treated with 20µM z-vad for an hour prior treatment with or without 1nM STS for 48 hours. caspase3/7 were then added and leave for 30min. Cells were imaged using EVOS microscope at power 10x to capture different fields (n=3), and significant was tested with one-way ANOVA with multiple comparison test (ns>0.05, * p≤0.05, **p≤0.01, ***p≤001, and ****p≤0001).. **B.** shows a representative image of each treatment conditions. The images were taken using the GFP filter (green) for the positive caspase cells and the bright field for the total unstained cells.

4.2.4 GC activates the GR in GBM cells

GR is phosphorylated at several sites including Ser-211, and this post-translational modification is a marker for the active form of the GR (Patt *et al.,* 2019). Dex activating GR through phosphorylation drives nuclear translocation of the GR, which permits interaction with DNA and effects on transcription. Once in the nucleus, GR can regulate hundreds of genes important for cell growth, cell cycle progression, and apoptosis (He *et al.,* 2014). I analysed the expression of GR and Ser-211 phosphorylation in response to Dex and Dex plus Reo treatment using Western blotting. Ligand induced phosphorylation of GR was evident after treatment with Dex alone and Dex and Reo combined (Figure 4.9.A). Western blots were quantitated (normalising against B-actin) which showed that there was no significant change in Ser-211 phosphorylation between Dex alone or Dex plus Reo (Figure 4.9.B). These data show that in GBM, GR activation is GC mediated and that co-treatment with Reo does not alter GR activation as assessed by phosphorylation of the Ser-211 residue.

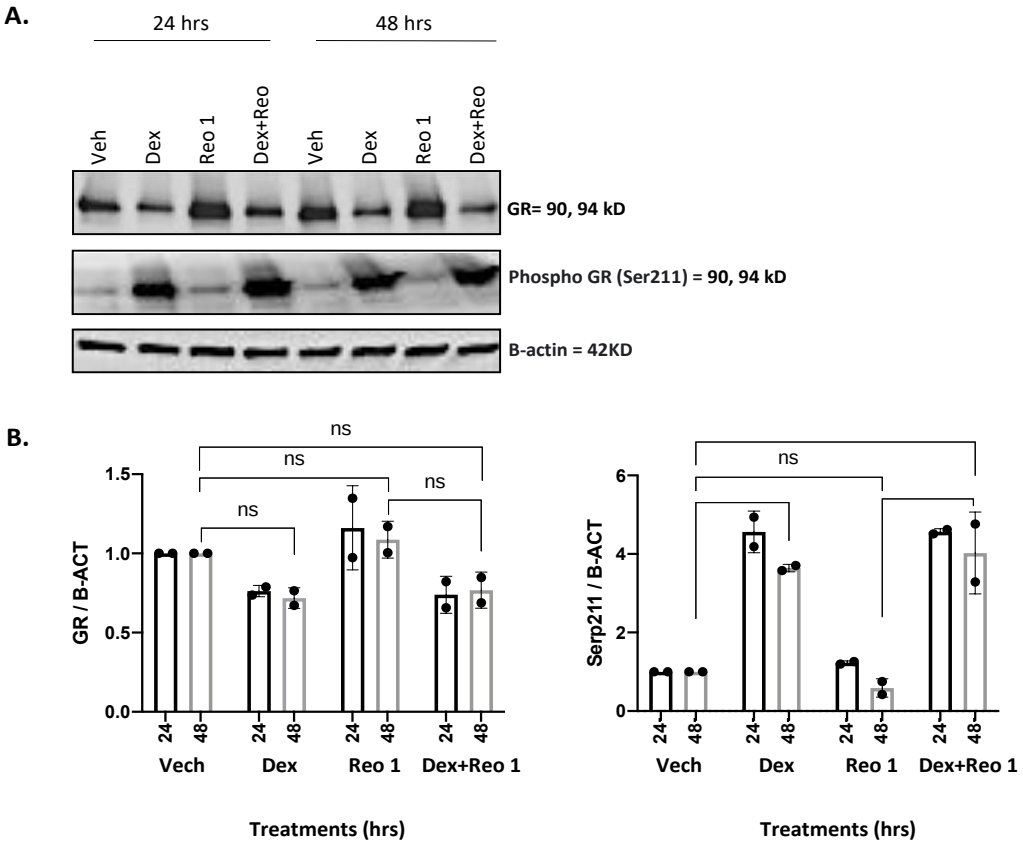

Figure 4-9 Dex activates Glucocorticoids receptor (GR) in MO59K cells.

Treated MO59K cells for 24 and 48 hours were lysed by RIPA buffer to extract proteins. **A.** Total GR and phosphorylated GR (Serp211) were detected by Western blot and **B.** the expression was normalised against B-actin for quantification and plotted for n=2 independent experiments (ns>0.05, * p≤0.05, **p≤0.01, ***p≤001, and ****p≤0001).

4.2.5 The effect of selective steroids combination treatment with reovirus in MO59K cells

GR regulates the expression of genes important in multiple pathways – most notably those that regulate cell fate, metabolism and inflammation. While Dex is the most potent anti-inflammatory known, long term use is often associated with side effects – typically relating to cell fate and metabolism. There has been significant effort in developing selective GCs that dissociate the anti-inflammatory effects (beneficial) from those on cell fate and metabolism (detrimental). Here, a small panel of selective steroids (AZD7594, Vamorolone, Compound A; see materials of methods) were investigated alongside Dex to determine the effect on Reo mediated direct killing of GBM cells. The MO59K cell line was treated with 100nM GC alone or co-treated with Reo for 48 hours and then stained with live/dead dye for flow cytometry analysis. As previously shown, Reo killed GBM cells and this was significantly reduced by Dex treatment. The selective steroids all reduced the killing of GBM by Reo but this reduction did not reach statistical significance compared to Reo alone, but the trend is similar to Dex. Surprisingly, the selective steroids appeared to have a cytotoxic effect in GBM cells in the absence of Reo (Figure 4.10).

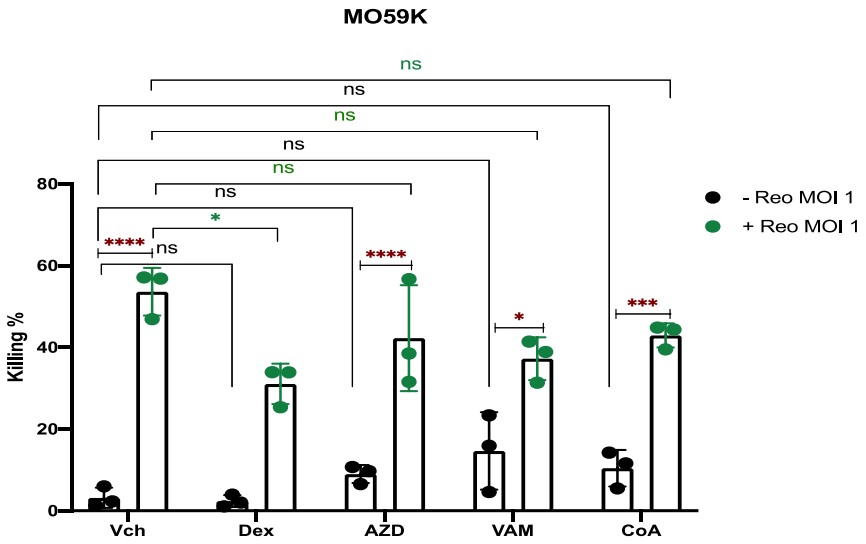

Figure 4-10 Screen of selective GCs as alternative to Dex in GBM treatment.

MO59K cells was treated with selective GCs (AZD, Vam, CoA) and Reo for 48 hours. The killing % was determined by Live/dead stain using flow cytometry. The data are presented as mean ± SEM for n=2 independent donors, and significance was tested using 2-way ANOVA with Tukey's multiple comparison test (ns>0.05, *p≤0.05, ** p≤0.01, ***p≤001, and ****p≤0001).

The results above show that Dex reduces Reo-mediated lysis of GBM cells. However, entry receptor expression, viral replication and caspase activation were unaffected by Dex treatment. I speculated that comparing the action of selective GC to Dex might provide a route to understanding the mechanism but unfortunately, there was no clear difference between Dex and the selective GC. I therefore used RNA-seq as a global approach to attempt to define the mechanisms of action.

4.2.6 Optimising samples condition for total RNA sequencing

It was necessary to optimise the timing of the analysis to allow biologically relevant effects of both Dex and Reo to be detected in the RNA-seq data. The killing assays demonstrated cell death at 48 or 72 hours, but the transcriptional changes that cause them likely occur much sooner. The combination treatment of Dex with Reo can have a complex, time-dependent effect on gene expression. For example, the transcriptional effects of Dex can occur as quickly as 1 hour of treatment, and typically peaks around 6 hours post treatment (Pascussi *et al.,* 2000). While transcriptional changes can still be detected 24-48 hours post treatment, the effect is smaller, and is gene dependent. Reo infects tumour cells within 4 hours, replicates within 16 hours post-infection and can remain for up to 48 hours (Irvin *et al.,* 2011). The anti-viral and anti-tumour immune response was reported to be detected by 24 hours post-infection.

A preliminary screening was first conducted on two cells lines, the long-established cell line MO59K and patient-derived GBM20 cell line. Cells were treated with Veh, Reo alone, or combined with Dex for mid and late time-points (8 and 24 hours). For this assessment, RNA was extracted from samples for RT-PCR to evaluate baseline of selected genes reported to be regulated by Dex or Reo (GILZ, RIG1, TNF, IL-6, IFTIM3, and IFNB); RIG1 and IFTIM3 are Reo regulated genes, Glucocorticoid-induced leucine zipper (GILZ, or TSC22D3) is a key Dex-regulated gene, while IL-6, IFNB, TNF are regulated by both Reo and Dex.

The results showed that IL-6, IFNB, TNF were not detectable 8 hours post-treatment in either cell line, but Reo significantly induced their expression (tens to hundreds of fold) after 24 hours (Figure 4.11.A-C). Combining Dex with Reo significantly reduced the gene expression of IL-6 and TNF in GBM20 in comparison to Reo alone, consistent with the ability of Dex to reduce expression of inflammatory mediators. TNF expression was reduced after 24 hours in MO59K cell line (Figure 4.11. A-C), although this did not reach statistical significance (p.value = 0.055). Expression of RIG-I was relatively unaffected by the different treatments, although Reo treated GBM20 cells showed a small (~1.5 fold) but statistically significant induction after 24 hours (Figure 4.12.A). IFITM3 expression increased significantly in both cell lines treated with Reo and this was not significantly changed following the addition of Dex, suggesting that Dex did not blunt this virus-mediated response (Figure 4.12.B). Both cell lines treated with Dex alone or combined with Reo showed significant increase in GILZ expression at early stage (8 hours), consistent with the long-established and potent GR-mediated induction of this gene by Dex (Zeiner *et al*., 2019). However, the kinetics of GILZ induction differed in MO59K and GBM20, with expression peaking at 8 hours in MO59K but persisting until at least 24 hours in GBM20 (Figure 4.12.C). Overall, both MO59K and GBM20 showed significant changes in gene expression profile at 24 hours post-treatment. Although GBM20 showed higher significant gene expression, and is more representative of GBM patient tumours features, it grows very slowly compared to MO59K and hence the latter cell line was used in the RNA-seq analysis.

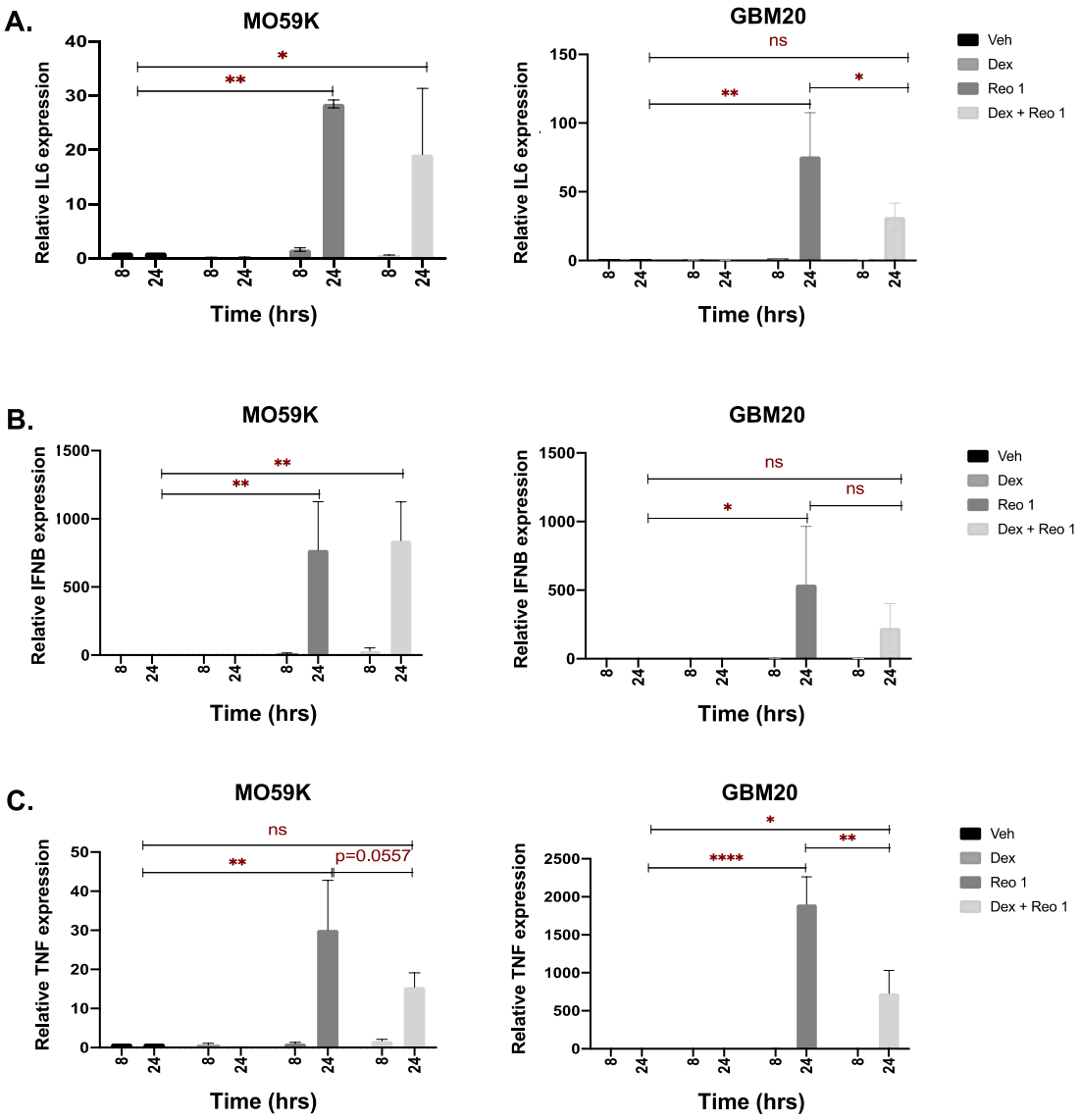

Figure 4-11 Effect of Dex on Reo regulating cytokines gene expression.

MO59K cells and GBM20 cells were treated with Veh, Dex, Reo, Dex plus Reo and the expression of a panel of Reo and Dex regulated genes were determined by qRT-PCR at indicated time points. Expression of **A.** IL-6, **B.** IFNB, and **C.** TNF genes were normalized to ACT-B. Graphs depict fold change in gene expression relative to Veh control. The data are presented as mean ± SEM for n=2 independent experiments and significance was tested with 2-way ANOVA with Tukey's multiple comparison test. (ns>0.05, * p≤0.05, **p≤0.01, ***p≤001, and ****p≤0001).

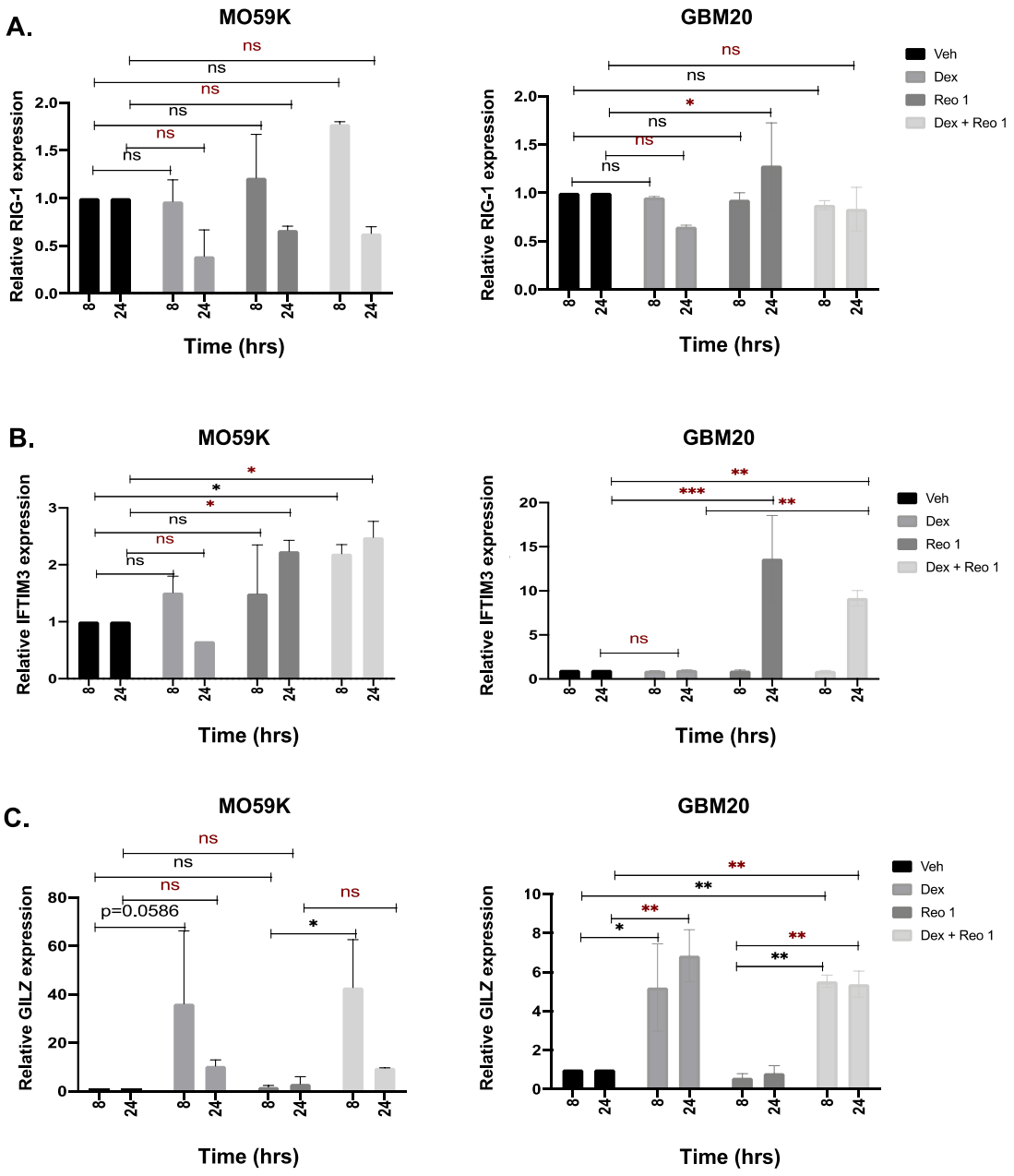

Figure 4-12 Effect of Dex on Reo regulating candidate gene expression.

MO59K cells and GBM20 cells were treated with Veh, Dex, Reo, Dex plus Reo and the expression of a panel of Reo and Dex regulated genes were determined by qRT-PCR at indicated time points. Expression of **A.** RIG-1, **B.** IFTIM3, and **C.** GILZ genes were normalized to ACT-B. Graphs depict fold change in gene expression relative to Veh control. Data show the mean ± SEM for n=2 independent experiments and significant was tested with 2-way ANOVA with Tukey's multiple comparison test (ns>0.05, * p≤0.05, **p≤0.01, ***p≤001, and ****p≤0001).

4.2.7 Sample preparation and the quality control for RNA-seq

RNA-seq analysis was used to understand the effect of Dex on Reo efficacy at the gene expression level. All RNA samples from MO59K cells treated with Veh, Reo or ReoDex, had passed the quality control (QC) test by Novogene with RIN score above 9 (Table 4.1). RNA sequencing was performed using Illumina platform carried out by Novogene (Cambridge, UK).

Table 4-1 RNA samples quality control (QC). All samples passed the QC with RIN score > 9

Culture model	Sample condition	Sample code
Single culture	MO59K_Veh	GBM_Veh_A GBM_Veh_B GBM_Veh_C
	MO59K_Reo MOI 1	GBM_Reo_A GBM_Reo_B GBM_Reo_C
	MO59K_Reo MOI 1 + 100nM Dex	GBM_ ReoDex_A GBM_ ReoDex _B GBM_ ReoDex _C

The quality control of the raw RNA-seq data was examined to ensure that the RNA samples are reliable. The raw data was formatted on FASTQ file, filtered to obtain clean reads, and mapped on hisat2 software. The gene expression was calculated by the number of mapped reads. The distribution of gene expression level was calculated using FPKM method and plotted in box bar, showing that the gene expression level was similar between the groups indicating that the replicates are comparable (Figure 4.13.A). Results of the principal component analysis (PCA) was plotted, showing clustering of replicates and clear separation of treatment groups (Figure 4.13.B). A heat map of DEGs demonstrated the hierarchical clustering with distinct expression pattern (Figure 4.13.C).

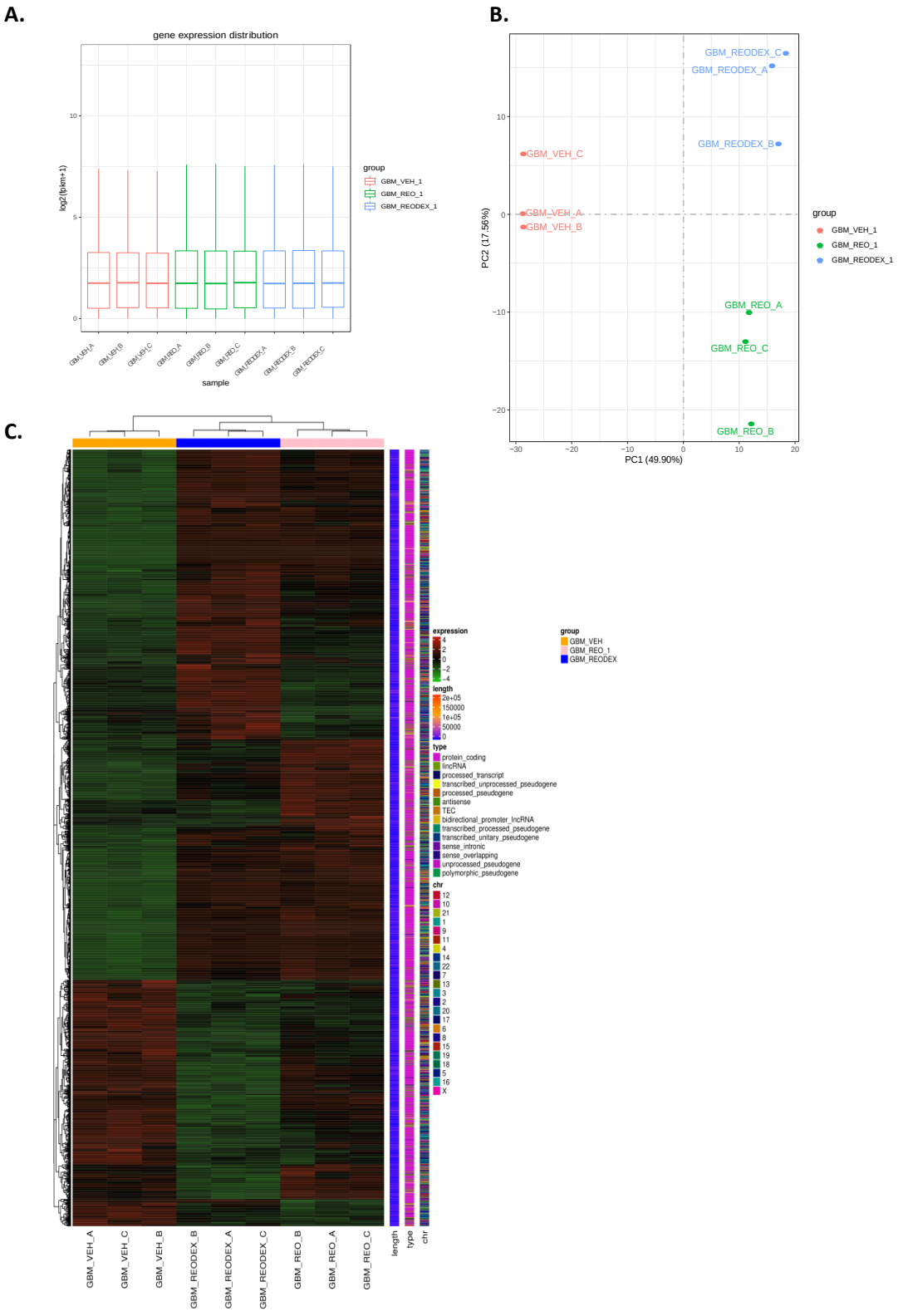

Figure 4-13 RNA-seq data quality.

A. The box plot of the gene expression distribution between the treatment groups based on log10 (FPKM+1) values. **B.** Principal component analysis (PCA) plot normalized expression values of GBM cells untreated and treated estimated raw counts of differentially expressed genes. **C.** Hierarchical clustering heatmap of RNA-seq. the heatmap shows the overall result in all treatment groups (three replicates each) displayed differences in gene expression levels. The colour scale illustrates a high relative expression level (red) and low relative expression level (green).

Figure 4.14 shows a representative image of the RNA-seq samples error rate distribution, data filtering and reference genome alignment. Table 4.2 shows the details of the clean reads results. Table 4.3 shows the reference genome comparison including the percentage of Exon, Intron, Intergenic reads, and Table 4.4 shows the error rate distribution.

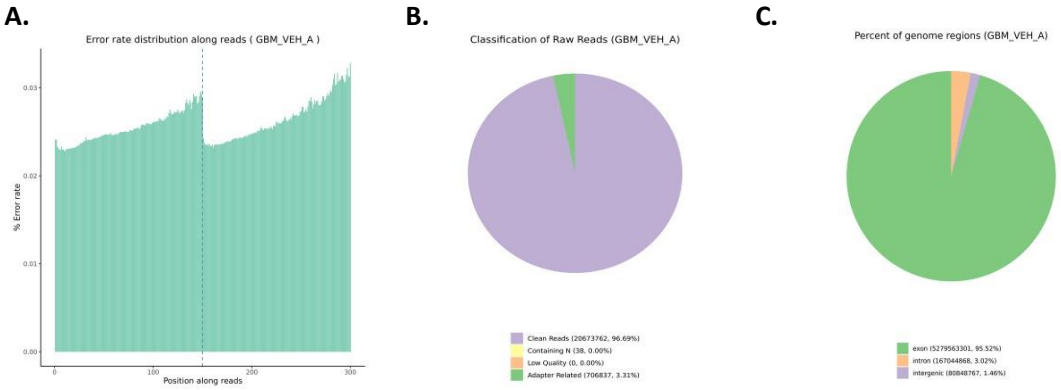

Figure 4-14 The quality control of the RNA-seq samples.

The representative images show **A.** the error rate distribution. **B.** Sample sequencing data filtering and **C.** reference genome alignment of the RNA-seq samples.

Table 4-2 The details of the transcriptome assembly result

Sample	library	raw_reads	raw_bases	clean_reads	clean_bases	error_rate	Q20	Q30	GC_pct
GBM_VEH_A	ERAS230059182 -1r	42761274	6.41G	41347524	6.2G	0.03	97.55	93.45	50.87
GBM_VEH_B	ERAS230059183 -1r	40212726	6.03G	38796398	5.82G	0.03	97.6	93.53	50.05
GBM_VEH_C	ERAS230059184 -1r	44757350	6.71G	43247624	6.49G	0.03	97.64	93.64	51.67
GBM_REO_A	ERAS230059185 -1r	44786278	6.72G	43209664	6.48G	0.03	97.67	93.7	51.03
GBM_REO_B	ERAS230059186 -1r	43996632	6.6G	42957946	6.44G	0.03	97.63	93.55	48.99
GBM_REO_C	ERRA230059187 -1a	61213996	9.18G	59848186	8.98G	0.03	96.95	92.24	50.62
GBM_REODEX_A	ERAS230059188 -1r	47730972	7.16G	45519552	6.83G	0.03	97.64	93.62	51.55
GBM_REODEX_B	ERAS230059189 -1r	62564314	9.38G	59502742	8.93G	0.03	97.43	93.29	50.36
GBM_REODEX_C	ERAS230059190 -1r	52989648	7.95G	50208570	7.53G	0.03	97.68	93.77	51.51

Table 4-3 Samples and reference genome comparison statistics

sample	exon	intron	intergenic
GBM_VEH_A	5279563301(95.5153%)	167044868(3.0221%)	80848767(1.4627%)
GBM_VEH_B	4963113721(95.0498%)	184359583(3.5307%)	74118691(1.4195%)
GBM_VEH_C	5603731600(95.3233%)	193535545(3.2922%)	81391565(1.3845%)
GBM_REO_A	5590415996(95.6977%)	173671218(2.9729%)	77658704(1.3294%)
GBM_REO_B	5669402563(96.0261%)	162633535(2.7546%)	71986179(1.2193%)
GBM_REO_C	8027867225(95.0041%)	295427314(3.4962%)	126727016(1.4997%)
GBM_REODEX_A	5950939799(95.3513%)	212251624(3.4009%)	77877075(1.2478%)
GBM_REODEX_B	7511950349(95.1380%)	272121141(3.4464%)	111769928(1.4156%)
GBM_REODEX_C	6422249261(94.1054%)	301964981(4.4247%)	100313278(1.4699%)

Table 4-4 RNA-seq error rate distribution reads.

sample	total_reads	total_map	unique_map	multi_map	read1_map	read2_map	positive_map	negative_map	splice_map	unsplice_map	proper_map
GBM_VEH_A	41347524	37044195(89.59%)	36022757(87.12%)	1021438(2.47%)	18053937(43.66%)	17968820(43.46%)	17957422(43.43%)	18065335(43.69%)	16947683(40.99%)	19075074(46.13%)	32051386(77.52%)
GBM_VEH_B	38796398	35003707(90.22%)	34107391(87.91%)	896316(2.31%)	17096903(44.07%)	17010488(43.85%)	16996052(43.81%)	17111339(44.11%)	15536663(40.05%)	18570728(47.87%)	29054186(74.89%)
GBM_VEH_C	43247624	39370063(91.03%)	38269250(88.49%)	1100813(2.55%)	19161518(44.31%)	19107732(44.18%)	19082670(44.12%)	19186580(44.36%)	18495816(42.77%)	19773434(45.72%)	34721022(80.28%)
GBM_REO_A	43209664	39144786(90.59%)	38073633(88.11%)	1071153(2.48%)	19051705(44.09%)	19021928(44.02%)	18981966(43.93%)	19091667(44.18%)	17963697(41.57%)	20109936(46.54%)	33029278(76.44%)
GBM_REO_B	42957946	39541698(92.05%)	38534104(89.7%)	1007594(2.35%)	19310574(44.95%)	19223530(44.75%)	19210771(44.72%)	19323333(44.98%)	17660429(41.11%)	20873675(48.59%)	34037710(79.23%)
GBM_REO_C	59848186	56449185(94.32%)	54871159(91.68%)	1578026(2.64%)	27520020(45.98%)	27351139(45.7%)	27412936(45.8%)	27458223(45.88%)	24172035(40.39%)	30699124(51.29%)	53249066(88.97%)
GBM_REODEX_A	45519552	41796374(91.82%)	40638388(89.28%)	1157986(2.54%)	20366716(44.74%)	20271672(44.53%)	20272424(44.54%)	20365964(44.74%)	19783434(43.46%)	20854954(45.82%)	36481810(80.15%)
GBM_REODEX_B	59502742	52942451(88.97%)	51474880(86.51%)	1467571(2.47%)	25791055(43.34%)	25683825(43.16%)	25649952(43.11%)	25824928(43.4%)	23389292(39.31%)	28085588(47.2%)	45049204(75.71%)
GBM_REODEX_C	50208570	45724559(91.07%)	44415808(88.46%)	1308751(2.61%)	22238813(44.29%)	22176995(44.17%)	22153783(44.12%)	22262025(44.34%)	20615341(41.06%)	23800467(47.4%)	39574688(78.82%)

4.2.8 Enrichment analysis of the DEGs

Bioinformatic analysis was carried out to profile the transcriptome of treated MO59K cells and compare between the treated groups indicated in Table 4.5.

Table 4-5 DEGs samples comparison.

Sample 1	Sample 2	Description
GBM_Veh	GBM_Reo	Genes regulated by Reo
GBM_Veh	GBM_ReoDex	Genes regulated by Reo and/or Dex
GBM_Reo	GBM_ReoDex	Genes regulated by Dex

The RNA-seq results displayed all the DEGs with cut offs of p.adj of ≤ 0.05 and Log2Fold Change of ≥1 or ≤ -1. Results identified 983 DEGs in GBM cells treated Reo in comparison to vehicle as showed in in the volcano plot (Figure 4.15.A), indicating the increase of upregulated genes upon Reo treatment (85%, red) than downregulated genes (15%, green). 1523 DEGs were identified in GBM treated ReoDex in comparison to vehicle (Figure 4.15.B), showing a skew in the percentage of upregulated genes upon the co-treatment (67%, red) toward more downregulated genes (33%, green). It also identified in 488 DEGs in GBM treated ReoDex in comparison to Reo alone (Figure 4.15.C), showing equal percentage between upregulated and downregulated genes (45%, red and 54%, green respectively).

Next, KEGG pathway enrichment analysis of the DEGs for Reo and ReoDex highlighted potential pathways that are important to understand how Dex impairs Reo efficacy to kill GBM cells. By applying a statistical cut-off of pathways to adj.p <0.05, several common terms were identified in all comparison analysis, including: TNF signalling pathway, viral protein interaction with cytokines and cytokines receptors, NF-kB signalling pathway, Interferon signalling, and apoptosis (Figure 4. 14, middle) as listed in Tables 7.7 and 7.8. Additionally, a protein-protein interaction network (PPI) was developed for the DEGs and identified the top 20 hub genes (Figure 4.14, right) which are presented in Table 4.6.

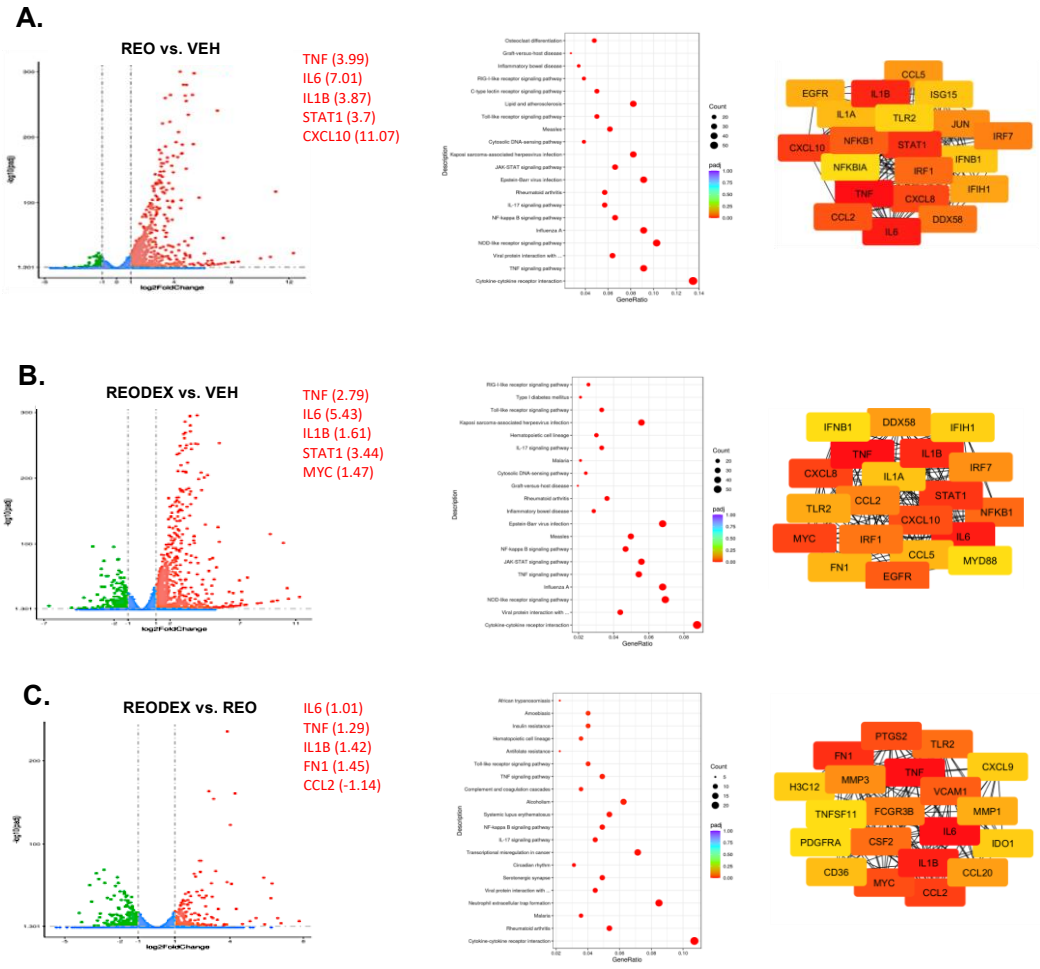

Figure 4-15 The DEGs identified in MO59K treated cells.

Volcano plot of the differentially expressed genes (DEGs) between **A.** Veh vs. Reo **B.** Veh vs. ReoDex and **C.** Reo vs. ReoDex. KEGG pathways enrichment analysis of the DEGs of the three comparison groups, and displaying the top enriched terms in a dot plot chart. The horizontal axis defines the ratio of DEGs annotated on each pathway term. The vertical axis defines the top 20 pathways with significant enrichment. STRING analysis for the PPI network, exported into cytoscape software to identify the top hub genes.

Table 4-6 Top hub genes in the single culture.

REO DEGs				REODEX DEGs				DEX modifying REO DEGs			
Rank	Name	score	Log 2FC	Rank	Name	score	Log 2FC	Rank	Name	score	Log 2FC
1	TNF	247	3.99	1	TNF	265	2.79	1	IL6	104	-1.57
1	IL6	228	7.01	2	IL6	257	5.43	1	TNF	104	-1.19
3	IL1B	217	3.87	3	IL1B	232	1.61	3	IL1B	96	-2.25
4	STAT1	196	3.70	4	STAT1	212	3.44	4	FN1	69	1.07
5	CXCL10	171	11.07	5	MYC	179	1.47	5	CCL2	67	-1.14
6	CXCL8	170	5.09	5	CXCL8	179	4.3	6	MYC	54	1.57
6	CCL2	157	4.69	7	CXCL10	178	10.1	7	PTGS2	54	-2.86
8	NFKB1	156	1.65	8	EGFR	176	1.37	8	VCAM1	47	-1.6
9	IRF1	154	2.50	9	NFKB1	170	1.1	9	CSF2	45	-1.18
10	DDX58	147	5.46	10	IRF1	159	2.58	10	TLR2	45	1.12
11	JUN	140	1.42	11	IRF7	148	3.83	11	FCGR3B	39	1.49
12	IRF7	141	3.69	12	CCL2	158	3.54	12	MMP3	37	-2.23
13	CCL5	139	6.12	13	DDX58	147	5.4	13	CCL20	36	1.37
14	IFIH1	135	4.77	14	TLR2	144	5.05	14	MMP1	35	-1.98
15	EGFR	134	1.11	15	CCL5	142	3.54	15	CD36	34	2.47
16	IL1A	130	4.76	16	FN1	142	1.19	16	CXCL9	32	-1.47
17	ISG15	129	4.99	17	IL1A	134	3.96	17	H3C12	32	1
18	TLR2	126	3.93	18	IFIH1	134	4.69	18	IDO1	32	-1.11
19	IFNB1	129	8.47	19	IFNB1	133	9.27	19	TNFSF11	30	-1.78
20	NFKBIA	125	1.94	20	MYD88	133	2.37	20	PDGFRA	30	1.25

Most of the hub genes were expressed by both Reo and ReoDex treatment group with high degree of connectivity. Notably, both MYC and FN1 genes were differentially expressed under ReoDex treatment, while JUN was differentially expressed under Reo treatment. MYC showed to be upregulated in GBM. It was reported that MYC promotes cell proliferation, programmed cell death, and was required for GBM stem cells survival (Annibali *et al.,* 2014; Wang *et al.,* 2008). Although it was demonstrated that GCs inhibit c-MYC in cancer, the combination treatment with Reo showed significant increase in MYC gene expression. Upregulation of MYC by ReoDex might mean that this combination of agents could be detrimental to patient outcomes. Similarly, FN1 (fibronectin-1) upregulation is associated with poor prognosis in GBM patients (Kabir *et al.,* 2022) and induction of FN1 by ReoDex might represent a barrier to this combination strategy. The top three ranked hub genes are TNF, IL-6 and IL-1B in all DEGs comparisons, all of which were upregulated by Reo and ReoDex, but downregulated with comparing Reo vs. ReoDex, suggesting that Dex downregulated the expression of these genes. Both PTGS2 and IDO1 genes expression were upregulated by Reo in comparison to ReoDex, suggest Dex role in reducing inflammation which benefit GBM patients to reduce brain oedema.

Expression of these identified hub genes was analysed in the RNA-seq data (Figure 4.16.A). A luminex assay was performed to validate TNF expression in MO59K cells, and results showed the significant increase expression of TNF under Reo treatment (Figure 4.16.B).

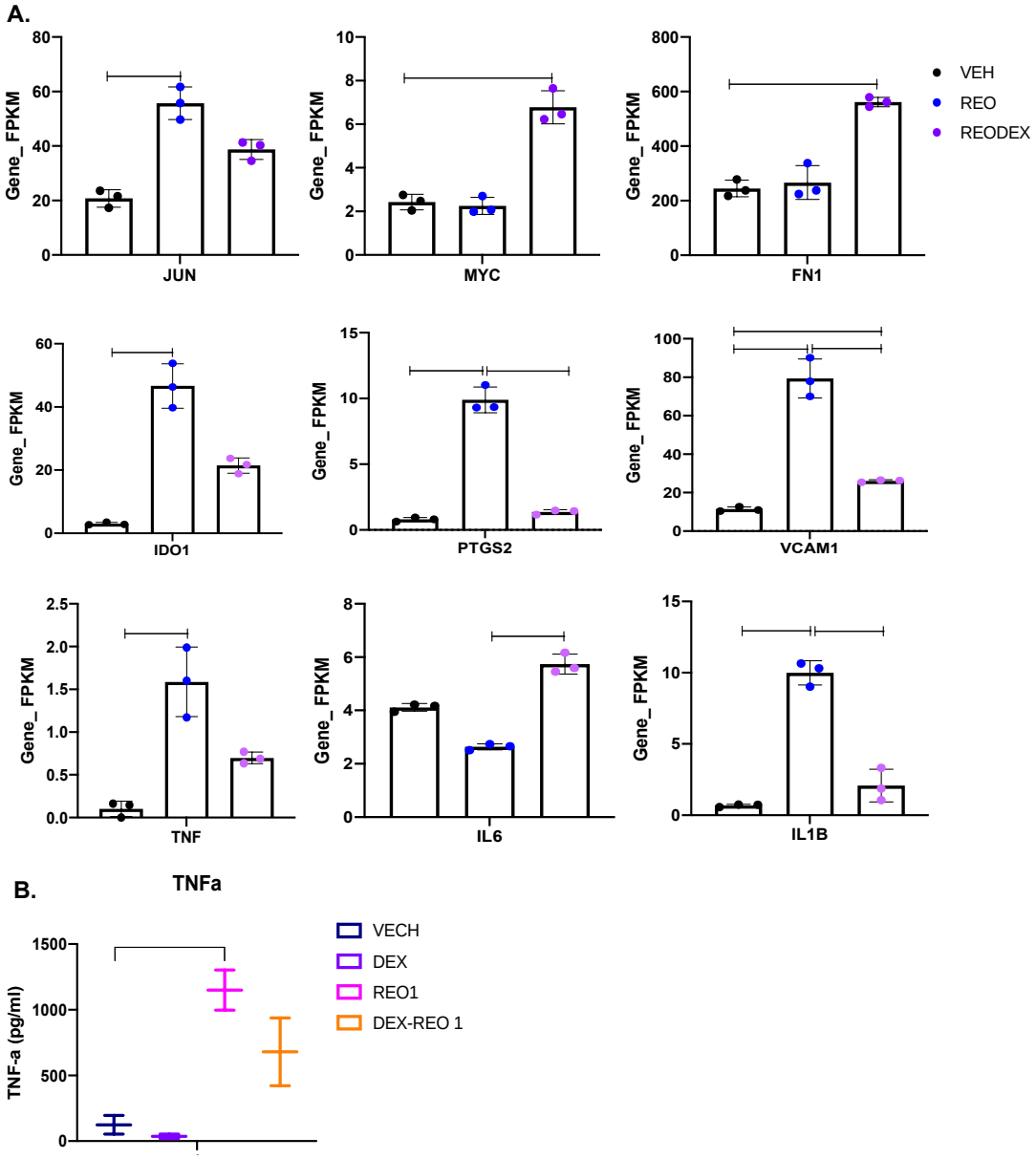

Figure 4-16 The expression of the top hub genes regulated by Dex.

A. The level of gene expression (-FPKM) of JUN, MYC, and FN1, IL-6, TNF, IL-1B as a top hub gene specific for Reo or ReoDex treatment. Data shows the mean ± SEM for n=3 independent samples one-way ANOVA with multiple comparison test. **B.** TNFa validation using Luminex assay from n=2 independent experiments, each in duplicate, and significance was tested with nonparametric one-way ANOVA with Dunn's multiple comparison test (ns $p>0.05$, *$p\leq0.05$, **$p\leq0.005$, ***$p\leq0.001$, and ****$p\leq0.001$).

Next, a Venn diagram was generated for the DEGs of the three comparison groups (Table 4.5) which identified 65 common genes (Figure 4.17.A). A heat map of the 65 common genes (Figure 4.17.B) showed that most of the genes are similarly up or downregulated among the three comparison, and five genes were differentially expressed (SLCO2B1, TNFSF18, TSC22D3, SLCO2A1, and SYBU). Dex was reported to induce TSC22D3 (GILZ), while downregulates TNFSF18 (GITR). TSC22D3 regulate immune cells activation such as T cells (Cannarile *et al.,* 2019), its promoter binds to FOXO, STAT6, NFAT, c-MYC, and reported to be induced by GCs in melanoma through the PI3k/Akt pathway (Grugan *et al.,* 2008). Figure 4.17.C showing that Dex influenced Reo by inducing TSC22D3 gene-FPMK level while downregulated TNFSF18. Among the 65 genes, an increase expression of DUSP1 by ReoDex was observed. DUSP1 is one of the most common GC target genes that inhibits several pathways including MAPK, ERK1/2 signalling (Mills *et al.,* 2017). DUSP1 is highly expressed in GBM tissue, and the gene FPMK level was upregulated by Reo alone or combined with Dex, but the combination treatment has significant increase in expression compared to Reo alone. This suggests that GR and Reo work cooperatively to regulate DUSP1.

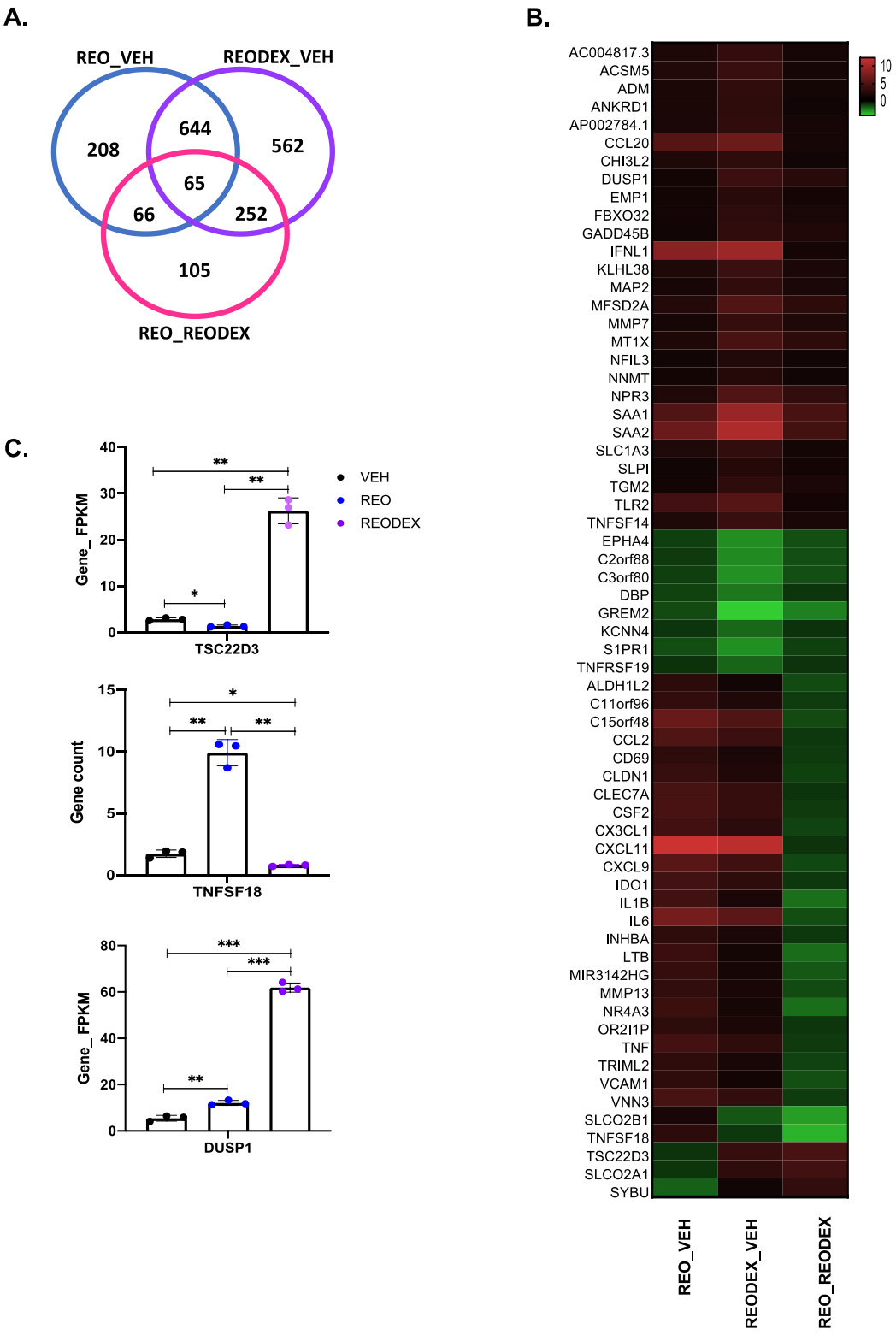

Figure 4-17 Identifying 65 overlapping DEGs between the comparison groups.

A. Venn diagram identified common genes between the three comparisons **B.** The heat map of the common 65 DEGs showing genes with similar or obesities direction between the three comparisons **C.** The level of gene expression (-FPKM) of TSC22D3, TNFSF18, and DUSP1 genes. The data are presented as mean ± SEM for n=3 independent samples, and significance was tested using a one-way ANOVA with multiple comparison test (ns p>0.05, *p≤0.05, **p≤0.005, ***p≤0.001, and ****p≤0.001).

I then compared the 65 common genes (those regulated by Reo, and also by ReoDex, but significantly different between treatments) and their relation to GBM overall survival (OS) and identified 12 genes (IL-6, TNFSF14, CCL2, CCL20, SAA1, SAA2, KCNN4, ADM, LTB, CHI3L2, MMP13, SLPI) to correlate with GBM prognosis. Gepia2 analysis showed the significant increase in gene expression level in GBM compared to normal samples in IL-6, CCL2, CCL20, SAA1, SAA2, ADM, SLPI, and CHI3L2 (Figure 4.18 and 4.19, right). GBM poor survival showed a significant association with LTB, MMP13, and KCNN4, TNFSF14, SAA1/2, CHI3L2, and ADM for which gene downregulation is associated with GBM poor survival (Figure 4.18 and 4.19, left).

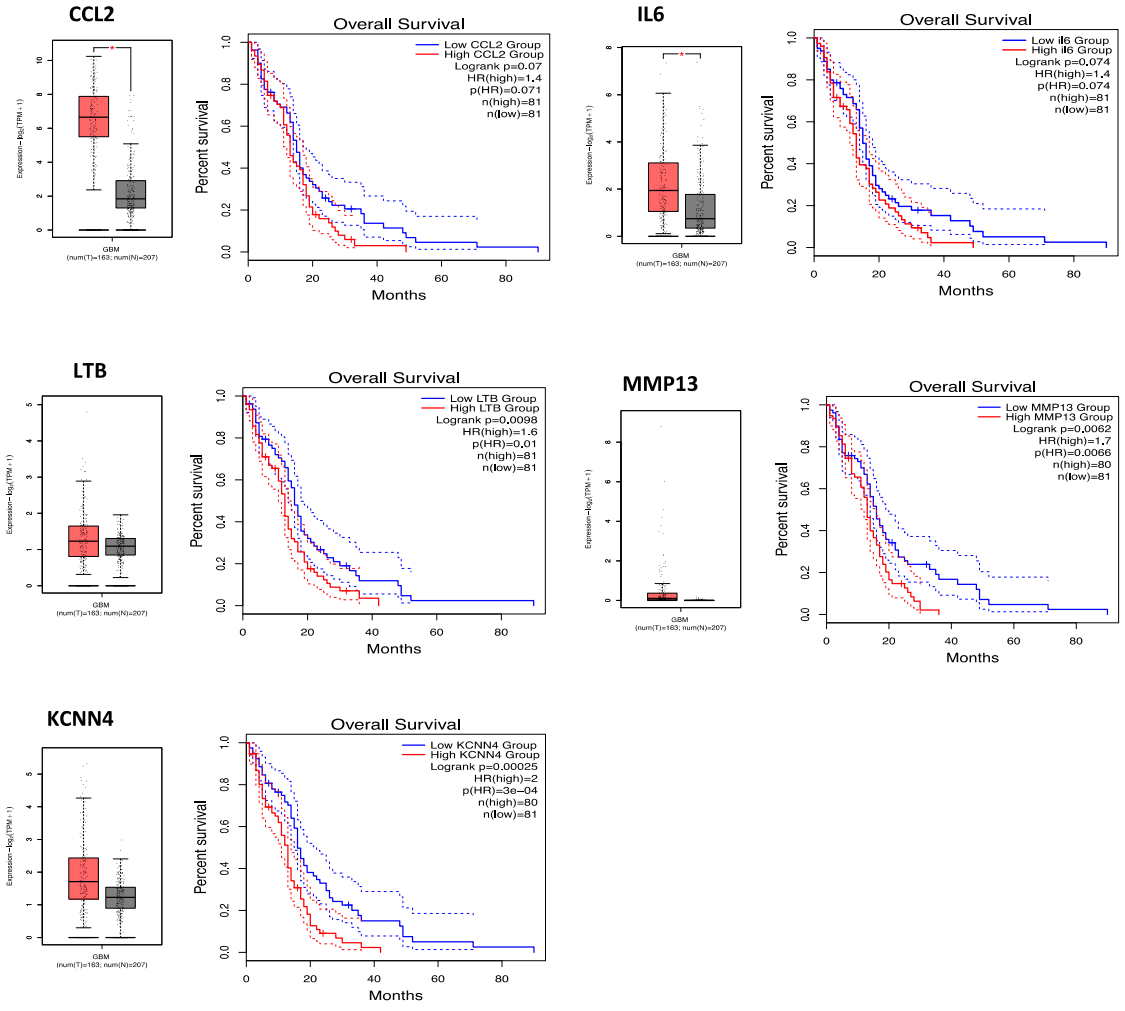

Figure 4-18 DEGs downregulated by ReoDex and associated with GBM prognosis.

Gepia2 website tool presented genes expression level on GBM tissue (red) compared to normal brain tissue (gray) in a box-plot (left side), and their association with GBM poor survival (left side) presented as a Kaplan-Meier survival curve based TCGA database.

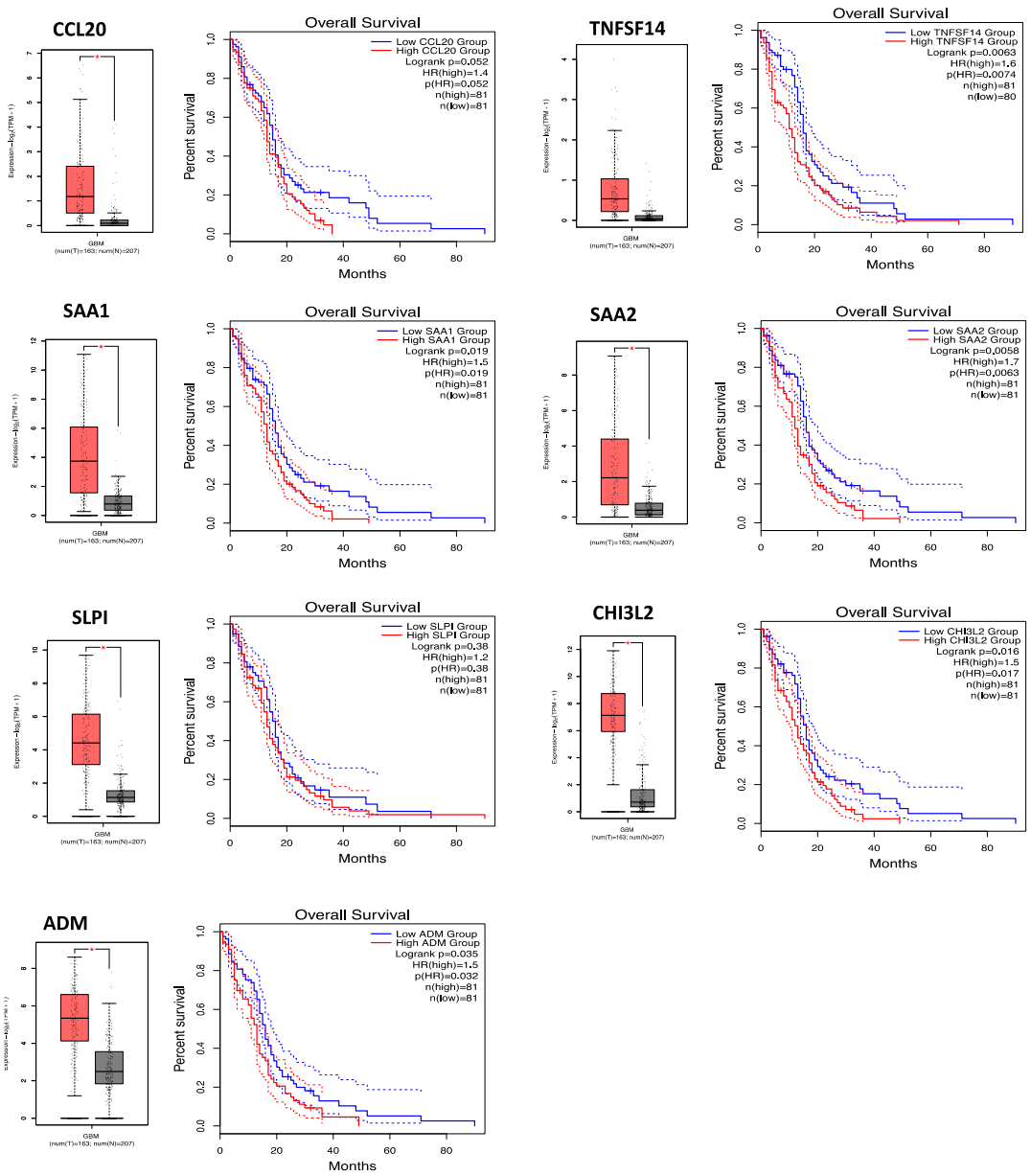

Figure 4-19 Upregulated DEGs by ReoDex and associated with GBM prognosis.

Gepia2 website tool presented genes expression level on GBM tissue (red) compared to normal brain tissue (gray) in a box-plot (left side), and their association with GBM poor survival (left side) presented as a Kaplan-Meier survival curve based TCGA database.

4.2.8.1 The effect of Dex on regulating Reo identified DEGs involved in GBM cell death pathways

Changes to the expression of apoptosis pathway genes is an obvious mechanism by which Dex might reduce Reo-mediated killing of GBM. Figure 4.20.A visualise the apoptosis pathway map and compares the DEGs list from the Reo and ReoDex datasets (adj.p 5.26E-04 vs. 0.035). I identified genes similarly

upregulated in both treatment groups such as TNFSF10 (TRAIL), Fas, PUMA (BBC3), and NFKBIA (IkBa). Though BIRC3 was expressed in both treatment groups, but the log2FC was more upregulated in ReoDex than Reo alone (3.82 vs. 2.93 respectively). It was reported that BIRC3 overexpression is associated with poor GBM survival, and induced apoptosis suppression (Gressot *et al.,* 2017). In addition, c-Jun and CASP7 were upregulated in Reo group only. Looking at the gene count of both genes, they were also expressed in the ReoDex group but they were not included in the DEGs list, likely because they did not meet the cut-off criteria, meaning the change in gene expression was not significant enough. It was reported that Reo activates Jun to activate JNK to induce apoptosis (Clarke *et al.,* 2001). Caspases are also activated upon Reo infection to induce apoptosis (Bourhill *et al.,* 2018). Interestingly, anti-apoptotic genes were upregulated in ReoDex group only which are BCL2L1 (BCL-xL) and CFLAR (FLIP), NOXA1. Previous studies have demonstrated that BCL-xL, a bcl-2 family, binds to BAX/BAK to prevent their activation, and inhibit apoptosis (Fanfone *et al.,* 2020). This could explain the mechanism in which GBM cell could survive under conditions like stress or DNA damage, and in our treatment conditions, infection by Reo and Dex. BCL2L1 was reported to contribute to cell proliferation and cell cycle progression (Janumyan *et al.,* 2003). CFLAR, another anti-apoptotic protein, inhibits apoptosis by prevent activation of caspase-8, evade immune surveillance. In addition to its role in apoptosis, CFLAR gene was demonstrated to play a role in necroptosis and autophagy (Safa *et al.,* 2013). NOXA, a BH3 protein in the Bcl-2 family to induce apoptosis. Dex was reported to reduce NOXA expression (Lynch *et al.,* 2010), which suggests Dex role in reducing apoptosis. MAP3K5 (ASK1) was differentially upregulated by ReoDex, and the FPKM level similar increase expression by Reo, suggesting that it did not meet the cut-off criteria. DDIT3, a DNA damage inducible transcript 3 gene was differentially expressed by Reo, and the RNA-seq data showed that the FPKM level was reduced by ReoDex, suggesting Dex reduces DDIT3 expression. GADD45B, a growth arrest and DNA damage-inducible 45 gene that regulate cell cycle, DNA damage and proliferation (Chen *et al.,* 2017) was identified. GADD45B expression was upregulated by ReoDex in comparison to Reo alone, suggest Dex role to induce its expression. Figure 4.20.B summarises the expression of genes of interest.

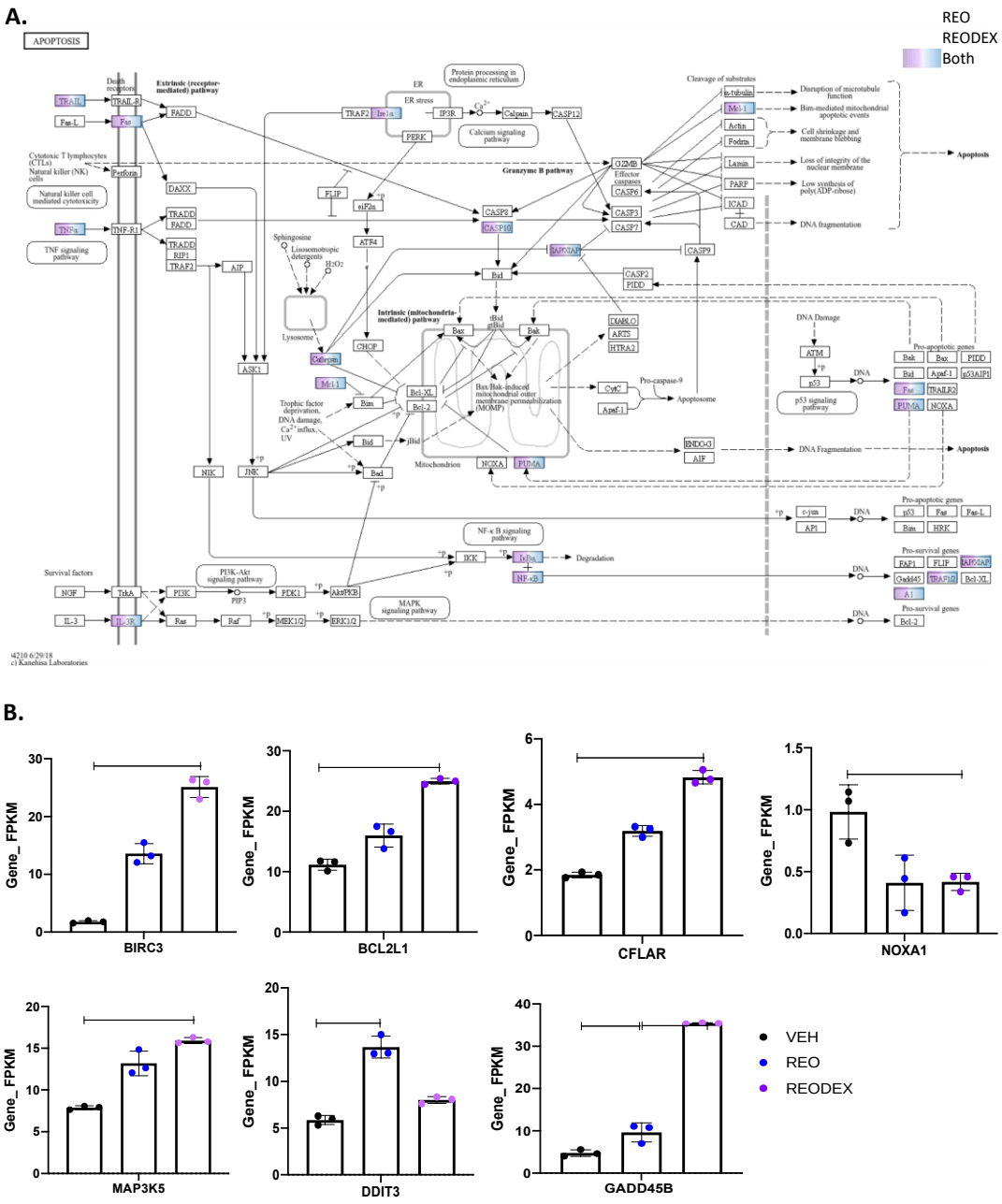

Figure 4-20 Dex influence Reo mediating apoptosis pathway.

A. The apoptosis pathway obtained from the KEGG enrichment analysis of DEGs in MO59K-treated Reo (purple) and ReoDex (Blue) alone or both (gradient). KEGG map was taken from (https://www.genome.jp/kegg/brite.html). The analysis identified unique genes that specifically expressed in ReoDex group which explain Dex influence on GBM cell death. These genes are **B.** RNA-seq data show the genes (-FPKM) level. The data are presented as mean ± SEM for n=3 independent samples, and significant was tested using one-way ANOVA with multiple comparison test (ns $p>0.05$, *$p\leq0.05$, **$p\leq0.005$, ***$p\leq0.001$, and ****$p\leq0.001$).

I next examined if GR (NR3C1) binds to the BCL2L1, CFLAR, and BIRC3 genes using ChIP-seq data visualised on the Cistrome data browser (Figure 4.21). Peak tracks of GR showed GR binding peaks upstream of promoters to BCL2L1, CFLAR and BIRC3 in A549, lung cancer and MCF7, breast cancer cell lines (no GBM ChIP-seq data was available). This would be supportive of a direct role for GR in regulating the expression of these genes.

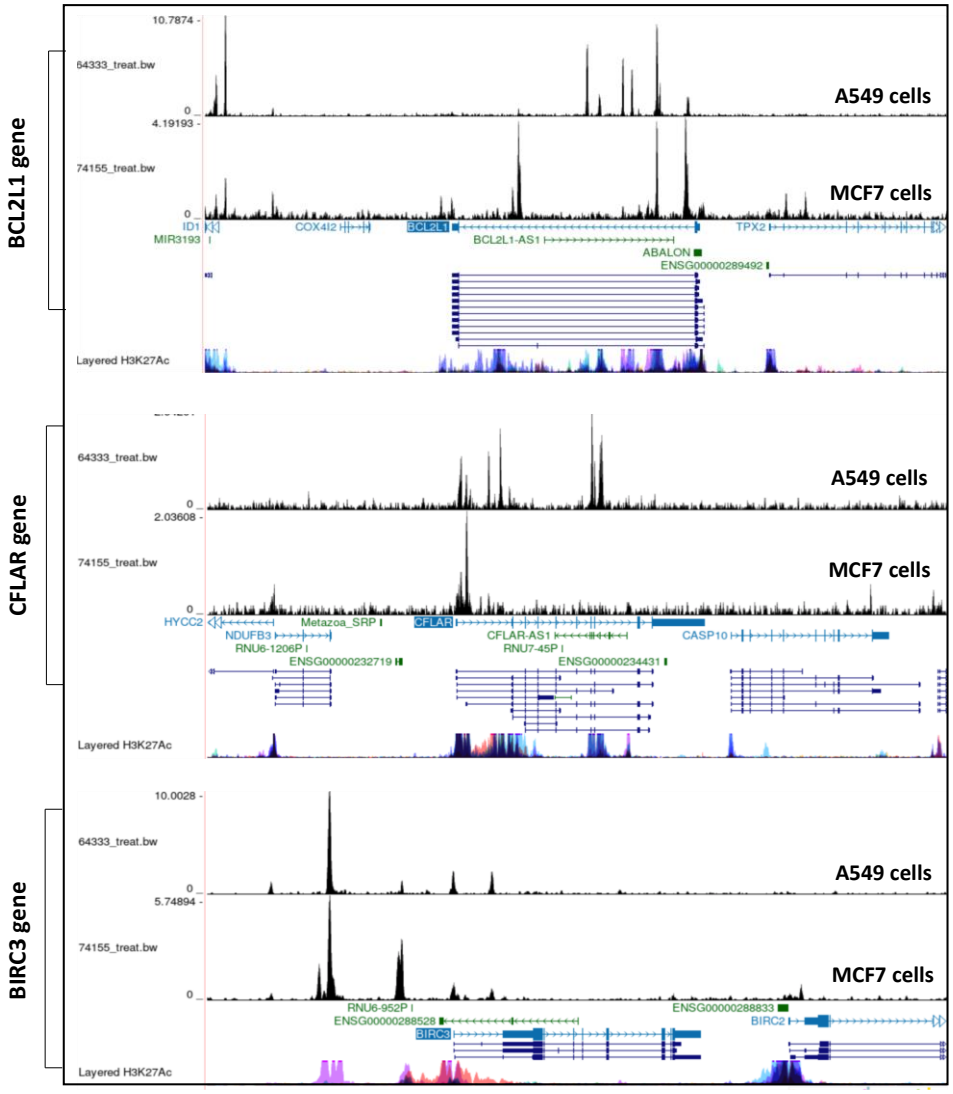

Figure 4-21 GR binding peaks on BCL2L1, CFLAR, and BIRC3 in different cell lines.

Snapshot of ChIP-seq peak tracks of GR (NR3C1) from Cistrome data browser demonstrating the binding site for BCL2L1, CFLAR, BIRC3 on A549 and MCF7 cell lines.

4.2.8.2 Dex regulates Reo effect on DEGs involved in viral protein interaction with cytokines

OVs, including Reo used in our study, mediate tumour killing by direct oncolysis and generating anti-viral and anti-tumour immune response. One of the top KEGG terms from my RNA-seq is viral protein interaction with cytokines and cytokine receptors (Figure 4.22.A). Genes involved in this pathway in MO59K treated directly with ReoDex showed changes in gene expression level of CCL2, CCL20, CX3CL1, CXCL9, CXCL11, CXCL13, LTBR, and TNFSF14/LIGHT as plotted with log2FC in Figure 4.22.B. TNFSF14/LIGHT gene is highly expressed in the mesenchymal subtype and reported to act as both anti- and pro-inflammatory gene, modulate immune response and link to MHC-II, suggesting its role in Macrophage and APC (Yang *et al.,* 2021). TNFRSF1B/TNFR2, binds TNF-α to activate immunosuppressive immune cells. Its expression was higher in ReoDex than Reo alone (log2FC 2.57 in ReoDex, 1.68 in Reo). Dex is reported to increase TNFR2 expression in the microglia cell line (Chantong *et al.,* 2012). CXCL9 and CXCL11 are pro-inflammatory genes, that recruit leukocytes. CXCL9 and CXCL11 are induced by IFN-y (from T and NK cell activation) and recruit T cells to promote antitumor immune responses. ReoDex treatment reduced the expression of CXCL9 and CXCL11 with log2FC -1.4, and -1.04 respectively, suggesting that Dex treatment might impair Reo from activating T and NK cells and recruitment to the tumour site. CCL2, which is reported to be upregulated in GBM, was also downregulated by ReoDex in comparison to Reo alone (log2FC -1.14). CCL2 can promote TME by recruiting TAMs. CCL20 (MIP-3a), a pro-inflammatory and immunomodulatory gene, recruit immune cells to site of inflammation and cancer. Gepia2 analysis found that both CCL2, CCL20 are highly expressed in GBM, and associated with poor survival. Since Dex reduce TNF, IL-1B, IL-6 which can induce CCL2, leading to reduce it expression as well. CCL20 was upregulated in GBM hypoxic sites. CXCL8/IL-8 is a pro-inflammatory cytokine that regulates GBM proliferation and invasion (Sharma et al., 2018). LTBR (lymphotoxin beta receptor), was upregulated by ReoDex only. It is highly expressed in GBM and associated with immune checkpoint, and DNA methylation in GBM, which can be used as marker for immunotherapy (Tang *et al.,* 2024). CXCL12 mediate CXCR7/ACKR3 are both downregulated by ReoDex, which suggest that Dex downregulate their expression. Previous studies showed

that CXCL12/ACKR3 were highly expressed in GBM, and CXCL12 expression recruit immune cells while ACKR3 promote ERK1/2 (Hattermann *et al.,* 2010).

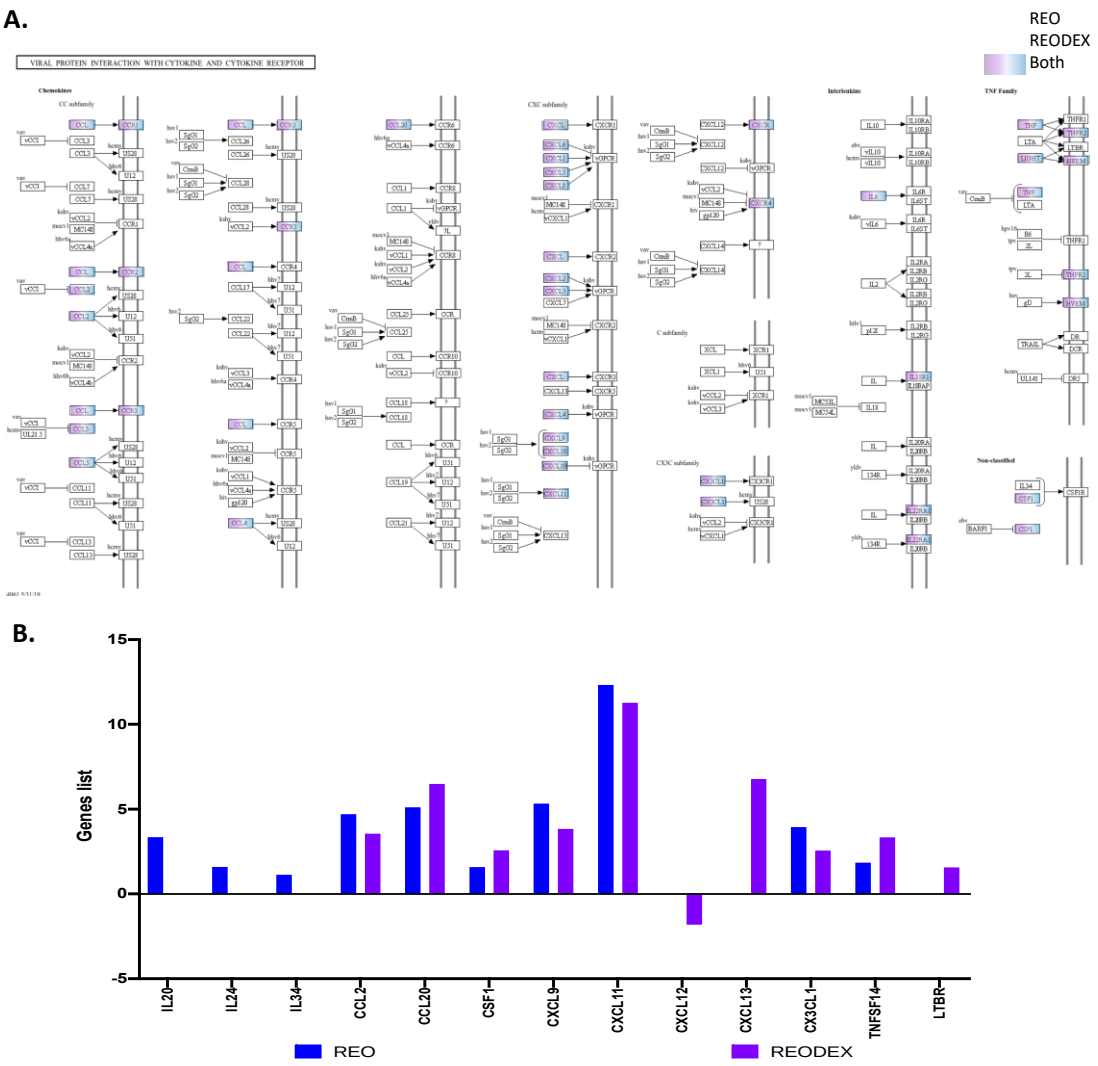

Figure 4-20 Dex mediated The viral protein interaction with cytokines and cytokines receptor pathway.

A. The pathway was obtained from the KEGG enrichment analysis of DEGs in MO59K-treated Reo (purple) and ReoDex (Blue) alone or both (gradient). **B.** A bar graph showing differential gene expression (log2FC) by Reo and ReoDEx treatment.

4.3 Discussion

The aim of this chapter was to identify the effects of the GCs (Dex) on GBM cells when combined with the OV (Reo). There is very little known on the role of GCs on OV efficacy and few studies have been conducted in this area. To achieve this, I firstly explored the combination treatment (pre-treatment, and co-treatment) of Dex with two different OVs (Reo and HSV-1) on long-established GBM cell lines (MO59K and A172). The data demonstrated that A172 cell line was susceptible to Reo, even in high virus concentration and long treatment period, up to 72 hours in both co- and pre-treatment groups. MO59K cells co-treated with Reo and Dex showed significant increase in the percentage of cell viability than Reo alone (Figure 4.1.D). This suggest that Dex has direct protection effect on Reo oncolysis to kill GBM cells. The pre-treated group did not show the protection effect of Dex on Reo efficacy to kill cells suggesting the importance of the timeline of Dex administration for GBM patients receiving oncolytic virus therapy. One explanation could be the early response of Dex which could involve pathways such as NF-KB inhibition which regulate inflammation and immune response (Auphan *et al.,* 1995). GR interacts with NF-kB in the nucleus to regulate gene expression and the inflammatory response (Bekhbat *et al.,* 2017). This observation was different when GBM cells were treated with HSV-1, where Dex has no effect of the virus ability to kill GBM cells (Figure 4.2), suggesting that Dex response differently between these DNA and RNA viruses.

The data in Figure 4.3 for the surface expression of JAM-1 and HVEM on GBM cells showed that JAM-1 is highly expressed in MO59K cells, as well as normal brain cell line (NP1), and two derived-patients cell lines (GBM20, GBM13). However, the expression of HVEM were almost equal among all cell lines. This promoted further exploration of the effect of OVs and Dex co-treatment on NP1, GBM20 and GBM13 to confirm the previous observation. As expected, the NP1 cell line was more resistant to OVs, confirming the selectivity of OVs to infect and kill tumour cells, without harming normal cells. GBM20 showed significant increase in resistance when Dex co-treated with OVs (Reo or HSV-1) and Dex (Figure 4.4. C and D). For the mechanistic analysis, I chose to focus on one OV, Reo, since it was explored in chapter 3, and the experimental data so far supported response to Reo as a Dex regulated target. Next, the death percentage of MO59K, GBM20, and GBM13 cell were then explored by flow cytometry for

further confirmation, and the results showed significant increase in cell death in in co-treated Dex and Reo than Reo alone (Figure 4.5).

Previous data raised questions to how Dex might protect GBM cells from direct killing by Reo; could Dex stop Reo from entering host cells?, or could Dex interrupt virus replication? To answer this, JAM-1 cell surface expression (the Reo entry receptor) was examined by flow cytometry, and no significant change were observed on Dex treated cells (Figure 4.6. A), suggesting that Dex does not affect Reo cell entry. Virus replication by plaque assay showed that Dex does not reduce the ability of Reo to infect and replicate in tumour cells (Figure 4.6. B), and this was supported by RT-qPCR for the σ3 genome segment (Figure 4.6.C). Reo infected cells were also visualized through immunofluorescence for the σNS protein (using antibody 2A9; Figure 4.7.A), and evaluated by flow cytometry, showing stable expression of σNS in GBM cells treated Reo alone or combined with Dex (Figure 4.7.C). Both σ3 outer capsid protein and σNS non-structural protein are required for virus replication. It was reported that the σNS assembled into factories, and their formation is required for Reo replication (Lee *et al.,* 2021). σ3 was reported to inhibit PKR activation by binding to dsRNA during virus infection (Guo *et al.,* 2021). Overall, my data showed that Dex does not impair Reo attachment to host cells through JAM-1 receptor, nor virus replication. I therefore speculated that Dex might impair Reo-mediated killing of GBM cells, e.g through inhibition of caspase activation. Several studies determined the mechanisms of Reo induced cell death including extrinsic apoptotic pathway by inducing TRAIL secretion which signals DR4/5-FADD complex lead to caspase 3 activation (Phillips *et al.,* 2018; Richardson-Burns *et al.,* 2002). Using the caspase inhibitor Z-VAD demonstrated that Reo killed GBM cells by caspase activation (Figure 4.8). However, although Reo induced caspase activation in GBM cells, Dex treatment did not inhibit this. (Figure 4.8). It was previously reported that Dex pre-treatment prior to TMZ reduced cleaved caspase 3, indicating an inhibitory effect of Dex (Das *et al.,* 2004). However, it seems that Dex does not inhibit Reo-mediated apoptosis through the caspase pathway. This led to using RNA-seq to explore other mechanisms for Dex to inhibit Reo mediated cell death such as necrosis, autophagy or cell cycle arrest. It was determined that GR signalling mediated transcriptional changes involved in cell growth arrest, and apoptosis in

hematologic malignancies (Greenstein *et al.,* 2002), and GR signalling might contribute to the inhibition of apoptosis in breast cancer (Moutsatsou *et al.,* 2008).

GR activation occurs in response to Dex treatment, but under some circumstances (eg. during mitosis), GR can be activated in the absence of its ligand. It was therefore tested if Reo treatment would change GR expression or activation on ser-211 as a control experiment. Western blot analysis showed that GR phosphorylated at ser-211 site is induced by Dex alone or combined with Reo with no significant difference between the two groups, suggesting that Reo does not interfere with Dex to induce GR phosphorylation (Figure 4.9).

The data so far revealed that Dex impairs Reo to kill GBM cells. Several selective glucocorticoids, namely AZD-7594 (AZD) and Vamorolone (Vam), are currently under pre-clinical studies for asthma and Duchenne muscular dystrophy (Brown *et al.,* 2019; Guglieri *et al.,* 2022) and they might offer a promising novel alternative to Dex in GBM treatment to potentially show fewer side effects. Vamorolone showed increased survival outcome in glioma animal model (Wells *et al.,* 2017). Compound A (CoA) was also proposed to have anti-inflammatory and anti-tumour activities (Lesovaya *et al.,* 2015). This led us to examine the effect of these candidates to treat GBM cells alone or in combination to Reo (Figure 4.10). I had hoped that one of the selective GCs would not protect against Reo mediated cell death and that differences in gene expression between ReoDex and Reo-Selective GC could then be used to more precisely identify the affected pathways. However, it appeared that each of the selective compounds showed a similar trend in response to Dex. While the effect was smaller than Dex, I did not think the differences would be large enough to compare using transcriptional profiling.

The question of how Dex impairs Reo efficacy to kill GBM cells was investigated using RNA-sequencing. This provides a genome wide view of all of the Dex regulated genes, and the pathways affected. Firstly, optimisation was carried out on two cells lines treated with Dex or Reo alone or in combination followed by RT-PCR to examine a panel of genes known to be regulated by GCs and OVs. The results showed that GBM20 was the best candidate for sequencing, however the growth of the cells line was slow and time-consuming (I calculated it would

take over 3 months to expand the cells for an RNA-seq experiment) and therefore MO59K were used for sequencing (Figure 4.11 and 4.12). Samples were prepared and sent to Novogene for sequencing and a preliminary bioinformatic report was generated by the company for analysis. The samples were efficient for analysis as they passed the QC criteria, and the heatmap showed consistent expression pattern among all samples (Figure 4.13). Overall the quality of the RNA-seq data was very good.

The comparison between the DEGs databases (Figure 4.15) identified top hub genes such as JUN in GBM treated Reo, while MYC and FN1 were identified in GBM treated with ReoDex (Figure 4.15.A, B, and C). Jun is an AP-1 transcription factor, and it has been showed that GCs inhibits c-Jun and Fos in GBM cells (Arcuri *et al.,* 1995). In parallel, Reo reported to induce apoptosis cell death (oncolysis) by upregulation of c-JUN N-terminal kinase (JNK) signalling pathway (Clark *et al.,* 2001). This suggest that Reo co-treated Dex could reduce Jun expression in comparison to Reo alone, which is consistent with the data from the RNA-seq. In GBM, MYC is overexpressed and associated with GBM stemness. MYC expression is also suppressed by GCs, however, the RNA-seq analysis on ReoDex treatment showed increased in MYC expression though the expression of MYC is low in Reo samples. An early study showed that MYC induces the cytopathic effect of Reo (Kim *et al.,* 2007). FN1 (fibronectin) is an extracellular matrix (ECM) protein involved in cell adhesion and a key mesenchymal subtype marker. The RNA-seq data in this study showed FN1 upregulated in GBM cells treated ReoDex only. According to a study by Yin *et al.,* and his colleague in 2016, Dex upregulated FN1 and MUC1 in ovarian cancer to increase cell adhesion (Yin *et al.,* 2016). Additionally, IL-6, TNF, and IL-1B were the top hub genes in both Reo and ReoDex dataset, as the anti-inflammatory cytokine (IL-6) was downregulated, and the pro-inflammatory cytokines (IL-1B and TNF) were upregulated in ReoDex in comparison to Reo alone. This showed that the presence of GCs changes the inflammatory response to Reo (Figure 4.16).

There were 65 common DEGs between the three comparison groups (Figure 4.17.A) and their expression (log2FC) plotted as a heat map (Figure 4.17.B), which showed the similarity of gene regulation among the three comparison,

while TNFSF18/GITR and TSC22D3/GILZ genes were differentially regulated. Figure 4.17.C showing that Dex influenced Reo by upregulating TSC22D3 gene expression while downregulating TNFSF18. TSC22D3 regulates immune cells activation such as T cells (Cannarile *et al.,* 2019), its promoter binds to FOXO, STAT6, NFAT, c-MYC, and its expression was induced by GCs in melanoma through PI3k/Akt pathway (Grugan *et al.,* 2008). Additionally, IL-6, CCL2, CCL20, SAA1, SAA2, ADM, SLPI, and CHI3L2 genes showed significant correlation with GBM poor survival (Figure 4.18 and 4.19).

The pathway enrichment analysis showed the top terms regulated by Reo, ReoDex or Dex. Common pathways among the three datasets included apoptosis which is essential to investigate to answer how Dex impaired Reo oncolysis. First, we evaluated death related pathways. Apoptosis and NF-kB pathways are controlled by several factors including cellular inhibitors of apoptosis (cIAPs) which function as E3 ligases (Bertrand *et al.,* 2008). BIRC3/IAP2 is a negative regulator that interacts with NF-kB pathway in response to inflammation. The NF-kB pathway induces pro-survival genes including BIRC3, which contribute to cell survival. This mechanism might allow GBM cells to survive despite the inflammatory environment and therapies that induce cell death, which in this study is represented by GCs and OV therapies. It has been reported that BIRC3 protected lung airway infected with influenza against necroptosis, promoting cell survival (Rodrigue-Gervais *et al.,* 2014). GCs was found to transactivate NF-kB, leading to activation of MYC, demonstrating a pro-survival mechanism by GCs in breast cancer (Khan *et al.,* 2013). The RNA-seq data confirmed the upregulation of BIRC3 expression in GBM cells treated with Reo and ReoDex (Figure 4.20.B). ChIP analysis identified GR (NR3C1) binding to BIRC3 promoter (Figure 4.21). Overall, this could suggest the cooperation between BIRC3, GCs, and NF-kB is essential to help cells resistance to apoptosis. CASP7 was upregulated by REO, while ReoDex group did not met the cut-offs criteria. This suggest that GCs did not influence Reo to activate Caspase7 to induce apoptosis. ReoDex induced anti-apoptotic genes including BCL-xL and CFLAR/FLIP, suggest that GCs mediate anti-apoptotic genes to block cells to undergo apoptosis initiated by Reo, and ChIP analysis showed that GR bind to BCL-xL and CFLAR promoter. It has been demonstrated that NOXA neutralize anti-apoptotic genes (Ploner *et al.,* 2008). The downregulated

expression of the pro-apoptotic gene NOXA/ PMAIP1 was significant with ReoDex treatment. This suggests that GCs downregulate NOXA, allowing anti-apoptotic gene expression, leading to GBM survival. A recent review by Afshari *et al*., 2022 has reported the role of Dex in promoting GBM which involves GR in altering anti-apoptotic genes. DDIT3 (CHOP) gene, is a member of the CCAAT/enhancer-binding protein (C/EBP) family of DNA-binding transcription factors, which play role in ER stress-induce apoptosis. ReoDex downregulation for DDIT3 expression suggest Dex inhibitory effect on DDIT3 gene. GADD45B upregulation in tumour increases cell cycle arrest and apoptosis in response to DNA damage and stress (Salvador *et al.,* 2013). Understating the role of GADD45B in the context of GBM and GCs is unclear and therefore more investigation is needed.

Next, I explored KEGG identified term in viral protein interaction with cytokines and cytokines receptor (Figure 4.22.A). Interestingly, many of cytokines/chemokines showed similar differential expression in both Reo and ReoDex treatment groups. There were however some genes that showed opposite regulation by Reo and ReoDex. For instance, TNFSF14/LIGHT is expressed in GBM cells, and involved in T cell activation and NF-kB signalling to promote inflammation (Han *et al.,* 2022). Beside the involvement in mesenchymal subtype signature, the increase in gene-FPKM level by ReoDex suggests that GC trigger inflammation through TNFSF14 and transitioning to more aggressive type of GBM. TNFRSF1B/TNFR2 induces immunosuppressive immune cells. It also recruited cIPA to mediate NF-kB and apoptosis pathway (D'Ignazio *et al.,* 2018). CXCL9, CXCL10 and CXCL11 are pro-inflammatory genes that activate T and NK cells. ReoDex treatment reduced their expression compared to Reo, suggesting that Dex impair Reo indirectly by reducing chemokines secretion to recruit T and NK cells. Dex is well known to inhibit the activation of immune cells such as NK and T cells activation and reduce T cell numbers through apoptosis (Iorgulescu *et al.,* 2021). CCL2 and CCL20 expression were downregulated by ReoDex compared to Reo alone, thus reducing immune cells infiltration to the GBM site. CCL20 is upregulated in hypoxic region in GBM. LTBR (lymphotoxin beta receptor), was upregulated by ReoDex only. It is highly expressed in GBM and associated with immune-checkpoint inhibitors, and DNA methylation in GBM, which can be used as marker for immunotherapy (Tang *et al.,* 2024).

CXCL12/ACKR3 axis are downregulated by ReoDex, which suggest being GCs regulated.

Overall, this study has identified a range of candidate pathways that could provide the mechanism by which Dex reduces the efficacy of Reo which is summarised in figure 4.23. The most promising candidates would be Dex-mediated inhibition of proinflammatory cytokines and chemokines, and also the upregulation of the anti-apoptotic proteins FLIP and BCL-xL. Further work is needed to validate these pathways in more detail.

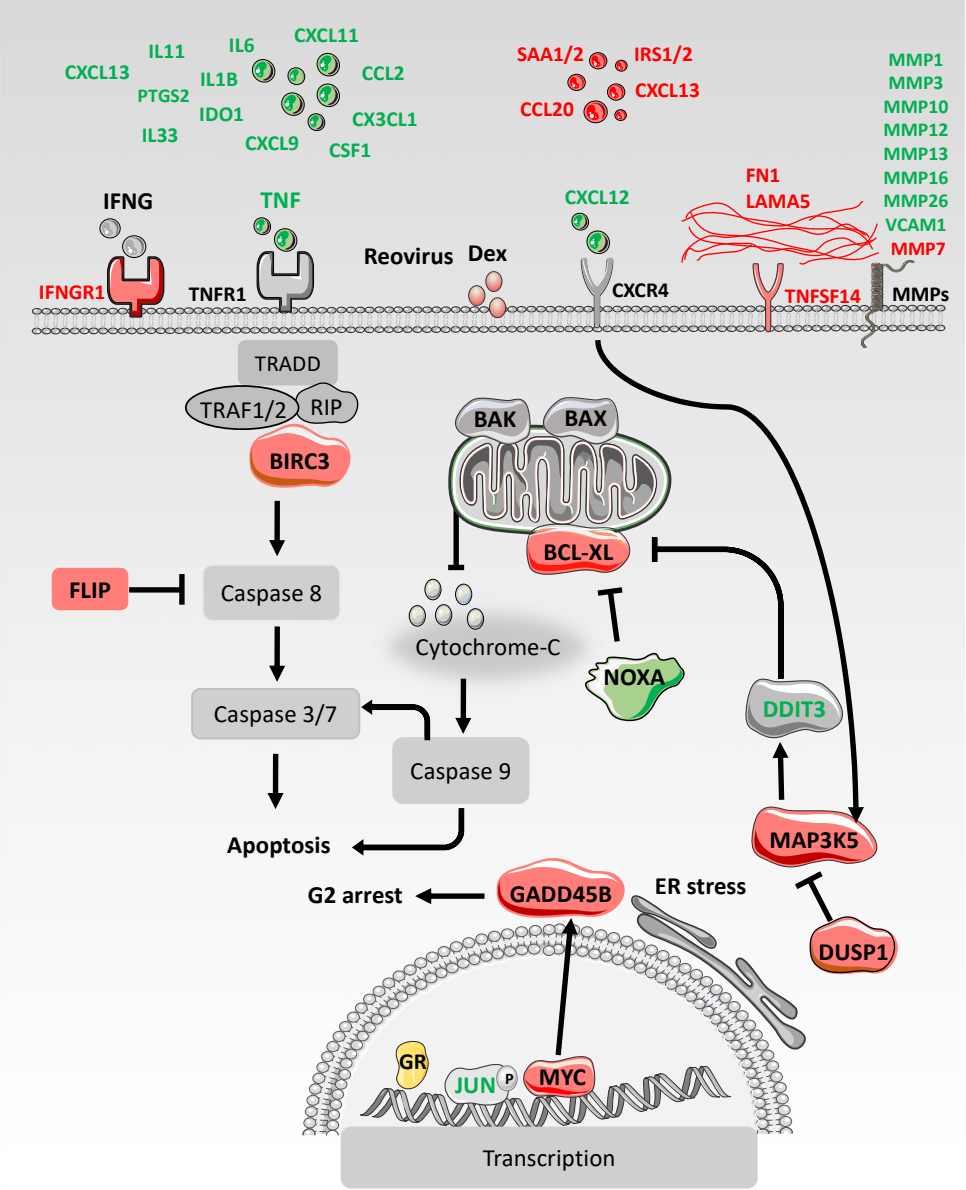

Figure 4-21 Summary of potential pathways and genes regulated by Dex modifying reovirus efficacy in MO59K cell line.

Genes upregulated by ReoDex (red), downregulated by ReoDex (green), genes upregulated by Reo (red text, gray background), downregulated by Reo (green text, gray background).

Chapter 5

The effect of GCs and Reo-mediating indirect killing in GBM

5.1 Introduction

Previous studies have shown that GCs control proliferation, survival, activation and differentiation of several immune cell types, including T cells, Treg, NK cells, DC, and macrophages (Cari *et al,* 2019). In chapter 4, I showed that local inflammation, interferons, and immune checkpoint pathways might play a role in GC modulating the effects of reovirus (Reo) on GBM and immune cells. In addition, chapter 5 demonstrated that Dex directly reduces the efficacy of Reo mediated killing of GBM cells. My analysis also revealed that in GBM cells Dex reduces the expression of secreted factors known to recruit immune cells, and that Dex also reduces expression of surface proteins on GBM cells that serve as attachment sites for T cells and NK cells. This would suggest that Dex might also reduce the recruitment and killing ability of T cells and NK cells in response to Reo, thereby impairing indirect killing by Reo. Therefore, it was important to understand the effects of combining GC with OV in the treatment of GBM and the crosstalk between GBM cells and immune cells in the TME.

<u>The aim of this chapter</u>

1. Use a coculture model to determine the effect of GCs on OV efficacy to indirectly kill GBM cells.
2. To determine the effect of GCs on OV activation of immune cell populations.
3. Use RNA-sequencing to investigate the crosstalk between GC and OV signaling responses in GBM cells.

5.2 Results

5.2.1 Dex impairs indirect killing of GBM cells following Reo treatment

I have shown that Dex impairs Reo direct killing in GBM cells. The anti-inflammatory and immunosuppressive effect of Dex and Reo-mediated immune response led me to investigate the effect of Dex on immune-mediated killing of GBM cells. GBM cells (MO59K, GBM20, and GBM13) were labelled with mito-tracker green and rested overnight. PBMCs were treated with vehicle (Veh), Dex, Reo or a combination ReoDex for 24 hours. Clinically, GBM patients receive Dex before and after surgery and/or during therapy. GBM cells were then cocultured with the treated PBMC for 4-5 hours and killing of GBM cells tested using a live/dead flow cytometry assay; any killing of GBM cells that occurs within five hours is immune-mediated and not a result of direct lysis by the virus as this is too short a time for viral replication and cytopathic effects. Figure 5.1.A show a representative image outlining the coculture conditions.

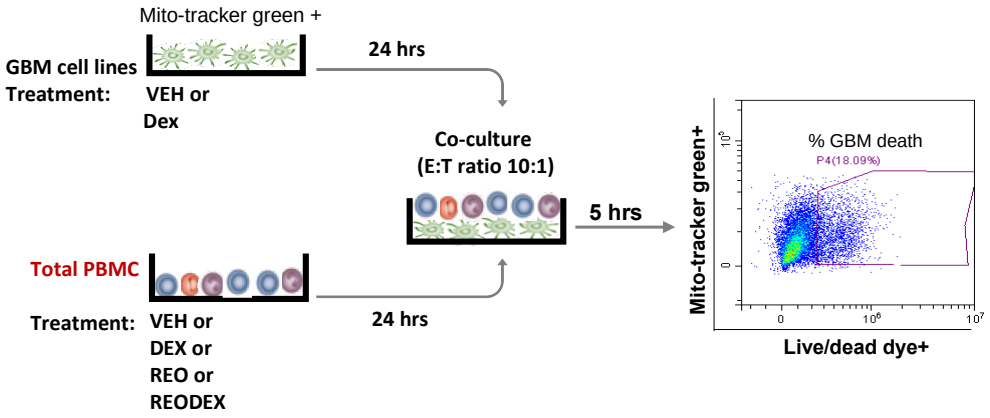

Figure 5-1 Schematic overview of the PBMC killing assay on a coculture model.

GBM cell lines (target cells) were tagged with mito-tracker green and rested for 24 hours before coculture. Total PBMC (effector cells) were treated with either Veh, 100nM Dex alone, Reo MOI1 alone, or combination of ReoDex for 24 hours. GBM cells were cocultured with Total PBMC. Target cells were cocultured with effector cells at E:T ratio of 10:1 for 5 hours. PBMCs killing effect on GBM cells was determined by Live/dead stain analyzed by flow cytometry, gating GBM cells with mito-tracker green.

Results in Figure 5.2 show that Reo activates immune mediated killing in MO59K cells and two patient derived cells lines, GBM13 and GBM20. Both MO59K and GBM20 cells showed significant reduction in PBMC killing response to Reo when cotreated with Dex. While GBM13 showed the same trend, the effect of Dex did not reach statistical significance.

In the previous chapter I identified a possible effect of Dex on regulating NK or T cell recruitment. NK cells are the main effector cells mediating the PBMC killing assay, and so the assay was repeated using the same coculture conditions except that the CD56+ cells (NK cells and NKT cells) were depleted using magnetic selection (Figure 5.2, right). This clearly demonstrates that the killing effect of Reo on GBM cells is dependent on NK cells, implicating them as a Dex target cell.

To further confirm that the indirect killing of GBM cell is NK cell mediated, I depleted PBMC with CD56 microbeads. I collected each of NK cell fraction (that contain NK cells only), and non-NK cell fraction (the remain of PBMC after depletion) each alone or re-combined them, then treated them with Reo for 24 hours. MO59K cells was cocultured with each fraction alone or combined for 4-5 hours to examine the killing percentage of MO59K cells by flow cytometry as explained in Figure 5.3.A. The results showed that neither NK cell fraction nor the non-NK cell fraction alone exhibited a killing effect on GBM cells, however when the two fractions are re-combined, a significant GBM killing was observed. This suggest that while NK cells mediate GBM cell killing, they need to interact with other immune cells to become activated by the Reo, more likely APC such as macrophages (Figure 5.3.B).

Overall, these results show that Reo treated PBMC kill GBM cells in an NK cell dependent manner and that Dex treatment impairs this reponse, possibly by blocking NK cell activation or by killing some NK cells directly, as has been reported in other models.

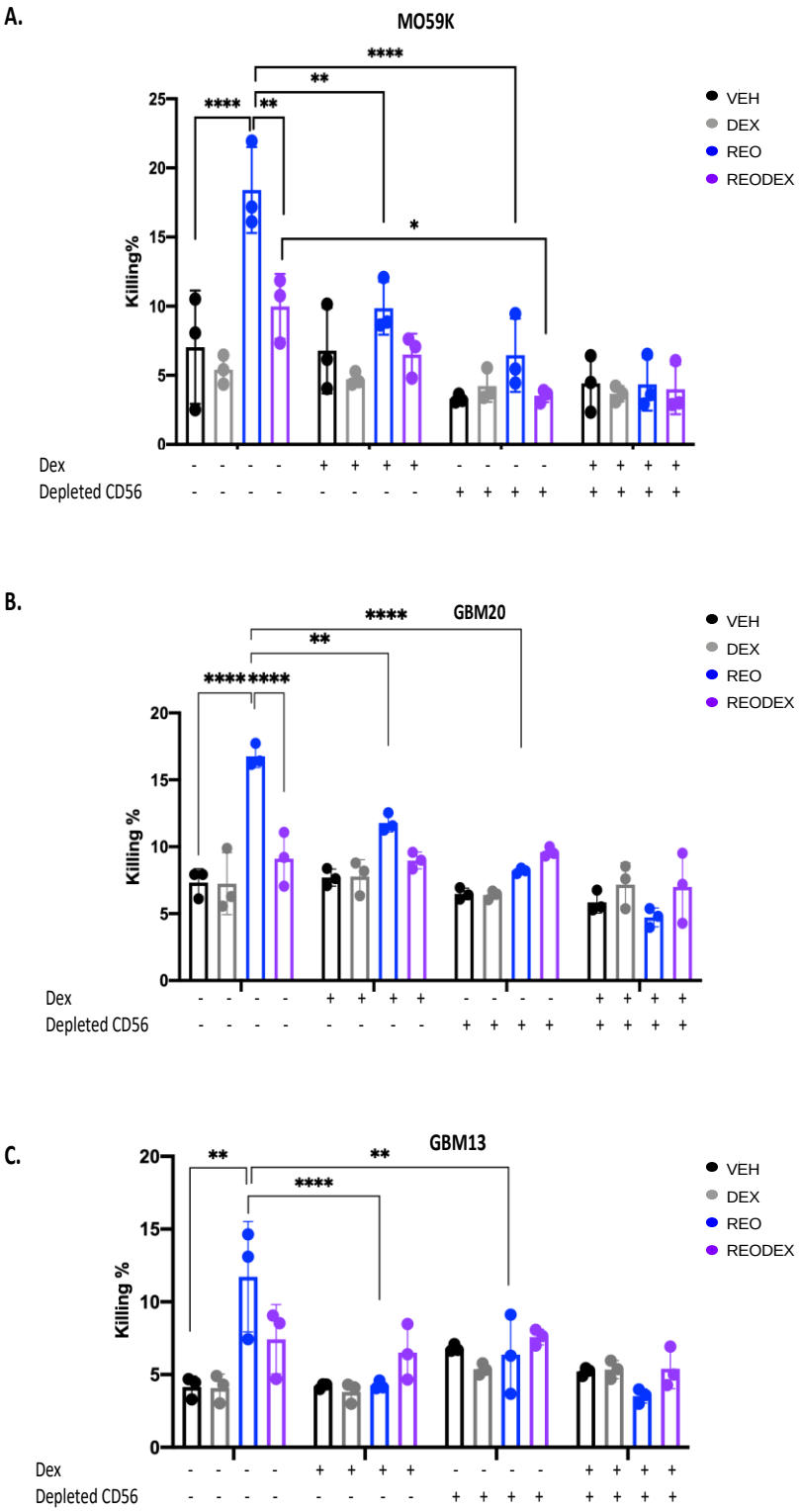

Figure 5-2 Dex significantly impairs indirect killing of GBM cells by Reo activated PBMC, and is NK mediated.

The killing percentage of **A.** MO59K **B.** GBM20 and **C.** GBM13 cells treated with Veh or Dex and cocultured with different treatment conditions of total PBMC or depleted NK PBMC or GBM cells pre-treated with Dex and o-cultured with different treatment conditions of total PBMC or depleted NK PBMC. Data show the mean ± SEM for n=3 independent donors and significant was tested with 2-way ANOVA with Tukey's multiple comparison test (ns p>0.05, *p≤0.05, **p≤0.005, ***p≤0.001, and ****p≤0.001).

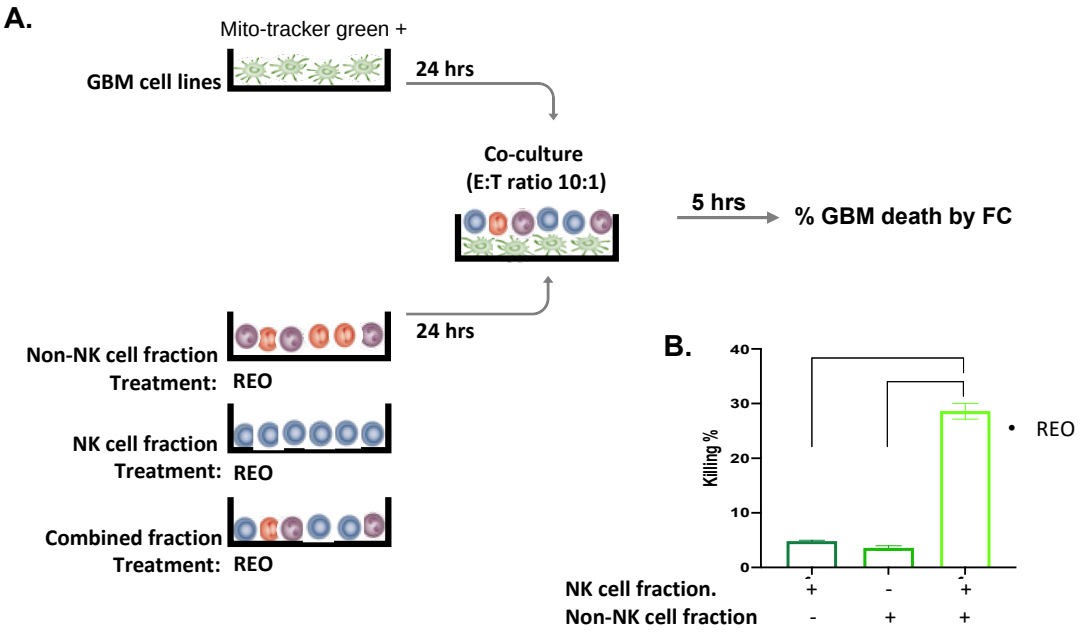

Figure 5-3 PBMC mediating killing require both NK and other immune cells.

A. a scheme image of MO59K cells. Coculture assay was repeated on reovirus-treated PBMC with non-NK fraction, NK fraction or combined assessed by flow cytometry after 5 hours. **B.** Graph depicts percentage killing of NK and Non-NK cell cotreatments alone and in combination. Graphs show the mean ± SEM for n=3 independent experiments and significance was tested using a one-way ANOVA with Tukey's multiple comparison test (ns p>0.05, *p≤0.05, **p≤0.005, ***p≤0.001, and ****p≤0.001). **

5.2.2 Effect of Dex on reovirus activating immune cells

The previous observation suggested Dex impaired the activation of PBMC by Reo and resulted in reduced immune-mediated killing of GBM cells. Dex is a potent anti-inflammatory agent and is known to modulate the phenotype of circulating monocytes (Moyes *et al.,* 2018), inhibits lymphocyte activation and induces apoptosis (Chitadze *et al.,* 2017). It was therefore important to test the effects of Dex on Reo-mediated activation of immune cells. I have focussed on T cells and NK cells as these are the cell types most likely responsible for the immune-mediated cell death of GBM cells seen in Figure 5.1, and monocytes which are important for their activation.

5.2.2.1 Myeloid-lineage cells

Healthy PBMCs were treated with Dex and Reo alone or in combination for different time points (24, 48 or 72 hours). The cytotoxic effect of treatment in

PBMC were assessed by flow cytometry using the Live/dead stain to measure the percentage of monocyte cell death defined by CD14+ marker (Figure 5.4.A). Results showed that neither Dex or Reo cause monocyte death. Next, I investigated the effects of Dex and Reo on the monocyte infiltration. PBMC were treated with Dex, Reo or both or 24 hours and the expression of CD163, HLA-DR markers. It has been reported that circulating myeloid cells in GBM patients receiving Dex express markers such as CD163, HLA-DR which are associated with high GBM grade (Marx *et al.,* 2022). There were significant increases in CD163 and HLA-DR expression when treated with Dex alone or in combination with Reo (Figure 5.4.B). PBMC treated with Dex alone expressed higher levels of CD163 than other treatment groups as determined by mean fluorescence intensity (MFI) (Figure 5.4.C). This suggest that Dex in combination with Reo is modulating the expression of CD163 marker.

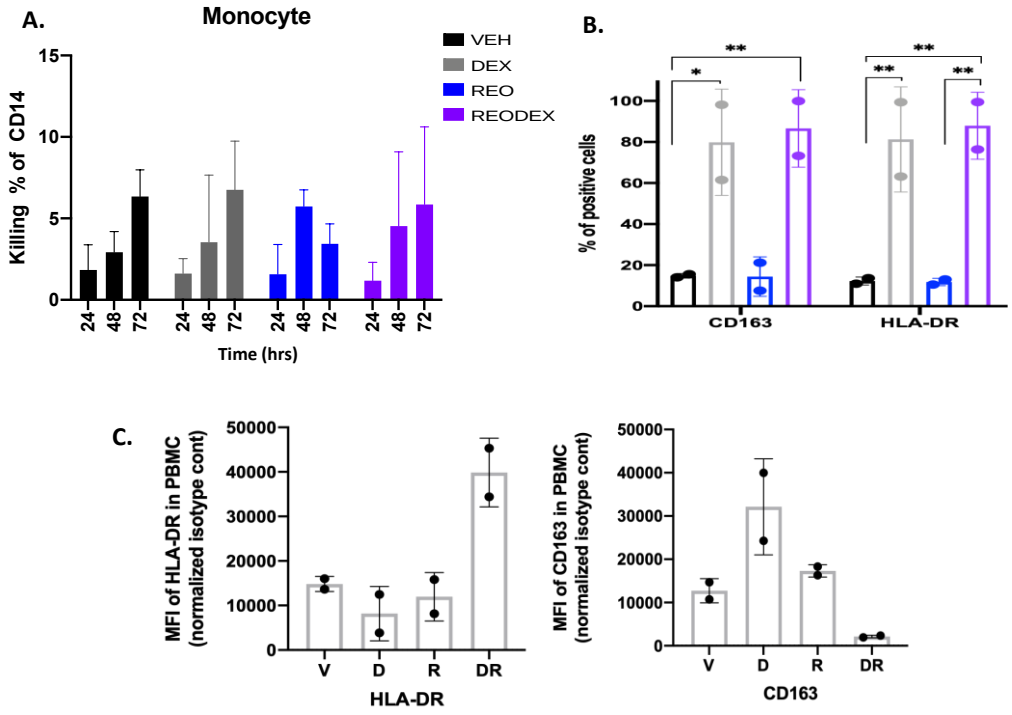

Figure 5-4 Dex and Reo do not cause myeloid cells death but influence its phenotype markers.

A. The death percentage of monocyte was determined by Flow cytometry using live/dead stain. Data show the mean ± SEM for n=3 independent donors. **B.** PBMC were treated with Veh, Dex, Reo or combination for 24 hours, and CD163, HLA-DR markers expression was determined by flow cytometry for CD14 cells plotted in percentage. **C.** shows the MFI of CD163, and HLA-DR markers were calculated on CD14+ cells and normalized by isotype control. Data show the mean ± SEM for n=2 independent experiments, and significance was tested with nonparametric one-way ANOVA with Dunn's multiple comparison test. test (ns p>0.05, *p≤0.05, **p≤0.005, ***p≤0.001, and ****p≤0.001).

5.2.2.2 T cells and NK cells

Healthy PBMCs were treated with Dex and Reo alone or in combination for 24, 48 or 72 hours. The cytotoxic effect of Dex treatment on PBMC was assessed by flow cytometry using the Live/dead stain, along with markers defining two specific immune sub-sets; T cells (CD3+), and NK cells (CD3neg CD56+). The results show that Dex induces death of NK cells but that this effect is reduced in the presence of Reo. Neither Dex nor Reo showed killing of T cells (Figure 5.5.A and B). Activated T cells and NK cells were identified by cell surface expression of CD69 and the MFI compared to isotype controls were calculated and plotted in Figure 5.5.C and D; activation of both NK cells and T cells remains low in the presence of Dex, while Reo significantly increased NK activation after 48 hours post infection, consistent with studies demonstrating Reo mediated activation of NK cells via type I interferon (El-Sherbiny *et al.,* 2015). Dex did not significantly influence the activation of NK or T cells in response to Reo, although there was a trend towards inhibition of NK cell activation.

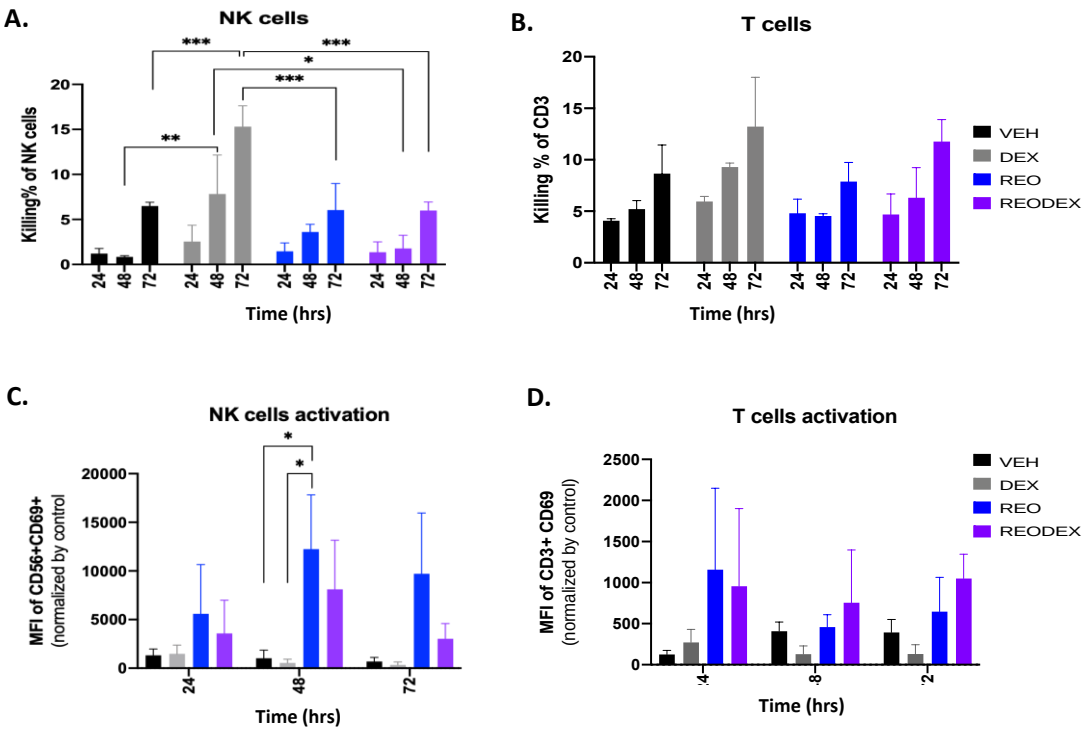

Figure 5-5 Dex significantly kills NK cells but does not affect NK cell activation.

PBMCs treated with Veh, 100nM Dex or Reo alone or in combination for 24 hours and **A.** death percentage of NK and **B.** T cells were determined by Flow cytometry using live/dead stain. **C.** NK and **D**. T cells were determined by CD69 expression and mean florescence intensity (MFI) was calculated and normalized by isotype control. Data shows the mean ± SEM for n=3 independent donors, and significance was tested with 2-way ANOVA with Tukey's multiple comparison test (ns $p>0.05$, *$p\leq0.05$, **$p\leq0.005$, ***$p\leq0.001$, and ****$p\leq0.001$).

5.2.2.3 The effect of selective steroids treatment on NK and T cells

Selective steroids (AZD, VAM, CoA) were also evaluated for their cytotoxic and inhibitory effect on immune cell populations. PBMC were treated with drugs alone or combined with Reo for 24 and 48 hours. The cytotoxic effect on NK and T cells were then assessed using flow cytometry for the percentage of positive live/dead stained cells. Neither VAM nor CoA showed cytotoxicity towards NK or T cells after 48 hours (Figure 5.6.A, B), whereas AZD significantly killed NK cells to a similar degree as Dex. These assays used PBMC from different donors to the previous figure and there was a clear inhibition of NK cell activation in response to Reo when treated with Dex. The fact that two other GR ligands, AZD and Vam produced a similar effect adds weight to this observation. In contrast to Dex, AZD and Vam treatment, CoA treatment did not decrease NK activation in response to Reo (Figure 5.6.C). More investigation is needed to validate this observation.

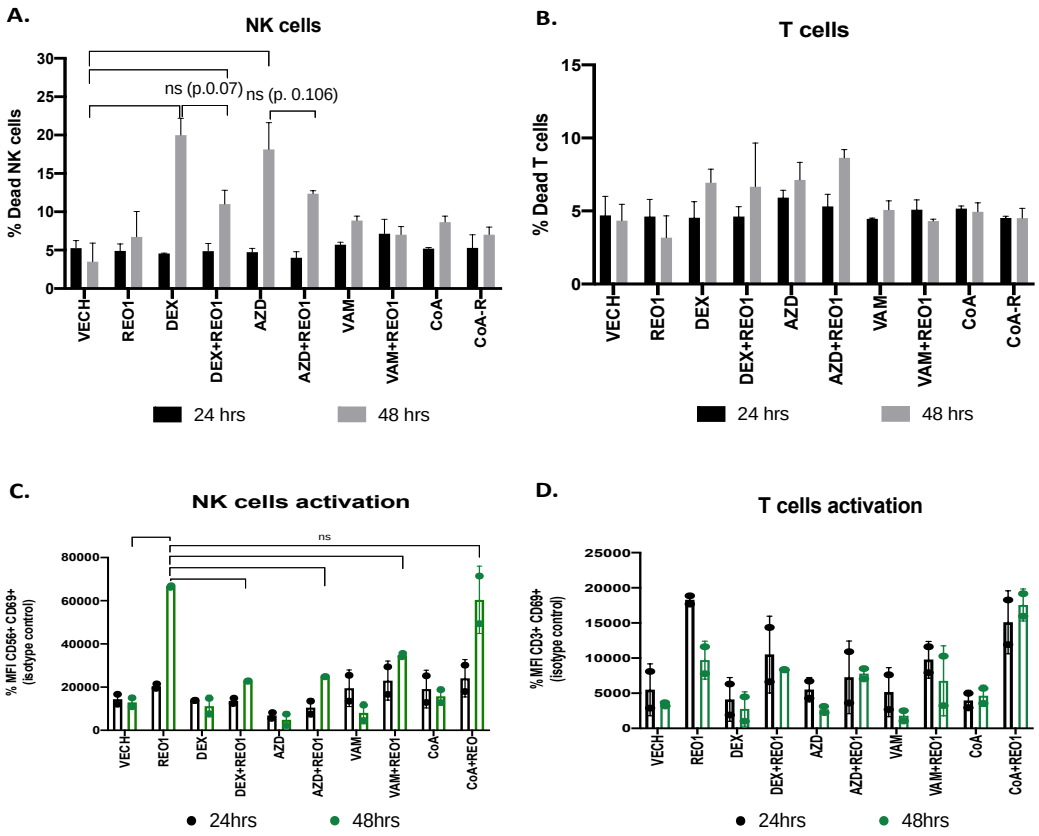

Figure 5-6 Screen of selective GCs as alternative to Dex in GBM treatment.

MO59K cells were treated with selective GRs (AZD, Vam, CoA) and Reo for 48 hours. **A.** Cytotoxicity percentage was determined by Live/dead stain using flow cytometry (n=3). **B.** NK cells and T cells killing percentage were determined by Live/dead stain using flow cytometry. **C.** Activation of NK and **D.** T cells were determined by MFI and normalized by isotype control. Data show the mean ± SEM for n=2 independent experiments and significance was tested using a one-way ANOVA with Dunn's multiple comparison test (ns p>0.05, *p≤0.05, **p≤0.005, ***p≤0.001, and ****p≤0.001).

5.2.3 Optimising samples condition for total RNA sequencing

The previous observation in this chapter showed that treatment of PBMC with Dex reduce NK cell activation in response to Reo, which in turn influences their efficacy to indirectly kill GBM cells, over a 5hr time period. However the optimisation completed for the RNA-seq in the previous chapter suggested a longer time period was required to measure gene expression changes in response to Dex. So I replicated the experiment for a longer time period (24 hours) to validate the initial findings, and the results showed similar killing response in MO59K cell line (Figure 5.7), confirming that 24hr treatment was also a suitable model.

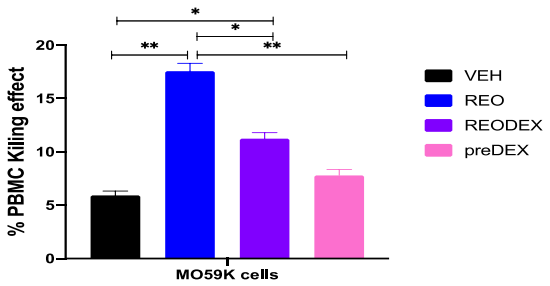

Figure 5-7 Pilot coculture model for the RNA-seq.

MO59K cells (untreated or pre-treated with 100nM Dex) and PBMCs (Veh, Dex, Reo alone or in combination for 24hours) at 10:1 E:T ratio for additional 24hours. PBMC killing MO59K cells were analyzed by Live/Dead stain on FC. Data show the mean ± SEM for n=3 independent donors and statistical analysis using paired T-test.

I therefore, conducted an RNA-seq analysis on the coculture model with a 24 hr end point for cell isolation and RNA extraction. Based on my previous results, the primary cells of interest to isolate in the coculture model included the GBM cells (MO59K), NK cells and monocytes. I used the cell sorter to isolate pure population of cells. To achieve the proposed plan, I firstly examined the gating strategy, cell purity, and RNA yield. The mixed suspension cells were prepared for cell sorting by suspending the cells in cold FACS buffer contain EDTA to reduce the stickiness of the cells. The gating strategy is explained in material and method chapter (Figure 3.1), and the number of sorted cells per population was 200,000 cells. MO59K cells were gated by size and absence of CD45 expression, to remove immune cells. Monocytes were gated by CD45+CD14+ markers, and NK cells by CD45+CD3-CD56+ markers. I then examined the purity of sorted cells by running a small subset of the gated cells. Results in figure 5.8.A,B and C

showed ~98% purity for NK cells, ~96% purity for macrophage, and 83% for MO59K cells. To refine and increase the purity of MO59K cells, I stained them with mito-tracker green prior to the coculture and used this marker in their isolation by FACS.

A.

NK cells purity

Statistics: 081223_005

Populations	Events	% Total	% Parent	*V 460/... Mean	*B 580/... Mean
All Events	10,000	100.00%	####	8	307
Singlets	9,845	98.45%	98.45%	7	309
PBMC's	9,738	97.38%	98.91%	7	312
CD45 pos	9,675	96.75%	99.35%	7	313
Monocytes	31	0.31%	0.32%	247	44
NK cells	9,556	95.56%	98.77%	5	316
Tumour cells	39	0.39%	0.40%	61	116
CD45 neg...	38	0.38%	97.44%	60	114

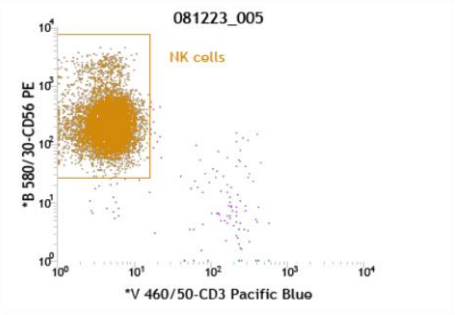

B.

Monocyte cells purity

Statistics: 121223_003

Populations	Events	% Total	% Parent	*V 460/... Mean	*B 580/... Mean
All Events	4,247	100.00%	####	68	18
Singlets	4,194	98.75%	98.75%	67	18
PBMC's	4,018	94.61%	95.80%	68	17
CD45 pos	4,004	94.28%	99.65%	68	17
Monocytes	3,848	90.61%	96.10%	64	15
NK cells	19	0.45%	0.47%	7	271
Tumour cells	44	1.04%	1.05%	82	112
CD45 neg...	33	0.78%	75.00%	108	148

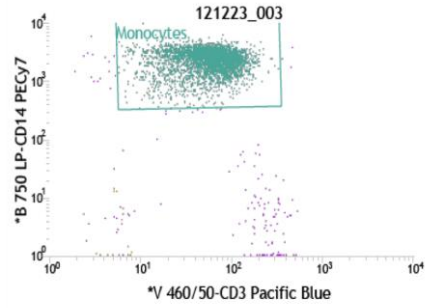

C.

MO59K cells purity

Statistics: 081223_006

Populations	Events	%Total	%Parent	*V 460/ ... Mean	*B 580/ ... Mean
All Events	2,155	100.00%	####	65	95
Singlets	1,899	88.12%	88.12%	65	93
PBMC's	184	8.54%	9.69%	119	48
CD45 pos	137	6.36%	74.46%	154	52
Monocytes	23	1.07%	16.79%	258	46
NK cells	24	1.11%	17.52%	5	217
Tumour cells	1,464	67.94%	77.09%	63	105
CD45 neg...	1,417	65.75%	96.79%	63	106

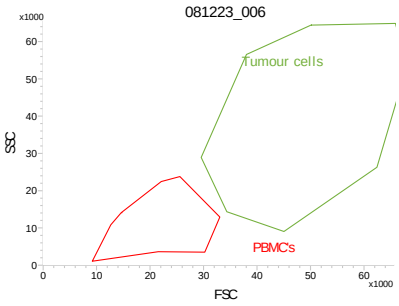

Figure 5-8 Cells population purity using the cell sorter.

MO59K cells cocultured with PBMC at 10:1 E:T ratio for 24 hours. Adhered cells were detached and collected alongside the suspension cells, washed with PBS, and resuspended in FACS buffer. Cells of interest were isolated by cell sorter. A small number of isolated cells were then sorted again to check the cells purity percentage of **A.** NK cells (CD45-CD3-CD56+), **B.** monocyte (CD45+CD14+), and **C.** MO59K cells (CD45- and cell weight).

The sorted cells were lysed for RNA extraction, and RNA concentration was quantified using the nanodrop to examine the yield RNA for each cell population. RNA extraction of MO59K cells was successful, yielding a good total RNA quantity. However, the total RNA concentration for macrophage (350ng) and NK cells (175ng) were low. To overcome the low RNA concentration, it was decided to increase the number of sorted cells up to 400,000 cells to achieve at least 400ng per sample. Due to several unfortunate circumstances namely the sorter being offline for repair for a period of time, and a reduced availability of PBMC donors at this late stage (large numbers of cells are required for sorting), I decided to focus only on the GBM cells for the RNA-seq. I tried two alternative culture methods that did not require sorting by Flow. The first method is to indirectly coculture MO59K cells with PBMC using transwell inserts with 0.4mm pore size, followed by isolating MO59K cells. Although this method gives a 100% purity for tumour cells, one disadvantage is the loss of direct cell-cell contact between immune cells and tumour cells, which would miss a lot of signalling pathways. The second method is using a direct coculture model, followed by MO59K cells isolation based on negative fraction of CD14 microbeads. Successful isolation was achieved by testing the purity of the isolated cells. After optimizing both methods, it was decided to prepare MO59K cells by negative fraction of CD14 microbeads for RNA-seq.

5.2.4 Sample preparation for MO59K cells and the quality control for RNA-seq

As previously described, the direct coculture of MO59K cells with treated-PBMCs was incubated for 24 hours, then tumor cells were washed several times with PBS to remove any PBMC, followed by trypsin to detach tumor cells. Monocytes would sometimes attach to the culture surface and therefore, CD14 microbead negative fraction was used to purify MO59K cells. To confirm the purity of the isolated tumour cells, a flow cytometry analysis was assessed for several immune cells markers including CD45, CD14, CD56, and CD3 with appropriate isotype control if needed. Results showed that 5.99% of MO59K cells expressed the CD56 marker, which is commonly expressed in neuronal cell lines. However, the

MO59K cells are also CD45 negative and CD14 negative and were ~95% pure, confirming that the isolated cells are tumour and not immune cells (Figure 5.9).

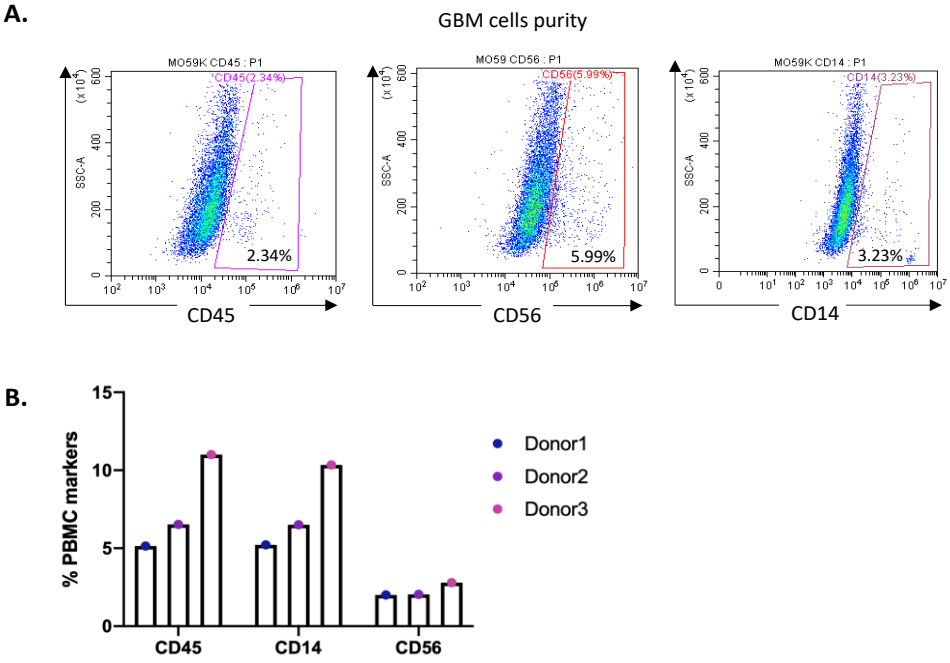

Figure 5-9 A representative validation of MO59K cells purity.

Flow cytometry analysis for **A.** MO59K cells and stained with CD45, CD56, and CD14 markers. **B.** showed the percentage of CD45, CD14, CD56 markers in the three PBMCs samples.

Next, RNA was then extracted from the isolated MO59K samples, and the RNA concentration was quantified by the nanodrop. Samples were prepared in triplicated by using three individual PBMC. All samples passed the quality control test by the company with RIN score above 9 (Table 5.1).

Table 5-1 RNA samples carried out by Novogene passed the QC RIN>9

Sample	Sample code
MO59K: PBMC_Veh	Veh _ Veh _A Veh _ Veh _B Veh _ Veh _C
MO59K: PBMC_Reo MOI 1	Veh _ Reo _A Veh _ Reo _B Veh _ Reo _C
MO59K: PBMC_ Reo MOI 1 + 100nM Dex	Veh _ ReoDex_A Veh _ ReoDex _B Veh _ ReoDex _C
MO59K+100nM Dex: PBMC_ Reo MOI 1	Dex _ Reo _A Dex _ Reo _B Dex _ Reo _C

PBMC treated with Reo before combining with MO59K cells was considered as the positive control. PBMC cotreated with ReoDex determine the effect of Dex on PBMC. Additionally, MO59K cells pre-treated with Dex determine how Dex might influence the GBM cell interaction with Reo-activated PBMC.

The sample code is written to describe the treatment of the MO59K cells followed by the treatment of the PBMC in a particular coculture. For example, Veh_ Veh refers to RNA-Seq data from MO59K cells in an experiment where vehicle treated M059K were cocultured with vehicle treated PBMC (the untreated controls) whereas Dex_Reo refers to MO59K transcriptome data from a coculture of Dex treated MO59K with Reo treated PBMC. The inclusion of A, B and C refers to the PBMC donor used.

The quality control of the raw RNA-seq data was examined to ensure that the RNA samples are reliable. A violin plot of the gene expression distribution was calculated based on FPKM method and showed that the gene expression level was similar between the groups indicating that the replicates are comparable (Figure 5.10.A). Results of the principal component analysis (PCA) was plotted, showing separation between most untreated and treated groups, although there was some separation amongst triplicates; this probably represents donor variability of the PBMC in the MO59K: PBMC cocultures (Figure 5.10.B). A heat map of DEGs demonstrated the hierarchical clustering with distinct expression pattern (Figure 5.10.C).

Although the QC summary shows all four treatment groups, the analysis will be divided into two parts – where Reo and Dex used as cotreatment on PBMC; and where GBM cells were treated with Dex and the PBMC were treated with Reo.

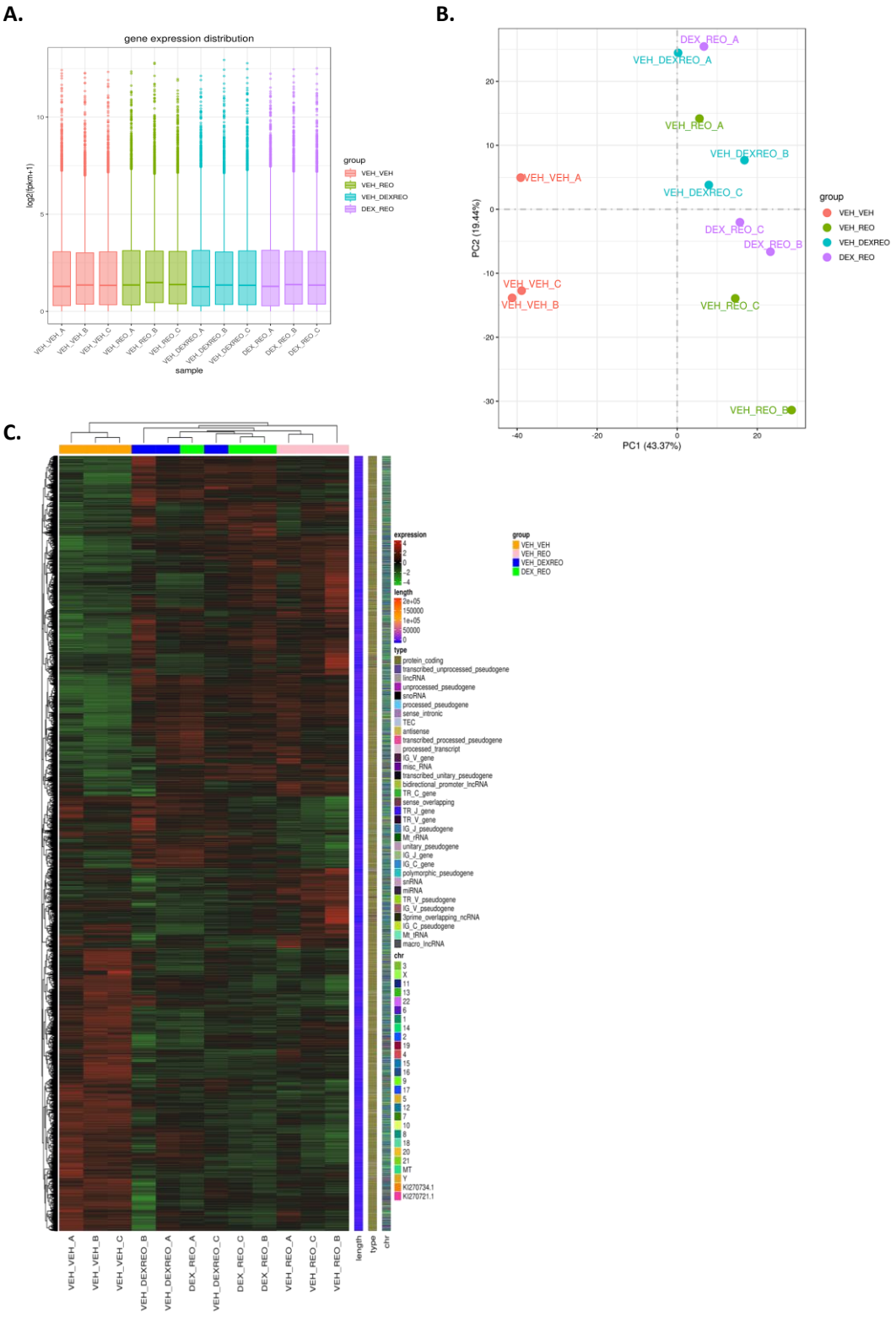

Figure 5-10 RNA-seq QC for the MO59K cells isolated from the coculture model

A. The gene expression distribution in box plot between groups based on log2 (FPKM+1). **B.** Principal component analysis (PCA) plot normalized expression values of MO59K cells untreated and treated replicates estimated raw counts of differentially expressed genes. **C.** The heat map of DEGs between the groups. The colour scale illustrates a high relative expression level (red) and low relative expression level (green).

Additional QC analysis for the RNA-seq samples shows the error rate distribution, data filtering and reference genome alignment (Figure 5.11). Table 5.2 shows the details of the clean reads results. Table 5.3 shows the reference genome comparison including the percentage of Exon, Intron, Intergenic reads, and Table 5.4 shows the error rate distribution.

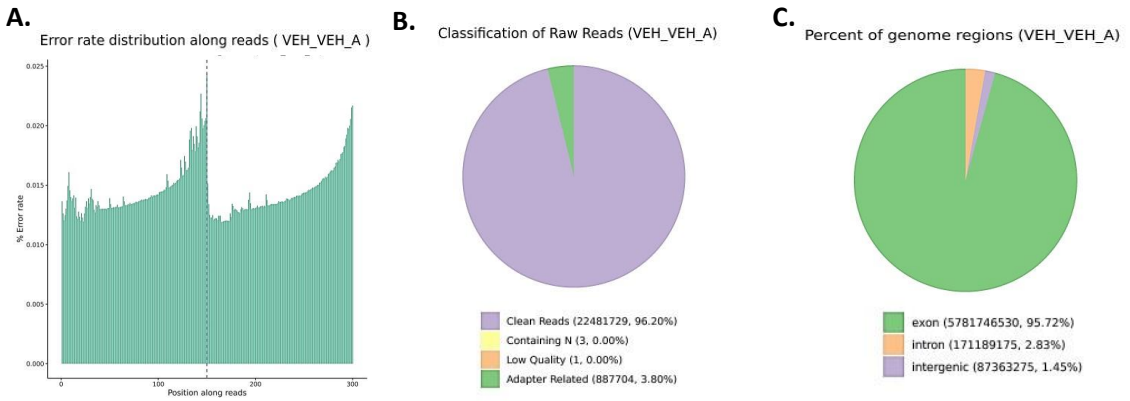

Figure 5-11 The quality control of the RNA-seq samples

The representative images show **A.** the error rate distribution. **B.** Sample sequencing data filtering and **C.** reference genome alignment of the RNA-seq samples.

Table 5-2 The details of the transcriptome assembly result

Sample	Library	raw_reads	raw_bases	clean_reads	clean_bases	error_rate	Q20	Q30	GC_pct
VEH_VEH_A	ERAS240023264 -2r	46738874	7.01G	44963458	6.74G	0.01	97.05	92.42	50.73
VEH_VEH_B	ERAS240023265 -1r	51334820	7.7G	51168982	7.68G	0.01	97.26	92.84	50.49
VEH_VEH_C	ERAS240023266 -1r	72477390	10.87G	72315710	10.85G	0.01	97.38	93.14	50.84
VEH_REO_A	ERAS240023268 -1r	53488312	8.02G	50526500	7.58G	0.01	97.44	93.23	50.23
VEH_REO_B	ERAS240023269 -1r	51598904	7.74G	49316136	7.4G	0.01	97.46	93.39	50.02
VEH_REO_C	ERAS240023270 -1r	2.08E+08	31.23G	1.91E+08	28.58G	0.01	97.89	94.4	50.88
VEH_DEXREO_A	ERAS240023272 -1r	1.41E+08	21.11G	1.29E+08	19.33G	0.01	97.86	94.24	50.2
VEH_DEXREO_B	ERAS240023273 -1r	59564492	8.93G	55941408	8.39G	0.01	97.64	93.77	46.99
VEH_DEXREO_C	ERAS240023274 -1r	43666486	6.55G	40181754	6.03G	0.01	98.19	95.16	50.82
DEX_REO_A	ERAS240023276 -1r	54632518	8.19G	49963444	7.49G	0.01	97.6	93.55	49.69
DEX_REO_B	ERAS240023277 -1r	60772562	9.12G	56294814	8.44G	0.01	97.65	93.75	49.85
DEX_REO_C	ERAS240023278 -1r	1.71E+08	25.62G	1.56E+08	23.33G	0.01	97.8	94.17	50.86

Table 5-3 Samples and reference genome comparison statistics

Sample	Exon	Intron	Intergenic
VEH_VEH_A	5781746530(95.7195%)	171189175(2.8341%)	87363275(1.4463%)
VEH_VEH_B	6362482274(94.5970%)	271868873(4.0421%)	91529039(1.3608%)
VEH_VEH_C	9478171405(95.7598%)	300143090(3.0324%)	119542492(1.2078%)
VEH_REO_A	6579978094(95.1325%)	246439670(3.5630%)	90227739(1.3045%)
VEH_REO_B	6089206265(93.2554%)	353922695(5.4203%)	86469143(1.3243%)
VEH_REO_C	24016813243(94.4984%)	1089566358(4.2871%)	308663257(1.2145%)
VEH_DEXREO_A	17016756867(96.2088%)	443636585(2.5082%)	226926899(1.2830%)
VEH_DEXREO_B	6458320504(94.3803%)	292280466(4.2713%)	92267356(1.3484%)
VEH_DEXREO_C	5218461915(95.6620%)	171879344(3.1508%)	64758629(1.1871%)
DEX_REO_A	6473113286(96.2113%)	169687549(2.5221%)	85217722(1.2666%)
DEX_REO_B	7178763149(95.2564%)	274077434(3.6368%)	83413055(1.1068%)
DEX_REO_C	20144306819(94.9597%)	832909252(3.9263%)	236301670(1.1139%)

Table 5-4 RNA-seq error rate distribution reads

sample	total_reads	total_map	unique_map	multi_map	read1_map	read2_map	positive_map	negative_map	splice_map	unsplice_map	proper_map
VEH_VEH_A	44963458	40366141(89.78%)	39348776(87.51%)	1017365(2.26%)	19679406(43.77%)	19669370(43.75%)	19617969(43.63%)	19730807(43.88%)	17743833(39.46%)	21604943(48.05%)	34946204(77.72%)
VEH_VEH_B	51168982	44970520(87.89%)	43739320(85.48%)	1231200(2.41%)	21927568(42.85%)	21811752(42.63%)	21814148(42.63%)	21925172(42.85%)	20079475(39.24%)	23659845(46.24%)	38934214(76.09%)
VEH_VEH_C	72315710	66137634(91.46%)	64357594(89.0%)	1780040(2.46%)	32270368(44.62%)	32087226(44.37%)	32118800(44.41%)	32238794(44.58%)	30494115(42.17%)	33863479(46.83%)	59081544(81.7%)
VEH_REO_A	50526500	46211550(91.46%)	45054832(89.17%)	1156718(2.29%)	22593306(44.72%)	22461526(44.45%)	22491321(44.51%)	22563511(44.66%)	20600631(40.77%)	24454201(48.4%)	40734442(80.62%)
VEH_REO_B	49316136	43631628(88.47%)	42522703(86.22%)	1108925(2.25%)	21307546(43.21%)	21215157(43.02%)	21228680(43.05%)	21294023(43.18%)	17401215(35.29%)	25121488(50.94%)	37861576(76.77%)
VEH_REO_C	1.91E+08	169843145(89.15%)	164806524(86.5%)	5036621(2.64%)	82575260(43.34%)	82231264(43.16%)	82251277(43.17%)	82555247(43.33%)	74626630(39.17%)	90179894(47.33%)	147357674(77.34%)
VEH_DEXREO_A	1.29E+08	118166007(91.72%)	114697307(89.03%)	3468700(2.69%)	57469728(44.61%)	57227579(44.42%)	57246012(44.43%)	57451295(44.59%)	55424526(43.02%)	59272781(46.01%)	103179928(80.09%)
VEH_DEXREO_B	55941408	45789622(81.85%)	44614688(79.75%)	1174934(2.1%)	22363525(39.98%)	22251163(39.78%)	22204005(39.69%)	22410683(40.06%)	18482537(33.04%)	26132151(46.71%)	33862458(60.53%)
VEH_DEXREO_C	40181754	36449378(90.71%)	35471923(88.28%)	977455(2.43%)	17779982(44.25%)	17691941(44.03%)	17708598(44.07%)	17763325(44.21%)	16410257(40.84%)	19061666(47.44%)	32184656(80.1%)
DEX_REO_A	49963444	44961697(89.99%)	43795705(87.66%)	1165992(2.33%)	21959276(43.95%)	21836429(43.7%)	21853936(43.74%)	21941769(43.92%)	21051959(42.13%)	22743746(45.52%)	38860762(77.78%)
DEX_REO_B	56294814	50367149(89.47%)	49045955(87.12%)	1321194(2.35%)	24583845(43.67%)	24462110(43.45%)	24479751(43.48%)	24566204(43.64%)	22034808(39.14%)	27011147(47.98%)	43350864(77.01%)
DEX_REO_C	1.56E+08	141734812(91.12%)	137629356(88.49%)	4105456(2.64%)	68972875(44.34%)	68656481(44.14%)	68698888(44.17%)	68930468(44.32%)	63686373(40.95%)	73942983(47.54%)	126425656(81.28%)

5.2.5 Cotreating PBMC with Reo and Dex; effect on the MO59K cell transcriptome

MO59K cells (vehicle treated) were cocultured with PBMC treated with Reo alone or in combination with Dex. This RNA-seq analysis identified three sets of differentially expressed gene (DEGs) based on the comparison:

- Veh_ Veh versus Veh _ Reo
- Veh _ Veh versus Veh _ReoDex
- Veh _Reo versus Veh _ReoDex

5.2.5.1 Differentially expressed genes (DEGs)

Figure 5.12 shows DEGs identified by the RNA-seq analysis. There were 2177 DEGs regulated by Reo treated PBMC (Veh_Reo versus Veh_Veh). Of these 2177 genes, the majority (1497, 69%), were upregulated in MO59K in response to culture with Reo-treated PBMC. Upregulated genes included cytokines (TNF, IFNB1, IL-1B, IL-6, IFNG), transcription factors (IRF1, TP53, STAT1) and chemokines CXCL8, CXCL10, CCL5). Gene set enrichment analysis (GSEA) revealed several pathways associated with viral infection and cytokine-cytokine receptor interactions. Furthermore, a protein-protein interaction network analysis (using STRING) highlighted the key hub genes as those involved in these pathways (Figure 5.12.A). I repeated this analysis for Veh_Veh versus Veh _ReoDex (Figure 5.12.B). The volcano plot was very similar in appearance to that in 5.12.A, suggesting that the inclusion of Dex was not modifying the transcriptome very much. Several MO59K genes induced by Reo treated PBMC were also induced by ReoDex treated PBMC and similar GSEA and hub genes were identified (Figure 5.12.C). Analysis of DEGs between Veh_Reo and Veh_ReoDex confirmed the relatively small effect of Dex treatment under these coculture conditions. Only 339 genes were differentially expressed between these groups and both GSEA and hub gene analysis (with the top 20 genes shown in Table 5.5) demonstrated that the inclusion of Dex did modify the response of PBMC to Reo and in turn impact on the MO59K transcriptome.

Pathway enrichment analysis was next graphed as bubble plot created using SRplot website tool, showing the top 10 terms by KEGG database identified common enriched pathways related inflammation (TNF, and NF-kB signalling

pathway), cell death (apoptosis, cellular senescence, necroptosis), viral infection (viral protein interaction with cytokine and cytokine receptor, NOD-like receptors, Toll-like receptors, RIG-like receptors), and TME (cytokine-cytokine receptor interaction, and NK cells mediated cytotoxicity) which is listed in Tables 7.9 to 7.10, and will be discussed in more detail in following sections.

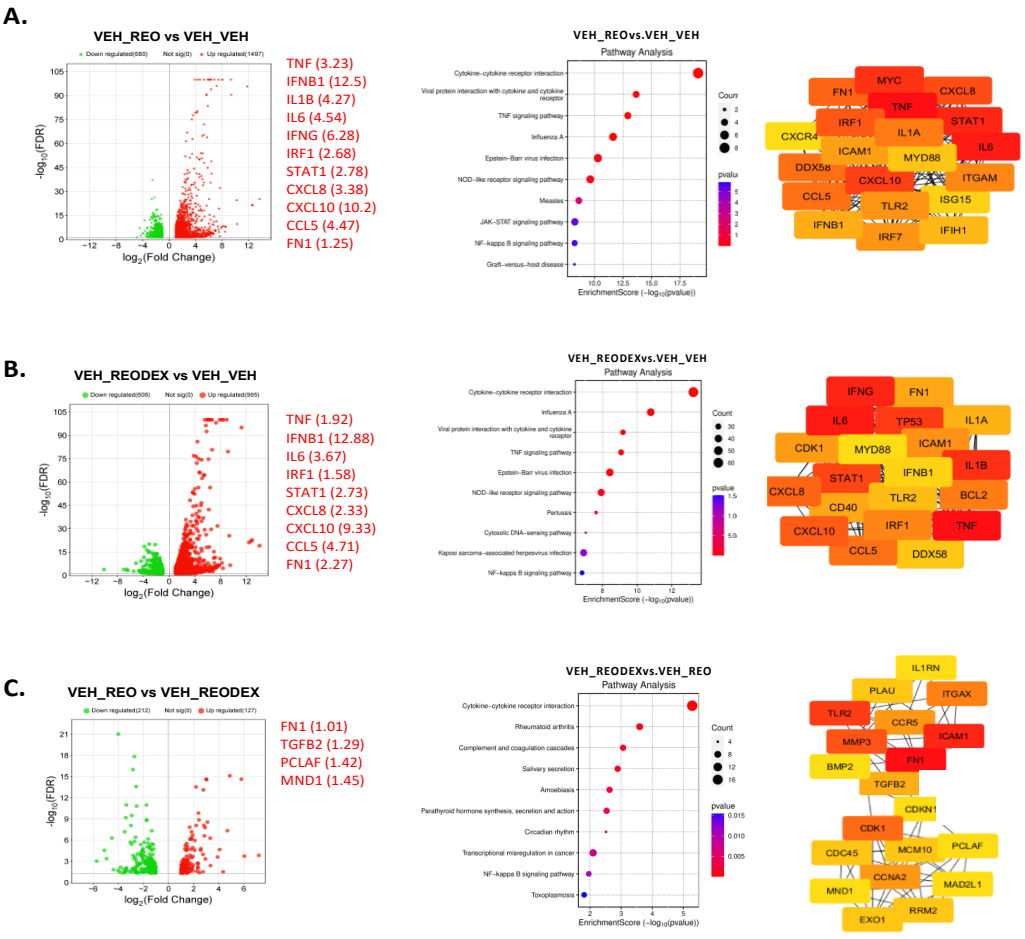

Figure 5-12 The DEGs of MO59K cells cocultured with different PBMC conditions.

For each of the three comparisons (**A-C**), show a volcano plot of DEGs (left panel), the GSEA analysis (using KEGG) and the PPI network of the top 20 hub genes for the three DEGs datasets via STRING and Cytoscape/cytoHubba. Genes listed adjacent to the volcano plots in red are a fraction of genes with greater expression, with the log2 fold change shown in brackets.

For both Reo and ReoDex treatments, induced genes are reminiscent of an anti-viral or inflammatory response; Reo is detected by the PBMC, inducing a type I interferon (IFN-I) response, as shown previously (El-sherbiny, 2015; Wantoch *et al.,* 2022). The treated PBMC are washed before coculture with the MO59K but it is possible that some Reo was transferred to the coculture. The top two hub genes for the Reo and ReoDex datasets were the pro-inflammatory genes TNF and IL-6. These were induced by both Reo and ReoDex but induction with ReoDex was lower, suggesting a role for Dex in inhibiting their expression and consistent with the anti-inflammatory action of Dex on these genes.

Table 5-5 List of the top 20 hub genes for the DEGs datasets

REO DEGs					REODEX DEGs					DEX modifying REO DEGs			
Rank	Name	score	Log 2FC		Rank	Name	score	Log 2FC		Rank	Name	score	Log 2FC
1	TNF	357	3.23		1	TNF	282	1.92		1	FN1	46	1.01
2	IL6	348	4.54		2	IL6	271	3.67		2	ICAM1	35	-1.27
3	IFNG	314	6.28		3	STAT1	223	2.73		3	TLR2	27	1.12
4	IL1B	312	4.27		4	MYC	187	1.73		4	MMP3	25	-3.99
5	TP53	309	-1.35		5	CXCL10	186	9.33		5	CDK1	23	1.02
6	STAT1	277	2.78		6	CXCL8	177	2.33		6	ITGAX	22	-1
7	CXCL10	229	10.2		7	IRF1	163	1.58		7	CCNA2	20	1.24
8	CXCL8	225	3.38		8	FN1	154	2.27		8	CCR5	20	-2.36
9	CCL5	201	4.47		9	DDX58	151	5.54		9	TGFB2	19	1.29
10	BCL2	194	2.25		10	CCL5	151	4.71		10	CDC45	18	1.28
11	IRF1	190	2.68		11	IL1A	145	4.33		11	PLAU	18	-1.67
12	ICAM1	188	2.33		12	ITGAM	144	-1.85		12	MCM10	18	1.15
13	CDK1	187	-1.96		13	TLR2	143	5.41		13	EXO1	18	1.1
14	FN1	183	1.25		14	IRF7	143	3.79		14	RRM2	18	1.07
15	CD40	183	2.7		15	ICAM1	139	1.06		15	PCLAF	17	1.42
16	IL1A	181	4.29		16	IFNB1	137	12.88		16	MAD211	17	1.07
17	TLR2	173	4.27		17	IFIH1	136	5.37		17	CDKNIA	17	-1.04
18	DDX58	170	5.26		18	MYD88	135	2.07		18	MND1	17	1.45
19	IFNB1	169	12.5		19	ISG15	134	4.56		19	BMP2	17	-2.18
20	MYD88	167	2.26		20	CXCR4	133	2.42		20	IL1RN	17	-1.84

Next, a Venn diagram was used to identify 44 shared DEGs between the different groups and their expression was visualised using a heatmap (Figure 5.13.A and B). These 44 genes are altered by Reo, and by ReoDex, but are significantly different between the two groups. 35 of the 44 genes were upregulated in both treatments, 4 were downregulated in both treatments, while 4 genes were up-regulated by Reo but downregulated by ReoDex (CST4, RIPOR3, TNFRSF11B/OBG, TNFRSF18), and only SLCO2A1 was downregulated by Reo but upregulated by ReoDex. Notably, DUSP1, which is a key GCs gene, showed higher differential expression by ReoDex than Reo alone (Figure 5.13.C).

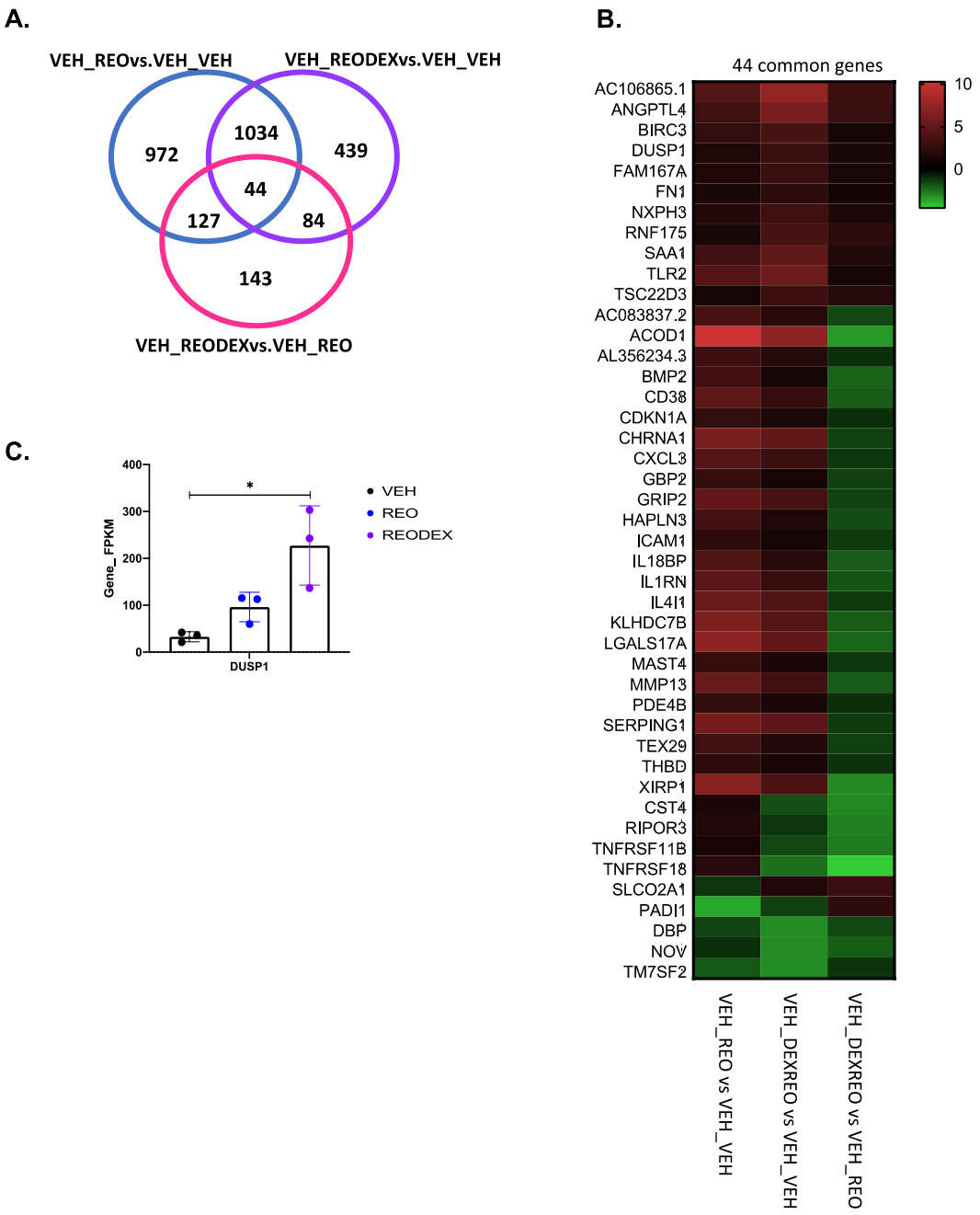

Figure 5-13 Identifying 44 overlapped genes between GBM cells cocultured different treatment conditions.

A. Venn diagram identified common genes between the three comparisons **B.** A heat map of the common 65 DEGs showing genes with similar or opposite direction between the three comparisons. **C.** DUSP1 expression increased by pre-Dex. significance was tested for n=3 independent samples using one-way ANOVA with multiple comparison test, where (ns p>0.05, *p≤0.05, **p≤0.005, ***p≤0.001, and ****p≤0.001).

5.2.5.2 Dex influenced Reo indirect mediating GBM killing through multiple death/proliferation pathways

I have shown previously (section 5.1) that PBMC co-treated with Reo plus Dex reduced the immune mediated killing of GBM cells in a coculture model. Therefore, I compared the DEGs of MO59K regulated by Reo and ReoDex to identify genes regulating cell death. Gene set enrichment analysis (using KEGG) showed that the apoptosis pathway was enriched in DEGs regulated by Reo and ReoDex (Figure 5.14.A). Caspase genes were similarly upregulated in both datasets. Relevant genes upregulated by Reo included FASLG, NTRK1, TRADD, BAK, ERN1, and PARP3 while TP53 was downregulated. In contrast, CASP8 was upregulated by ReoDex and MAPK3/ERK was downregulated. Interestingly, the BIRC3 gene showed increased expression by ReoDex (log2FC 3.61) in comparison to Reo (log2FC 2.48). BIRC3 is a member of the inhibitor apoptosis gene (IAPs), a negative regulator of NF-kB and inhibits apoptosis. This suggest that Dex might block the apoptosis pathway through BIRC3, which, as shown above, is associated with GBM poor prognosis. Figure 5.14.B shows the relative expression levels of apoptosis genes in the MO59K cells cocultured with the Reo and ReoDex treated PBMC. Many genes on the apoptosis pathway are regulated (see also 6.15.A) and many show that Dex inhibits the Reo mediated induction of apoptotic gene expression. Additionally, CDKNIA (p21) is a cyclin-dependent kinase inhibitor that inhibits the cell cycle at G1, with its overexpression reported to induce apoptosis in GBM (Gousias *et al.,* 2022); this gene was downregulated by ReoDex (Figure 5.14.B). Furthermore, positive regulators of the GBM cell cycle, CCNA2, and CDK1 (Yang *et al.,* 2020; Doan *et al.,* 2019) were increased by ReoDex, suggesting that Dex might induce GBM growth and tumour progression.

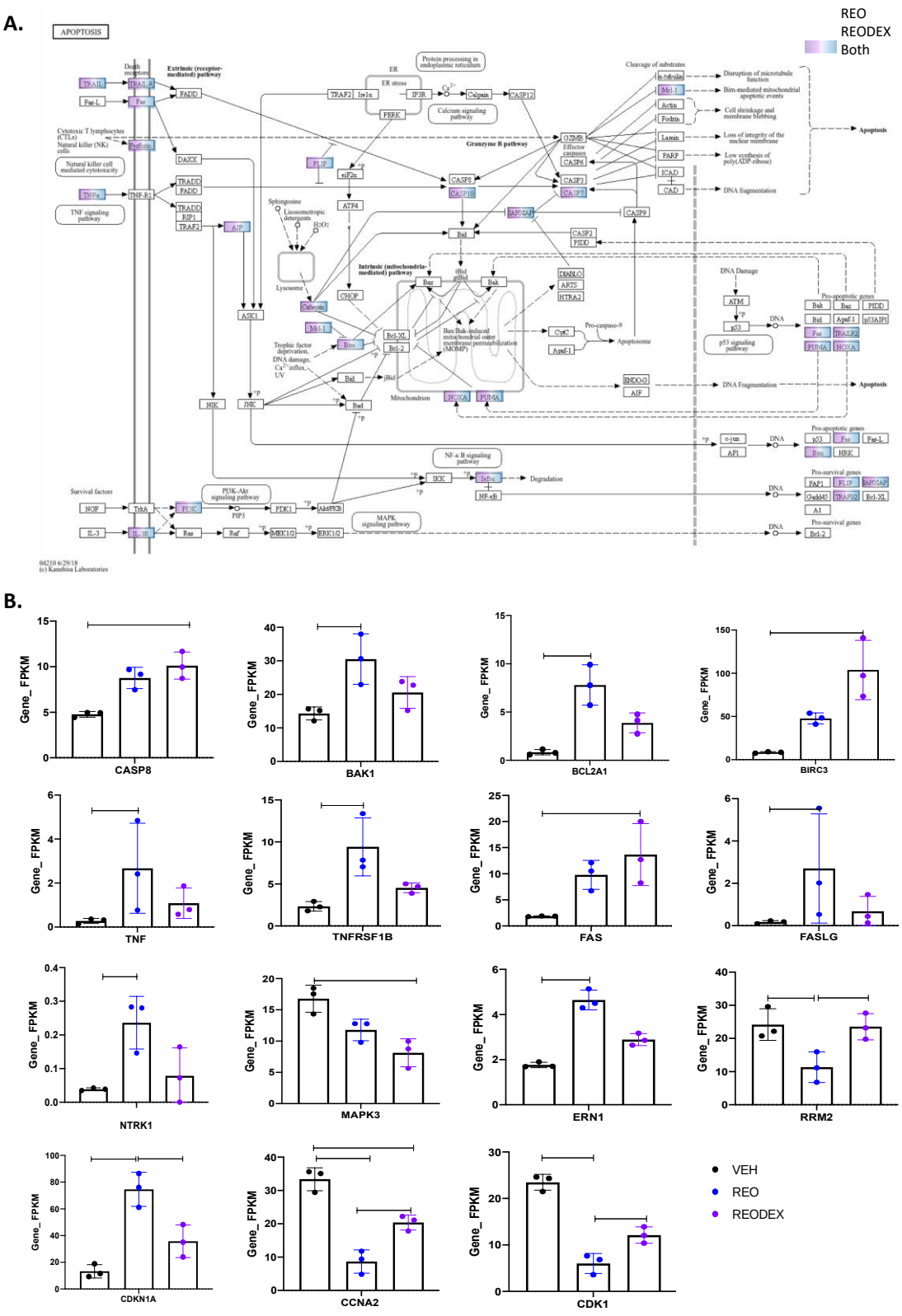

Figure 5-14 Dex modulates Reo induced apoptosis pathway.

Apoptosis pathway map obtained from the KEGG enrichment analysis. The map shows the genes involved in apoptosis pathways with respect to the DEGs regulated by Reo only (blue), ReoDex only (purple), or both (gradient). **B.** The RNA-seq genes count by FPKM for mutable genes regulated by Dex to decrease GBM cell death in response to Reo-treated PBMC. significance was tested for n= 3 independent samples using one-way ANOVA with multiple comparison test, where (ns $p>0.05$, *$p\leq0.05$, **$p\leq0.005$, ***$p\leq0.001$, and ****$p\leq0.001$).

The IFNG gene was induced by Reo and strongly inhibited by ReoDex. Several other inflammatory pathways were similarly regulated, including the IFN response factor (IRF1) and TNF superfamily members. This suggests that the immunosuppressive effects of Dex might reduce type I and type II interferon responses, which is likely to reduce immune control of GBM (Figure 5.15.A). Figure 5.15.B and C showed that expression of TNFSF14/LIGHT, and its receptor TNFRSF14 were regulated by these treatments. TNFRSF14 is a regulatory cytokine that plays essential roles in immunity as it can stimulate NK cells to produce IFN-γ through NF-κB signalling pathway, and is reported to be highly expressed in mesenchymal GBM subtype (Han *et al.,* 2022). Expression of TNFSF14 was induced by Reo and inhibited by ReoDex, suggesting that Dex regulates its expression, and its ability to activate NK cells. Expression of the CD40 gene was induced in MO59K as a result of Reo treatment of PBMC (Figure 5.15.D). CD40 is usually expressed by immune cells but can also be expressed in tumour cells. Interestingly, the high expression of the CD40/CD40L axis in GBM is associated with better patient survival (Chonan *et al.,* 2015), suggesting that this response to Reo might be beneficial. In addition, PLAU (uPA) is a serine protease that promotes several signalling pathways. PLAU regulates ECM turnover and promotes angiogenesis. Gepia2 analysis showed its high expression in GBM and LGG tissue in comparison to normal brain, and correlated with GBM poor survival as measured by Kaplan-Meier curve on GBM samples alone (n=81) with non-significant HR (1.3) but significant with HR 4.6 when combined with LGG (n=338); ReoDex samples showed significant reduction in PLAU expression (Figure 5.15.E).

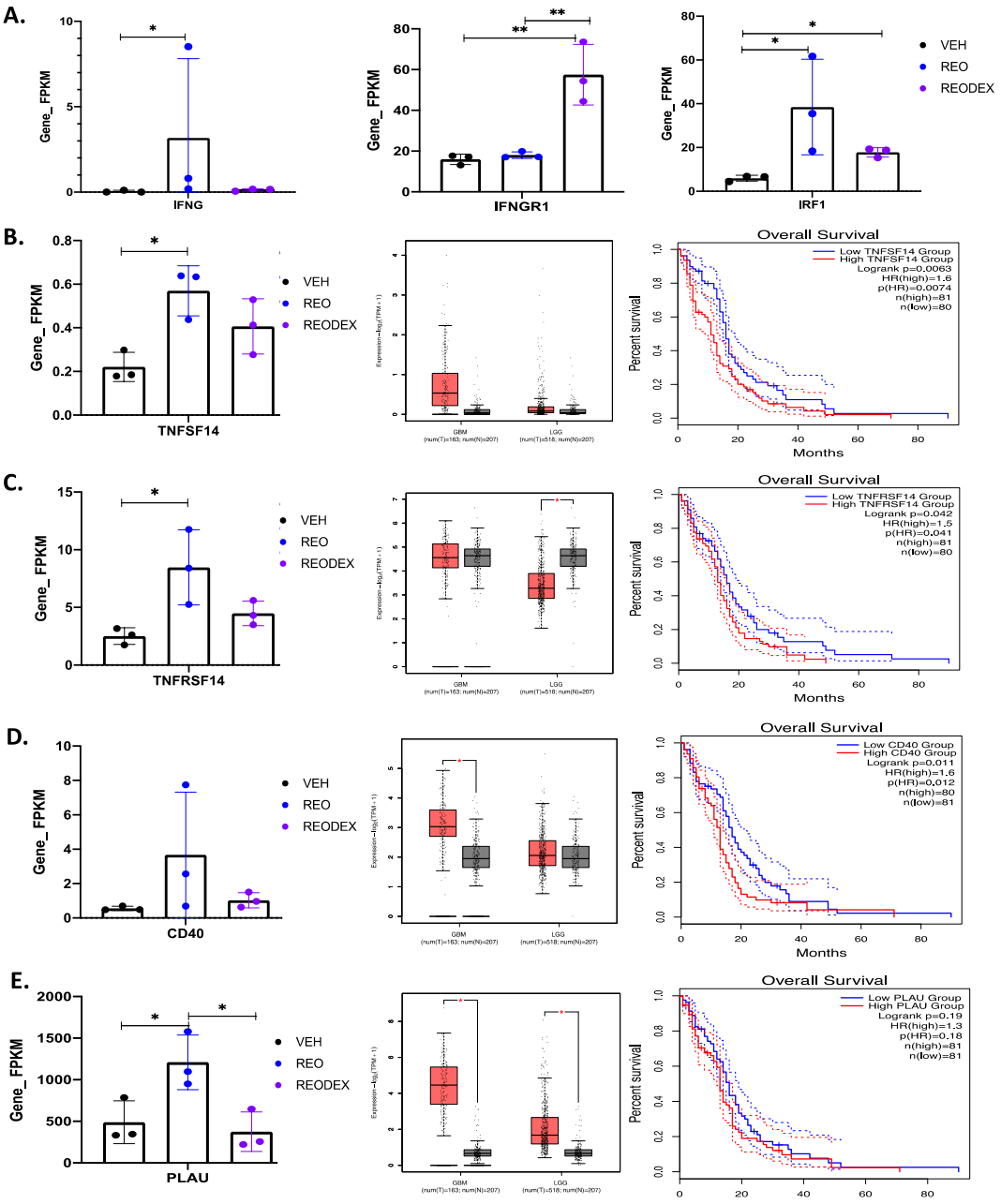

Figure 5-15 Genes promoted by NF-kB pathway.

Summary of kye gene within NF-kB pathway, where the left panel shown FKPM from the RNA-seq data, central panels show the expression in normal vs. tumour samples in the TCGA dataset using gepia2 analysis, and right panels show survival plots demonstrated by the Kaplan Meier Curve **A.** IFN-γ/IFNGR1 axis; **B, C.** TNFSF14/TNFRSF14 axis; **D.** CD40; and **E.** PLAU genes. Statistical significance of gene expression level (FKPM) was tested for n=3 independent samples using one-way ANOVA with multiple comparison test (ns p>0.05, *p≤0.05, **p≤0.005, ***p≤0.001, and ****p≤0.001).

5.2.5.3 Viral mediated regulation of apoptosis is essential for successful virus replication pathway

Another pathway identified by GSEA was viral protein interaction with cytokines (illustrated in Figure 5.16.A) with many genes highlighted as being regulated by Reo, ReoDex or both. In particular, a large number of chemokine and chemokine receptor genes were identified (Figure 5.16.B), suggesting that these treatments might alter the recruitment of immune cells to brain tumours.

A.

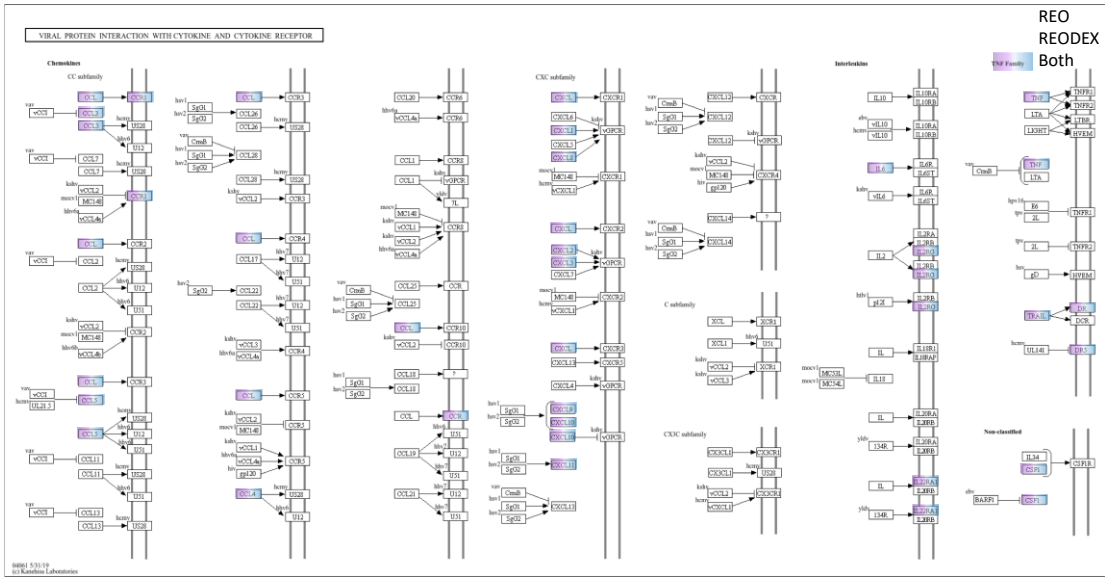

B.

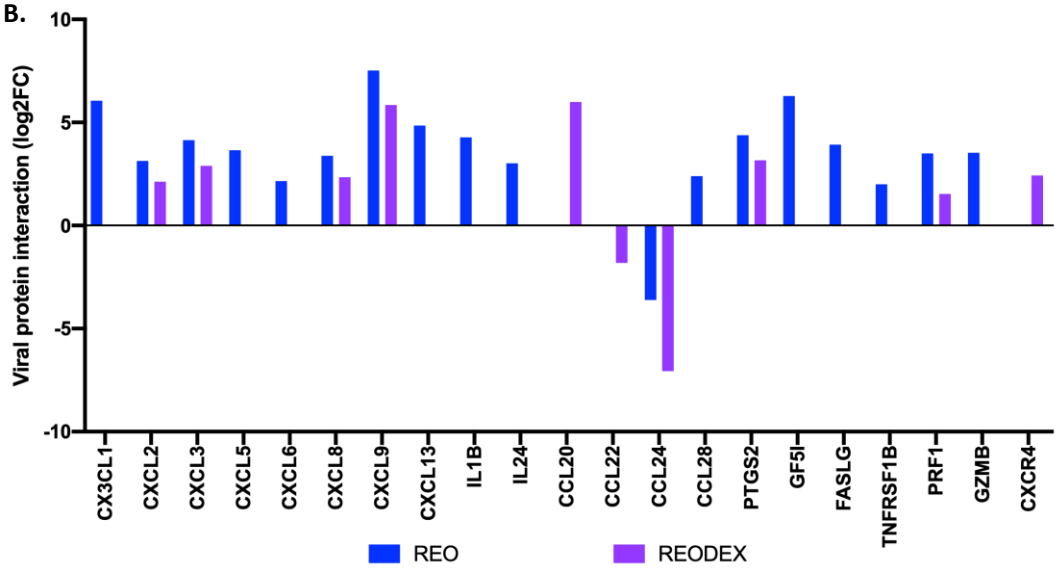

Figure 5-16 Dex regulated viral protein interaction with cytokines and cytokines receptors

A. The map was obtained from KEGG (https://www.genome.jp/kegg/brite.html). Expressed genes were highlighted based on the coculture PBMC conditions, Reo (blue), ReoDex (burble) and gradient when expressed in both datasets. **B.** highlight the DEGs involved in the viral interaction with cytokines based on the log2FC.

Expression of CXCL8, CXCL9, CXCL10 was significantly increased in GBM tissue in comparison to normal brain tissue, and this correlated with GBM poor survival (Figure 5.17).

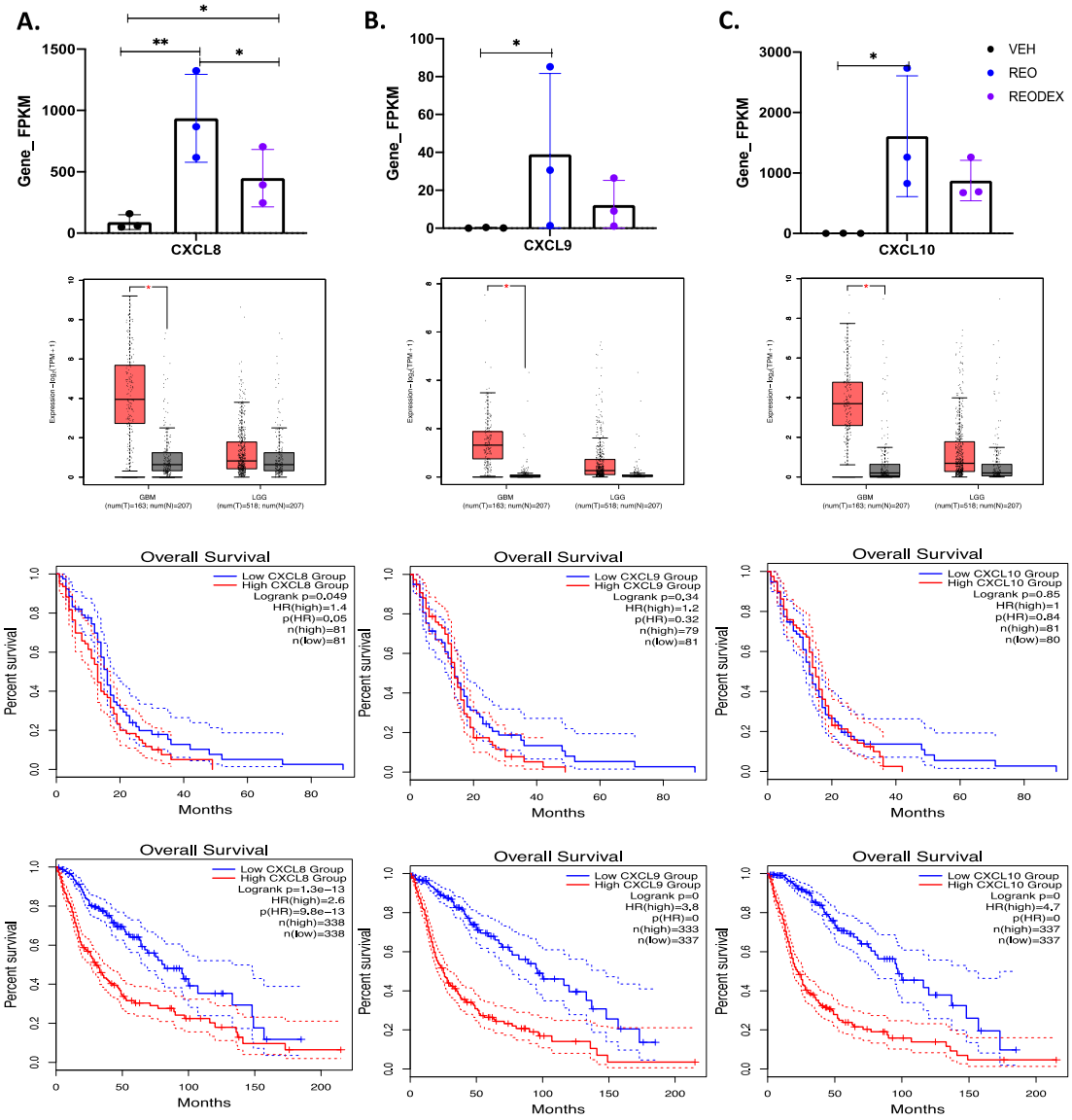

Figure 5-17 Genes promoted by chemokines.

Dex regulated **A.** CXCL8 **B.** CXCL9**, C.** CXCL10 genes. All genes showed their RNA level measured by FPKM level (top). Statistical significance was tested for n=3 independent samples using one-way ANOVA with multiple comparison test (ns p>0.05, *p≤0.05, **p≤0.005, ***p≤0.001, and ****p≤0.001). Gepia2 analysis (middle) showed significant increase expression in GBM tissue in comparison normal brain tissue. Chemokines showed increase correlation with GBM poor survival, as shown in the Kaplan Meier Curve (bottom) on GBM samples alone (n=81) or combined with LGG (n=338).

5.2.5.4 Natural killer cell mediated cytotoxicity was enriched in Reo treatment group

The MO59K data also showed changes in the expression of RAET1L/ULBP6, being induced by Reo (log2FC 3.12) and further induced by ReoDex (log2FC 4.53), suggesting that Dex induces its expression. The RAET1L protein is a cell surface molecule that binds to the NKG2D activating receptor on NK cells to induce NK cell cytotoxicity (Ma and Kuang, 2016). This suggest that DEX might increase NK cytotoxicity to GBM cells. Expression of other NK cell ligands was altered by treatments; CD48 (a ligand of 2B4/CD244) and HLA-G (a ligand of KIR2DL4 and ILT family members) were both upregulated by Reo and reduced by ReoDex. CD48 has both activating and inhibitory activity on NK cells but HLA-G is associated with inhibition of NK cell activity. Interestingly, ICAM1 expression showed a reduction in log2FC from 2.33 by Reo to 1 by ReoDex. ICAM1 is a cell adhesion molecule that bind to LFA1 on NK cells to promote NK cell adhesion and cytotoxicity (Jeong *et al.,* 2018). This suggests that ICAM1 downregulation reduces NK cells ability to adhere to tumour target cells and reduces NK cell killing of the tumour. NK cells mediating cytotoxicity pathway was mapped by KEGG (Figure 5.18.A), and the expression of these genes is shown in Figure 5.18.B.

Interestingly, the MO59K data identified perforin (PRF1) and granzyme B (GZMB) as upregulated by Reo. These genes are essential and highly expressed components of the NK cell and T cell cytotoxic machinery, and are not expressed by GBM cells. The detection of transcripts of these genes suggests that the isolated GBM cells are contaminated with NK cells. However, the fact they are only detected in sample incubated with PBMC treated with Reo and not ReoDex provides a valuable insight – that Reo promotes contamination with NK cells, but this is not observed with ReoDex.

After coculture, the GBM cells are washed several times to remove non-adherent immune cells. This leave me to speculate that Reo is driving recruitment of NK cells to attach to the GBM cells, and that Dex is somehow blocking this. This would also be consistent with some of my in vitro findings, and also data from my single culture RNA-seq.

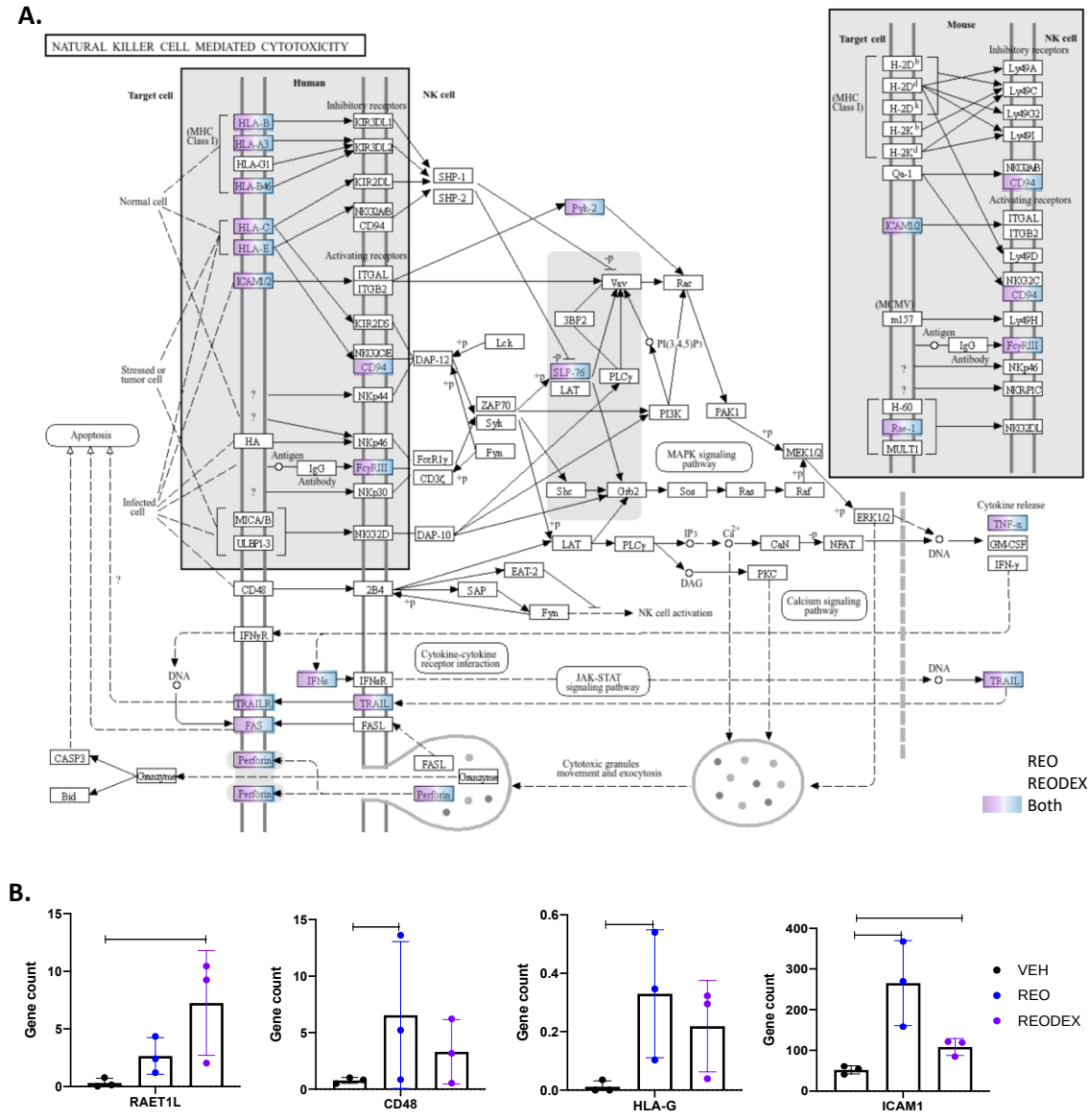

Figure 5-18 Dex regulates ligands on GBM cells to regulate NK function.

A. The pathway was obtained from the KEGG enrichment analysis of DEGs in MO59K-treated Reo (purple) and ReoDex (Blue) alone or both (gradient). KEGG map was taken from (https://www.genome.jp/kegg/brite.html). **B.** proposed ligands on GBM cells (RAET1L, CD48, HLA-G, ICAM1) interact with NK cells receptors to modulate NK cytotoxicity. Statistical significance was tested for n=3 independent samples using a one-way ANOVA with multiple comparison test, (ns p>0.05, *p≤0.05, **p≤0.005, ***p≤0.001, and ****p≤0.001).

5.2.5.5 The ECM pathway

The matrix metalloproteinase genes MMP13, MMP10, MMP12 and MMP14 were downregulated by ReoDex, while fibronectin (FN1) was upregulated in comparison to Reo. Among identified MMPs, MMP14 expression was significantly higher in GBM tissue in comparison to normal brain tissue (Figure 5.19.A). Previous study demonstrated MMP14 association with M2 in GBM to impair GBM progression (Li *et al.,* 2023). FN1 (Fibronectin-1), is an ECM protein that is upregulated in GBM tissue and correlated with worse GBM survival (Figure 5.19.B). It was demonstrated that Dex promotes cell adhesion through increasing FN1 expression in ovarian cancer (Giorgievski *et al.,* 2019). Overall, ECM plays an essential role in GBM invasion through inflammation. The increase ed expression of ECM molecules is linked to worse prognosis in GBM patients.

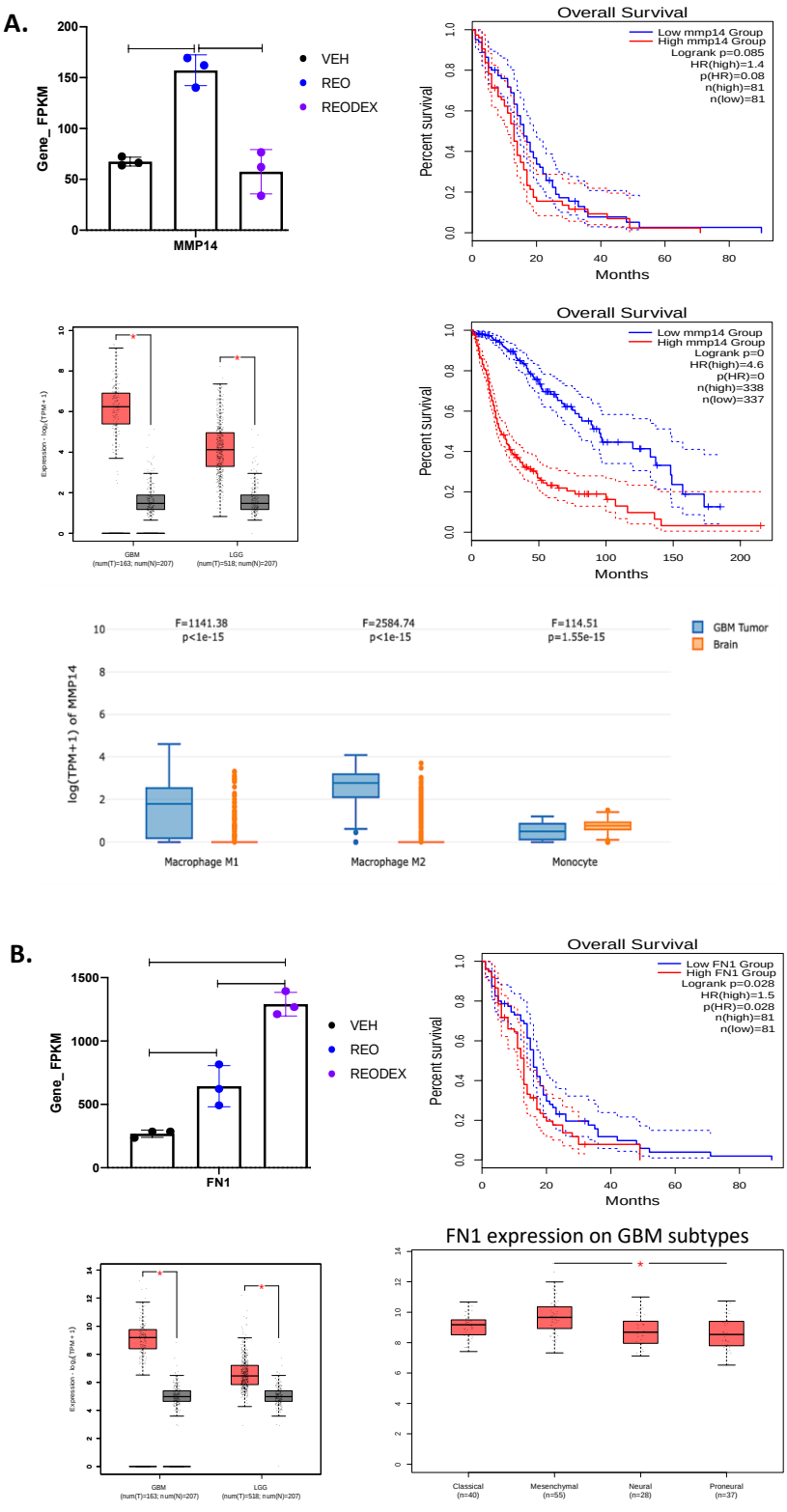

Figure 5-19 Dex regulates cell adhesion genes to promote GBM invasion.

Dex regulated ECM genes by **A.** downregulating MMP14 and **B.** upregulating FN1 expression. MMP14 and FN1 RNA level measured by FPKM level. Statistical significance was tested for n=3 using one-way ANOVA with multiple comparison test (ns p>0.05, *p≤0.05, **p≤0.005, ***p≤0.001, and ****p≤0.001). Gepia2 analysis showed a significant increase in the expression of MMP14 and FN1 in GBM tissue compared to normal brain tissue. Kaplan Meier Curve analysis using the gepia2 tool demonstrated a correlation between these genes and poor survival in GBM.

5.2.6 RNA-seq analysis of MO59K cells pre-treated with Dex and cocultured with Reo activated PBMC

MO59K cells were pre-treated with Dex for 24 hours and then cocultured with PBMC untreated or treated with Reo. This was compared to MO59K cells (vehicle-treated) cocultured with PBMCs treated with Reo. This RNA-seq analysis identified two new sets of the DEGs based on the comparison:

- Veh_ Veh and Veh _Reo (Reo) (as in previous section)
- Veh _ Veh versus Dex_ Reo (pre-Dex GBM and Reo-PBMC)
- Veh _Reo and Dex_ Reo

Figure 5.20.A shows DEGs identified by the RNA-seq analysis. There were 2201 DEGs regulated by pre-Dex (Veh_Veh vs. Dex_Reo). Gene set analysis (GSEA) revealed several pathways associated TNF signalling and viral infection and cytokine-cytokine receptor interactions as listed in tables 7.12 and 7.13. Furthermore, PPI network analysis (using STRING) highlighted the key hub genes as those involved in these pathways. Figure 5.20.B shows only 199 DEGs between Veh_Reo vs. Dex_Reo, suggesting the minimal effect of Dex in modifying the transcriptome.

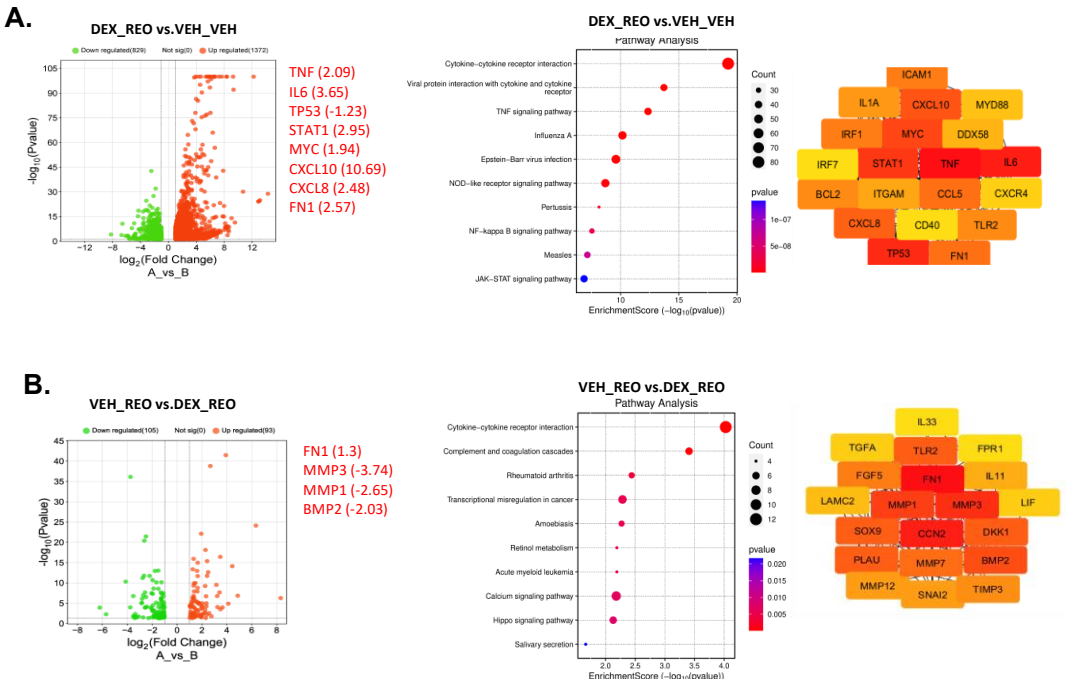

Figure 5-19 The DEGs of Dex treated GBM cultured with Reo-activated PBMC.

Volcano plot of the DEGs comparing pre-Dex GBM in response to Reo- PBMC (left), the shift between pre-Dex GBM in response to Reo-PBMC to the baseline (right). Red dots represent upregulated genes, and green dots represent the downregulated genes**.** The top 20 hub genes including the list of the genes with score and log2FC value.

Table 5-6 List of the top 20 hub genes for the DEGs datasets

preDEX DEGs					preDEX modifying REO DEGs			
Rank	Name	score	Log 2FC		Rank	Name	score	Log 2FC
1	TNF	333	2.09		1	FN1	35	1.3
2	IL6	326	3.65		2	CCN2	22	-
3	TP53	301	-1.23		3	MMP3	21	-3.74
4	STAT1	262	2.95		4	MMP1	20	-2.65
5	MYC	238	1.94		5	BMP2	17	-2.03
6	CXCL10	218	10.69		6	PLAU	16	-1.47
7	CXCL8	217	2.48		6	SOX9	16	-1.24
8	FN1	186	2.57		6	TLR2	16	1.59
8	CCL5	186	4.79		6	DKK1	16	1.1
10	ICAM1	181	2.2		10	MMP7	15	1.98
10	IRF1	181	2.7		11	FGF5	14	-1.38
12	BCL2	175	1.48		12	TIMP3	13	-1.22
12	TLR2	175	5.89		13	SNAI2	12	1.35
14	IL1A	173	4.23		13	MMP12	12	-2.71
15	ITGAM	172	-1.68		15	IL11	11	-2.5
16	DDX58	167	5.52		16	LAMC2	10	-1.29
17	MYD88	162	2.13		17	TGFA	9	-1.43
18	CXCR4	161	2.63		17	LIF	9	-1.17
19	IRF7	160	3.96		19	FPR1	8	3.15
19	CD40	160	1.24		19	IL33	8	-2.85

The top 2 genes with the highest hub score were TNF and IL-6, whose expression were downregulated in MO59K cells pretreated with Dex (Table 5.6). MYC, IL-11, and FPR1 were differentially expressed in pre-Dex. The RNA-seq gene level (FPKM) showed IL-11 downregulation and FPR1, MYC upregulation in comparison to the baseline (Figure 5.21.A). Gepia2 analysis however showed a non-significant MYC and FPR1 genes expression in GBM tissue in comparison to normal tissue (Figure 5.21.B). FPR1 (formyl peptide receptor 1) encodes a G protein coupled receptor which transactivate EGFR to promote GBM growth and invasion (Liu *et al.,* 2012). The pro-inflammatory IL-11 increases GBM proliferation and survival as its also influence immune cells within the GBM TME. It is well known that GCs supress the pro-inflammatory cytokines TNF, IL-11 and IL-6.

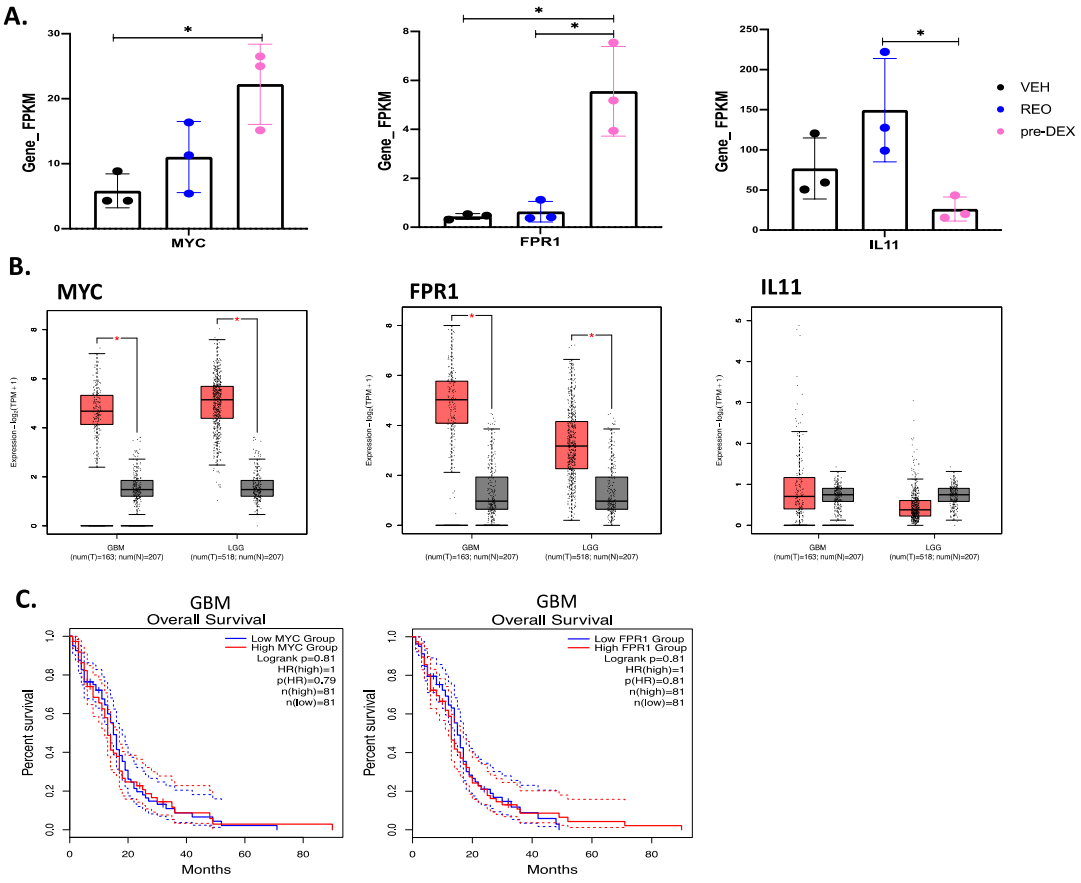

Figure 5-20 The pre-Dex GBM hub genes.

A. MYC and PFR1 were upregulated while ITGAM and IL-11 were downregulated in response to pre-Dex treatment. Data shows the mean ± SEM for n=3 independent samples, and significance was tested using one-way ANOVA with multiple comparison test (ns p>0.05, *p≤0.05, **p≤0.005, ***p≤0.001, and ****p≤0.001. **B.** MYC and PFR1 expression were significantly upregulated in GBM samples compared to normal samples as assessed by using the Gepia2 web tool. **C.** Kaplan-Meier survival curve was generated for GBM samples (n=81) for the genes showing non-significant correlation with poor GBM survival.

DKK1 is one of the hub genes identified in the Veh_Reo vs. Dex_Reo set, and the FPKM level showed significant increase by pre-Dex in comparison to Reo or Veh (Figure 5.22). DKK1 (Dickkopf Wnt signalling pathway inhibitor 1) gene is a Wnt/B inhibitor and its overexpression activates PI3K/AKT pathway (Li *et al.,* 2022). Promoter hypermethylation of the DKK1 gene is frequent in GBM and induced by Dex (Moors *et al.,* 2012), suggesting its potential as targeted therapy or biomarker. GR interacts with DKK1 promoter in human neural stem/ progenitor cells and increases in its expression leads to inhibition of stem cells proliferation

and stimulates glial cells differentiation. DKK-1 levels were Increased in the cerebrospinal fluid of GBM patients (Zhou *et al.,* 2010), suggesting DKK1 role in GBM tumorigenesis.

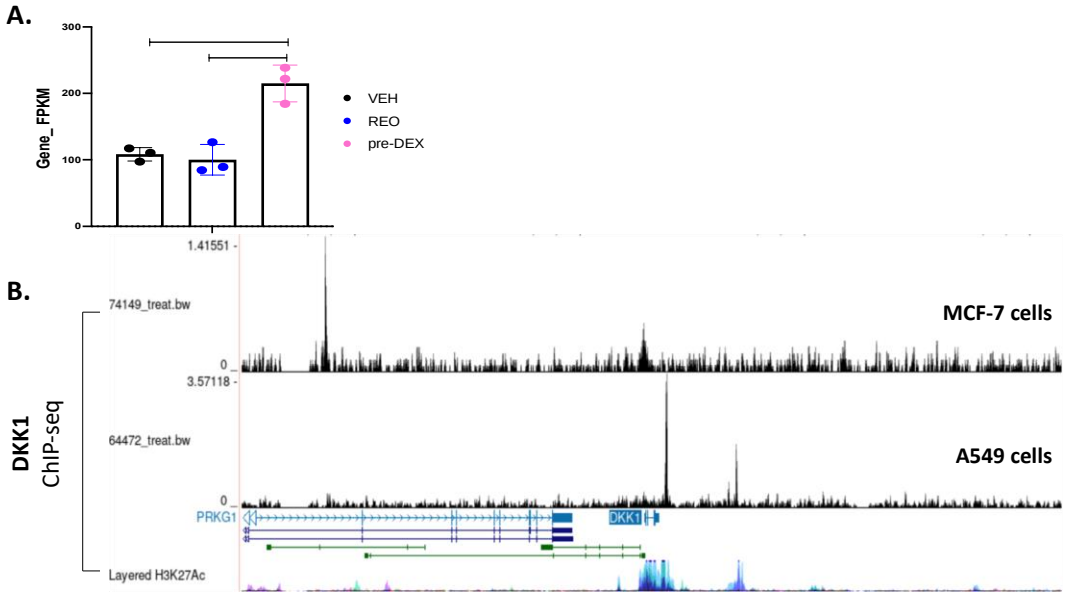

Figure 5-21 Pre-Dex treatment on GBM cells induces DKK1 gene expression.

A. The pre-Dex treatment induces DKK1 expression. Data show the mean ± SEM for n=3 independent samples, and significance was tested for n=3 independent samples using one-way ANOVA with multiple comparison test (ns $p>0.05$, *$p\leq0.05$, **$p\leq0.005$, ***$p\leq0.001$, and ****$p\leq0.001$. **B.** ChIP analysis showed GR (NR3C1) binding to DKK1 promoter in lung and breast cancer cell lines.

Next, a Venn diagram was plotted to compare the DEGs of GBM cells pretreated with Dex and incubated with Reo-activated PBMC compared with Vehicle treated GBM cells incubated with Reo-activated PBMC, and genes that were different between both treatment conditions. This identified 25 common genes (Figure 5.23.A). A heat map was generated using Prism for the 25 common genes using the log2FC values (Figure 5.23.B). Most of the DEGs (15 out of 25) were upregulated to a greater degree after pretretment with Dex. DUSP1 provides an example (Figure 5.23.C). Nine of the remaining genes showed downregulated expression in comparison to Reo treatment alone. SLCO2A1 was downregulated in the Reo only group and upregulated following Dex pretreatment, while TNFRSF11B/OPG and CST4 were upregulated in Reo only and downregulated in both Dex treatment groups.

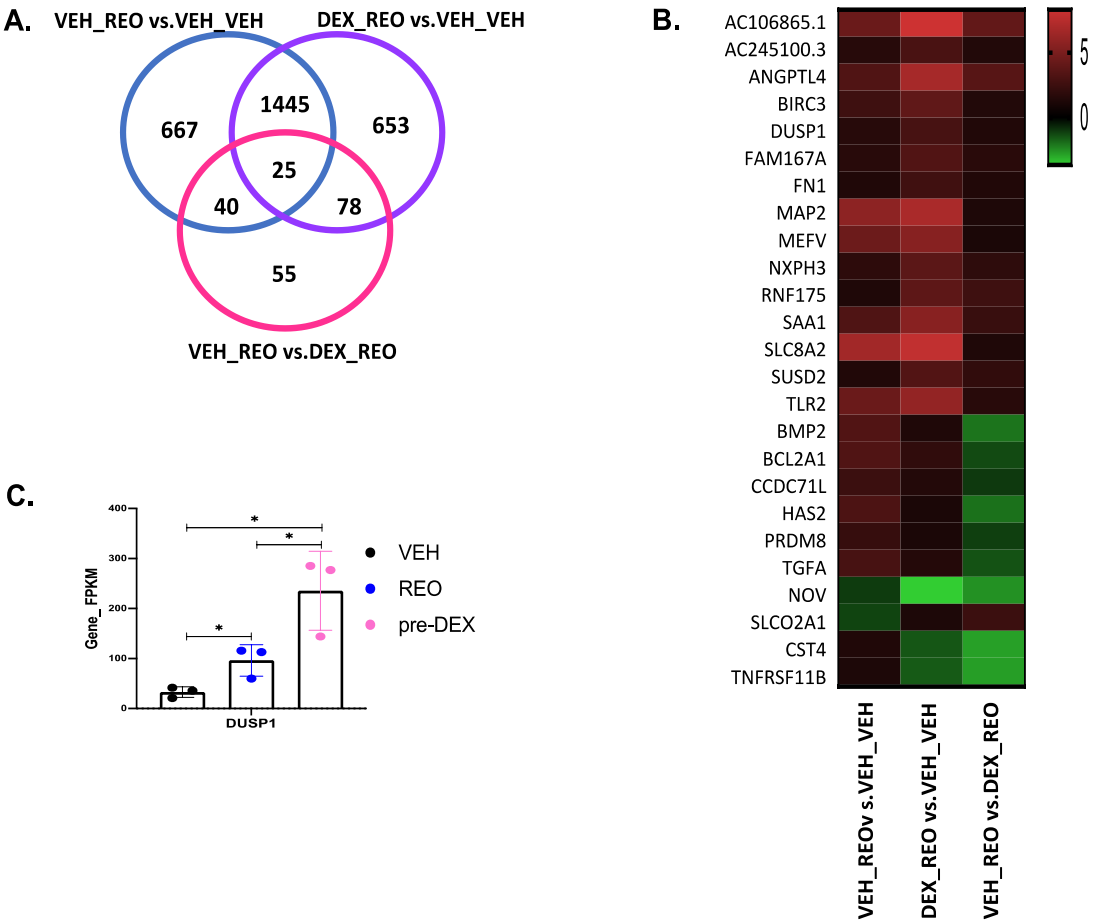

Figure 5-22 Identifying 25 common DEGs between GBM cells untreated or pre-treated with Dex in response to Reo- PBMC.

A. Venn diagram identified common genes between the three comparisons, untreated GBM (blue), pre-Dex (purple), and the differences between them (pink). **B.** Heat map of the 25 genes showing the upregulated genes (red) and downregulated genes (green). **C.** DUSP1 expression is induced by pre-Dex treatment, for n=3 independent samples using one-way ANOVA with multiple comparison test (ns $p>0.05$, *$p\leq0.05$, **$p\leq0.005$, ***$p\leq0.001$, and ****$p\leq0.001$).

5.2.6.1 Dex influences PBMC mediated killing of GBM cells through multiple death/proliferation pathways

I compared the DEGs of MO59K cells that change in response to incubation with Reo activated PBMC where GBM cells have been treated with or without Dex to identify genes regulating cell death. Gene set enrichment analysis by KEGG identified the apoptosis pathway (Figure 5.24.A). The gene expression of the anti-apoptotic gene BCL2L1 (BCL-xL) and BIRC3 were signifyingly upregulated only in the Dex pretreated group, while BAK1 gene expression was increased in both pre-Dex and Reo datasets (Figure 5.24.B). This might suggest a role for Dex in

directly blocking apoptosis pathway through upregulation of anti-apoptotic mediators, to promote cell survival. Among death receptors involved in this model, TNF expression has significant increase in Reo which was reduced in the pre-Dex, suggesting that TNF mediated GBM cells death might be an important mechanism by which Dex could reduce cell death. Additionally, GADD45A and cyclin D (CCND3) were upregulated by pre-Dex (Figure 5.24.B). GADD45A is a stress response gene involved in cell cycle arrest and apoptosis (Mak *et al.,* 2004). CCND3 promotes G1/S cell cycle transition (Büschges *et al.,* 1999). ERN1 was differentially upregulated by Reo, and the RNA-seq FPKM showed reduction in expression by pre-Dex (Figure 5.24.B). This might suggest that Dex is promoting cell cycle arrest in order to evade apoptosis in response to Reo.

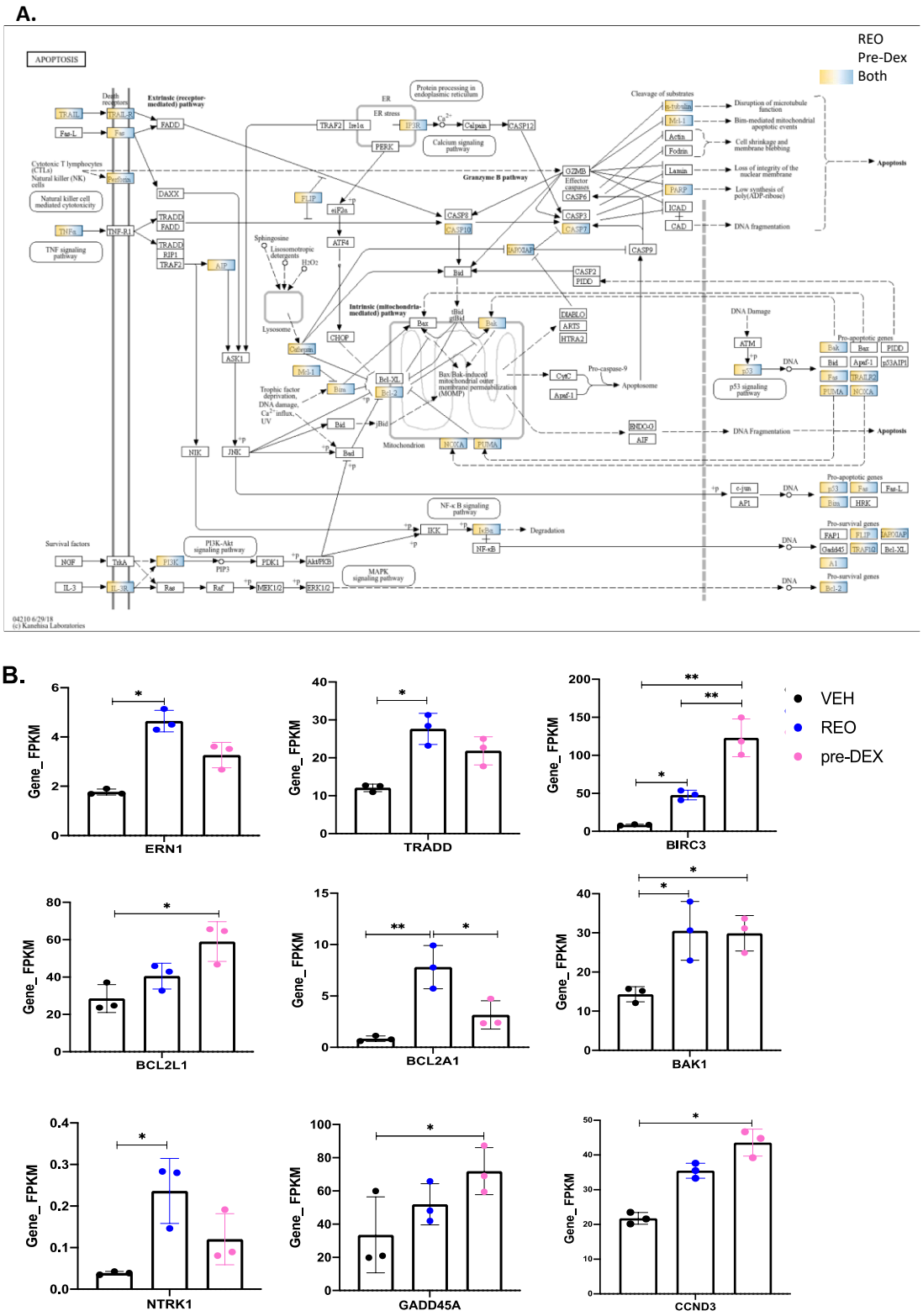

Figure 5-23 Pre-Dex treatment regulate Apoptosis pathway.

A. The pathway was obtained from the KEGG enrichment analysis of DEGs in MO59K conducted in response to Reo-PBMC (blue), pre-Dex GBM (yellow), or both (gradient). KEGG map was obtained from (https://www.genome.jp/kegg/brite.html). B. Notable genes included TNF, anti-apoptotic genes (BCL-xL, BIRC3, BCL2L1, BCL2A1), pro-apoptotic gene (BAK1), TRAAD, and ERN1. Data are shown as mean ± SEM for n=3 independent samples with statistical significance assessed using one-way ANOVA with multiple comparison test (ns p>0.05, *p≤0.05, **p≤0.005, ***p≤0.001, and ****p≤0.001).

5.2.6.2 Viral protein interaction with cytokines and cytokines receptors

Figure 5.25.A illustrated viral protein interaction with cytokines pathway identified by GSEA, highlighting genes regulated by Reo, pre-Dex or both. Several chemokines and chemokine receptors were identified as summarised in Figure 5.25.B. Pre-Dex treatment of GBM cells seems to reduce expression of these receptors and in turn reduce response to proinflammatory mediators. This suggest that pre-Dex treatments might alter the recruitment of immune cells to brain tumours.

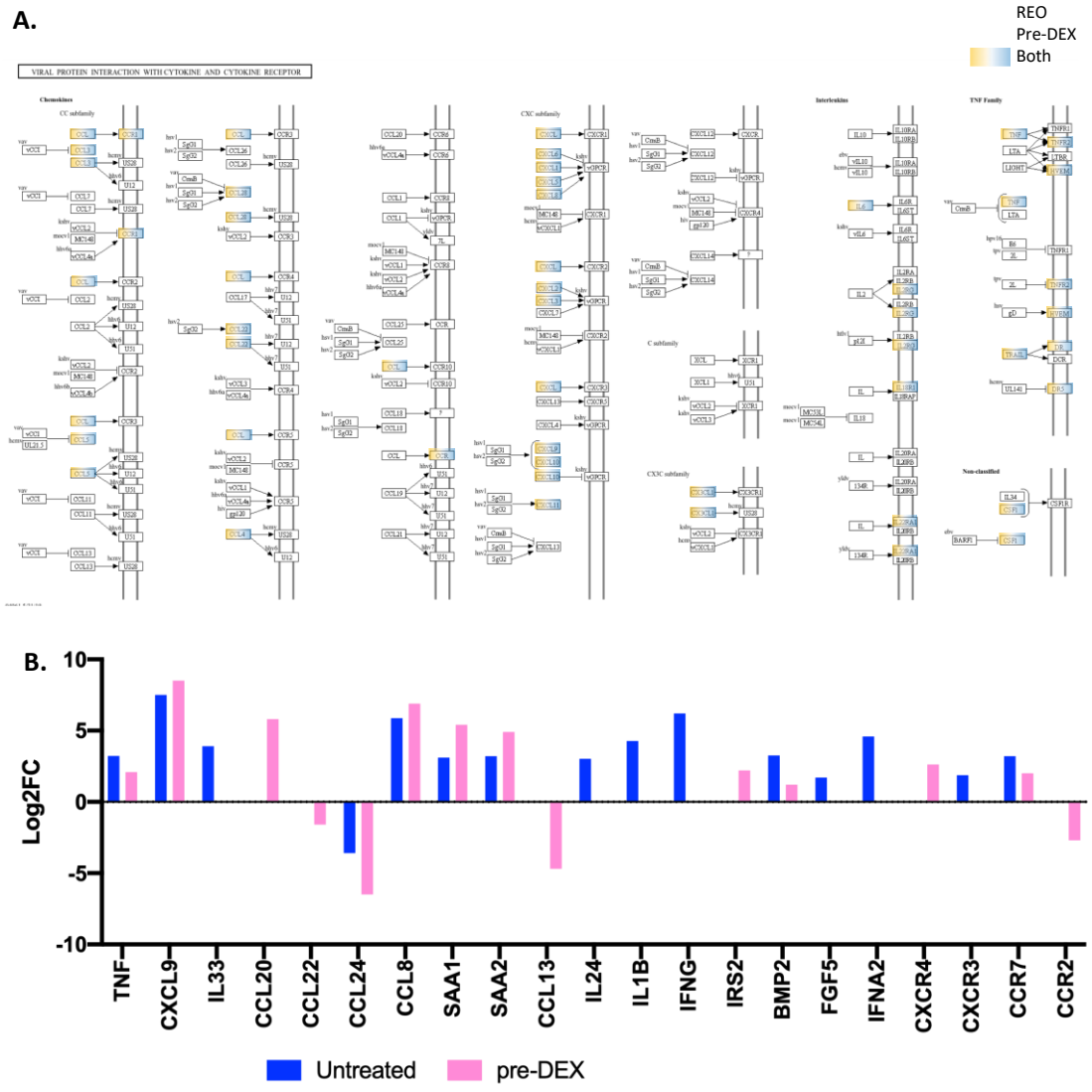

Figure 5-24 Cytokines and chemokines involved in immune response influence by pre-Dex treatment.

A. Viral protein interaction with cytokines and cytokines receptors pathway KEGG map was taken from (https://www.genome.jp/kegg/brite.html). Untreated GBM in response to Reo-activated PBMC **B.** List of the cytokines/ chemokines expressed as log2FC.

I also explored the cytokines pathway – circulating immunomodulatory mediators. TGFBR2 expression was differentially increased by Pre-DEX, and TGFB2 was differentially decreased by Reo (Figure 5.26.A). TGFB2, is a TGF-β ligand expressed in GBM cells that initiates SMAD signalling, which contributes to shaping ECM by inducing MMP2 to promote angiogenesis. This suggests that Dex might regulate the induction of TGFB2 expression. To prove that GR binds to TGFB2 promoter, I analysed ChIP data using Cistrome website (Figure 5.26.B). A recent study on GBM samples has identified TNFRSF18 genes which related to NK cells activation and migration to tumour site, predicting the response to immunotherapy (Hwang *et al.,* 2023).

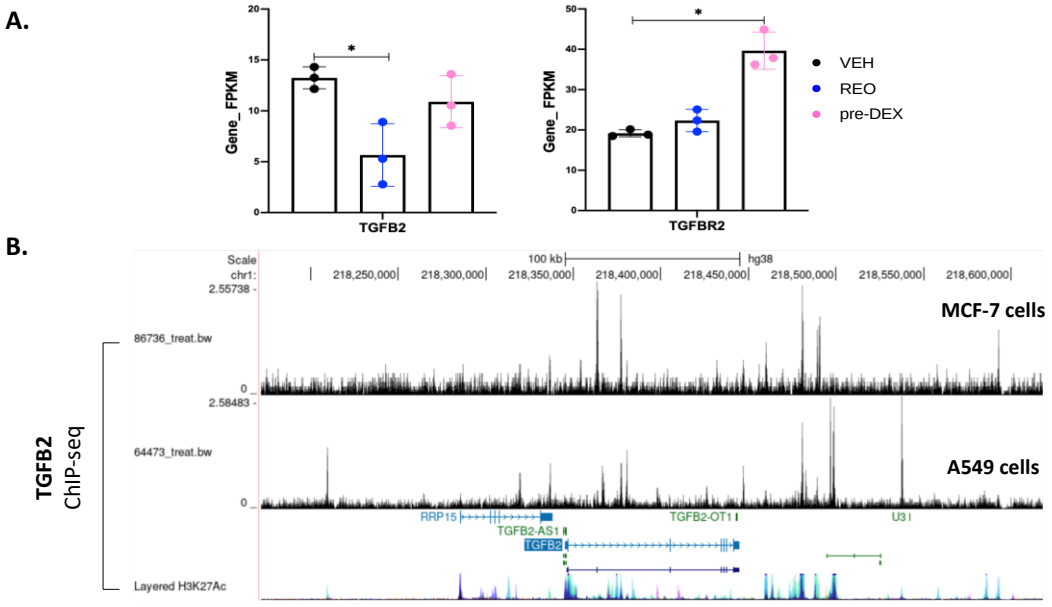

Figure 5-25 Identification of TGFB: TGRBR2 involved in pre-Dex treated GBM cells.

A. TGFB2 and TGFBR2 expression by FPKM level. Data show the mean ± SEM for n=3 independent samples, and significance was tested with one-way ANOVA with multiple comparison test (ns p>0.05, *p≤0.05, **p≤0.005, ***p≤0.001, and ****p≤0.001). **B.** ChIP analysis showed GR binds to TGFB2 promoter in MCF-7 and A549 cell lines.

5.2.6.3 NK cell mediated cytotoxicity pathway is enriched by KEGG

Genes involved in the NK cell-mediated cytotoxicity pathway are illustrated in Figure 5.27. Interferons related genes such as IFNB1, IFNA2, IFN-γ, IFNGR1 were identified. The RNA-seq FPKM in pre-Dex showed significant increased expression in IFNGR1. In addition, FASLG which bind to FAS to induce apoptosis was differentially upregulated by GBM in response to Reo-PBMC and the FPKM showed reduction in the expression in pre-Dex GBM and suggest Dex role to

regulate its expression. NK cytotoxicity markers (PRF1, GZMB) were expressed in GBM in response to Reo-PBMC, confirming NK cells activation to mediate indirect GBM killing. These genes were abolished in the pre-Dex (Figure 5.28.A). The presence of NK marker suggested a level of contamination in the isolated GBM cells method. This was observed in the other analysis where the PBMC had been treated with Dex. Interestingly, this might suggest that Dex is acting on the GBM cells to reduce the ability of NK cells to adhere and also altering the recruitment and activation of NK cells (Figure 5.28.B). In addition, interferons such as IFNG, IFNA2, and TNF showed increased expression level in untreated GBM, while a degree of reduction was observed in pre-Dex treatment, although it was not significant. IFNG and IFNA2, and TNF were validated using the Luminex assay (Figure 5.28.C) showing consistent results with the RNA-seq data.

Additionally, CD247, HAL-G, and CD48 were identified, suggesting their interaction with NK cells cytotoxicity to kill GBM cells. HLA-G and CD247 were upregulated by GBM in response to Reo-PBMC. The FPKM level for CD48 showed decrease shift in expression from logf2FC of 3 by untreated GBM to 2 by pre-Dex GBM. CD40 expression was upregulated in untreated GBM, suggesting pre-Dex role to reduce its expression to impair NK cytotoxicity. CD58 was differentially increased by pre-Dex which suggest binding to NK cells to induce its cytotoxicity. CD247 and HLA-G were reduced in pre-Dex in response to Reo-PBMC, suggesting Dex influence on their expression to interact with NK cells to induce its cytotoxic effect (Figure 5.28.D).

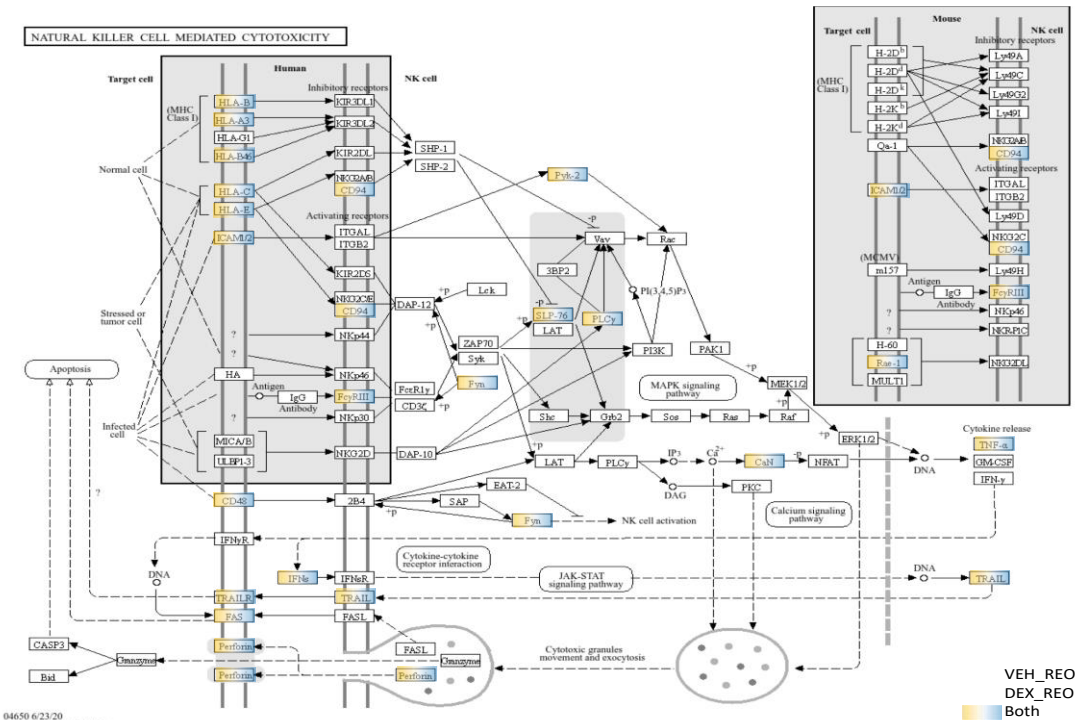

Figure 5-26 NK mediated cytotoxicity pathway revealed NK markers.

KEGG map was taken from https://www.genome.jp/kegg/brite.html. Analysis of DEGs in MO59K in response to Reo-PBMC (blue) and pre-Dex GBM (yellow) alone or both (gradient).

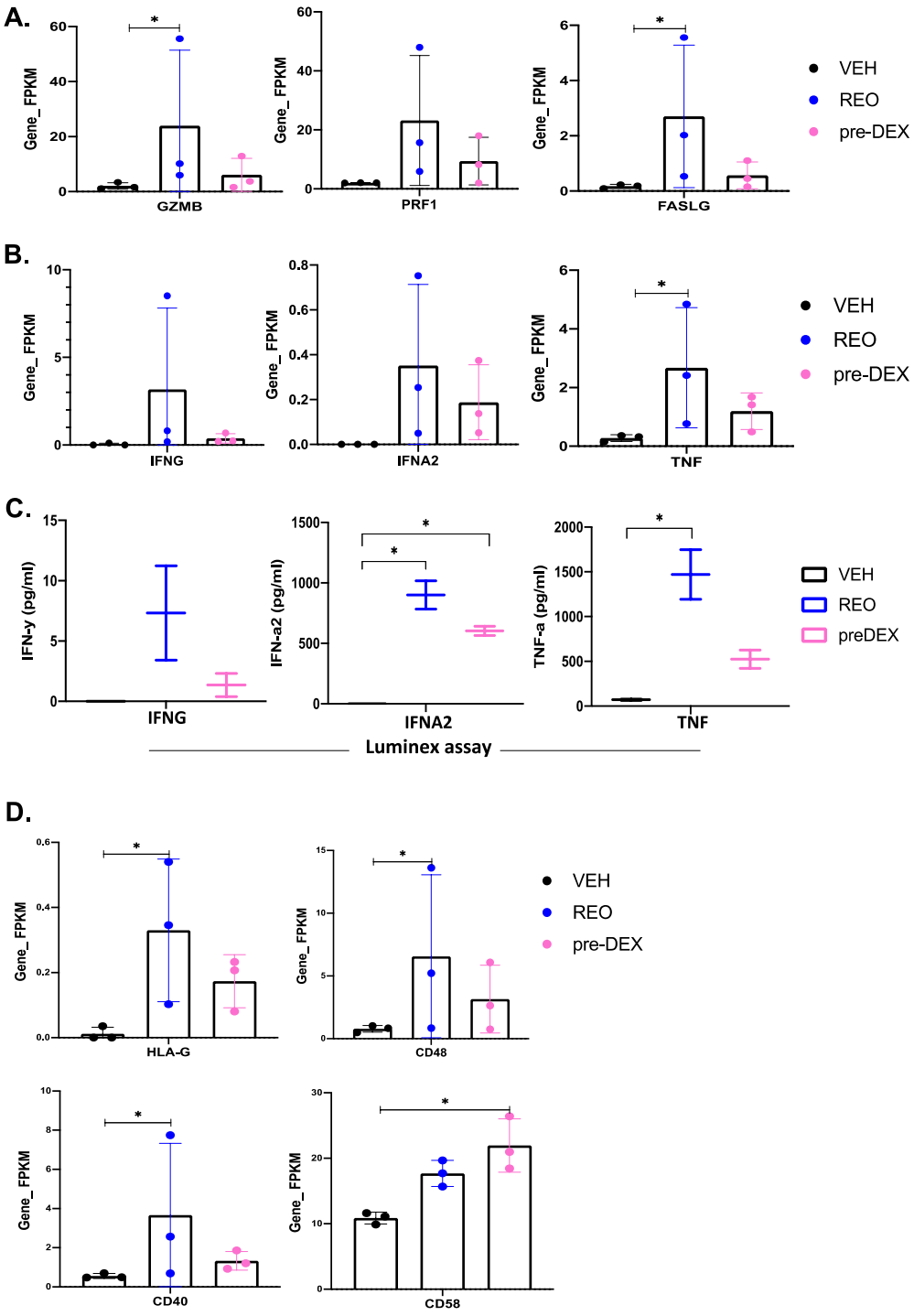

Figure 5-27 Pre-Dex treatment identified death signals and ligands on GBM mediating NK cytotoxicity.

A. NK markers (GZMB, PRF1, FASLG) were expressed in Reo-treated PBMC, but not the pre-Dex GBM cells. **B.** Interferons genes-FPKM level (IFN-γ, IFNa2, TNF) plotted showing the increase of expression on Reo-treated PBMC were lost in the presence of Dex (n=3) **C.** Results were validated by Luminex assay (n=2) and significance was tested using a nonparametric one-way ANOVA with Dunn's multiple comparison test. **D.** GBM ligands (HAL-G, CD48, CD40, CD58) FPKM level. The gene expression count (FPKM) shows the mean ± SEM n=3 independent samples, and significance was tested using one-way ANOVA with multiple comparison test (ns $p>0.05$, *$p\leq0.05$, **$p\leq0.005$, ***$p\leq0.001$, and ****$p\leq0.001$).

5.2.6.4 The ECM pathway

The ECM genes MMP1, MMP3, MMP10, and MMP12 were downregulated by pre-Dex while MMP7 and FN1 were upregulated (Figure 5.29). FN1 regulates GBM proliferation through the PI3K/AKT pathway (Jing-bing *et al.,* 2018). MMP7 was upregulated in pre-Dex GBM in response to Reo-PBMC. Gepia2 analysis showed that MMP7 is highly expressed in GBM tissue in comparison to normal brain tissue. Previous study has showed that MMP7 elevated in GBM through ERK and JNK pathway (Mu *et al.,* 2018).

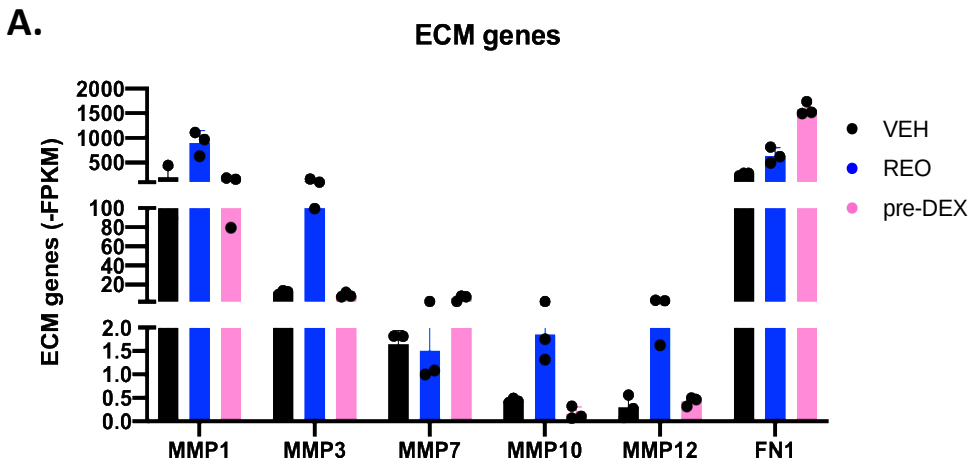

Figure 5-28 The extracellular matrix (ECM) genes.

The plot shows the genes list displayed in a bar graph comparing the gene expression level (-FPKM) of ECM genes, and only MMP7 and FN1 expression were higher in pre-Dex GBM cells.

5.3 Discussion

This chapter explored the effect of Dex on indirect Reo killing efficacy on GBM cells cocultured PBMC and showed that ReoDex co-treated PBMC decreased GBM cell death significantly. GBM cells indirect killing was evaluated again with depleting NK cells before PBMC treatment followed by coculture with GBM cells and the results showed limited cell death indicating that the indirect killing effect was NK mediated. Several studies raised concern in term of Dex administration time and dose that influence immunotherapies (McGranahan *et al.,* 2019). GBM cells were Dex pre-treated in response to Reo activated PBMC and results showed that pre-Dex impaired Reo activated PBMC to kill GBM cells (Figure 5.2). GBM cells cocultured with different fractions of CD56 depleted PBMC and treated with Reo showed that NK cells alone do not kill GBM cells, suggesting the need of APC (macrophage) to activate NK cytotoxic effect to kill GBM cells (Figure 5.3). The results showed the contribution of immune cells in GBM killing. Therefore, the next step was to evaluate T cells, NK cells and myeloid cell for cell death and activation.

GCs reported to suppress T cells and induce its apoptosis (Xing et al., 2015). A previous study showed that Dex reduces the production of IFN on NK cells and induces apoptosis on both T cell and NK cells (Montani *et al.,* 1999), while reducing TAMs and promote macrophage polarization (Jiang *et al.,* 2017). Reo on the other hand mediates antiviral and antitumor immunity by inducing the number of T cells and NK cells and their activation (White *et al.,* 2008). Though GCs and OV modulate immune cells in various ways. However, the immunological change by GC and OV combination treatment is not well studied.

The data in this chapter showed that Dex alone or ReoDex co-treatment increased CD163 and HLA-DR expression in myeloid cells (Figure 5.4). I generated TAMs to investigate M1-M2 phenotype markers (Figure 7.3, chapter 7), however, more donors are needed to confirm the result. Dex showed its ability to kill NK cells and reduce its activation, and combining Dex and Reo reduce NK activation (Figure 5.5). Candidates selective glucocorticoids (CoA, AZD, Vam) were used to examine their cytotoxic effect in combination to Reo on PBMCs. The percentage of T and NK cells were relatively low by Vam and CoA alone or combined to Reo, but only CoA combined Reo showed significant increase in NK

activation. Overall, unlike Dex, CoA does not impair Reo to kill GBM cells, nor reduced NK activation, indicating that CoA is a potential alternative to Dex for treating patients with GBM (Figure 5.6). It would be interesting to have more investigation on CoA on GBM cells *in vitro* and *in vivo* for GBM in for safety and survival.

The crosstalk between immune cells and GBM cells during Dex and Reo treatment is complex. Therefore, RNA-seq of the coculture system was performed to gain insight into the targeted genes regulated by Dex and Reo activated pathways, which might explain how Dex limits the therapeutic benefit of OV in GBM. Multiple attempts were performed with purpose to sort cells from the coculture model using cell sorter, selecting to sort each of GBM cells, NK cells, and macrophages from the coculture model (Figure 5.8). However, time and cost required to optimize the model using the cells sorter, along with the unfortunate breakdown of the machine limited the successful sorting. More optimisation for future work is recommended by increasing the number of sorted NK and macrophage cells for achieve better RNA yield, and adding mito tracker-green dye on GBM cells to increase the isolated cell purity. Looking at alternative method for isolation, I intend to use CD45 microbeads to remove all immune cells from GBM cells, however, limitation of the lake of CD45 microbeads in the lab led to use CD14 microbeads with possible contamination to isolate GBM cells using negative faction of CD14 microbeads and cell purity was validated by flow cytometry to verify the isolation efficiency and cell purity (Figure 5.9).

RNA-seq analysis of ReoDex co-treatment in the coculture model:

The RNA-seq analysis was conducted on MO59K cells isolated from cocultured model of PBMCs treated with Veh, Reo, or ReoDex. The DEGs analysis was performed for the three comparisons, Veh_Veh vs. Veh_Reo (labelled as Reo), Veh_Veh vs. Veh_ReoDex (labelled as ReoDex) and Reo vs. ReoDex. Pathway enrichment analysis was used to explore how Dex influences Reo's ability to activate anti-viral and anti-tumour immune responses. This approach highlighted changes in gene expression linked to key signalling pathways in GBM (Figure 5.12).

RNA-seq KEGG analysis was enriched in apoptosis pathway (Figure 5.14). ReoDex upregulated the apoptosis inhibitor, BIRC3, regulated NF-kB to reduce apoptosis. BIRC3 increase gene expression was found to be correlated with poor GBM survival, induced GBM stemness (Wu *et al.,* 2021), increased in the hypoxic microenvironment and mesenchymal phenotype (Wang *et al.,* 2017). The anti-apoptotic gene, BCL2A1 and BAK1 were downregulated which block apoptosis through blocking cytochrome-c release from the mitochondria to induce apoptosis. Trk receptor (NTRK1) was reported to regulate GBM growth through MAPK/ERK and PI3K/AKT downstream signaling (Wang *et al.,* 2020). However, MAPK3 (ERK) expression was reduced by ReoDex suggest Dex role in reducing cell proliferation. ERN1 (IRE1) mediates ER stress signalling and is associated with apoptosis. Its expression was reduced by ReoDex which has been reported to have anti-tumour effect and interacts with GR receptor (Riabovolet *et al.,* 2019). DUSP1 which is a key GCs target gene was upregulated by ReoDex. Previous studies showed that GCs attenuates MAPK through DUSP1 (Hoppstadter *et al.,* 2019). SOCS3 was also inhibited by ReoDex which suggests reduction in tumour growth. The interaction between these genes suggests GC role to supress MAPK pathway leading to reduce GBM proliferation. The transcription factor MYC reported to involve with GBM growth through genes involved in cell cycle progression (Bretones *et al.,* 2015) including CDKNIA (p21) which was inhibited by ReoDex. ReoDex increased the expression of CDK1 which is required for mitosis phase, and CCNA2 regulating G1-S and G2-M cell cycle transition. It has been shown that Dex inhibits CDKNIA (Chen *et al.,* 2016). MYC, a key GCs gene, was differentially upregulated by ReoDex confirms the role of Dex in mediating GBM cells growth and survival. This suggest that Dex regulate cell division of GBM cells to induce its proliferation and progression. GBM cells cocultured with PBMC treated with OV trigger cell death through FAS/FASLG axis. FASLG expression on GBM cells was reduced by ReoDex, suggesting that Dex reduces Reo ability to efficiently kill GBM cells. Dex might inhibit the apoptosis pathway through FAS/FASLG axis.

IFNG was differentially upregulated by Reo but was abolished by ReoDex. IFNG binds to IFNGR1 which is differentially upregulated by ReoDex (Figure 5.15.A). This suggest that Dex reduced Reo to enhance the anti-tumour immune response. IRF1 expression was reduced by ReoDex suggests that GBM cells

became susceptible to Reo mediated by Dex (Ehrlich and Bacharach, 2021). In addition, TNFSF14/LIGHT and its receptor TNFRSF14 expression were upregulated by Reo, and that effect was reduced by ReoDex (Figure 5.15.B and C). The TNFSF14/ TNFRSF14 interaction activates immune cells upon infection. TNFSF14 is expressed in the mesenchymal subtype, and reported to promotes cell adhesion (Han *et al.,* 2022).

Viral protein interaction with cytokine and cytokine receptor signalling identified several genes regulated by ReoDex (Figure 5.16). The pro-inflammatory chemokines CXCL2 and CXCL3 expression were reduced by ReoDex**.** CXCL2 and 3 are highly expressed in GBM and contribute to macrophage/microglia (Codrici *et al.,* 2022). CXCL2 and CXCL3 are ligands that bind to CXCR2 receptor indicating the significant involvement of CXCL2-3/CXCR2 signalling pathway in GBM prognosis and angiogenesis (Acker *et al.,* 2020). CXCL8 was reduced by ReoDex, promotes cell invasion, and TAM recruitment. Inflammatory chemokines are essential for induction of immune response to GBM (Han *et al.,* 2021). Immune cell infiltration, such as T and NK cells, has been reported to be mediated through CXCL9,10,11, and CX3CL1 (Tokunaga *et al.,* 2018). Results showed that ReoDex downregulated CXCL8, CXCL9, CXCL10 expression (Figure 5.17), suggesting lower recruitment of the cytotoxic T and NK cells. CCL22, and CCL24 which were downregulated by ReoDex while CCL20 was upregulated. It has been shown that CCL20 and CCL22 recruit Treg to the tumour site to reduce CTLs (Codrici *et al.,* 2022). GBM treatment with GCs might curtail the oncolytic activity required to recruit and activate the anti-tumour immune response.

The NK cell cytotoxicity pathway was enriched in genes that act as ligands expressed in GBM cells to bind NK receptors (Figure 5.18). Several studies have reported interaction between NK cells receptors and tumour cells, such as ICAM1 binding to LFA1 (Jeong *et al.,* 2018), CD40 binding to CD40L (Chonan *et al.,* 2015), RAET1L binding to NKG2D (Ma and Kuang, 2016), CD48 binding to 2B4 (Zou *et al.,* 2018), and HLA-G binding to KIR2DL4 (Murad *et al.,* 2022). The expression of ICAM1, CD40, and HLA-G was reduced by ReoDex, suggesting Dex role in reducing the ability of NK cells to adhere to GBM cells and NK cytotoxic function. Validation of the NK cells receptors in coculture model by flow cytometry is recommended for future work.

RNA-seq analysis of pre-Dex treatment in the coculture model:

Next, RNA-seq analysis was conducted to compare between Veh_Veh vs. Veh_Reo (referred as Reo), Dex_Veh vs. Veh_Reo (referred as pre-Dex), and Veh_Reo vs Dex_Reo. This comparison allows to investigate the effect of direct Dex administration on GBM cells and how it may influence Reo-treated PBMC in the coculture model. DEGs were identified in each comparison, and the GSEA analysis identified pathways involved in cell death, cytokines and chemokines, and NK cytotoxicity (Figure 5.20). The pro-inflammatory cytokines TNF, IL-6, IL-11 were downregulated by pre-DEX. This suggests that Dex may benefit GBM patients by reducing and oedema inflammation as anti-inflammatory drug. Collectively, upregulation of DUSP1, MYC, and FPR1 by pre-Dex was observed (Figure 5.21, 6.23). Key GC genes (MYC and DUSP1) were upregulated by pre-Dex, confirming that the data is robust. DKK1 was also identified as a top hub gene upregulated by pre-DEX, suggesting Dex role in promoting GBM growth through the Wnt pathway. ChIP analysis in Figure 5.22 showed that GR binds to the DKK1 promoter, suggesting that GR might regulate gene transcription.

GSEA analysis identified apoptosis pathway regulated by pre-Dex (Figure 5.24). BIRC3 and BCL-xL showed to be upregulated and BCL2A1 was downregulated, suggesting pre-Dex role to regulate apoptosis through the expression of apoptosis inhibitory genes. ER stress mediator, ERN1 expression was downregulated by pre-DEX, suggest that Dex reduced ER stress- induced apoptosis. Moreover, cell cycle arrest was upregulated in GADD45A and CCND3 expression, suggesting Dex role in enhancing cell cycle signalling. Notably, pre-Dex treatment in this coculture model shows similarities with GBM single culture by modifying GADD45 and BCL-xL genes and similarities with ReoDex coculture in modifying cell cycle and ER-stress related genes.

GSEA analysis on Pre-Dex was enriched in viral protein interaction with cytokines signalling (Figure 5.25). Pre-Dex upregulated CCL20 and SSA1,2 expression while downregulating CCL22, CCL24, and CCL13 expression. TGFBR2 was upregulated by pre-Dex, and TGFB2 expression was reduced by Reo compared to Veh but increased compared to pre-Dex. The ChIP analysis showed that GR binds to TGFB2 promoter (Figure 5.26), suggesting crosstalk with Dex to modulate GBM TME. Previous studies showed that TGFBR2 upregulates the

GBM mesenchymal subtype (Wang *et al.,* 2018). CXCR4 chemokine receptor which binds to CXCL12, was differentially upregulated by pre-Dex, and has been reported to involved in mesenchymal subtype progression and linked to poor OS in GBM patients (Wurth *et al.,* 2014).

The NK cell cytotoxicity pathway was enriched by pre-Dex (Figure 5. 27), and identified death signals genes (GZMB, PRF1) which were upregulated by Reo and the FPKM level showed the reduction of these genes by pre-Dex. Though this result shows a level of contamination in the RNA samples, but the fact that these genes do not express in Veh, suggests NK cells possible response in pre-Dex treatment. The RNA-FPKM also showed that pre-Dex reduced IFNG, IFNA2, and TNF expression in comparison to Reo, which was validated by the Luminex assay (Figure 5.28). Similar to ReoDex coculture, pre-Dex reduced the expression of GBM ligands that interacts with the immune cells (NK) receptors such as HLA-G, CD48, CD40 as well as upregulate CD58 that bind to CD2 in NK cells, suggesting NK that Dex reduce the ability of NK cells to bind GBM cells and reduce NK cytotoxic function.

Finally, the ECM pathway showed downregulation in MMPs genes except MMP7 and upregulation on FN1 which is similar to the observation on the ReoDex coculture analysis (Figure 5.29). This confirms Dex role in regulating ECM remodelling and its association with GBM invasion.

Figure 5.30 and Figure 5.31 summaries the highlight findings of GBM cells isolated from the coculture model.

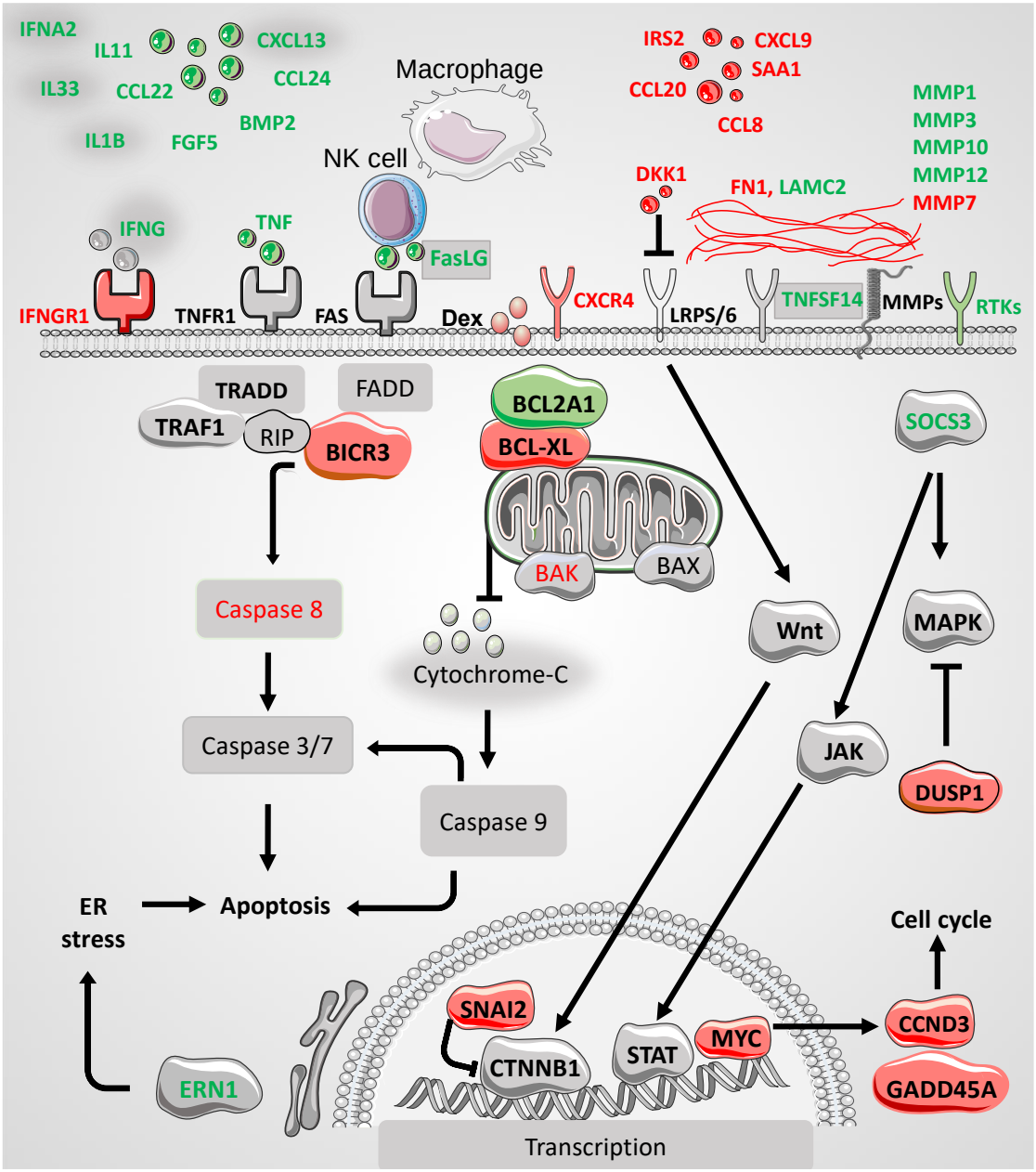

Figure 5-29 Summary of potential pathways and genes regulated by pre-Dex modifying Reo-treated PBMC in MO59K cell line in coculture model.

Genes upregulated by ReoDex (red), downregulated by ReoDex (Green), genes upregulated by Reo (red text), downregulated by Reo (Green text).

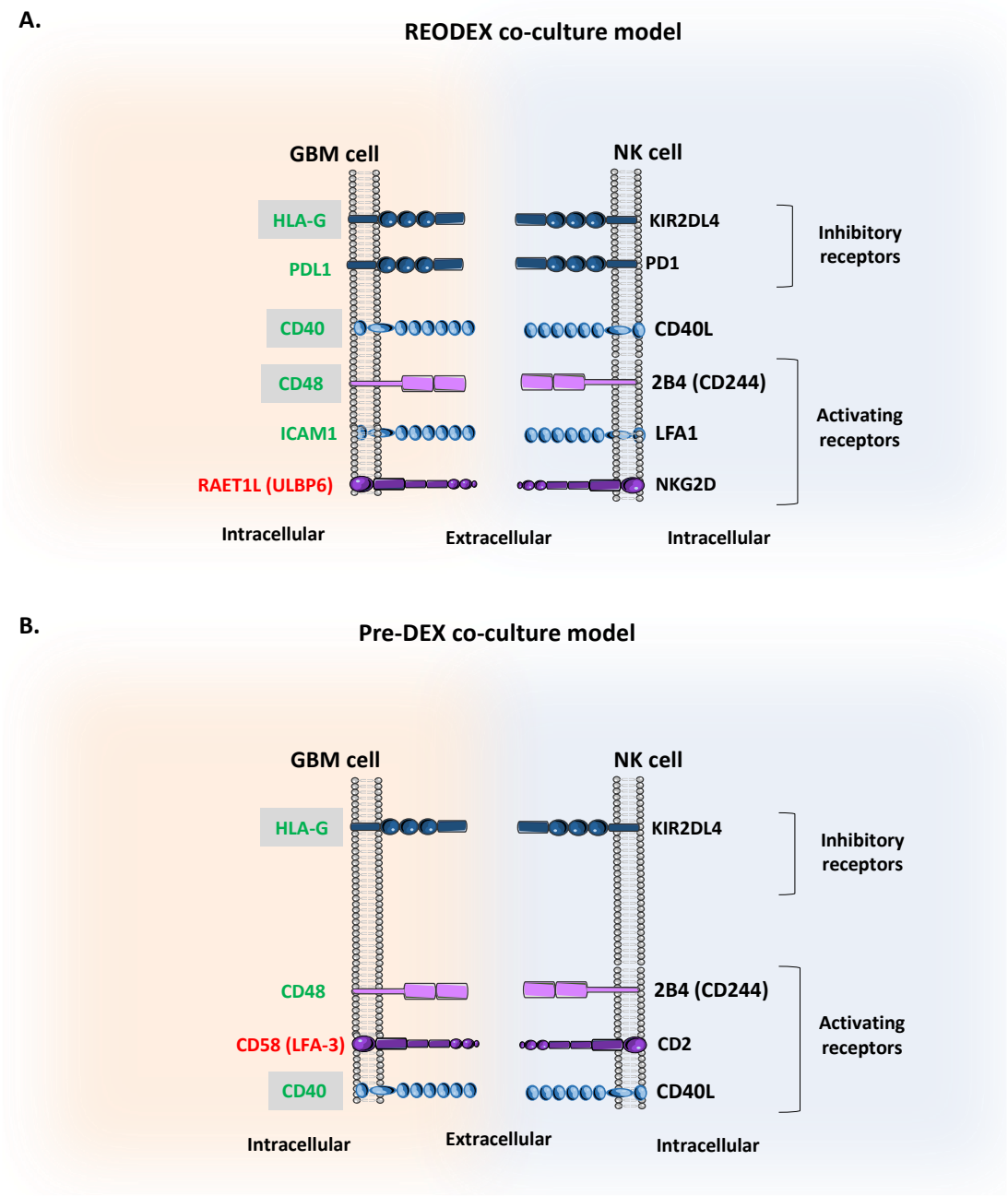

Figure 5-30 Ligand-mediated interactions between GBM cells and NK cell receptors.

GBM cells were **A.** isolated from the ReoDex-treated coculture model or **B.** GBM cells pre-treated Dex and isolated from the Reo-treated coculture model, expressed ligands that bind to both inhibitory and activating NK cells receptors, modulating NK cells function. Downregulation of HLA-G ligand enhances NK-mediated killing of GBM cells. In contrast, the downregulation of CD48 and CD40 impair NK cytotoxicity. ICAM1 downregulation reduces NK cells adhesion to GBM cells and limits production of cytotoxic factors (eg. IFNy, PRF1, GZMB), therapy reducing NK-mediated killing of GBM cells. Conversely, upregulation of CD58 increases NK cell adhesion to GBM cells, while upregulation of RAET1L enhances NK cells cytotoxicity. Additionally, PD-L1 downregulation diminishes interaction with PD-1 on NK cells, facilitating NK cells activation. *Ligand key: Dex upregulated (red), Dex downregulated (green), Dex non-significantly downgauged (green in gray box).

Chapter 6

Discussion and future perspectives

Despite decades of research, GBM prognosis remains poor, and advances in treatment are much needed (Yalamarty *et al*., 2023). In recent years, there have been growing concerns regarding the use of GCs, a frequently prescribed anti-inflammatory drug, on the impact of both existing and emerging immunotherapies in GBM (Kalfeist *et al.,* 2022). In particular, it was not known how GCs would impact the efficacy of OV treatment. GCs modulate the transcription of genes that control diverse pathways – including those involved in stress, metabolism, proliferation, differentiation, motility and adhesion. In addition, GCs mediate effects in a cell specific manner, which means that GC regulated genes can differ between tumour and immune cells, or even between specific immune subtypes. To add further complexity, OV can mediate killing by directly inducing death of tumour cells, or by activating cytotoxic immune cells to induce cell death (Muller *et al.,* 2020). The interplay between GC and OV, and also between tumour cells and immune cells provides a complex problem that required further investigation.

Shortly after starting my PhD, the laboratories were closed due to the COVID pandemic, and so I started by analysing public transcriptome data for Dex and reovirus treated GBM cells and immune cells. This work uncovered enrichment of GC regulated pathways (AP-1 and MAPK) and identified NRs in MO59K cells treated GCs. Regulation of pro-inflammatory cytokines (IL-6, IL-11), anti-apoptotic gene (BIRC3), and PD-L1 were identified in GBM patients treated with OV. It has been demonstrated previously that IL-6 and IL-11 can activate STAT3 signalling, stimulating GBM migration and growth (Yu *et al.,* 2009), Dex inhibited apoptosis through BIRC3 (Thorne *et al.,* 2023), and PDL1 was expressed in GBM (Nduom *et al.,* 2015). Predicted crosstalk between GC and Reo included IL-6, AP-1 and TNF signaling pathways. GC treatment in immune cells predicted ATP synthesis in CD4 T cells, induction of M2-like macrophage markers, and expression of the GR target gene TSC22D3 in monocytes. It has been demonstrated that GCs inducing apoptosis in T cells require ATP (Ashwell *et al.,* 2000), increase M2-phenotype and TSC22D3 expression (Tedesco *et al.,* 2015; Jubb *et al.,* 2016). Reo treated monocytes predicted NOD-like receptor pathway

for virus recognition (Wicherska-Pawłowska *et al.,* 2021), and TNF pathway. This suggested that the immune response to the virus in the presence of GC may play a role in how OV differs from GC in regulating genes. Unfortunately, there was limitation to access NK cell transcriptome data, and therefore it was necessary to study the combination treatment in an *in vitro* setting.

Dex impairs direct killing by reovirus by modulating death pathways:

Reovirus, is naturally selective to productively infect tumour cells, allowing for virus replication and subsequent cell death, termed direct oncolysis (Zhao *et al.,* 2016). The data in this study explored how Dex impairs direct oncolysis by reovirus to kill GBM cells. Cell viability assays demonstrated that reovirus promotes oncolysis in a dose dependent manner and increased over time, and that Dex impaired the killing effect of reovirus in MO59K cells line and two patient-derived cell lines. The effect of Dex was not on the expression of reovirus entry receptor (JAM-1), suggesting that Dex does not impair reovirus entry to the host cells. Dex treatment had no effect on reovirus replication, the number of reovirus factories, or their subcellular localisation. Overall, the effect of Dex on GBM cells is not to alter the entry or processing of the virus, but instead the cells response to viral infection. As Dex is known to control multiple pathways relating to immunity, cell fate and metabolism, RNA-seq was used to quantify the transcriptomes of cells treated with reovirus alone or in combination with Dex.

Dex impairs indirect killing by reovirus by reducing NK cell activation:

Reovirus can also stimulate host anti-tumour immune responses to indirectly kill tumour cells (Muller *et al.,* 2020). To investigate this, an *in vitro* coculture assay was developed, and GBM cells in the presence or absence of Dex were cocultured with Veh-PBCM, reovirus-primed PBMC, or reovirus plus Dex primed PBMC. Cytotoxicity assays demonstrated that Dex impaired PBMC mediated killing in response to reovirus. However, Dex could regulate the activity of NK cells as Dex killed some NK cells, and reduced NK cell activation of others. This suggested a possible role for NK cell in mediating the indirect killing, which was confirmed by depleting NK cells and eliminating the response to reovirus. Given that Dex impairs NK cell activation, this suggest that Dex effects on NK function are of particular importance.

Dex impairs indirect killing by reovirus by reducing NK cell recruitment:

Most GBM patients receive GCs before surgery or other treatments. Therefore, the coculture model was repeated after pre-treating GBM cells with Dex prior coculture with reovirus activated PBMC. This demonstrated that pre-Dex treatment abolished reovirus-primed PBMC to kill GBM cells, suggesting that Dex protected cells from signals promoting killing in response to reovirus.

RNA-seq identifies pathways for GC and reovirus crosstalk:

Despite differences in the combination of the GC and reovirus target cell (Figure 6.1), RNA-seq analysis identified multiple common pathways among the three culture models.

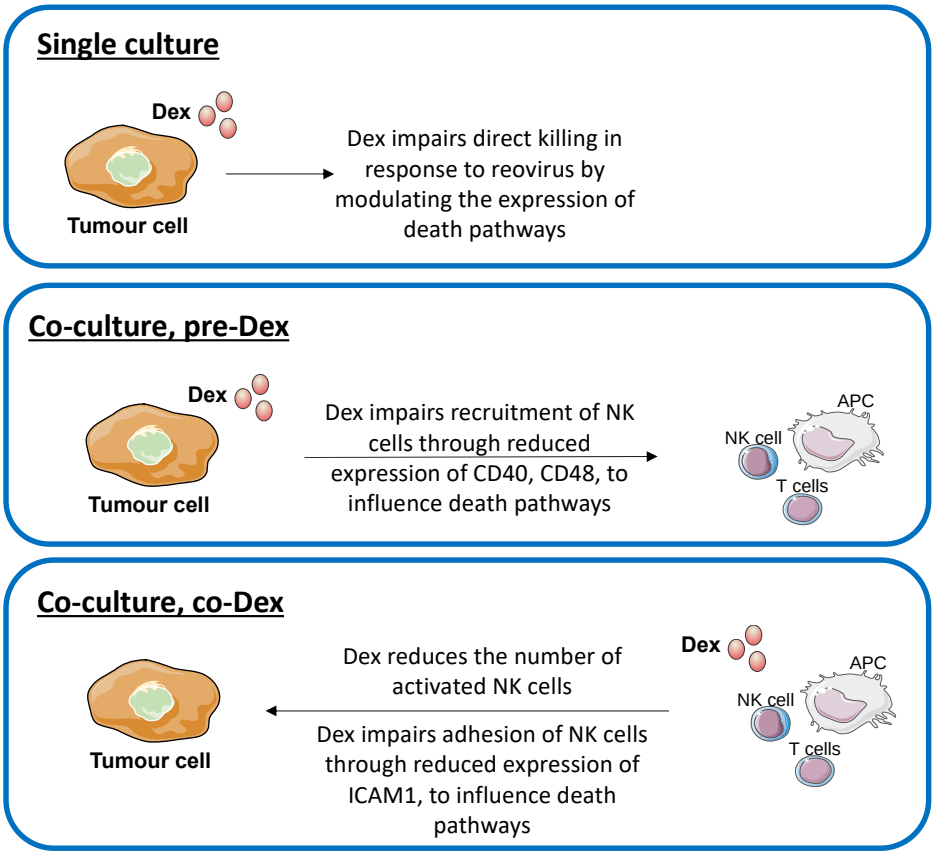

Figure 6-1 Overview of GBM cells sequenced culture model.

RNA-seq analysis of GBM cells in the single culture (top) predicted death pathways regulating Dex on reovirus efficacy, the coculture pre-Dex (middle) predicted impaired NK recruitment, influencing death pathway, and coculture co-Dex (down) reduced NK activation, and reduce NK adhesion to mediate death pathway.

For the coculture experiment, multiple attempts were made using the cell sorter to isolate the target cells (GBM cells, NK cells, and Monocyte) was conducted. However, this resulted in low RNA yields for immune cells and low purity of GBM cells and needed more refinement. An alternative method would have been to use anti-CD45 microbeads, but more limited resources guided to isolated attached GBM cells after multiple washes to remove PBMC and used negative fraction CD14 microbeads. Validation on cells purity was conducted using CD45, CD14, CD56 markers and used samples with ~90% purity. While this method resulted in contamination during data analysis, it provided preliminary insights into potential pathways. Recommendation to use the cell sorter in the future, with higher number of isolated cells is advised.

Inflammatory pathways: Due to Dex immunosuppressive effect, it was expected that a downregulation of pro-inflammatory factors such IL-6, IL-1B, IL-11, IL-33, PTGS2 (COX2), and IDO1 would be observed. This is beneficial for GBM patients to reduce inflammation and neurological symptoms, and improve the patient's quality of life. PTGS2 and IDO1 are main immunosuppressive factors, and reducing their expression could be beneficial for GBM patients by reducing inflammation in the brain oedema (Dietrich *et al.,* 2011). However, CXCL9,11,13 and CX3CL1 downregulation suggest reductions in T and NK recruitment, thus reduce anti-tumour immune response. CXCL9,10,11 were reported as anti-tumor immune T cells function markers and their expression reduced by Dex (Xu *et al.,* 2020), CCL2 downregulation suggested a decrease in monocyte and TAM recruitment. It has been demonstrated that CCL2 is highly expressed in GBM, recruits TAMs, Treg and NK cells, and that Dex reduced its expression (Urbantat *et al.,* 2021). CCL20 expression was upregulated by Dex suggesting increased infiltration of Th17 cells, and promotion of invasion through HIF-1 and NF-kB (Jin *et al.,* 2018).

Death pathways: In all three datasets, reduced TNF expression was ranked as the top hub gene, suggesting its central role in mediating signalling pathways. TNF binds to its receptor TNFR1 to regulate cell death signalling. Dex upregulated the expression of the anti-apoptotic gene, BIRC3, in all three analyses to reduce cell death. This was observed in chapter 4 *in-silico* analysis and a previous study has reported Dex inhibits apoptosis by through BIRC3

(Thorne *et al.,* 2023). Single culture also showed an increase in FLIP mediating TRAIL-included apoptosis which was observed by Jeon et al., 2020, and the anti-apoptotic genes (BCL-xL). Likewise, the pre-Dex model also upregulated BCL-xL, suggesting the need of Dex presence in culture to active the gene, and maybe its promoter binds to GR by tethering. BCL2 in coculture model and BCL2A1 in the pre-Dex model were downregulated. Overall, upregulation of the anti-apoptotic genes dominates to block the release of cytochrome c to subsequently reduce apoptosis.

Cell cycle pathways: All three models observed upregulation in GR target gene, MYC which regulates cell cycle progression in the G1- to S phase transition (Rogatsky *et al.,* 1997) but with different gene interactions. For example, upregulation of the growth arrest marker, GADD45B and Cyclin D3 (CCND3) was observed in single culture. Similarly, pre-Dex model showed GADD45A and CCND3 upregulation to regulate cell cycle. Dex induces cell cycle progression by upregulating GADD45B expression, DNA damage and apoptosis (Salvador *et al*., 2013). GADD45A is reported to be regulated by P53, and CCND3 promotes the cell cycle, and its association to cell proliferation (Meng *et al.,* 2012). The coculture model downregulated CDKN1A (p21) and upregulated of CDK1 and CCNA2, which are required for cell cycle progression which suggests greater cell proliferation. CDK1 regulates cell cycle G2/M transition and form a complex with CCNA and CCNB, and it has been demonstrated that CCNA2 overexpression increases tumour progression (Uhlen *et al.,* 2010). CDK1/ cyclin B increase tumour spreading and invasion (Fang *et al.,* 2019). Overall, this model suggests GR is linked to cell cycle progression as a transcriptional activator interfering with cyclin D genes and MYC, regulating cell metabolism and reduced transcription of p21.

Stress pathways: It has previously been reported that high doses of Dex can increase the expression of ER stress proteins and promote ER stress through calcium influx (Guo *et al.,* 2021). Dex upregulated CXCR4 expression and downregulated CXCL12 (SDF-1), this leads to activation of Ca+ influx regulating ER stress, MAPK, PI3/AKT and RAS/ERK regulating cell survival, stemness, and chemotaxis (Tseng *et al.,* 2011). In single culture, MAP3K5 (ASK1) expression was upregulated and the ER stress marker, DDIT3 (CHOP) expression was

downregulated. DDIT3 is reported to induce apoptosis and thus, this data suggest apoptosis reduction through DDIT3 inhibition. MAP3K5 is stress-induced apoptosis signal-regulating kinase 1 (ASK1) that activate JNK, p83, and MAPK pathway required for apoptosis (Takeda *et al.,* 2011), while DDIT3 is inhibitor of forming complex with CCAAT enhancer binding proteins β (CEBPβ) to regulate cellular differentiation, and its knockdown restores GBM cell viability (Tsai *et al.,* 2017). In the coculture and pre-Dex models, RTK receptor was downregulated. RTKs mediate several downstream signalling including MAPK (Regad, 2015). SOCS3 was downregulated in pre-Dex while ERN1 and MAPK3 (ERK2) were additionally downregulated in the coculture model. This suggests that GR/MAPK crosstalk is a nongenomic mechanism. It has been demonstrated that SOCS3 activates ERK/MAPK pathway in GBM (Dai *et al.,* 2021). Decreased expression of ERN1 deregulates p53 and inhibits GBM growth (Minchenko *et al.,* 2014). DUSP1 overexpression has been reported in several cancers, and inactivates MAPK pathway (Wang *et al.,* 2016). DUSP1 upregulation in the three model suggest it as the main mediator in ER stress.

Cell-cell interactions: Both coculture models and the pre-Dex model showed distinct signalling from the single culture. One example is that both coculture and pre-Dex model showed downregulation of FASLG expression by Dex. FASLG binds to its receptor FAS, triggering apoptosis, and promoting tumour evasion. Furthermore, the RNA-seq analysis predicted NK cells cytotoxicity pathway to be enriched, and identified ligands expressed on GBM cells that interact with NK activating or inhibitory receptors to activate or repress NK cytotoxicity. Dex modulated expression of several ligands, for example HLA-G interacting with KIR2DL4 on NK cells was downregulated, suggesting increase NK cell ability to kill GBM cells. CD247 (PD-L1) expression was downregulated in GBM cells, suggesting reduction of interaction with PD-1 on NK cells. Dex also downregulated CD48 and CD40 expressions which interact with 2B4 and CD40L respectively, leading to impaired NK cytotoxicity. ICAM1 downregulation reduces NK cell adhesion to GBM cells, and limits production of cytotoxic factors to kill GBM cells. Only the coculture model specifically downregulated ICAM1 expression on GBM. ICAM1 interacts with LFA1 on the NK cell and it is possible that downregulation of ICAM1 expression might require cell-cell interaction. Conversely, the pre-Dex model showed an upregulated CD58 expression on

GBM which interacts with CD2 on NK cells, an interaction that is important in NK activation.

Cell-matrix interactions: Additionally, the coculture model showed an increase in TGFB2 expression which is reported to contribute to angiogenesis and ECM activation (Dieterich *et al.,* 2012). The ChIP analysis showed that GR binds to the TGFB2 promoter, suggesting crosstalk to GR. ECM has been identified in the gene ontology in all three models. Studies showed that Dex modulates ECM through MMPs, to allow cell migration (Harkness *et al.,* 2000). Dex downregulates MMP10, 13 while upregulate MMP7 which correlate with GBM poor survival. MMP7 is involved in immune escape, the TME, and the cell cycle, promoting tumour progression. This study showed that Dex upregulates FN1 which bind to MMPs through integrin receptors and stimulates their expression in all three models, while the coculture model showed upregulation in LAMA5 expression and the pre-Dex model showed downregulation in LAMC2 expression. FN1 is reported to be involved in GBM invasion and associated with GBM poor survival (Kabir *et al.,* 2022), LAMA5, and LAMC2 induce cell proliferation (Diao *et al.,* 2023; Ling *et al.,* 2011). Therefore, transcriptional regulation of MMPs is suggested to involve TNF to stimulate MMPs through NFKB, TGFB, and CXCR4/CXCL12.

Collectively, the results presented in this thesis demonstrate that Dex impairs Reo's ability of to kill GBM cells as summarized in Figure 6.2. RNA-seq analysis highlights potential signalling pathways by which Dex impacts Reo efficiency on GBM cells. One is that GR might interact with transcription factors identified in the RNA-seq within the context of Dex and Reo crosstalk. This work requires further investigation that may lead to targeted strategies that improve GBM patient survival.

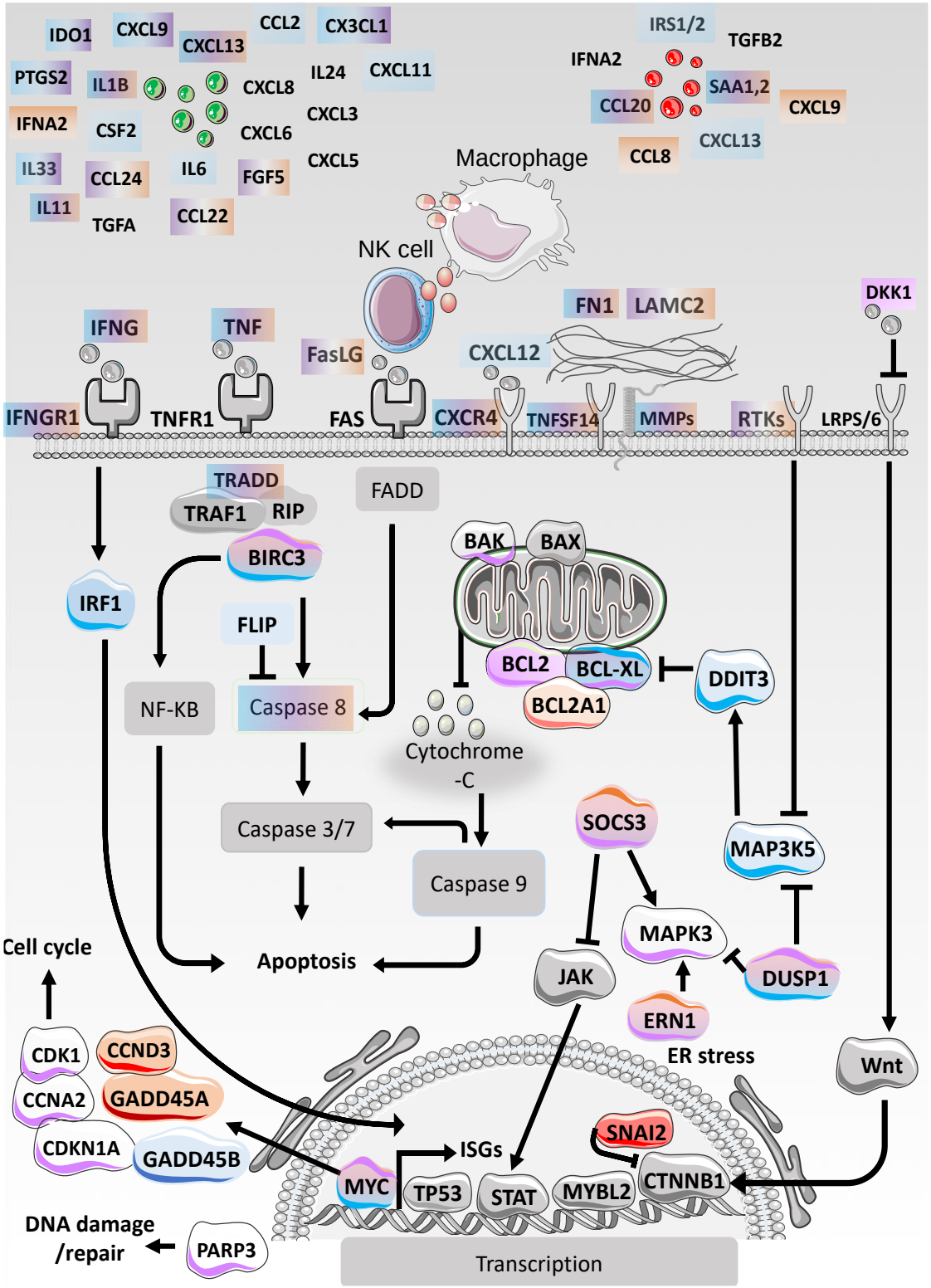

Figure 6-2 Summary of Dex influence reovirus killing efficacy through multiple signalling pathways.

Genes regulated in single culture (blue), coculture (purple), pre-Dex coculture (orange).

Future work:

Cell communication and Reo/Dex crosstalk: Due to time constraints, there are a few key experiments that need to be completed. Firstly, I have demonstrated that the effect of Dex on indirect killing is mediated by NK cells, since the effect of Dex was significantly reduced after depletion of NK cells with magnetic beads. I did not however complete similar studies to deplete T cells and therefore cannot exclude them as a possible effector of the Dex effect. I also plan to deplete macrophages to determine if they play a role in the altered activation of NK cells I observed (and T cells if that seems appropriate). This will be important to clearly define which immune subtypes are important for future studies.

This project has generated a significant amount of transcriptome data across three different culture models. There are therefore several avenues to develop this work further.

TAMs: Tumour associated macrophage (TAM) generated *in vitro* using GBM cell lines cocultured with PBMCs for 7 days, and TAM was isolated using CD14 microbeads. Generated TAMs were treated with Veh, Dex, Reo, ReoDex for 24hrs and M1/M2 markers were used to check the phenotype shift between M1 and M2 in TAMs assessed by flow cytometry. Experiments were conducted in 2 donors, and preliminary results showed consistence increase M2-like phenotype marker (CD163) by Dex group, while M1-like phenotype marker (CD86) showed consistence increase in reovirus group (Figure 7.3). More donors are needed to conclude Dex effect on TAMs.

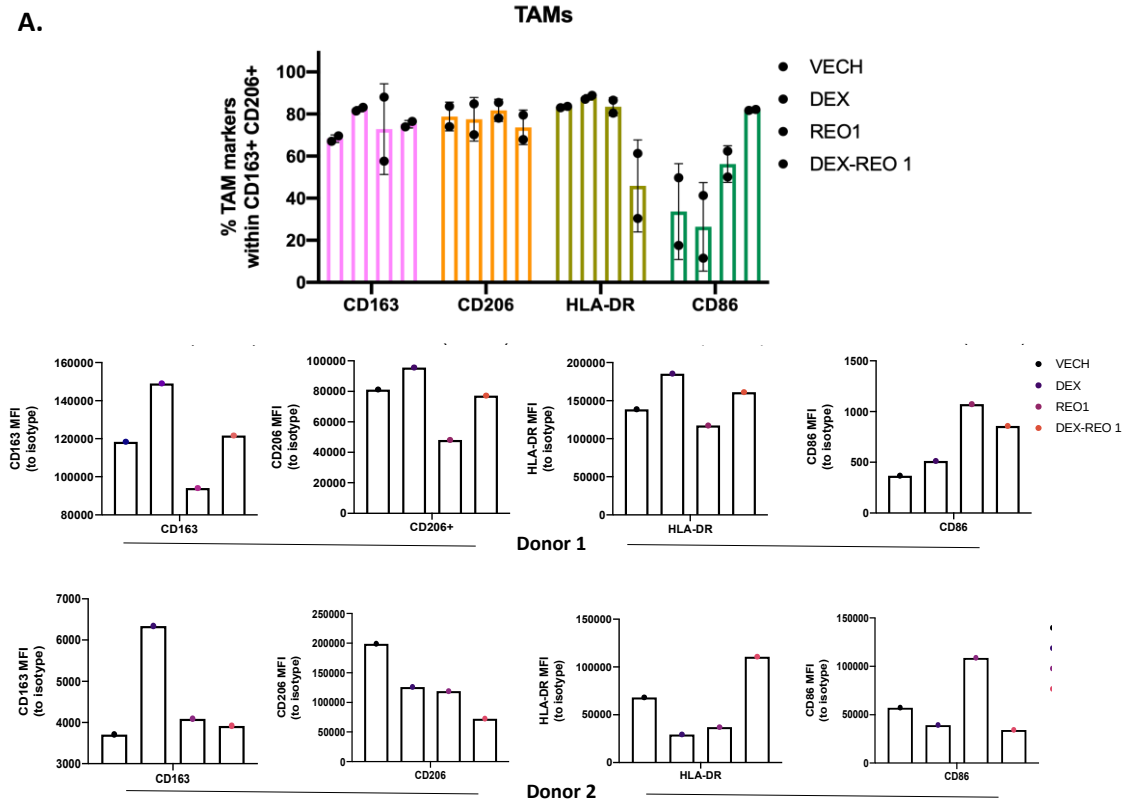

Figure 6-3 Dex effect on TAMs phenotype.

PBMC were treated with Veh, Dex, Reo 1 and combination for 24hrs, and M1/M2 markers expression were determined by flow cytometry. MFI was calculated and normalized by isotype control. Data shows the mean ± SEM for n=2 independent donors.

Recent clinical trials are currently focusing on selective GCs such as AZD-3514 in prostate cancer. I have already screened several selective GCs on GBM cells and immune cells, however expanding the investigation on patients derived cells and indirect killing assay would give more insight on their potential as alternative to Dex and other OV are needed.

Functional validation of transcriptome analysis: Validation experiments after the RNA-seq of GBM cells would be done on the patient derived GBM20 cells to screen identified target genes. I have already validated some cytokines by Luminex essay. Following up validation experiments would be Western blot for the anti-apoptotic molecules (eg. BIRC3, BCL-xL, BCL2, FLIP). Cell cycle analysis to validate Dex and reovirus effect on GBM cell cycle progression would be assessed by flow cytometry. It will be interesting to validate identified NK cells

receptors (eg. LFA1, 2B4, KIR2DL4, CD40L) that interact with GBM cells ligands using flow cytometry.

Validate findings in more physiologically relevant models: At the start of this study, there was a plan to validate findings using spheroid models. It would be interesting to develop a coculture model in spheroids with patient derived cells or organoids to investigate Dex effect on OV therapy as a pre-clinical model. Designing a reliable GBM model is challenging due to its complexity. In this study, I used a 2D direct coculture model with human PBMC which provide some intracellular interaction between tumour cells and immune cells. However, the 2D culture model grow differently from the original tumour as its display changes in cells morphology and lake to capture the whole complex cellular and molecular interaction of the TME. The 3D cultures such as spheroids and organoids offer more biologically and relevant system to mimic GBM heterogenicity, better functional dynamic between tumour and immune cells interaction, and enable better drug response. 3D bioprinting coculture model offer a robust and high throughput model GBM which include the ECM, vasculature, BBB, and TME interaction. Moreover, *in vivo* models such as patient-derived xenograft (PDX) and genetically engineered mouse model (GEMM) were successfully generated and recapitulate original tumour tissue with its complex TME, although the methodology to maintain the tumour growth is complex and require ethical consideration. The integration of both 3D and in vivo models provide comprehensive understanding of GBM biology, explores gene regulation, immune interaction and development of effective treatment for GBM clinically meaningful insight into therapeutic strategies for GBM patients.

Although the focus of this study is on GCs and Reo, this can be expanded to other oncolytic viruses that are in clinical trials such as HSV-1 and adenovirus. There have been obstacles to study GCs in clinical trial since most GBM patients do receive GCs as standard during their treatment. However, it could be feasible to conduct a study to compare GBM patients in OV clinical trial, specifically comparing those who recently received GCs to those who have not receives GCs for at least a month.

In conclusion, GBM represents one of the most aggressive and therapeutically challenging cancers, due to its genetic heterogeneity, interactions with the TME and resistance to current therapies. These findings underline how standard treatments, like Dex, often prescribed for managing GBM-associated edema, may inadvertently hinder the efficacy of promising immunotherapies like OV. By modulating immune and apoptotic pathways, Dex appears to create an environment that favors GBM survival. Dex was found to decrease the expression of anti-inflammatory factors which suggest detrimental effects for GBM patients. Important targets that might reduce the efficacy of Reo to kill GBM cells are induction of anti-apoptotic genes, dysregulated interaction between GBM ligands and NK receptors affecting adhesion and recruitment to the tumour site, reduced NK cytotoxicity and the potential crosstalk between GC and Reo in mediating ER stress or cell cycle stress. Altogether, this provides a compelling case for re-evaluating the use of immunosuppressive agents in GBM management. Furthermore, it underscores the need for combination therapies that can mitigate the immunosuppressive effects of Dex while enhancing anti-tumor immunity.

References

1. Price, M., Ballard, C., Benedetti, J., Neff, C., Cioffi, G., Waite, K.A., Kruchko, C., Barnholtz-Sloan, J.S. and Ostrom, Q.T., 2024. CBTRUS statistical report: primary brain and other central nervous system tumors diagnosed in the United States in 2017–2021. *Neuro-oncology*, *26*(Supplement_6), pp.vi1-vi85.
2. Stupp, R., Mason, W.P., Van Den Bent, M.J., Weller, M., Fisher, B., Taphoorn, M.J., Belanger, K., Brandes, A.A., Marosi, C., Bogdahn, U. and Curschmann, J., 2005. Radiotherapy plus concomitant and adjuvant temozolomide for glioblastoma. *New England journal of medicine*, *352*(10), pp.987-996.
3. Thakkar, J.P., Dolecek, T.A., Horbinski, C., Ostrom, Q.T., Lightner, D.D., Barnholtz-Sloan, J.S. and Villano, J.L., 2014. Epidemiologic and molecular prognostic review of glioblastoma. *Cancer epidemiology, biomarkers & prevention*, *23*(10), pp.1985-1996
4. Zong, H., Verhaak, R.G. and Canoll, P., 2012. The cellular origin for malignant glioma and prospects for clinical advancements. *Expert review of molecular diagnostics*, *12*(4), pp.383-394.
5. Louis, D.N., Perry, A., Reifenberger, G., Von Deimling, A., Figarella-Branger, D., Cavenee, W.K., Ohgaki, H., Wiestler, O.D., Kleihues, P. and Ellison, D.W., 2016. The 2016 World Health Organization classification of tumors of the central nervous system: a summary. *Acta neuropathologica*, *131*, pp.803-820.
6. Whitfield, B.T. and Huse, J.T., 2022. Classification of adult-type diffuse gliomas: Impact of the World Health Organization 2021 update. Brain pathology, 32(4), p.e13062
7. Wang, Q., Hu, B., Hu, X., Kim, H., Squatrito, M., Scarpace, L., DeCarvalho, A.C., Lyu, S., Li, P., Li, Y. and Barthel, F., 2017. Tumor evolution of glioma-intrinsic gene expression subtypes associates with immunological changes in the microenvironment. Cancer cell, 32(1), pp.42-56.
8. Brennan, C.W., Verhaak, R.G., McKenna, A., Campos, B., Noushmehr, H., Salama, S.R., Zheng, S., Chakravarty, D., Sanborn, J.Z., Berman, S.H. and Beroukhim, R., 2013. The somatic genomic landscape of glioblastoma. *cell*, *155*(2), pp.462-477.
9. Neftel, C., Laffy, J., Filbin, M.G., Hara, T., Shore, M.E., Rahme, G.J., Richman, A.R., Silverbush, D., Shaw, M.L., Hebert, C.M. and Dewitt, J., 2019. An integrative model of cellular states, plasticity, and genetics for glioblastoma. *Cell*, *178*(4), pp.835-849.
10. Boyrie, S., Delmas, C., Lemarié, A., Lubrano, V., Dahan, P., Malric, L., Luis, J., Gilhodes, J., Tosolini, M., Mouly, L. and Lehmann, M., 2018. RND1 regulates migration of human glioblastoma stem-like cells according to their anatomical localization and defines a prognostic signature in glioblastoma. *Oncotarget*, *9*(73), p.33788.
11. Gerritsen, J.K.W., Broekman, M.L.D., De Vleeschouwer, S., Schucht, P., Nahed, B.V., Berger, M.S. and Vincent, A.J.P.E., 2022. Safe surgery for glioblastoma: Recent advances and modern challenges. Neuro-oncology practice, 9(5), pp.364-379.
12. Hou, L.C., Veeravagu, A., Hsu, A.R. and Victor, C.K., 2006. Recurrent glioblastoma multiforme: a review of natural history and management options. *Neurosurgical focus*, *20*(4), p.E3
13. Lee, S.Y., 2016. Temozolomide resistance in glioblastoma multiforme. *Genes & diseases*, *3*(3), pp.198-210.
14. Murnyák, B., Kouhsari, M.C., Hershkovitch, R., Kálmán, B., Marko-Varga, G., Klekner, Á. and Hortobágyi, T., 2017. PARP1 expression and its correlation with survival is tumour molecular subtype dependent in glioblastoma. Oncotarget, 8(28), p.46348.
15. Lesueur, P., Lequesne, J., Grellard, J.M., Dugué, A., Coquan, E., Brachet, P.E., Geffrelot, J., Kao, W., Emery, E., Berro, D.H. and Castera, L., 2019. Phase I/IIa

study of concomitant radiotherapy with olaparib and temozolomide in unresectable or partially resectable glioblastoma: OLA-TMZ-RTE-01 trial protocol. *BMC cancer*, *19*, pp.1-11.
16. Gilbert, M.R., Dignam, J.J., Armstrong, T.S., Wefel, J.S., Blumenthal, D.T., Vogelbaum, M.A., Colman, H., Chakravarti, A., Pugh, S., Won, M. and Jeraj, R., 2014. A randomized trial of bevacizumab for newly diagnosed glioblastoma. *New England Journal of Medicine*, *370*(8), pp.699-708.
17. Reddy, R.G., Bhat, U.A., Chakravarty, S. and Kumar, A., 2020. Advances in histone deacetylase inhibitors in targeting glioblastoma stem cells. *Cancer Chemotherapy and Pharmacology*, *86*, pp.165-179.
18. Magaña-Maldonado, R., Chávez-Cortez, E.G., Olascoaga-Arellano, N.K., López-Mejía, M., Maldonado-Leal, F.M., Sotelo, J. and Pineda, B., 2016. Immunological evasion in glioblastoma. *BioMed research international*, *2016*(1), p.7487313.
19. Xuan, W., Lesniak, M.S., James, C.D., Heimberger, A.B. and Chen, P., 2021. Context-dependent glioblastoma–macrophage/microglia symbiosis and associated mechanisms. Trends in immunology, 42(4), pp.280-292.
20. Yuan, J., Levitin, H.M., Frattini, V., Bush, E.C., Boyett, D.M., Samanamud, J., Ceccarelli, M., Dovas, A., Zanazzi, G., Canoll, P. and Bruce, J.N., 2018. Single-cell transcriptome analysis of lineage diversity in high-grade glioma. *Genome medicine*, *10*, pp.1-15.
21. Zeiner, P.S., Preusse, C., Golebiewska, A., Zinke, J., Iriondo, A., Muller, A., Kaoma, T., Filipski, K., Müller-Eschner, M., Bernatz, S. and Blank, A.E., 2019. Distribution and prognostic impact of microglia/macrophage subpopulations in gliomas. *Brain pathology*, *29*(4), pp.513-529.
22. Würth, R., Bajetto, A., Harrison, J.K., Barbieri, F. and Florio, T., 2014. CXCL12 modulation of CXCR4 and CXCR7 activity in human glioblastoma stem-like cells and regulation of the tumor microenvironment. Frontiers in cellular neuroscience, 8, p.144
23. Held-Feindt, J., Hattermann, K., Müerköster, S.S., Wedderkopp, H., Knerlich-Lukoschus, F., Ungefroren, H., Mehdorn, H.M. and Mentlein, R., 2010. CX3CR1 promotes recruitment of human glioma-infiltrating microglia/macrophages (GIMs). *Experimental cell research*, *316*(9), pp.1553-1566.
24. Haage, V., Semtner, M., Vidal, R.O., Hernandez, D.P., Pong, W.W., Chen, Z., Hambardzumyan, D., Magrini, V., Ly, A., Walker, J. and Mardis, E., 2019. Comprehensive gene expression meta-analysis identifies signature genes that distinguish microglia from peripheral monocytes/macrophages in health and glioma. Acta neuropathologica communications, 7, pp.1-18.
25. Alban, T.J., Alvarado, A.G., Sorensen, M.D., Bayik, D., Volovetz, J., Serbinowski, E., Mulkearns-Hubert, E.E., Sinyuk, M., Hale, J.S., Onzi, G.R. and McGraw, M., 2018. Global immune fingerprinting in glioblastoma patient peripheral blood reveals immune-suppression signatures associated with prognosis. *JCI insight*, *3*(21).
26. Millrud, C.R., Bergenfelz, C. and Leandersson, K., 2017. On the origin of myeloid-derived suppressor cells. *Oncotarget*, *8*(2), p.3649.
27. Lakshmanachetty, S., Cruz-Cruz, J., Hoffmeyer, E., Cole, A.P. and Mitra, S.S., 2021. New insights into the multifaceted role of myeloid-derived suppressor cells (MDSCs) in high-grade gliomas: from metabolic reprograming, immunosuppression, and therapeutic resistance to current strategies for targeting MDSCs. *Cells*, *10*(4), p.893
28. Raychaudhuri, B., Rayman, P., Ireland, J., Ko, J., Rini, B., Borden, E.C., Garcia, J., Vogelbaum, M.A. and Finke, J., 2011. Myeloid-derived suppressor cell accumulation and function in patients with newly diagnosed glioblastoma. *Neuro-oncology*, *13*(6), pp.591-599.
29. Hussain, S.F., Yang, D., Suki, D., Aldape, K., Grimm, E. and Heimberger, A.B., 2006. The role of human glioma-infiltrating microglia/macrophages in mediating antitumor immune responses. *Neuro-oncology*, *8*(3), pp.261-279.

30. Humphries, W., Wei, J., Sampson, J.H. and Heimberger, A.B., 2010. The role of tregs in glioma-mediated immunosuppression: potential target for intervention. *Neurosurgery Clinics*, *21*(1), pp.125-137.
31. Djediai, S., Gonzalez Suarez, N., El Cheikh-Hussein, L., Rodriguez Torres, S., Gresseau, L., Dhayne, S., Joly-Lopez, Z. and Annabi, B., 2021. MT1-MMP cooperates with TGF-β receptor-mediated signaling to trigger SNAIL and induce epithelial-to-mesenchymal-like transition in U87 glioblastoma cells. *International Journal of Molecular Sciences*, *22*(23), p.13006.
32. Smyth, M.J., Teng, M.W., Swann, J., Kyparissoudis, K., Godfrey, D.I. and Hayakawa, Y., 2006. CD4+ CD25+ T regulatory cells suppress NK cell-mediated immunotherapy of cancer. *The Journal of Immunology*, *176*(3), pp.1582-1587
33. Raskov, H., Orhan, A., Christensen, J.P. and Gögenur, I., 2021. Cytotoxic CD8+ T cells in cancer and cancer immunotherapy. British journal of cancer, 124(2), pp.359-367
34. Mirzaei, R., Sarkar, S. and Yong, V.W., 2017. T cell exhaustion in glioblastoma: intricacies of immune checkpoints. Trends in immunology, 38(2), pp.104-115.
35. Carlino, M.S., Larkin, J. and Long, G.V., 2021. Immune checkpoint inhibitors in melanoma. *The Lancet*, *398*(10304), pp.1002-1014.
36. Nduom, E.K., Wei, J., Yaghi, N.K., Huang, N., Kong, L.Y., Gabrusiewicz, K., Ling, X., Zhou, S., Ivan, C., Chen, J.Q. and Burks, J.K., 2015. PD-L1 expression and prognostic impact in glioblastoma. *Neuro-oncology*, *18*(2), pp.195-205.
37. Berghoff, A.S., Kiesel, B., Widhalm, G., Wilhelm, D., Rajky, O., Kurscheid, S., Kresl, P., Wöhrer, A., Marosi, C., Hegi, M.E. and Preusser, M., 2017. Correlation of immune phenotype with IDH mutation in diffuse glioma. *Neuro-oncology*, *19*(11), pp.1460-1468.
38. Pombo Antunes, A.R., Scheyltjens, I., Duerinck, J., Neyns, B., Movahedi, K. and Van Ginderachter, J.A., 2020. Understanding the glioblastoma immune microenvironment as basis for the development of new immunotherapeutic strategies. *Elife*, *9*, p.e52176.
39. Paul, S. and Lal, G., 2017. The molecular mechanism of natural killer cells function and its importance in cancer immunotherapy. Frontiers in immunology, 8, p.1124
40. Thomas, D.A. and Massagué, J., 2005. TGF-β directly targets cytotoxic T cell functions during tumor evasion of immune surveillance. *Cancer cell*, *8*(5), pp.369-380.
41. Eisele, G., Wischhusen, J., Mittelbronn, M., Meyermann, R., Waldhauer, I., Steinle, A., Weller, M. and Friese, M.A., 2006. TGF-β and metalloproteinases differentially suppress NKG2D ligand surface expression on malignant glioma cells. *Brain*, *129*(9), pp.2416-2425
42. Wiendl, H., Mitsdoerffer, M., Hofmeister, V., Wischhusen, J., Bornemann, A., Meyermann, R., Weiss, E.H., Melms, A. and Weller, M., 2002. A functional role of HLA-G expression in human gliomas: an alternative strategy of immune escape. *The Journal of Immunology*, *168*(9), pp.4772-4780.
43. Lin, A. and Yan, W.H., 2015. Human leukocyte antigen-G (HLA-G) expression in cancers: roles in immune evasion, metastasis and target for therapy. *Molecular Medicine*, *21*, pp.782-791.
44. Codrici, E., Popescu, I.D., Tanase, C. and Enciu, A.M., 2022. Friends with benefits: chemokines, glioblastoma-associated microglia/macrophages, and tumor microenvironment. International journal of molecular sciences, 23(5), p.2509.
45. Colwell, N., Larion, M., Giles, A.J., Seldomridge, A.N., Sizdahkhani, S., Gilbert, M.R. and Park, D.M., 2017. Hypoxia in the glioblastoma microenvironment: shaping the phenotype of cancer stem-like cells. *Neuro-oncology*, *19*(7), pp.887-896.
46. Gray, G.K., McFarland, B.C., Nozell, S.E. and Benveniste, E.N., 2014. NF-κB and STAT3 in glioblastoma: therapeutic targets coming of age. Expert review of neurotherapeutics, 14(11), pp.1293-1306.
47. Joseph, J.V., Conroy, S., Pavlov, K., Sontakke, P., Tomar, T., Eggens-Meijer, E., Balasubramaniyan, V., Wagemakers, M., den Dunnen, W.F. and Kruyt, F.A., 2015.

Hypoxia enhances migration and invasion in glioblastoma by promoting a mesenchymal shift mediated by the HIF1α–ZEB1 axis. Cancer letters, 359(1), pp.107-116.
48. Fu, S., Liang, M., Wang, Y., Cui, L., Gao, C., Chu, X., Liu, Q., Feng, Y., Gong, W., Yang, M. and Li, Z., 2018. Dual-modified novel biomimetic nanocarriers improve targeting and therapeutic efficacy in glioma. *ACS applied materials & interfaces*, *11*(2), pp.1841-1854.
49. Bhowmik, A., Khan, R. and Ghosh, M.K., 2015. Blood brain barrier: a challenge for effectual therapy of brain tumors. BioMed research international, 2015(1), p.320941.
50. Abbott, N.J., 2002. Astrocyte–endothelial interactions and blood–brain barrier permeability. Journal of anatomy, 200(5), pp.523-534.
51. Llaguno, S.R.A., Wang, Z., Sun, D., Chen, J., Xu, J., Kim, E., Hatanpaa, K.J., Raisanen, J.M., Burns, D.K., Johnson, J.E. and Parada, L.F., 2015. Adult lineage-restricted CNS progenitors specify distinct glioblastoma subtypes. Cancer cell, 28(4), pp.429-440.
52. Fidoamore, A., Cristiano, L., Antonosante, A., d'Angelo, M., Di Giacomo, E., Astarita, C., Giordano, A., Ippoliti, R., Benedetti, E. and Cimini, A., 2016. Glioblastoma stem cells microenvironment: the paracrine roles of the niche in drug and radioresistance. Stem cells international, 2016(1), p.6809105
53. Calabrese, C., Poppleton, H., Kocak, M., Hogg, T.L., Fuller, C., Hamner, B., Oh, E.Y., Gaber, M.W., Finklestein, D., Allen, M. and Frank, A., 2007. A perivascular niche for brain tumor stem cells. Cancer cell, 11(1), pp.69-82.
54. Brown, D.V., Filiz, G., Daniel, P.M., Hollande, F., Dworkin, S., Amiridis, S., Kountouri, N., Ng, W., Morokoff, A.P. and Mantamadiotis, T., 2017. Expression of CD133 and CD44 in glioblastoma stem cells correlates with cell proliferation, phenotype stability and intra-tumor heterogeneity. PLoS One, 12(2), p.e0172791.
55. Trépant, A.L., Bouchart, C., Rorive, S., Sauvage, S., Decaestecker, C., Demetter, P. and Salmon, I., 2015. Identification of OLIG2 as the most specific glioblastoma stem cell marker starting from comparative analysis of data from similar DNA chip microarray platforms. Tumor Biology, 36, pp.1943-1953.
56. Sherry, M.M., Reeves, A., Wu, J.K. and Cochran, B.H., 2009. STAT3 is required for proliferation and maintenance of multipotency in glioblastoma stem cells. Stem cells, 27(10), pp.2383-2392.
57. Bouffet, E., Larouche, V., Campbell, B.B., Merico, D., De Borja, R., Aronson, M., Durno, C., Krueger, J., Cabric, V., Ramaswamy, V. and Zhukova, N., 2016. Immune checkpoint inhibition for hypermutant glioblastoma multiforme resulting from germline biallelic mismatch repair deficiency. *Journal of clinical oncology*, *34*(19), pp.2206-2211
58. Wang, X., Guo, G., Guan, H., Yu, Y., Lu, J. and Yu, J., 2019. Challenges and potential of PD-1/PD-L1 checkpoint blockade immunotherapy for glioblastoma. *Journal of Experimental & Clinical Cancer Research*, *38*, pp.1-13
59. Curigliano, G., Gelderblom, H., Mach, N., Doi, T., Tai, D., Forde, P.M., Sarantopoulos, J., Bedard, P.L., Lin, C.C., Hodi, F.S. and Wilgenhof, S., 2021. Phase I/Ib clinical trial of sabatolimab, an anti–TIM-3 antibody, alone and in combination with spartalizumab, an anti–PD-1 antibody, in advanced solid tumors. Clinical Cancer Research, 27(13), pp.3620-3629.
60. Lim, M., Ye, X., Piotrowski, A.F., Desai, A.S., Ahluwalia, M.S., Walbert, T., Fisher, J.D., Desideri, S., Belcaid, Z., Jackson, C. and Nabors, L.B., 2019. Updated phase I trial of anti-LAG-3 or anti-CD137 alone and in combination with anti-PD-1 in patients with recurrent GBM.
61. Rotte, A., Sahasranaman, S. and Budha, N., 2021. Targeting TIGIT for immunotherapy of cancer: update on clinical development. Biomedicines, 9(9), p.1277.
62. Strohl, W.R. and Naso, M., 2019. Bispecific T-cell redirection versus chimeric antigen receptor (CAR)-T cells as approaches to kill cancer cells. *Antibodies*, *8*(3), p.41.

63. Bagley, S.J., Desai, A.S., Linette, G.P., June, C.H. and O'Rourke, D.M., 2018. CAR T-cell therapy for glioblastoma: recent clinical advances and future challenges. *Neuro-oncology*, *20*(11), pp.1429-1438.
64. Brown, M.P., Ebert, L.M. and Gargett, T., 2019. Clinical chimeric antigen receptor-T cell therapy: a new and promising treatment modality for glioblastoma. *Clinical & Translational Immunology*, *8*(5), p.e1050.
65. Haslauer, T., Greil, R., Zaborsky, N. and Geisberger, R., 2021. CAR T-cell therapy in hematological malignancies. *International Journal of Molecular Sciences*, *22*(16), p.8996.
66. Swartz, A.M., Li, Q.J. and Sampson, J.H., 2014. Rindopepimut: a promising immunotherapeutic for the treatment of glioblastoma multiforme. *Immunotherapy*, *6*(6), pp.679-690.
67. Weller, M., Butowski, N., Tran, D.D., Recht, L.D., Lim, M., Hirte, H., Ashby, L., Mechtler, L., Goldlust, S.A., Iwamoto, F. and Drappatz, J., 2017. Rindopepimut with temozolomide for patients with newly diagnosed, EGFRvIII-expressing glioblastoma (ACT IV): a randomised, double-blind, international phase 3 trial. *The lancet oncology*, *18*(10), pp.1373-1385.
68. Reardon, D.A., Desjardins, A., Vredenburgh, J.J., O'Rourke, D.M., Tran, D.D., Fink, K.L., Nabors, L.B., Li, G., Bota, D.A., Lukas, R.V. and Ashby, L.S., 2020. Rindopepimut with bevacizumab for patients with relapsed EGFRvIII-expressing glioblastoma (ReACT): results of a double-blind randomized phase II trial. *Clinical Cancer Research*, *26*(7), pp.1586-1594.
69. Hilf, N., Kuttruff-Coqui, S., Frenzel, K., Bukur, V., Stevanović, S., Gouttefangeas, C., Platten, M., Tabatabai, G., Dutoit, V., van der Burg, S.H. and thor Straten, P., 2019. Actively personalized vaccination trial for newly diagnosed glioblastoma. Nature, 565(7738), pp.240-245.
70. Keskin, D.B., Anandappa, A.J., Sun, J., Tirosh, I., Mathewson, N.D., Li, S., Oliveira, G., Giobbie-Hurder, A., Felt, K., Gjini, E. and Shukla, S.A., 2019. Neoantigen vaccine generates intratumoral T cell responses in phase Ib glioblastoma trial. *Nature*, *565*(7738), pp.234-239.
71. Ahluwalia, M.S., Reardon, D.A., Abad, A.P., Curry, W.T., Wong, E.T., Figel, S.A., Mechtler, L.L., Peereboom, D.M., Hutson, A.D., Withers, H.G. and Liu, S., 2023. Phase IIa study of SurVaxM plus adjuvant temozolomide for newly diagnosed glioblastoma. Journal of Clinical Oncology, 41(7), pp.1453-1465.
72. Migliorini, D., Dutoit, V., Allard, M., Grandjean Hallez, N., Marinari, E., Widmer, V., Philippin, G., Corlazzoli, F., Gustave, R., Kreutzfeldt, M. and Blazek, N., 2019. Phase I/II trial testing safety and immunogenicity of the multipeptide IMA950/poly-ICLC vaccine in newly diagnosed adult malignant astrocytoma patients. Neuro-oncology, 21(7), pp.923-933.
73. Wen, P.Y., Reardon, D.A., Armstrong, T.S., Phuphanich, S., Aiken, R.D., Landolfi, J.C., Curry, W.T., Zhu, J.J., Glantz, M., Peereboom, D.M. and Markert, J.M., 2019. A randomized double-blind placebo-controlled phase II trial of dendritic cell vaccine ICT-107 in newly diagnosed patients with glioblastoma. *Clinical Cancer Research*, *25*(19), pp.5799-5807
74. Liau, L.M., Ashkan, K., Tran, D.D., Campian, J.L., Trusheim, J.E., Cobbs, C.S., Heth, J.A., Salacz, M., Taylor, S., D'Andre, S.D. and Iwamoto, F.M., 2018. First results on survival from a large Phase 3 clinical trial of an autologous dendritic cell vaccine in newly diagnosed glioblastoma. *Journal of translational medicine*, *16*, pp.1-9.
75. Cenciarini, M., Valentino, M., Belia, S., Sforna, L., Rosa, P., Ronchetti, S., D'Adamo, M.C. and Pessia, M., 2019. Dexamethasone in glioblastoma multiforme therapy: mechanisms and controversies. Frontiers in molecular neuroscience, 12, p.65.
76. Gibbs, J., Ince, L., Matthews, L., Mei, J., Bell, T., Yang, N., Saer, B., Begley, N., Poolman, T., Pariollaud, M. and Farrow, S., 2014. An epithelial circadian clock controls pulmonary inflammation and glucocorticoid action. *Nature medicine*, *20*(8), pp.919-926.

77. Matthews, L., Johnson, J., Berry, A., Trebble, P., Cookson, A., Spiller, D., Rivers, C., Norman, M., White, M. and Ray, D., 2011. Cell cycle phase regulates glucocorticoid receptor function. *PLoS One*, *6*(7), p.e22289.
78. Distelhorst, C.W., 2002. Recent insights into the mechanism of glucocorticosteroid-induced apoptosis. *Cell Death & Differentiation*, *9*(1), pp.6-19.
79. Salvador, E., Shityakov, S. and Förster, C., 2014. Glucocorticoids and endothelial cell barrier function. Cell and tissue research, 355, pp.597-605.
80. Hollenberg, S.M., Weinberger, C., Ong, E.S., Cerelli, G., Oro, A., Lebo, R., Brad Thompson, E., Rosenfeld, M.G. and Evans, R.M., 1985. Primary structure and expression of a functional human glucocorticoid receptor cDNA. *Nature*, *318*(6047), pp.635-641.
81. Oakley, R.H. and Cidlowski, J.A., 2013. The biology of the glucocorticoid receptor: new signaling mechanisms in health and disease. Journal of Allergy and Clinical Immunology, 132(5), pp.1033-1044.
82. Yang, N., Ray, D.W. and Matthews, L.C., 2012. Current concepts in glucocorticoid resistance. *Steroids*, *77*(11), pp.1041-1049.
83. LEWIS-TUFFIN, L.J. and Cidlowski, J.A., 2006. The physiology of human glucocorticoid receptor β (hGRβ) and glucocorticoid resistance. Annals of the New York Academy of Sciences, 1069(1), pp.1-9.
84. Ray, D.W., 1996. Molecular mechanisms of glucocorticoid resistance. Journal of endocrinology, 149(1), pp.1-5.
85. de Lange, P., Segeren, C.M., Koper, J.W., Wiemer, E., Sonneveld, P., Brinkmann, A.O., White, A., Brogan, I.J., de Jong, F.H. and Lamberts, S.W., 2010. Expression in hematological malignancies of a glucocorticoid receptor splice variant that augments glucocorticoid receptor-mediated effects in transfected cells. Cancer research, 61(10), pp.3937-3941.
86. Timmermans, S., Souffriau, J. and Libert, C., 2019. A general introduction to glucocorticoid biology. Frontiers in immunology, 10, p.1545.
87. Liu, B., Zhang, T.N., Knight, J.K. and Goodwin, J.E., 2019. The glucocorticoid receptor in cardiovascular health and disease. Cells, 8(10), p.1227.
88. Song, I.H. and Buttgereit, F., 2006. Non-genomic glucocorticoid effects to provide the basis for new drug developments. Molecular and cellular endocrinology, 246(1-2), pp.142-146.
89. Leis, H., Page, A., Ramírez, A., Bravo, A., Segrelles, C., Paramio, J., Barettino, D., Jorcano, J.L. and Pérez, P., 2004. Glucocorticoid receptor counteracts tumorigenic activity of Akt in skin through interference with the phosphatidylinositol 3-kinase signaling pathway. Molecular endocrinology, 18(2), pp.303-311.
90. Flaherty, R.L., Owen, M., Fagan-Murphy, A., Intabli, H., Healy, D., Patel, A., Allen, M.C., Patel, B.A. and Flint, M.S., 2017. Glucocorticoids induce production of reactive oxygen species/reactive nitrogen species and DNA damage through an iNOS mediated pathway in breast cancer. Breast Cancer Research, 19, pp.1-13.
91. Cain, D.W. and Cidlowski, J.A., 2017. Immune regulation by glucocorticoids. Nature Reviews Immunology, 17(4), pp.233-247.
92. Ratman, D., Berghe, W.V., Dejager, L., Libert, C., Tavernier, J., Beck, I.M. and De Bosscher, K., 2013. How glucocorticoid receptors modulate the activity of other transcription factors: a scope beyond tethering. Molecular and cellular endocrinology, 380(1-2), pp.41-54.
93. Rogatsky, I. and Ivashkiv, L.B., 2006. Glucocorticoid modulation of cytokine signaling. Tissue antigens, 68(1), pp.1-12
94. Kalfeist, L., Galland, L., Ledys, F., Ghiringhelli, F., Limagne, E. and Ladoire, S., 2022. Impact of glucocorticoid use in oncology in the immunotherapy era. Cells, 11(5), p.770
95. Gustafson, M.P., Lin, Y., New, K.C., Bulur, P.A., O'Neill, B.P., Gastineau, D.A. and Dietz, A.B., 2010. Systemic immune suppression in glioblastoma: the interplay between CD14+ HLA-DRlo/neg monocytes, tumor factors, and dexamethasone. Neuro-oncology, 12(7), pp.631-644

96. Moyes, K.W., Davis, A., Hoglund, V., Haberthur, K., Lieberman, N.A., Kreuser, S.A., Deutsch, G.H., Franco, S., Locke, D., Carleton, M.O. and Gilbertson, D.G., 2018. Effects of tumor grade and dexamethasone on myeloid cells in patients with glioma. *Oncoimmunology*, *7*(11), p.e1507668.
97. Ingawale, D.K. and Mandlik, S.K., 2020. New insights into the novel anti-inflammatory mode of action of glucocorticoids. Immunopharmacology and immunotoxicology, 42(2), pp.59-73.
98. Liberman, A.C., Budziñski, M.L., Sokn, C., Gobbini, R.P., Steininger, A. and Arzt, E., 2018. Regulatory and mechanistic actions of glucocorticoids on T and inflammatory cells. Frontiers in endocrinology, 9, p.235
99. Chen, L., Jondal, M. and Yakimchuk, K., 2018. Regulatory effects of dexamethasone on NK and T cell immunity. Inflammopharmacology, 26, pp.1331-1338
100. Morgan, D.J. and Davis, D.M., 2017. Distinct effects of dexamethasone on human natural killer cell responses dependent on cytokines. Frontiers in immunology, 8, p.432
101. Riccardi, C., Cifone, M.G. and Migliorati, G., 1999. Glucocorticoid hormone-induced modulation of gene expression and regulation of T-cell death: role of GITR and GILZ, two dexamethasone-induced genes. *Cell Death & Differentiation*, *6*(12), pp.1182-1189.
102. Zappasodi, R., Sirard, C., Li, Y., Budhu, S., Abu-Akeel, M., Liu, C., Yang, X., Zhong, H., Newman, W., Qi, J. and Wong, P., 2019. Rational design of anti-GITR-based combination immunotherapy. Nature medicine, 25(5), pp.759-766.
103. Rudak, P.T., Gangireddy, R., Choi, J., Burhan, A.M., Summers, K.L., Jackson, D.N., Inoue, W. and Haeryfar, S.M., 2019. Stress-elicited glucocorticoid receptor signaling upregulates TIGIT in innate-like invariant T lymphocytes. Brain, Behavior, and Immunity, 80, pp.793-804.
104. Xing, K., Gu, B., Zhang, P. and Wu, X., 2015. Dexamethasone enhances programmed cell death 1 (PD-1) expression during T cell activation: an insight into the optimum application of glucocorticoids in anti-cancer therapy. BMC immunology, 16, pp.1-9.
105. Pitter, K.L., Tamagno, I., Alikhanyan, K., Hosni-Ahmed, A., Pattwell, S.S., Donnola, S., Dai, C., Ozawa, T., Chang, M., Chan, T.A. and Beal, K., 2016. Corticosteroids compromise survival in glioblastoma. Brain, 139(5), pp.1458-1471
106. Zhou, L., Shen, Y., Huang, T., Sun, Y., Alolga, R.N., Zhang, G. and Ge, Y., 2021. The prognostic effect of dexamethasone on patients with glioblastoma: a systematic review and meta-analysis. Frontiers in Pharmacology, 12, p.727707.
107. Kaup, B., Schindler, I., Knüpfer, H., Schlenzka, A., Preiβ, R. and Knüpfer, M.M., 2001. Time-dependent inhibition of glioblastoma cell proliferation by dexamethasone. Journal of neuro-oncology, 51, pp.105-110.
108. Iorgulescu, J.B., Gokhale, P.C., Speranza, M.C., Eschle, B.K., Poitras, M.J., Wilkens, M.K., Soroko, K.M., Chhoeu, C., Knott, A., Gao, Y. and Lim-Fat, M.J., 2021. Concurrent dexamethasone limits the clinical benefit of immune checkpoint blockade in glioblastoma. Clinical Cancer Research, 27(1), pp.276-287.
109. Wong, E.T., Lok, E., Gautam, S. and Swanson, K.D., 2015. Dexamethasone exerts profound immunologic interference on treatment efficacy for recurrent glioblastoma. British journal of cancer, 113(2), pp.232-241
110. Luedi, M.M., Singh, S.K., Mosley, J.C., Hatami, M., Gumin, J., Sulman, E.P., Lang, F.F., Stueber, F., Zinn, P.O. and Colen, R.R., 2017. A dexamethasone-regulated gene signature is prognostic for poor survival in glioblastoma patients. *Journal of neurosurgical anesthesiology*, *29*(1), pp.46-58.
111. Luedi, M.M., Singh, S.K., Mosley, J.C., Hassan, I.S., Hatami, M., Gumin, J., Andereggen, L., Sulman, E.P., Lang, F.F., Stueber, F. and Fuller, G.N., 2018. Dexamethasone-mediated oncogenicity in vitro and in an animal model of glioblastoma. *Journal of neurosurgery*, *129*(6), pp.1446-1455
112. Kostopoulou, O.N., Mohammad, A.A., Bartek Jr, J., Winter, J., Jung, M., Stragliotto, G., Söderberg-Nauclér, C. and Landázuri, N., 2018. Glucocorticoids

promote a glioma stem cell-like phenotype and resistance to chemotherapy in human glioblastoma primary cells: Biological and prognostic significance. *International Journal of Cancer*, *142*(6), pp.1266-1276.
113. Martens, B. and Drebert, Z., 2019. Glucocorticoid-mediated effects on angiogenesis in solid tumors. The Journal of Steroid Biochemistry and Molecular Biology, 188, pp.147-155
114. Keskin, D.B., Anandappa, A.J., Sun, J., Tirosh, I., Mathewson, N.D., Li, S., Oliveira, G., Giobbie-Hurder, A., Felt, K., Gjini, E. and Shukla, S.A., 2019. Neoantigen vaccine generates intratumoral T cell responses in phase Ib glioblastoma trial. *Nature*, *565*(7738), pp.234-239.
115. Giles, A.J., Hutchinson, M.K.N., Sonnemann, H.M., Jung, J., Fecci, P.E., Ratnam, N.M., Zhang, W., Song, H., Bailey, R., Davis, D. and Reid, C.M., 2018. Dexamethasone-induced immunosuppression: mechanisms and implications for immunotherapy. Journal for immunotherapy of cancer, 6, pp.1-13.
116. Nayak, L., Molinaro, A.M., Peters, K., Clarke, J.L., Jordan, J.T., de Groot, J., Nghiemphu, L., Kaley, T., Colman, H., McCluskey, C. and Gaffey, S., 2021. Randomized phase II and biomarker study of pembrolizumab plus bevacizumab versus pembrolizumab alone for patients with recurrent glioblastoma. Clinical Cancer Research, 27(4), pp.1048-1057.
117. Van Putten, E.H., Kleijn, A., Van Beusechem, V.W., Noske, D., Lamers, C.H., De Goede, A.L., Idema, S., Hoefnagel, D., Kloezeman, J.J., Fueyo, J. and Lang, F.F., 2022. Convection enhanced delivery of the oncolytic adenovirus Delta24-RGD in patients with recurrent GBM: a phase I clinical trial including correlative studies. Clinical Cancer Research, 28(8), pp.1572-1585.
118. Kaufman, H.L., Kohlhapp, F.J. and Zloza, A., 2015. Oncolytic viruses: a new class of immunotherapy drugs. *Nature reviews Drug discovery*, *14*(9), pp.642-662.
119. Lichty, B.D., Breitbach, C.J., Stojdl, D.F. and Bell, J.C., 2014. Going viral with cancer immunotherapy. *Nature Reviews Cancer*, *14*(8), pp.559-567.
120. Prestwich, R.J., Harrington, K.J., Pandha, H.S., Vile, R.G., Melcher, A.A. and Errington, F., 2008. Oncolytic viruses: a novel form of immunotherapy. Expert review of anticancer therapy, 8(10), pp.1581-1588
121. El-Sherbiny, Y.M., Holmes, T.D., Wetherill, L.F., Black, E.V.I., Wilson, E.B., Phillips, S.L., Scott, G.B., Adair, R.A., Dave, R., Scott, K.J. and Morgan, R.S.M., 2015. Controlled infection with a therapeutic virus defines the activation kinetics of human natural killer cells in vivo. Clinical & Experimental Immunology, 180(1), pp.98-107.
122. Andtbacka, R.H., Collichio, F., Harrington, K.J., Middleton, M.R., Downey, G., Öhrling, K. and Kaufman, H.L., 2019. Final analyses of OPTiM: a randomized phase III trial of talimogene laherparepvec versus granulocyte-macrophage colony-stimulating factor in unresectable stage III–IV melanoma. *Journal for immunotherapy of cancer*, *7*, pp.1-11.
123. Todo, T., Ito, H., Ino, Y., Ohtsu, H., Ota, Y., Shibahara, J. and Tanaka, M., 2022. Intratumoral oncolytic herpes virus G47Δ for residual or recurrent glioblastoma: a phase 2 trial. Nature medicine, 28(8), pp.1630-1639.
124. Martikainen, M. and Essand, M., 2019. Virus-based immunotherapy of glioblastoma. Cancers, 11(2), p.186.
125. Desjardins, A., Gromeier, M., Herndon, J.E., Beaubier, N., Bolognesi, D.P., Friedman, A.H., Friedman, H.S., McSherry, F., Muscat, A.M., Nair, S. and Peters, K.B., 2018. Recurrent glioblastoma treated with recombinant poliovirus. *New England Journal of Medicine*, *379*(2), pp.150-161.
126. Lang, F.F., Conrad, C., Gomez-Manzano, C., Yung, W.A., Sawaya, R., Weinberg, J.S., Prabhu, S.S., Rao, G., Fuller, G.N., Aldape, K.D. and Gumin, J., 2018. Phase I study of DNX-2401 (Delta-24-RGD) oncolytic adenovirus: replication and immunotherapeutic effects in recurrent malignant glioma. *Journal of clinical oncology*, *36*(14), pp.1419-1427.
127. Nassiri, F., Patil, V., Yefet, L.S., Singh, O., Liu, J., Dang, R.M., Yamaguchi, T.N., Daras, M., Cloughesy, T.F., Colman, H. and Kumthekar, P.U., 2023. Oncolytic

DNX-2401 virotherapy plus pembrolizumab in recurrent glioblastoma: a phase 1/2 trial. Nature medicine, 29(6), pp.1370-1378
128. Kleijn, A., Kloezeman, J., Treffers-Westerlaken, E., Fulci, G., Leenstra, S., Dirven, C., Debets, R. and Lamfers, M., 2014. The in vivo therapeutic efficacy of the oncolytic adenovirus Delta24-RGD is mediated by tumor-specific immunity. *PloS one*, *9*(5), p.e97495.
129. Kleijn, A., van den Bossche, W., Haefner, E.S., Belcaid, Z., Burghoorn-Maas, C., Kloezeman, J.J., Pas, S.D., Leenstra, S., Debets, R., de Vrij, J. and Dirven, C.M., 2017. The sequence of Delta24-RGD and TMZ administration in malignant glioma affects the role of CD8+ T cell anti-tumor activity. Molecular Therapy-Oncolytics, 5, pp.11-19.
130. Harrow, S., Papanastassiou, V., Harland, J., Mabbs, R., Petty, R., Fraser, M., Hadley, D., Patterson, J., Brown, S.M. and Rampling, R., 2004. HSV1716 injection into the brain adjacent to tumour following surgical resection of high-grade glioma: safety data and long-term survival. *Gene therapy*, *11*(22), pp.1648-1658.
131. Todo, T., Rabkin, S.D., Chahlavi, A. and Martuza, R.L., 1999. Corticosteroid administration does not affect viral oncolytic activity, but inhibits antitumor immunity in replicationcompetent herpes simplex virus tumor therapy. *Human gene therapy*, *10*(17), pp.2869-2878.
132. Todo2022
133. Samson, A., Scott, K.J., Taggart, D., West, E.J., Wilson, E., Nuovo, G.J., Thomson, S., Corns, R., Mathew, R.K., Fuller, M.J. and Kottke, T.J., 2018. Intravenous delivery of oncolytic reovirus to brain tumor patients immunologically primes for subsequent checkpoint blockade. *Science translational medicine*, *10*(422), p.eaam7577.
134. Phillips, M.B., Stuart, J.D., Rodríguez Stewart, R.M., Berry, J.T., Mainou, B.A. and Boehme, K.W., 2018. Current understanding of reovirus oncolysis mechanisms. *Oncolytic virotherapy*, pp.53-6
135. DeAntoneo, C., Danthi, P. and Balachandran, S., 2022. Reovirus activated cell death pathways. Cells, 11(11), p.1757.
136. Barton, E.S., Chappell, J.D., Connolly, J.L., Forrest, J.C. and Dermody, T.S., 2001. Reovirus receptors and apoptosis. Virology, 290(2), pp.173-180.
137. Antar, A.A., Konopka, J.L., Campbell, J.A., Henry, R.A., Perdigoto, A.L., Carter, B.D., Pozzi, A., Abel, T.W. and Dermody, T.S., 2009. Junctional adhesion molecule-A is required for hematogenous dissemination of reovirus. Cell host & microbe, 5(1), pp.59-71
138. Chandran, K., Zhang, X., Olson, N.H., Walker, S.B., Chappell, J.D., Dermody, T.S., Baker, T.S. and Nibert, M.L., 2001. Complete in vitro assembly of the reovirus outer capsid produces highly infectious particles suitable for genetic studies of the receptor-binding protein. Journal of Virology, 75(11), pp.5335-5342.
139. Antczak, J.B. and Joklik, W.K., 1992. Reovirus genome segment assortment into progeny genomes studied by the use of monoclonal antibodies directed against reovirus proteins. Virology, 187(2), pp.760-776.
140. Tenorio, R., Fernández de Castro, I., Knowlton, J.J., Zamora, P.F., Sutherland, D.M., Risco, C. and Dermody, T.S., 2019. Function, architecture, and biogenesis of reovirus replication neoorganelles. Viruses, 11(3), p.288.
141. Coffey, M.C., Strong, J.E., Forsyth, P.A. and Lee, P.W., 1998. Reovirus therapy of tumors with activated Ras pathway. Science, 282(5392), pp.1332-1334.
142. Gong, J. and Mita, M.M., 2014. Activated ras signaling pathways and reovirus oncolysis: an update on the mechanism of preferential reovirus replication in cancer cells. Frontiers in oncology, 4, p.167.
143. Sadler, A.J. and Williams, B.R., 2008. Interferon-inducible antiviral effectors. Nature reviews immunology, 8(7), pp.559-568.
144. Shmulevitz, M., Pan, L.Z., Garant, K., Pan, D. and Lee, P.W., 2010. Oncogenic Ras promotes reovirus spread by suppressing IFN-β production through negative regulation of RIG-I signaling. Cancer research, 70(12), pp.4912-4921

145. Sharpe, A.H. and Fields, B.N., 1982. Reovirus inhibition of cellular RNA and protein synthesis: role of the S4 gene. Virology, 122(2), pp.381-391.
146. Richardson-Burns, S.M., Kominsky, D.J. and Tyler, K.L., 2002. Reovirus-induced neuronal apoptosis is mediated by caspase 3 and is associated with the activation of death receptors. Journal of neurovirology, 8(5), pp.365-380.
147. O'DONNELL, S.M., Hansberger, M.W. and Dermody, T.S., 2003. Viral and cellular determinants of apoptosis induced by mammalian reovirus. International reviews of immunology, 22(5-6), pp.477-503.
148. Thirukkumaran, C.M., Shi, Z.Q., Luider, J., Kopciuk, K., Gao, H., Bahlis, N., Neri, P., Pho, M., Stewart, D., Mansoor, A. and Morris, D.G., 2012. Reovirus as a viable therapeutic option for the treatment of multiple myeloma. *Clinical Cancer Research*, *18*(18), pp.4962-4972.
149. Berger, A.K., Hiller, B.E., Thete, D., Snyder, A.J., Perez Jr, E., Upton, J.W. and Danthi, P., 2017. Viral RNA at two stages of reovirus infection is required for the induction of necroptosis. Journal of virology, 91(6), pp.10-1128
150. Errington, F., Steele, L., Prestwich, R., Harrington, K.J., Pandha, H.S., Vidal, L., De Bono, J., Selby, P., Coffey, M., Vile, R. and Melcher, A., 2008. Reovirus activates human dendritic cells to promote innate antitumor immunity. The Journal of Immunology, 180(9), pp.6018-6026
151. Schulz, O., Diebold, S.S., Chen, M., Näslund, T.I., Nolte, M.A., Alexopoulou, L., Azuma, Y.T., Flavell, R.A., Liljeström, P. and Reis e Sousa, C., 2005. Toll-like receptor 3 promotes cross-priming to virus-infected cells. Nature, 433(7028), pp.887-892
152. Katayama, Y., Tachibana, M., Kurisu, N., Oya, Y., Terasawa, Y., Goda, H., Kobiyama, K., Ishii, K.J., Akira, S., Mizuguchi, H. and Sakurai, F., 2018. Oncolytic reovirus inhibits immunosuppressive activity of myeloid-derived suppressor cells in a TLR3-dependent manner. The Journal of Immunology, 200(8), pp.2987-2999.
153. White, C.L., Twigger, K.R., Vidal, L., De Bono, J.S., Coffey, M., Heinemann, L., Morgan, R., Merrick, A., Errington, F., Vile, R.G. and Melcher, A.A., 2008. Characterization of the adaptive and innate immune response to intravenous oncolytic reovirus (Dearing type 3) during a phase I clinical trial. Gene therapy, 15(12), pp.911-920.
154. Pandha, H.S., Heinemann, L., Simpson, G.R., Melcher, A., Prestwich, R., Errington, F., Coffey, M., Harrington, K.J. and Morgan, R., 2009. Synergistic effects of oncolytic reovirus and cisplatin chemotherapy in murine malignant melanoma. Clinical cancer research, 15(19), pp.6158-6166.
155. Roulstone, V., Twigger, K., Zaidi, S., Pencavel, T., Kyula, J.N., White, C., McLaughlin, M., Seth, R., Karapanagiotou, E.M., Mansfield, D. and Coffey, M., 2013. Synergistic cytotoxicity of oncolytic reovirus in combination with cisplatin–paclitaxel doublet chemotherapy. Gene therapy, 20(5), pp.521-528.
156. Hamano, S., Mori, Y., Aoyama, M., Kataoka, H., Tanaka, M., Ebi, M., Kubota, E., Mizoshita, T., Tanida, S., Johnston, R.N. and Asai, K., 2015. Oncolytic reovirus combined with trastuzumab enhances antitumor efficacy through TRAIL signaling in human HER2-positive gastric cancer cells. *Cancer Letters*, *356*(2), pp.846-854.
157. McEntee, G., Kyula, J.N., Mansfield, D., Smith, H., Wilkinson, M., Gregory, C., Roulstone, V., Coffey, M. and Harrington, K.J., 2016. Enhanced cytotoxicity of reovirus and radiotherapy in melanoma cells is mediated through increased viral replication and mitochondrial apoptotic signalling. Oncotarget, 7(30), p.48517.
158. Maitra, R., Ghalib, M.H. and Goel, S., 2012. Reovirus: a targeted therapeutic—progress and potential. Molecular cancer research, 10(12), pp.1514-1525.
159. Villalona-Calero, M.A., Lam, E., Otterson, G.A., Zhao, W., Timmons, M., Subramaniam, D., Hade, E.M., Gill, G.M., Coffey, M., Selvaggi, G. and Bertino, E., 2016. Oncolytic reovirus in combination with chemotherapy in metastatic or recurrent non–small cell lung cancer patients with K RAS-activated tumors. Cancer, 122(6), pp.875-883.
160. Rajani, K., Parrish, C., Kottke, T., Thompson, J., Zaidi, S., Ilett, L., Shim, K.G., Diaz, R.M., Pandha, H., Harrington, K. and Coffey, M., 2016. Combination therapy

with reovirus and anti-PD-1 blockade controls tumor growth through innate and adaptive immune responses. Molecular Therapy, 24(1), pp.166-174
161. Polson, E.S., Kuchler, V.B., Abbosh, C., Ross, E.M., Mathew, R.K., Beard, H.A., da Silva, B., Holding, A.N., Ballereau, S., Chuntharpursat-Bon, E. and Williams, J., 2018. KHS101 disrupts energy metabolism in human glioblastoma cells and reduces tumor growth in mice. Science translational medicine, 10(454), p.eaar2718
162. Wurdak, H., Zhu, S., Romero, A., Lorger, M., Watson, J., Chiang, C.Y., Zhang, J., Natu, V.S., Lairson, L.L., Walker, J.R. and Trussell, C.M., 2010. An RNAi screen identifies TRRAP as a regulator of brain tumor-initiating cell differentiation. Cell stem cell, 6(1), pp.37-47.
163. Da Silva, B., Mathew, R.K., Polson, E.S., Williams, J. and Wurdak, H., 2018. Spontaneous glioblastoma spheroid infiltration of early-stage cerebral organoids models brain tumor invasion. SLAS DISCOVERY: Advancing Life Sciences R&D, 23(8), pp.862-868.
164. Simpson, G.R., Han, Z., Liu, B., Wang, Y., Campbell, G. and Coffin, R.S., 2006. Combination of a fusogenic glycoprotein, prodrug activation, and oncolytic herpes simplex virus for enhanced local tumor control. *Cancer research*, *66*(9), pp.4835-4842.
165. Robinson, M.D., McCarthy, D.J. and Smyth, G.K., 2010. edgeR: a Bioconductor package for differential expression analysis of digital gene expression data. *bioinformatics*, *26*(1), pp.139-140.
166. Reyes, M., Vickers, D., Billman, K., Eisenhaure, T., Hoover, P., Browne, E.P., Rao, D.A., Hacohen, N. and Blainey, P.C., 2019. Multiplexed enrichment and genomic profiling of peripheral blood cells reveal subset-specific immune signatures. Science advances, 5(1), p.eaau9223
167. Goujon, C., Moncorgé, O., Bauby, H., Doyle, T., Ward, C.C., Schaller, T., Hué, S., Barclay, W.S., Schulz, R. and Malim, M.H., 2013. Human MX2 is an interferon-induced post-entry inhibitor of HIV-1 infection. *Nature*, *502*(7472), pp.559-562.
168. Berkeley, R.A., Steele, L.P., Mulder, A.A., Van Den Wollenberg, D.J., Kottke, T.J., Thompson, J., Coffey, M., Hoeben, R.C., Vile, R.G., Melcher, A. and Ilett, E.J., 2018. Antibody-neutralized reovirus is effective in oncolytic virotherapy. Cancer immunology research, 6(10), pp.1161-1173.
169. Chen, E.Y., Tan, C.M., Kou, Y., Duan, Q., Wang, Z., Meirelles, G.V., Clark, N.R. and Ma'ayan, A., 2013. Enrichr: interactive and collaborative HTML5 gene list enrichment analysis tool. BMC bioinformatics, 14, pp.1-14.
170. Tang, D., Chen, M., Huang, X., Zhang, G., Zeng, L., Zhang, G., Wu, S. and Wang, Y., 2023. SRplot: A free online platform for data visualization and graphing. PLoS One, 18(11), p.e0294236
171. Szklarczyk, D., Kirsch, R., Koutrouli, M., Nastou, K., Mehryary, F., Hachilif, R., Gable, A.L., Fang, T., Doncheva, N.T., Pyysalo, S. and Bork, P., 2023. The STRING database in 2023: protein–protein association networks and functional enrichment analyses for any sequenced genome of interest. *Nucleic acids research*, *51*(D1), pp.D638-D646.
172. Close, H.J., Stead, L.F., Nsengimana, J., Reilly, K.A., Droop, A., Wurdak, H., Mathew, R.K., Corns, R., Newton-Bishop, J., Melcher, A.A. and Short, S.C., 2020. Expression profiling of single cells and patient cohorts identifies multiple immunosuppressive pathways and an altered NK cell phenotype in glioblastoma. *Clinical & Experimental Immunology*, *200*(1), pp.33-44.
173. Kumar, R. and Thompson, E.B., 2005. Gene regulation by the glucocorticoid receptor: structure: function relationship. The Journal of steroid biochemistry and molecular biology, 94(5), pp.383-394.
174. Marques, A.H., Silverman, M.N. and Sternberg, E.M., 2009. Glucocorticoid dysregulations and their clinical correlates: From receptors to therapeutics. Annals of the New York Academy of Sciences, 1179(1), pp.1-18

175. Atsaves, V., Leventaki, V., Rassidakis, G.Z. and Claret, F.X., 2019. AP-1 transcription factors as regulators of immune responses in cancer. Cancers, 11(7), p.1037
176. Karki, K., Li, X., Jin, U.H., Mohankumar, K., Zarei, M., Michelhaugh, S.K., Mittal, S., Tjalkens, R. and Safe, S., 2020. Nuclear receptor 4A2 (NR4A2) is a druggable target for glioblastomas. *Journal of Neuro-oncology*, *146*, pp.25-39
177. Mohan, H.M., Aherne, C.M., Rogers, A.C., Baird, A.W., Winter, D.C. and Murphy, E.P., 2012. Molecular pathways: the role of NR4A orphan nuclear receptors in cancer. *Clinical cancer research*, *18*(12), pp.3223-3228
178. Yu, H., Park, J., Lee, J., Choi, K. and Choi, C., 2012. Constitutive expression of MAP kinase phosphatase-1 confers multi-drug resistance in human glioblastoma cells. Cancer Research and Treatment: Official Journal of Korean Cancer Association, 44(3), p.195
179. Wang, Y., Xie, X., Li, S., Zhang, D., Zheng, H., Zhang, M. and Zhang, Z., 2021. Co-overexpression of RIOK1 and AKT1 as a prognostic risk factor in glioma. Journal of Cancer, 12(19), p.5745
180. Berard, A.R., Severini, A. and Coombs, K.M., 2015. Differential reovirus-specific and herpesvirus-specific activator protein 1 activation of secretogranin II leads to altered virus secretion. *Journal of Virology*, *89*(23), pp.11954-11964.
181. Wang, D., Berglund, A., Kenchappa, R.S., Forsyth, P.A., Mulé, J.J. and Etame, A.B., 2016. BIRC3 is a novel driver of therapeutic resistance in Glioblastoma. Scientific reports, 6(1), p.21710.
182. Mahajan-Thakur, S., Bien-Möller, S., Marx, S., Schroeder, H. and Rauch, B.H., 2017. Sphingosine 1-phosphate (S1P) signaling in glioblastoma multiforme—A systematic review. International Journal of Molecular Sciences, 18(11), p.2448
183. Gril, B., Paranjape, A.N., Woditschka, S., Hua, E., Dolan, E.L., Hanson, J., Wu, X., Kloc, W., Izycka-Swieszewska, E., Duchnowska, R. and Pęksa, R., 2018. Reactive astrocytic S1P3 signaling modulates the blood–tumor barrier in brain metastases. *Nature communications*, *9*(1), p.2705.
184. Pol, J.G., Workenhe, S.T., Konda, P., Gujar, S. and Kroemer, G., 2020. Cytokines in oncolytic virotherapy. *Cytokine & Growth Factor Reviews*, *56*, pp.4-27.
185. Yang, H., Xia, L., Chen, J., Zhang, S., Martin, V., Li, Q., Lin, S., Chen, J., Calmette, J., Lu, M. and Fu, L., 2019. Stress–glucocorticoid–TSC22D3 axis compromises therapy-induced antitumor immunity. *Nature medicine*, *25*(9), pp.1428-1441.
186. Ma, J., Chen, C.C. and Li, M., 2021. Macrophages/microglia in the glioblastoma tumor microenvironment. International journal of molecular sciences, *22*(11), p.5775.
187. Seker, F., Cingoz, A., Sur-Erdem, I., Erguder, N., Erkent, A., Uyulur, F., Esai Selvan, M., Gümüş, Z.H., Gönen, M., Bayraktar, H. and Wakimoto, H., 2019. Identification of SERPINE1 as a regulator of glioblastoma cell dispersal with transcriptome profiling. Cancers, 11(11), p.1651
188. Yi, Y.S., Son, Y.J., Ryou, C., Sung, G.H., Kim, J.H. and Cho, J.Y., 2014. Functional roles of Syk in macrophage-mediated inflammatory responses*. Mediators of inflammation, 2014(1), p.270302*
189. Moncayo, G., Grzmil, M., Smirnova, T., Zmarz, P., Huber, R.M., Hynx, D., Kohler, H., Wang, Y., Hotz, H.R., Hynes, N.E. and Keller, G., 2018. SYK inhibition blocks proliferation and migration of glioma cells and modifies the tumor microenvironment. Neuro-oncology, 20(5), pp.621-631.
190. Dedobbeleer, M., Willems, E., Freeman, S., Lombard, A., Goffart, N. and Rogister, B., 2017. Phosphatases and solid tumors: focus on glioblastoma initiation, progression and recurrences. *Biochemical Journal*, *474*(17), pp.2903-2924
191. Bermudez, O., Pagès, G. and Gimond, C., 2010. The dual-specificity MAP kinase phosphatases: critical roles in development and cancer. American Journal of Physiology-Cell Physiology
192. Mills, B.N., Albert, G.P. and Halterman, M.W., 2017. Expression profiling of the MAP kinase phosphatase family reveals a role for DUSP1 in the glioblastoma stem cell niche. Cancer Microenvironment, 10, pp.57-68

193. Jiang, L., Hindmarch, C.C., Rogers, M., Campbell, C., Waterfall, C., Coghill, J., Mathieson, P.W. and Welsh, G.I., 2016. RNA sequencing analysis of human podocytes reveals glucocorticoid regulated gene networks targeting non-immune pathways. Scientific reports, 6(1), p.35671
194. Abraham, S.M., Lawrence, T., Kleiman, A., Warden, P., Medghalchi, M., Tuckermann, J., Saklatvala, J. and Clark, A.R., 2006. Antiinflammatory effects of dexamethasone are partly dependent on induction of dual specificity phosphatase 1. The Journal of experimental medicine, 203(8), pp.1883-1889.
195. Gauthier, M., Chakraborty, K., Oriss, T.B., Raundhal, M., Das, S., Chen, J., Huff, R., Sinha, A., Fajt, M., Ray, P. and Wenzel, S.E., 2017. Severe asthma in humans and mouse model suggests a CXCL10 signature underlies corticosteroid-resistant Th1 bias. JCI insight, 2(13).
196. Cahill, K.E., Morshed, R.A. and Yamini, B., 2015. Nuclear factor-κB in glioblastoma: insights into regulators and targeted therapy. Neuro-oncology, 18(3), pp.329-339
197. Miyar, A., Habibi, I., Ebrahimi, A., Mansourpour, D., Mokarizadeh, A., Rajabi, A., Farshgar, R., Eshaghzadeh, M., Zamani-Ahmadmahmudi, M. and Nodushan, S.M.H.T., 2016. Predictive and prognostic value of TLR9 and NFKBIA gene expression as potential biomarkers for human glioma diagnosis. Journal of the neurological sciences, 368, pp.314-317.
198. Bredel, M., Scholtens, D.M., Yadav, A.K., Alvarez, A.A., Renfrow, J.J., Chandler, J.P., Yu, I.L., Carro, M.S., Dai, F., Tagge, M.J. and Ferrarese, R., 2011. NFKBIA deletion in glioblastomas. New England Journal of Medicine, 364(7), pp.627-637
199. Desmet, S.J. and De Bosscher, K., 2017. Glucocorticoid receptors: finding the middle ground. The Journal of clinical investigation, 127(4), pp.1136-1145
200. Mohamed, A., Konda, P., Eaton, H.E., Gujar, S., Smiley, J.R. and Shmulevitz, M., 2020. Closely related reovirus lab strains induce opposite expression of RIG-I/IFN-dependent versus-independent host genes, via mechanisms of slow replication versus polymorphisms in dsRNA binding σ3 respectively. PLoS Pathogens, 16(9), p.e1008803
201. Das, A., Banik, N.L., Patel, S.J. and Ray, S.K., 2004. Dexamethasone protected human glioblastoma U87MG cells from temozolomide induced apoptosis by maintaining Bax: Bcl-2 ratio and preventing proteolytic activities. Molecular cancer, 3, pp.1-10
202. Patt, M., Gysi, J., Faresse, N., Cidlowski, J.A. and Odermatt, A., 2020. Protein phosphatase 1 alpha enhances glucocorticoid receptor activity by a mechanism involving phosphorylation of serine-211. Molecular and cellular endocrinology, 518, p.110873.
203. He, L.X., Yang, L., Liu, T., Li, Y.N., Huang, T.X., Zhang, L.L., Luo, J. and Liu, C.T., 2023. Group 3 innate lymphoid cells secret neutrophil chemoattractants and are insensitive to glucocorticoid via aberrant GR phosphorylation. Respiratory Research, 24(1), p.90.
204. Annibali, D., Whitfield, J.R., Favuzzi, E., Jauset, T., Serrano, E., Cuartas, I., Redondo-Campos, S., Folch, G., Gonzàlez-Juncà, A., Sodir, N.M. and Massó-Vallés, D., 2014. Myc inhibition is effective against glioma and reveals a role for Myc in proficient mitosis. Nature communications, 5(1), p.4632
205. Wang, J., Wang, H., Li, Z., Wu, Q., Lathia, J.D., McLendon, R.E., Hjelmeland, A.B. and Rich, J.N., 2008. c-Myc is required for maintenance of glioma cancer stem cells. PloS one, 3(11), p.e3769.
206. Kabir, F. and Apu, M.N.H., 2022. Multi-omics analysis predicts fibronectin 1 as a prognostic biomarker in glioblastoma multiforme. Genomics, 114(3), p.110378.
207. Cannarile, L., Delfino, D.V., Adorisio, S., Riccardi, C. and Ayroldi, E., 2019. Implicating the role of GILZ in glucocorticoid modulation of T-cell activation. Frontiers in Immunology, 10, p.1823.
208. Grugan, K.D., Ma, C., Singhal, S., Krett, N.L. and Rosen, S.T., 2008. Dual regulation of glucocorticoid-induced leucine zipper (GILZ) by the glucocorticoid

receptor and the PI3-kinase/AKT pathways in multiple myeloma. The Journal of steroid biochemistry and molecular biology, 110(3-5), pp.244-254
209. Kim, M., Osborne, N.R., Zeng, W., Donaghy, H., McKinnon, K., Jackson, D.C. and Cunningham, A.L., 2012. Herpes simplex virus antigens directly activate NK cells via TLR2, thus facilitating their presentation to CD4 T lymphocytes. The Journal of Immunology, 188(9), pp.4158-4170.
210. Li, C., Ma, L., Liu, Y., Li, Z., Wang, Q., Chen, Z., Geng, X., Han, X., Sun, J. and Li, Z., 2019. TLR2 promotes development and progression of human glioma via enhancing autophagy. Gene, 700, pp.52-59.
211. Gressot, L.V., Doucette, T., Yang, Y., Fuller, G.N., Manyam, G., Rao, A., Latha, K. and Rao, G., 2017. Analysis of the inhibitors of apoptosis identifies BIRC3 as a facilitator of malignant progression in glioma. Oncotarget, 8(8), p.12695.
212. Clarke, P., Meintzer, S.M., Widmann, C., Johnson, G.L. and Tyler, K.L., 2001. Reovirus infection activates JNK and the JNK-dependent transcription factor c-Jun. Journal of virology, 75(23), pp.11275-11283.
213. Bourhill, T., Mori, Y., Rancourt, D.E., Shmulevitz, M. and Johnston, R.N., 2018. Going (reo) viral: Factors promoting successful reoviral oncolytic infection. Viruses, 10(8), p.42
214. Fanfone, D., Idbaih, A., Mammi, J., Gabut, M. and Ichim, G., 2020. Profiling anti-apoptotic BCL-xL protein expression in glioblastoma tumorspheres. Cancers, 12(10), p.2853.
215. Janumyan, Y.M., Sansam, C.G., Chattopadhyay, A., Cheng, N., Soucie, E.L., Penn, L.Z., Andrews, D., Knudson, C.M. and Yang, E., 2003. Bcl-xL/Bcl-2 coordinately regulates apoptosis, cell cycle arrest and cell cycle entry. The EMBO journal, 22(20), pp.5459-5470.
216. Safa, AR., 2013. Roles of c-FLIP in apoptosis, necroptosis, and autophagy. Journal of carcinogenesis & mutagenesis.
217. Lynch, J.T., Rajendran, R., Xenaki, G., Berrou, I., Demonacos, C. and Krstic-Demonacos, M., 2010. The role of glucocorticoid receptor phosphorylation in Mcl-1 and NOXA gene expression. Molecular cancer, 9, pp.1-15
218. Yang, Y., Lv, W., Xu, S., Shi, F., Shan, A. and Wang, J., 2021. Molecular and clinical characterization of LIGHT/TNFSF14 expression at transcriptional level via 998 samples with brain glioma. Frontiers in Molecular Biosciences, 8, p.567327.
219. Chantong, B., Kratschmar, D.V., Nashev, L.G., Balazs, Z. and Odermatt, A., 2012. Mineralocorticoid and glucocorticoid receptors differentially regulate NF-kappaB activity and pro-inflammatory cytokine production in murine BV-2 microglial cells. Journal of neuroinflammation, 9, pp.1-14.
220. Tang, Q., Yuan, Y., Li, L., Xu, Y., Ji, W., Xiao, S., Han, Y., Miao, W., Cai, J., You, P. and Chen, M., 2024. Comprehensive analysis reveals that LTBR is a immune-related biomarker for glioma. Computers in Biology and Medicine, 174, p.108457
221. Hattermann, K., Held-Feindt, J., Lucius, R., Müerköster, S.S., Penfold, M.E., Schall, T.J. and Mentlein, R., 2010. The chemokine receptor CXCR7 is highly expressed in human glioma cells and mediates antiapoptotic effects. Cancer research, 70(8), pp.3299-3308.
222. Xiang, Z., Zhou, Z., Song, S., Li, J., Ji, J., Yan, R., Wang, J., Cai, W., Hu, W., Zang, L. and Zhu, Z., 2021. Dexamethasone suppresses immune evasion by inducing GR/STAT3 mediated downregulation of PD-L1 and IDO1 pathways. Oncogene, 40(31), pp.5002-5012
223. Gorgisen, G. and Yaren, Z., 2020. Insulin receptor substrate 1 overexpression promotes survival of glioblastoma cells through AKT1 activation. Folia Neuropathologica, 58(1), pp.38-44.
224. Xu, L., Chen, Y., Dutra-Clarke, M., Mayakonda, A., Hazawa, M., Savinoff, S.E., Doan, N., Said, J.W., Yong, W.H., Watkins, A. and Yang, H., 2017. BCL6 promotes glioma and serves as a therapeutic target. Proceedings of the National Academy of Sciences, 114(15), pp.3981-3986
225. Foltyn, M., Luger, A.L., Lorenz, N.I., Sauer, B., Mittelbronn, M., Harter, P.N., Steinbach, J.P. and Ronellenfitsch, M.W., 2019. The physiological mTOR complex

1 inhibitor DDIT4 mediates therapy resistance in glioblastoma. British Journal of Cancer, 120(5), pp.481-487.
226. Yang, Q., Wei, B., Peng, C., Wang, L. and Li, C., 2022. Identification of serum exosomal miR-98–5p, miR-183–5p, miR-323–3p and miR-19b-3p as potential biomarkers for glioblastoma patients and investigation of their mechanisms. Current Research in Translational Medicine, 70(1), p.103315
227. Duncan, C.G., Killela, P.J., Payne, C.A., Lampson, B., Chen, W.C., Liu, J., Solomon, D., Waldman, T., Towers, A.J., Gregory, S.G. and McDonald, K.L., 2010. Integrated genomic analyses identify ERRFI1 and TACC3 as glioblastoma-targeted genes. Oncotarget, 1(4), p.265
228. K Karnati, H., Panigrahi, M., A Shaik, N., H Greig, N., Bagadi, A.R., A Kamal, M. and Kapalavayi, N., 2014. Down regulated expression of Claudin-1 and Claudin-5 and up regulation of β-catenin: association with human glioma progression. CNS & Neurological Disorders-Drug Targets (Formerly Current Drug Targets-CNS & Neurological Disorders), 13(8), pp.1413-1426
229. Lim, S.Y., Ahn, S.H., Park, H., Lee, J., Choi, K., Choi, C., Choi, J.H., Park, E.M. and Choi, Y.H., 2014. Transcriptional regulation of adrenomedullin by oncostatin M in human astroglioma cells: implications for tumor invasion and migration. Scientific reports, 4(1), p.6444.
230. Peñuelas, S., Anido, J., Prieto-Sánchez, R.M., Folch, G., Barba, I., Cuartas, I., García-Dorado, D., Poca, M.A., Sahuquillo, J., Baselga, J. and Seoane, J., 2009. TGF-β increases glioma-initiating cell self-renewal through the induction of LIF in human glioblastoma. Cancer cell, 15(4), pp.315-327
231. Grosset, C., Taupin, J.L., Lemercier, C., Moreau, J.F., Reiffers, J. and Ripoche, J., 1999. Leukaemia inhibitory factor expression is inhibited by glucocorticoids through post-transcriptional mechanisms. Cytokine, 11(1), pp.29-36
232. Aldaz, P., Auzmendi-Iriarte, J., Durántez, M., Lasheras-Otero, I., Carrasco-Garcia, E., Zelaya, M.V., Bragado, L., Olías-Arjona, A., Egaña, L., Samprón, N. and Morilla, I., 2021. Identification of a dexamethasone mediated radioprotection mechanism reveals new therapeutic vulnerabilities in glioblastoma. Cancers, 13(2), p.361.
233. Arcuri, C., Tardy, M., Rolland, B., Armellini, R., Menghini, A.R. and Bocchini, V., 1995. Glutamine synthetase gene experession in a glioblastoma cell-line of clonal origin: Regulation by dexamethasone and dibutyryl cyclic AMP. Neurochemical research, 20, pp.1133-1139
234. Lee, C.H., Raghunathan, K., Taylor, G.M., French, A.J., Tenorio, R., Fernández de Castro, I., Risco, C., Parker, J.S. and Dermody, T.S., 2021. Reovirus nonstructural protein σNS recruits viral RNA to replication organelles. Mbio, 12(4), pp.10-1128
235. Guo, Y., Hinchman, M.M., Lewandrowski, M., Cross, S.T., Sutherland, D.M., Welsh, O.L., Dermody, T.S. and Parker, J.S., 2021. The multi-functional reovirus σ3 protein is a virulence factor that suppresses stress granule formation and is associated with myocardial injury. PLoS Pathogens, 17(7), p.e1009494.
236. Richardson-Burns, S.M., Kominsky, D.J. and Tyler, K.L., 2002. Reovirus-induced neuronal apoptosis is mediated by caspase 3 and is associated with the activation of death receptors. Journal of neurovirology, 8(5), pp.365-380.
237. Greenstein, S., Ghias, K., Krett, N.L. and Rosen, S.T., 2002. Mechanisms of glucocorticoid-mediated apoptosis in hematological malignancies. Clinical cancer research, 8(6), pp.1681-1694.
238. Moutsatsou, P. and Papavassiliou, A.G., 2008. The glucocorticoid receptor signalling in breast cancer. Journal of cellular and molecular medicine, 12(1), pp.145-163.
239. Brown, M.N., Fuhr, R., Beier, J., Su, H.L., Chen, Y., Forsman, H., Hamrén, U.W., Jackson, H. and Aggarwal, A., 2019. Efficacy and safety of AZD7594, an inhaled non-steroidal selective glucocorticoid receptor modulator, in patients with asthma: a phase 2a randomized, double blind, placebo-controlled crossover trial. Respiratory research, 20, pp.1-11.
240. Guglieri, M., Clemens, P.R., Perlman, S.J., Smith, E.C., Horrocks, I., Finkel, R.S., Mah, J.K., Deconinck, N., Goemans, N., Haberlova, J. and Straub, V., 2022.

Efficacy and safety of vamorolone vs placebo and prednisone among boys with Duchenne muscular dystrophy: a randomized clinical trial. JAMA neurology, 79(10), pp.1005-1014
241. Wells, E., Kambhampati, M., Damsker, J.M., Gordish-Dressman, H., Yadavilli, S., Becher, O.J., Gittens, J., Stampar, M., Packer, R.J. and Nazarian, J., 2017. Vamorolone, a dissociative steroidal compound, reduces pro-inflammatory cytokine expression in glioma cells and increases activity and survival in a murine model of cortical tumor. Oncotarget, 8(6), p.9366.
242. Lesovaya, E., Yemelyanov, A., Swart, A.C., Swart, P., Haegeman, G. and Budunova, I., 2015. Discovery of Compound A–a selective activator of the glucocorticoid receptor with anti-inflammatory and anti-cancer activity. Oncotarget, 6(31), p.30730
243. Kim, M., 2015. Naturally occurring reoviruses for human cancer therapy. BMB reports, 48(8), p.454.
244. Yin, L., Fang, F., Song, X., Wang, Y., Huang, G., Su, J., Hui, N. and Lu, J., 2016. The pro-adhesive and pro-survival effects of glucocorticoid in human ovarian cancer cells. J Mol Endocrinol, 57(1), pp.61-72.
245. Bertrand, M.J., Milutinovic, S., Dickson, K.M., Ho, W.C., Boudreault, A., Durkin, J., Gillard, J.W., Jaquith, J.B., Morris, S.J. and Barker, P.A., 2008. cIAP1 and cIAP2 facilitate cancer cell survival by functioning as E3 ligases that promote RIP1 ubiquitination. Molecular cell, 30(6), pp.689-700.
246. Rodrigue-Gervais, I.G., Labbé, K., Dagenais, M., Dupaul-Chicoine, J., Champagne, C., Morizot, A., Skeldon, A., Brincks, E.L., Vidal, S.M., Griffith, T.S. and Saleh, M., 2014. Cellular inhibitor of apoptosis protein cIAP2 protects against pulmonary tissue necrosis during influenza virus infection to promote host survival. Cell host & microbe, 15(1), pp.23-35
247. Khan, S., Lopez-Dee, Z., Kumar, R. and Ling, J., 2013. Activation of NFkB is a novel mechanism of pro-survival activity of glucocorticoids in breast cancer cells. Cancer letters, 337(1), pp.90-95.
248. Ploner, C., Rainer, J., Niederegger, H., Eduardoff, M., Villunger, A., Geley, S. and Kofler, R., 2008. The BCL2 rheostat in glucocorticoid-induced apoptosis of acute lymphoblastic leukemia. Leukemia, 22(2), pp.370-377.
249. Afshari, A.R., Sanati, M., Aminyavari, S., Shakeri, F., Bibak, B., Keshavarzi, Z., Soukhtanloo, M., Jalili-Nik, M., Sadeghi, M.M., Mollazadeh, H. and Johnston, T.P., 2022. Advantages and drawbacks of dexamethasone in glioblastoma multiforme. Critical Reviews in Oncology/Hematology, 172, p.103625.
250. Ehrlich, M. and Bacharach, E., 2021. Oncolytic virotherapy: the cancer cell side. Cancers, 13(5), p.939.
251. Han, M., Sun, Y., Zhao, W., Xiang, G., Wang, X., Jiang, Z., Xue, Z. and Zhou, W., 2022. Comprehensive characterization of TNFSF14/LIGHT with implications in prognosis and immunotherapy of human gliomas. Frontiers in Immunology, 13, p.1025286.
252. D'Ignazio, L., Batie, M. and Rocha, S., 2018. TNFSF14/LIGHT, a non-canonical NF-κB stimulus, induces the HIF pathway. Cells, 7(8), p.102.
253. Fabre, M.S., Stanton, N.M., Slatter, T.L., Lee, S., Senanayake, D., Gordon, R.M., Castro, M.L., Rowe, M.R., Taha, A., Royds, J.A. and Hung, N., 2020. The oncogene BCL6 is up-regulated in glioblastoma in response to DNA damage, and drives survival after therapy. PLoS One, 15(4), p.e0231470.
254. Zhao, W., Qin, W., Pan, J., Wu, Y., Bauman, W.A. and Cardozo, C., 2009. Dependence of dexamethasone-induced Akt/FOXO1 signaling, upregulation of MAFbx, and protein catabolism upon the glucocorticoid receptor. Biochemical and biophysical research communications, 378(3), pp.668-672.
255. Praveen Kumar, V.R., Sehgal, P., Thota, B., Patil, S., Santosh, V. and Kondaiah, P., 2014. Insulin like growth factor binding protein 4 promotes GBM progression and regulates key factors involved in EMT and invasion. Journal of neuro-oncology, 116, pp.455-464

256. Cari, L., De Rosa, F., Nocentini, G. and Riccardi, C., 2019. Context-dependent effect of glucocorticoids on the proliferation, differentiation, and apoptosis of regulatory T cells: a review of the empirical evidence and clinical applications. International journal of molecular sciences, 20(5), p.1142.
257. Marx, S., Wilken, F., Miebach, L., Ispirjan, M., Kinnen, F., Paul, S., Bien-Möller, S., Freund, E., Baldauf, J., Fleck, S. and Siebert, N., 2022. Immunophenotyping of Circulating and Intratumoral Myeloid and T Cells in Glioblastoma Patients. Cancers, 14(23), p.5751.
258. Chitadze, G., Flüh, C., Quabius, E.S., Freitag-Wolf, S., Peters, C., Lettau, M., Bhat, J., Wesch, D., Oberg, H.H., Luecke, S. and Janssen, O., 2017. In-depth immunophenotyping of patients with glioblastoma multiforme: Impact of steroid treatment. Oncoimmunology, 6(11), p.e1358839.
259. Mantovani, A., Sozzani, S., Locati, M., Allavena, P. and Sica, A., 2002. Macrophage polarization: tumor-associated macrophages as a paradigm for polarized M2 mononuclear phagocytes. Trends in immunology, 23(11), pp.549-555.
260. Jayasingam, S.D., Citartan, M., Thang, T.H., Mat Zin, A.A., Ang, K.C. and Ch'ng, E.S., 2020. Evaluating the polarization of tumor-associated macrophages into M1 and M2 phenotypes in human cancer tissue: technicalities and challenges in routine clinical practice. Frontiers in oncology, 9, p.1512
261. Chonan, M., Saito, R., Shoji, T., Shibahara, I., Kanamori, M., Sonoda, Y., Watanabe, M., Kikuchi, T., Ishii, N. and Tominaga, T., 2015. CD40/CD40L expression correlates with the survival of patients with glioblastomas and an augmentation in CD40 signaling enhances the efficacy of vaccinations against glioma models. Neuro-oncology, 17(11), pp.1453-1462.
262. Gousias, K., Theocharous, T. and Simon, M., 2022. Mechanisms of cell cycle arrest and apoptosis in glioblastoma. Biomedicines, 10(3), p.564.
263. Yang, C., Sofroni, K., Wijnker, E., Hamamura, Y., Carstens, L., Harashima, H., Stolze, S.C., Vezon, D., Chelysheva, L., Orban-Nemeth, Z. and Pochon, G., 2020. The Arabidopsis Cdk1/Cdk2 homolog CDKA; 1 controls chromosome axis assembly during plant meiosis. The EMBO Journal, 39(3), p.e101625.
264. Doan, P., Musa, A., Candeias, N.R., Emmert-Streib, F., Yli-Harja, O. and Kandhavelu, M., 2019. Alkylaminophenol induces G1/S phase cell cycle arrest in glioblastoma cells through p53 and cyclin-dependent kinase signaling pathway. Frontiers in pharmacology, 10, p.330
265. Urbantat, R.M., Vajkoczy, P. and Brandenburg, S., 2021. Advances in chemokine signaling pathways as therapeutic targets in glioblastoma. Cancers, 13(12), p.2983.
266. Zeren, N., Afzal, Z., Morgan, S., Marshall, G., Uppiliappan, M., Merritt, J. and Coniglio, S.J., 2023. The chemokine receptor CCR1 mediates microglia stimulated glioma invasion. International Journal of Molecular Sciences, 24(6), p.513
267. Shimba, A. and Ikuta, K., 2020, December. Control of immunity by glucocorticoids in health and disease. In Seminars in Immunopathology (Vol. 42, No. 6, pp. 669-680). Berlin/Heidelberg: Springer Berlin Heidelberg.
268. Babazadeh, S.M., Zolfaghari, M.R., Zargar, M., Baesi, K., Hosseini, S.Y. and Ghaemi, A., 2023. Interleukin-24-mediated antitumor effects against human glioblastoma via upregulation of P38 MAPK and endogenous TRAIL-induced apoptosis and LC3-II activation-dependent autophagy. BMC cancer, 23(1), p.519.
269. Zou, C., 2019. CD48 is a key molecule of immunomodulation affecting prognosis in glioma. 597 Onco Targets Ther 12, 4181-4193, doi: 10.2147/OTT. S198762, 598.
270. Jeong, J.U., Uong, T.N.T., Chung, W.K., Nam, T.K., Ahn, S.J., Song, J.Y., Kim, S.K., Shin, D.J., Cho, E., Kim, K.W. and Cho, D., 2018. Effect of irradiation-induced intercellular adhesion molecule-1 expression on natural killer cell-mediated cytotoxicity toward human cancer cells. Cytotherapy, 20(5), pp.715-727.
271. Inoue, A., Takahashi, H., Harada, H., Kohno, S., Ohue, S., Kobayashi, K., Yano, H., Tanaka, J. and Ohnishi, T., 2010. Cancer stem-like cells of glioblastoma

characteristically express MMP-13 and display highly invasive activity. International journal of oncology, 37(5), pp.1121-1131.
272. Gjorgjevski, M., Hannen, R., Carl, B., Li, Y., Landmann, E., Buchholz, M., Bartsch, J.W. and Nimsky, C., 2019. Molecular profiling of the tumor microenvironment in glioblastoma patients: correlation of microglia/macrophage polarization state with metalloprotease expression profiles and survival. Bioscience reports, 39(6), p.BSR20182361
273. Liu, M., Zhao, J., Chen, K., Bian, X., Wang, C., Shi, Y. and Wang, J.M., 2012. G protein-coupled receptor FPR1 as a pharmacologic target in inflammation and human glioblastoma. International immunopharmacology, 14(3), pp.283-288
274. Li, C., Wang, T., Gu, J., Qi, S., Li, J., Chen, L., Wu, H., Shi, L., Song, C., Li, H. and Zhu, L., 2022. SMARCC2 mediates the regulation of DKK1 by the transcription factor EGR1 through chromatin remodeling to reduce the proliferative capacity of glioblastoma. Cell death & disease, 13(11), p.990
275. Moors, M., Bose, R., Johansson-Haque, K., Edoff, K., Okret, S. and Ceccatelli, S., 2012. Dickkopf 1 mediates glucocorticoid-induced changes in human neural progenitor cell proliferation and differentiation. Toxicological Sciences, 125(2), pp.488-495.
276. Zhou, Y., Liu, F., Xu, Q. and Wang, X., 2010. Analysis of the expression profile of Dickkopf-1 gene in human glioma and the association with tumor malignancy. Journal of Experimental & Clinical Cancer Research, 29, pp.1-7.
277. Guo, L., Li, S.Y., Ji, F.Y., Zhao, Y.F., Zhong, Y., Lv, X.J., Wu, X.L. and Qian, G.S., 2014. Role of Angptl4 in vascular permeability and inflammation. Inflammation Research, 63, pp.13-22.
278. Wang, D., Berglund, A., Kenchappa, R.S., Forsyth, P.A., Mulé, J.J. and Etame, A.B., 2016. BIRC3 is a novel driver of therapeutic resistance in Glioblastoma. Scientific reports, 6(1), p.21710.
279. Zhang, H., Xu, Y., Deng, G., Yuan, F., Tan, Y., Gao, L., Sun, Q., Qi, Y., Yang, K., Geng, R. and Jiang, H., 2021. SAA1 knockdown promotes the apoptosis of glioblastoma cells via downregulation of AKT signaling. Journal of Cancer, 12(9), p.2756.
280. Winkler, R. and Lu, H., 2023. Cell-Specific Regulation of Inflammatory Cytokines and Acute-Phase Proteins by the Glucocorticoid Receptor. Mediators of Inflammation, 2023(1), p.4399998.
281. Conaway, H.H., Henning, P., Lie, A., Tuckermann, J. and Lerner, U.H., 2019. Glucocorticoids employ the monomeric glucocorticoid receptor to potentiate vitamin D3 and parathyroid hormone–induced osteoclastogenesis. The FASEB Journal, 33(12), p.14394.
282. Wang, H.H., Chang, T.Y., Lin, W.C., Wei, K.C. and Shin, J.W., 2017. GADD45A plays a protective role against temozolomide treatment in glioblastoma cells. Scientific reports, 7(1), p.8814.
283. Chan, T.Y.H., Wong, J.S.Y., Kiang, K.M.Y., Sun, C.W.Y. and Leung, G.K.K., 2023. The duality of CXCR3 in glioblastoma: unveiling autocrine and paracrine mechanisms for novel therapeutic approaches. Cell Death & Disease, 14(12), p.835.
284. Elemam, N.M., Talaat, I.M. and Maghazachi, A.A., 2022. CXCL10 chemokine: a critical player in RNA and DNA viral infections. Viruses, 14(11), p.2445.
285. Hwang, S., Lim, J., Kang, H., Jeong, J.Y., Joung, J.G., Heo, J., Jung, D., Cho, K. and An, H.J., 2023. Predictive biomarkers for the responsiveness of recurrent glioblastomas to activated killer cell immunotherapy. Cell & bioscience, 13(1), p.17.
286. Narushima, Y., Kozuka-Hata, H., Koyama-Nasu, R., Tsumoto, K., Inoue, J.I., Akiyama, T. and Oyama, M., 2016. Integrative network analysis combined with quantitative phosphoproteomics reveals transforming growth factor-beta receptor type-2 (TGFBR2) as a novel regulator of glioblastoma stem cell properties. Molecular & Cellular Proteomics, 15(3), pp.1017-1031.

287. Sachdeva, R., Wu, M., Johnson, K., Kim, H., Celebre, A., Shahzad, U., Graham, M.S., Kessler, J.A., Chuang, J.H., Karamchandani, J. and Bredel, M., 2019. BMP signaling mediates glioma stem cell quiescence and confers treatment resistance in glioblastoma. Scientific reports, 9(1), p.14569.
288. Jing-Ping, L., 2018. Effects of fibronectin 1 on cell proliferation, senescence and apoptosis of human glioma cells through the PI3K/AKT signaling pathway. Cellular Physiology and Biochemistry, 48(3), pp.1382-1396.
289. Yang, H.W., Menon, L.G., Black, P.M., Carroll, R.S. and Johnson, M.D., 2010. SNAI2/Slug promotes growth and invasion in human gliomas. BMC cancer, 10, pp.1-12.
290. Krusche, B., Ottone, C., Clements, M.P., Johnstone, E.R., Goetsch, K., Lieven, H., Mota, S.G., Singh, P., Khadayate, S., Ashraf, A. and Davies, T., 2016. EphrinB2 drives perivascular invasion and proliferation of glioblastoma stem-like cells. Elife, 5, p.e14845.
291. Moreno, M., Pedrosa, L., Paré, L., Pineda, E., Bejarano, L., Martínez, J., Balasubramaniyan, V., Ezhilarasan, R., Kallarackal, N., Kim, S.H. and Wang, J., 2017. GPR56/ADGRG1 inhibits mesenchymal differentiation and radioresistance in glioblastoma. Cell reports, 21(8), pp.2183-2197.
292. Steponaitis, G., Kazlauskas, A., Skiriute, D., Vaitkiene, P., Skauminas, K. and Tamasauskas, A., 2019. Significance of amphiregulin (AREG) for the outcome of low and high grade astrocytoma patients. Journal of Cancer, 10(6), p.1479.
293. Gao, X.Y., Zang, J., Zheng, M.H., Zhang, Y.F., Yue, K.Y., Cao, X.L., Cao, Y., Li, X.X., Han, H., Jiang, X.F. and Liang, L., 2021. Temozolomide treatment induces HMGBM1 to promote the formation of glioma stem cells via the TLR2/NEAT1/Wnt pathway in glioblastoma. Frontiers in cell and developmental biology, 9, p.620883.
294. Hu, F., Ku, M.C., Markovic, D., Dzaye, O., Lehnardt, S., Synowitz, M., Wolf, S.A. and Kettenmann, H., 2014. Glioma-associated microglial MMP9 expression is upregulated by TLR2 signaling and sensitive to minocycline. International Journal of Cancer, 135(11), pp.2569-2578.
295. Mu, N., Gu, J., Liu, N., Xue, X., Shu, Z., Zhang, K., Huang, T., Chu, C., Zhang, W., Gong, L. and Zhao, H., 2018. PRL-3 is a potential glioblastoma prognostic marker and promotes glioblastoma progression by enhancing MMP7 through the ERK and JNK pathways. Theranostics, 8(6), p.1527.
296. Montani, M.S., Tuosto, L., Giliberti, R., Stefanini, L., Cundari, E. and Piccolella, E., 1999. Dexamethasone induces apoptosis in human T cell clones expressing low levels of Bcl-2. Cell Death & Differentiation, 6(1), pp.79-86.
297. Jiang, K., Weaver, J.D., Li, Y., Chen, X., Liang, J. and Stabler, C.L., 2017. Local release of dexamethasone from macroporous scaffolds accelerates islet transplant engraftment by promotion of anti-inflammatory M2 macrophages. Biomaterials, 114, pp.71-81.
298. Chen, C., Sun, C., Tang, D., Yang, G., Zhou, X. and Wang, D., 2016. Identification of key genes in glioblastoma-associated stromal cells using bioinformatics analysis. Oncology Letters, 11(6), pp.3999-4007.
299. Wu, Q., Berglund, A.E., MacAulay, R.J. and Etame, A.B., 2021. A novel role of BIRC3 in stemness reprogramming of glioblastoma. International Journal of Molecular Sciences, 23(1), p.297.
300. Wang, Y., Long, P., Wang, Y. and Ma, W., 2020. NTRK fusions and TRK inhibitors: potential targeted therapies for adult glioblastoma. Frontiers in Oncology, 10, p.593578.
301. Riabovol, O.O., Tsymbal, D.O., Minchenko, D.O., Lebid-Biletska, K.M., Sliusar, M.Y., Rudnytska, O.V. and Minchenko, O.H., 2019. Effect of glucose deprivation on the expression of genes encoding glucocorticoid receptor and some related factors in ERN1-knockdown U87 glioma cells. Endocrine Regulations, 53(4), pp.237-249.
302. Hoppstädter, J. and Ammit, A.J., 2019. Role of dual-specificity phosphatase 1 in glucocorticoid-driven anti-inflammatory responses. Frontiers in immunology, 10, p.1446.

303. Martínez-Sabadell, A., Arenas, E.J. and Arribas, J., 2022. Ifnγ signaling in natural and therapy-induced antitumor responses. Clinical Cancer Research, 28(7), pp.1243-1249.
304. Peng, L., Fu, J., Chen, Y., Ming, Y., He, H., Zeng, S., Zhong, C. and Chen, L., 2022. Transcription factor SNAI2 exerts pro-tumorigenic effects on glioma stem cells via PHLPP2-mediated Akt pathway. Cell Death & Disease, 13(6), p.516.
305. Wei, Q., Liang, G., zeng, R., Li, Y., Hong, A., Wang, H., Feng, S., Wang, Y. and Wang, Y., 2023. Glucocorticoid receptor activation induces NK cells to produce AREG and restricts their anti-tumor activity in skin cancer. bioRxiv, pp.2023-09.
306. Chédeville, A.L., Lourdusamy, A., Monteiro, A.R., Hill, R. and Madureira, P.A., 2020. Investigating glioblastoma response to hypoxia. Biomedicines, 8(9), p.310.
307. Tsai, Y.T., Wu, A.C., Yang, W.B., Kao, T.J., Chuang, J.Y., Chang, W.C. and Hsu, T.I., 2019. ANGPTL4 induces TMZ resistance of glioblastoma by promoting cancer stemness enrichment via the EGFR/AKT/4E-BP1 cascade. International Journal of Molecular Sciences, 20(22), p.5625.
308. Acker, G., Zollfrank, J., Jelgersma, C., Nieminen-Kelhä, M., Kremenetskaia, I., Mueller, S., Ghori, A., Vajkoczy, P. and Brandenburg, S., 2020. The CXCR2/CXCL2 signalling pathway–an alternative therapeutic approach in high-grade glioma. European journal of cancer, 126, pp.106-115.
309. Phesse, T., Flanagan, D. and Vincan, E., 2016. Frizzled7: a promising Achilles' heel for targeting the Wnt receptor complex to treat cancer. Cancers, 8(5), p.50
310. Büschges, R., Weber, R.G., Actor, B., Lichter, P., Collins, V.P. and Reifenberger, G., 1999. Amplification and expression of cyclin D genes (CCND1 CCND2 and CCND3) in human malignant gliomas. Brain pathology, 9(3), pp.435-442
311. Bretones, G., Delgado, M.D. and León, J., 2015. Myc and cell cycle control. Biochimica et Biophysica Acta (BBA)-Gene Regulatory Mechanisms, 1849(5), pp.506-516
312. Wang, Q., Cai, J., Fang, C., Yang, C., Zhou, J., Tan, Y., Wang, Y., Li, Y., Meng, X., Zhao, K. and Yi, K., 2018. Mesenchymal glioblastoma constitutes a major ceRNA signature in the TGF-β pathway. Theranostics, 8(17), p.4733.
313. Murad, S., Michen, S., Becker, A., Füssel, M., Schackert, G., Tonn, T., Momburg, F. and Temme, A., 2022. NKG2C+ NK cells for immunotherapy of glioblastoma multiforme. International journal of molecular sciences, 23(10), p.5857.
314. Tokunaga, R., Zhang, W.U., Naseem, M., Puccini, A., Berger, M.D., Soni, S., McSkane, M., Baba, H. and Lenz, H.J., 2018. CXCL9, CXCL10, CXCL11/CXCR3 axis for immune activation–a target for novel cancer therapy. Cancer treatment reviews, 63, pp.40-47.
315. Han, Z.J., Li, Y.B., Yang, L.X., Cheng, H.J., Liu, X. and Chen, H., 2021. Roles of the CXCL8-CXCR1/2 axis in the tumor microenvironment and immunotherapy. Molecules, 27(1), p.137.
316. Yalamarty, S.S.K., Filipczak, N., Li, X., Subhan, M.A., Parveen, F., Ataide, J.A., Rajmalani, B.A. and Torchilin, V.P., 2023. Mechanisms of resistance and current treatment options for glioblastoma multiforme (GBM). Cancers, 15(7), p.2116.
317. Müller, L., Berkeley, R., Barr, T., Ilett, E. and Errington-Mais, F., 2020. Past, present and future of oncolytic reovirus. Cancers, 12(11), p.3219.
318. Yu, H., Pardoll, D. and Jove, R., 2009. STATs in cancer inflammation and immunity: a leading role for STAT3. Nature reviews cancer, 9(11), pp.798-809
319. Thorne, A., Bansal, A., Necker-Brown, A., Mostafa, M.M., Gao, A., Georgescu, A., Kooi, C., Leigh, R. and Newton, R., 2023. Differential regulation of BIRC2 and BIRC3 expression by inflammatory cytokines and glucocorticoids in pulmonary epithelial cells. PLoS One, 18(6), p.e0286783.
320. Ashwell, J.D., Lu, F.W. and Vacchio, M.S., 2000. Glucocorticoids in T cell development and function. Annual review of immunology, 18(1), pp.309-345.
321. Tedesco, S., Bolego, C., Toniolo, A., Nassi, A., Fadini, G.P., Locati, M. and Cignarella, A., 2015. Phenotypic activation and pharmacological outcomes of spontaneously differentiated human monocyte-derived macrophages. Immunobiology, 220(5), pp.545-554.

322. Jubb, A.W., Young, R.S., Hume, D.A. and Bickmore, W.A., 2016. Enhancer turnover is associated with a divergent transcriptional response to glucocorticoid in mouse and human macrophages. The Journal of Immunology, 196(2), pp.813-822.
323. Wicherska-Pawłowska, K., Wróbel, T. and Rybka, J., 2021. Toll-like receptors (TLRs), NOD-like receptors (NLRs), and RIG-I-like receptors (RLRs) in innate immunity. TLRs, NLRs, and RLRs ligands as immunotherapeutic agents for hematopoietic diseases. International journal of molecular sciences, 22(24), p.13397.
324. Zhao, X., Chester, C., Rajasekaran, N., He, Z. and Kohrt, H.E., 2016. Strategic combinations: the future of oncolytic virotherapy with reovirus. Molecular cancer therapeutics, 15(5), pp.767-773.
325. Piette, C., Munaut, C., Foidart, J.M. and Deprez, M., 2006. Treating gliomas with glucocorticoids: from bedside to bench. Acta neuropathologica, 112, pp.651-664.
326. Dietrich, J., Rao, K., Pastorino, S. and Kesari, S., 2011. Corticosteroids in brain cancer patients: benefits and pitfalls. Expert review of clinical pharmacology, 4(2), pp.233-242.
327. Xu, L., Xia, H., Ni, D., Hu, Y., Liu, J., Qin, Y., Zhou, Q., Yi, Q. and Xie, Y., 2020. High-dose dexamethasone manipulates the tumor microenvironment and internal metabolic pathways in anti-tumor progression. International Journal of Molecular Sciences, 21(5), p.1846.
328. Jin, P., Shin, S.H., Chun, Y.S., Shin, H.W., Shin, Y.J., Lee, Y., Kim, D., Nam, D.H. and Park, J.W., 2018. Astrocyte-derived CCL20 reinforces HIF-1-mediated hypoxic responses in glioblastoma by stimulating the CCR6-NF-κB signaling pathway. Oncogene, 37(23), pp.3070-3087.
329. Jeon, M.Y., Woo, S.M., Seo, S.U., Kim, S.H., Nam, J.O., Kim, S., Park, J.W., Kubatka, P., Min, K.J. and Kwon, T.K., 2020. Dexamethasone inhibits TRAIL-induced apoptosis through c-FLIP (L) upregulation and DR5 downregulation by GSK3β activation in cancer cells. Cancers, 12(10), p.2901.
330. Rogatsky, I., Trowbridge, J.M. and Garabedian, M.J., 1997. Glucocorticoid receptor-mediated cell cycle arrest is achieved through distinct cell-specific transcriptional regulatory mechanisms. Molecular and cellular biology.
331. Salvador, J.M., Brown-Clay, J.D. and Fornace Jr, A.J., 2013. Gadd45 in stress signaling, cell cycle control, and apoptosis. Gadd45 stress sensor genes, pp.1-19.
332. Meng, X., Lu, P., Bai, H., Xiao, P. and Fan, Q., 2012. Transcriptional regulatory networks in human lung adenocarcinoma. Molecular Medicine Reports, 6(5), pp.961-966.
333. Uhlen, M., Oksvold, P., Fagerberg, L., Lundberg, E., Jonasson, K., Forsberg, M., Zwahlen, M., Kampf, C., Wester, K., Hober, S. and Wernerus, H., 2010. Towards a knowledge-based human protein atlas. Nature biotechnology, 28(12), pp.1248-1250.
334. Fang, L., Du, W.W., Awan, F.M., Dong, J. and Yang, B.B., 2019. The circular RNA circ-Ccnb1 dissociates Ccnb1/Cdk1 complex suppressing cell invasion and tumorigenesis. Cancer letters, 459, pp.216-226.
335. Guo, Y., Hao, D. and Hu, H., 2021. High doses of dexamethasone induce endoplasmic reticulum stress-mediated apoptosis by promoting calcium ion influx-dependent CHOP expression in osteoblasts. Molecular Biology Reports, 48, pp.7841-7851.
336. Tseng, D., Vasquez-Medrano, D.A. and Brown, J.M., 2011. Targeting SDF-1/CXCR4 to inhibit tumour vasculature for treatment of glioblastomas. British journal of cancer, 104(12), pp.1805-1809.
337. Takeda, K., Naguro, I., Nishitoh, H., Matsuzawa, A. and Ichijo, H., 2011. Apoptosis signaling kinases: from stress response to health outcomes. Antioxidants & redox signaling, 15(3), pp.719-761.
338. Tsai, S.F., Tao, M., Ho, L.I., Chiou, T.W., Lin, S.Z., Su, H.L. and Harn, H.J., 2017. Isochaihulactone-induced DDIT3 causes ER stress-PERK independent apoptosis in glioblastoma multiforme cells. Oncotarget, 8(3), p.4051.

339. Dai, L., Li, Z., Tao, Y., Liang, W., Hu, W., Zhou, S., Fu, X. and Wang, X., 2021. Emerging roles of suppressor of cytokine signaling 3 in human cancers. Biomedicine & Pharmacotherapy, 144, p.112262.
340. Minchenko, D.O., Danilovskyi, S.V., Kryvdiuk, I.V., Bakalets, T.V., Lypova, N.M., Karbovskyi, L.L. and Minchenko, O.H., 2014. Inhibition of ERN1 modifies the hypoxic regulation of the expression of TP53-related genes in U87 glioma cells. Cell Pathology, 1(1), pp.18-26.
341. Wang, J., Zhou, J.Y., Kho, D., Reiners Jr, J.J. and Wu, G.S., 2016. Role for DUSP1 (dual-specificity protein phosphatase 1) in the regulation of autophagy. Autophagy, 12(10), pp.1791-1803.
342. Dieterich, L.C., Mellberg, S., Langenkamp, E., Zhang, L., Zieba, A., Salomäki, H., Teichert, M., Huang, H., Edqvist, P.H., Kraus, T. and Augustin, H.G., 2012. Transcriptional profiling of human glioblastoma vessels indicates a key role of VEGF-A and TGFβ2 in vascular abnormalization. The Journal of pathology, 228(3), pp.378-390.
343. Harkness, K.A., Adamson, P., Sussman, J.D., Davies-Jones, G.A.B., Greenwood, J. and Woodroofe, M., 2000. Dexamethasone regulation of matrix metalloproteinase expression in CNS vascular endothelium. Brain, 123(4), pp.698-709.
344. Diao, B., Sun, C., Yu, P., Zhao, Z. and Yang, P., 2023. LAMA5 promotes cell proliferation and migration in ovarian cancer by activating Notch signaling pathway. The FASEB Journal, 37(9), p.e23109.
345. Ling, G., Wang, S., Song, Z., Sun, X., Liu, Y., Jiang, X., Cai, Y., Du, M. and Ke, Y., 2011. Transforming growth factor-β is required for vasculogenic mimicry formation in glioma cell line U251MG. Cancer biology & therapy, 12(11), pp.978-988.

Chapter 7

Appendices

List of tables for the DEGs re-analysed in chapter 3 (Table 7-1 to 7-6) and the DEGs KEGG analysis in chapters 4 (Table 7-7 to 7-8) for the single culture and chapter 5 for the coculture models (Table 7-9 to 7-13).

Table 7-1 Overlaying genes between GC-GBM and OV-GBM patients

DEGs	OV regulated Log FC	GC regulated Log FC
RGMB	1.66026	-0.80406
SOX4	1.03287	-0.70438
FST	1.32358	-0.65955
IL6	2.22138	-1.29671
CLDN1	1.33001	-0.59154
IL11	1.64861	-0.86603
JUN	1.75469	-0.60305
CYP24A1	3.80865	-0.88399
S1PR3	-1.12153	0.66863
BIRC3	-1.11216	1.01432

Upregulated	OV regulated Log FC	GC regulated Log FC
TRIM29	1.3329	0.86894
A4GALT	1.92264	0.69314
KLF4	2.44845	0.95528
CEBPD	1.34448	1.75118
ZFP36	1.36666	0.72156
SGK1	0.96318	0.74360
DUSP1	1.87293	1.22179
SOCS3	2.20157	0.61008
CTGF	1.50997	0.74074
ANGPTL4	1.95108	2.83426
PLAT	1.79919	0.67585
SERPINE1	1.0922	0.68298
TGFBR3	1.24228	0.72394
FSTL3	1.32358	0.64221
HOXC11	5.52669	0.70141
NFKBIA	0.83977	0.66229
IGFBP4	0.92164	0.69892

Table 7-2 Overlaying genes between IFN-GBM and OV-GBM patients

DEGs	OV regulated logFC	IFN regulated logFC
FAM71A	2.9858	-0.7228941
ABHD16B	1.43744	-0.5529548
TSPAN6	1.33912	-0.6468376
NDRG1	1.21317	-0.6554911
SEMA4F	1.25478	-0.5150903
CFH	-1.45751	1.0822916
IL1RL1	-2.66984	1.0353097
MNX1	2.83327	-0.739615
MAGED2	0.904137	-0.7967577
ONECUT2	1.77305	-0.58943
NRG1	-1.93548	0.6668943
STK32A	1.87993	-0.7403222
CRISPLD1	1.4147	-0.9058458
MYO7B	2.73099	-1.1105287
SLC22A17	1.15328	-0.8984576
PI16	1.38574	-0.8158488
FZD1	1.34932	-0.6313838
KLF15	1.7703	-1.1789025

Downregulated	OV regulated logFC	IFN regulated logFC
LCN15	-3.46659	-0.5133724
AKT1	-1.37838	-0.915801
C12orf56	-2.60932	-0.7347851

Upregulated	OV regulated logFC	IFN regulated logFC
FST	2.91753	1.3156347
ANGPTL4	1.95108	0.7114654
TRIB3	1.26133	0.9118298
FAM110C	1.26149	0.5922405
IFI16	1.40263	0.62941
TMEM248	0.923597	0.6200637
TTC30B	1.3545	0.5275302
MYCL	1.2114	0.6450955
HAS2	1.48968	0.5635458
NDN	2.00774	1.0643651
SHISA5	1.21122	1.1491846
MATN4	2.10569	0.6236479
CCL3	3.01802	1.1890119
SLC4A11	1.64565	0.6241011
CCL3L1	2.6107	0.6129126
COL4A6	2.1285	0.5152144
CAPSL	4.85634	0.8368357
VGF	1.49228	0.7716131
IGFBP3	2.30055	0.8366357
HLA-C	3.30826	0.866732
HLA-B	4.05474	0.9669211
POFUT1	0.966279	0.6482645
EGR2	2.67361	0.6590318
LGALS3BP	1.55178	1.1407546
HLA-A	2.01104	0.8035851
DPY19L2	1.85022	0.6530661
BCL2L11	1.43764	0.6088915
IFI6	1.25611	4.4751464
BTN3A3	0.876641	0.8299325
KCNA5	2.69663	0.9589411
SESN2	0.953732	1.0728313
AIM2	2.37808	1.0523335

Table 7-3 27 Overlaying genes between CD4 treated GC and OV-GBM patients

Gene name	OV regulated Log FC	GC regulated Log FC
C5orf55	1.2827	3.1266
CD24	1.2998	3.8372
KDELC2	0.9490	4.7044
LRRC2	1.0956	3.4077
MAP7D3	1.2114	2.8737
SLC35E3	3.9000	4.1924
SLC9A7	1.3189	4.2834

Gene name	OV regulated logFC	IFN regulated logFC
DBI	-1.1978	-2.4610
NEAT1	-1.5045	-1.6821
S100A9	-1.4699	-3.3336
XIST	-9.5312	-2.1878

Gene name	OV regulated Log FC	GC regulated Log FC
ATXN7L3B	1.0856	-1.90471
BNIPL	-1.54256	3.154185
BTN3A3	0.876641	-2.60024
CCL3	3.01802	-2.46292
CCL4	2.9353	-3.19549
CD3D	0.205014	-1.53265
DUSP1	1.87293	-2.30472
GABBR1	5.92053	-1.8227
MCM6	1.03548	-2.91642
MEGF6	2.93225	-2.97626
MYC	1.57413	-2.56381
PBXIP1	0.850798	-2.17456
SUMF2	1.74702	-2.22292
TMEM107	1.56618	-1.82458
POU2AF1	-2.93029	3.112396
TXNIP	-1.96557	3.475597

7-4 29 Overlaying genes between Monocyte treated GC and OV-GBM patients

Gene name	OV regulated Log FC	GC regulated Log FC
ATP6AP1	3.47553	1.966631
CCL3L1	2.6107	3.223598
DDX5	1.39065	1.43077
FOS	2.81945	1.641198
GRN	0.84726	1.726189
HLA-A	2.01104	1.602254
HLA-B	4.05474	1.600765
HLA-C	3.30826	2.387296
KDELC2	0.949026	2.002357
PDIA4	1.00047	2.399481
RPN1	0.980742	1.525972
SERPINE1	1.0922	3.701105
SLC35E3	3.90004	1.962846
ZFP36	1.36666	1.580453

Gene name	OV regulated Log FC	GC regulated Log FC
AHR	1.65472	-2.757957
BTG2	1.53286	-1.702709
C17orf76-AS1	1.81328	-1.919046
EGR1	2.37868	-2.670039
EGR2	2.67361	-2.692962
IRF2BPL	0.851275	-4.742123
PCMTD2	1.33114	-2.374412
LGMN	0.904595	-1.936101
POGLUT1	1.33919	-2.565121
PRKAR1A	1.00339	-1.71275
PRPS2	1.67053	-3.623497
RGS18	-1.46768	2.453281
S100A8	-2.2744	2.459439

Gene name	OV regulated logFC	IFN regulated logFC
PAPOLA	-1.39849	-1.393735
PPBP	-2.38411	-3.026403

Table 7-5 201 Overlaying genes between OV-monocyte and OV-monocyte

DEGs	OV Monocyte Log FC	GC Monocyte Log FC
ACSL5	1.9160214	-2.2536755
ADAM17	1.8704704	-3.8986181
ADAP2	1.8299307	-2.6296006
ADK	-4.315978	2.58345453
ALOX5AP	-4.386184	4.91493786
ANTXR2	2.3750726	-1.7702301
APOL2	4.1995443	-2.1566701
ARHGDIB	-3.263087	2.14275442
ARID5B	3.4053431	-4.1003302
ATP5A1	-1.576222	1.95395925
B4GALT1	2.0948460	-3.4934592
BAZ1A	2.2747873	-1.9910509
BCL10	1.5205259	-3.724151
BIRC2	1.5605934	-1.7084608
BTG3	2.8932900	-1.7083487
C15orf48	3.0761688	-2.7892877
C1orf162	-6.182863	3.79590088
C9orf72	1.6631560	-2.1579294
CALM2	-1.896014	1.48415491
CAMK2D	2.0402880	-2.6384127
CARD16	2.4688380	-1.7349205
CASP4	2.8446416	-2.3971038
CCL2	5.6516812	-2.3399747
CCL7	8.9127480	-2.9811267
CD163	-1.792800	3.62861015
CD83	5.2015741	-3.9792553
CDS2	1.5756733	-2.6111902
CLK1	2.1736193	-1.8464672
COTL1	-2.7910830	1.51650995
CREM	3.6117981	-2.0104203
CXCL3	3.5703832	-3.802953
CXCR4	-2.5758596	1.94257454
RNF19B	3.590873053	-1.6436909
RPL15	-1.834467467	1.38247655
RPL3	-1.638318169	1.962292
RPL36A	-1.536651465	2.8134978
RPL7	-1.875322302	1.5020369
RPLP0	-1.607560781	1.63789654
RPS18	-1.587802272	1.52645655
RRAGC	2.042389606	-1.8478854
RUFY3	1.82615331	-2.321293
S100A4	-6.715729665	2.1862692
S100A6	-2.534050656	1.60841765
S100A8	-2.976618138	2.45943902
SCP2	-1.807725459	1.93094183
SERPINA1	-1.517634202	2.26174978
CYBB	-2.3337059	-1.6468494
DAPP1	2.2134104	-1.829312
DENND1B	4.2926621	-2.5012958
DNMT3A	-2.0179375	-3.3011758
DOCK4	1.6850513	-1.8736071
DOCK5	-1.5800012	-2.6702746
DPYD	-1.8225519	3.03427748
EAF1	2.1039822	-3.7785122
EBP	-2.4543178	-2.5059552
EDEM1	1.9757324	-1.3153847
EGR1	-3.3727662	-2.670039
EIF4G3	-3.1934405	-1.925565
EPM2AIP1	1.6505351	-2.6000326
EREG	2.9131480	-3.7420638
FAH	-2.2413667	2.65908443
FAM105A	-2.778573	1.93900683
FCGR2B	-3.875940	2.30613903
FCGR3A	-1.5185169	2.37266713
FGD4	-2.233560	2.13903126
FNDC3B	2.789031	-2.0919354
FOS	-4.195671	1.64119757
FPR1	-5.622461	4.26422121
GAPDH	-1.598926	1.89353846
GPR137B	1.764161	-1.9983495
GPR82	-4.159727	2.04503652
HERPUD2	1.624229	-2.5526031
HK2	1.700387	-2.1278761
HTRA1	-6.031604	2.4834819
IDH1	-1.562713	2.4237828
IFNGR1	-2.306404	2.4187006
IL8	1.754590	-1.2332134
INSR	-4.418922	-1.878209
ITGB8	4.430416	-3.018448
KLF6	3.002189	-1.6587698
KLHL28	2.085138	-1.5289471
SSBP2	-1.919166037	3.15883575
STAB1	-4.740089861	2.29204368
SYK	-1.595966568	2.25647679
TBXAS1	-5.890405563	1.8362742
TDP2	2.077062038	-2.1776526
TLK1	1.593891205	-3.4142476
TMEM14C	-1.983096954	1.58636701
TMTC3	2.174481009	-3.1879365
TNFAIP2	2.598331319	-2.2378942
TNFAIP3	4.178266455	2.23014664
TRIM38	2.682049894	-2.6195862
SERPINE1	-3.392465357	3.70110501
SLA	-1.806524898	4.22996549
SLC11A1	-3.947171857	1.95264422
KPNB1	2.001709	-1.9921506
LATS2	1.809180	-2.3407728
LGMN	2.39960	-1.9361007
LYPLA1	-1.6933014	1.89462876
MARCKS	2.9586868	-1.7603592
METTL7A	-5.5759028	2.67209519
MGAT4A	-3.5829776	2.52279771
MLLT6	1.6958965	-2.1853875
MRC1	-5.1325538	3.40485184
MS4A6A	-2.9044804	4.32083109
MSR1	4.8735647	-2.1968929
MXD1	3.3096856	-3.0024508
MYCBP	-1.7040189	1.92020787
NAMPT	3.4424634	-1.6595369
NIN	-2.0764591	1.98773373
NRIP3	2.3702371	-3.6742286
PARP14	3.4193511	-1.9359577
PDK4	-4.2244941	1.95577715
PHACTR2	1.8169339	-2.5001623
PLA2G7	1.522442	-2.2951082
PLAUR	1.9981100	-1.7483528
PLEK	2.0915509	-1.5906057
PLP2	-2.4495312	1.5753501
POGLUT1	1.5239624	-2.5651209
PPP2R2A	2.5207426	-2.017461
PRDM1	1.8019511	-3.8927617
PSMD11	1.572322	-2.9435163
PTGER2	2.6692745	-1.7070306
RAP2C	1.9375602	-2.6065819
RDX	1.9256893	-1.9827675
REPS2	-2.7741963	2.23697554
RGS18	-5.668900	2.45328095
RGS2	-2.1282491	1.39771862
RIT1	1.76708411	-3.6751266
RNASE6	-4.5853869	2.58856132
TSC22D2	1.912522092	-2.9414468
TTC39C	-1.730603001	-2.3761525
VAMP5	3.276991137	1.88775483
VAMP8	-1.824467878	1.35203344
VCPIP1	2.118600386	-1.8377988
VRK2	2.335410085	-1.873086
WNT5A	5.517523354	-1.6673179
WTAP	3.121577379	-2.7736378
ZC3HAV1	2.747570306	-1.6707451
ZDHHC20	-1.930093828	2.29594368
SLC1A3	1.662195468	3.94369126
SLC41A2	3.897495647	-4.2493421
SORL1	-6.579013103	2.60590965
SOS1	2.078155474	-2.0648549
SRXN1	1.94414878	-2.2330435

Upregulated	OV Monocyte Log FC	GC Monocyte Log FC
ACSL1	3.86741313	2.08901446
CCL3L1	5.24435961	3.22359807
CASP8	1.63215541	2.18693808
CXCL10	8.24546486	3.2106235
CXorf38	1.57064348	1.74515956
HLA-A	1.96095803	1.6022541
HLA-B	1.91291413	1.60076471
HLA-C	1.97493983	2.38729576
IFITM1	7.12052374	2.47670205
IFITM2	4.28117827	3.7049259
IFITM3	4.22906359	2.63459237
MYL12A	1.83547309	1.33794633
NAPA	2.43051857	2.22793338
NT5C3	6.33513563	3.34320266
PPM1K	3.19917945	1.70479373
PRRG4	2.49536517	2.21954915
RGS1	2.67016317	2.81462438
RSAD2	6.15158591	1.74228132
SAMSN1	3.30361498	1.26251916
SMCHD1	3.00995375	2.13717837
TLR2	1.5886813	1.35311911

Downregulated	OV Monocyte Log FC	GC Monocyte Log FC
AKR1C3	-3.737947	-1.638355
ARHGAP18	-2.8121027	-2.1940912
ATXN1	-1.6924069	-3.9603295
CLEC7A	-1.9126584	-1.4939939
CD9	-3.7412609	-1.7967682
CD180	-1.5153653	-2.8839828
CD36	-3.0989846	-2.9710024
EVI5	-1.7511668	-1.5373482
GLT25D1	-3.8803346	-2.216563
EVI2A	-1.9334734	-1.5871245
HBEGF	-1.8649901	-2.0080479
KCNE3	-1.9094236	-2.4437754
LIPA	-1.8068219	-2.1211419
LYZ	-4.2695411	-1.589055
MAF	-3.7201567	-2.9148221
ME1	-1.8168334	-2.2137259
NUCKS1	-1.899839	-1.606785
PAPSS2	-2.7118467	-2.2007729
PCMTD2	-2.7849438	-2.3744122
PFKFB2	-4.3515016	-2.5871323
PID1	-8.2720966	-3.0425262
PMEPA1	-1.7905744	-1.7779576
PPP3CA	-2.6302785	-3.1649981
PRKCB	-1.7958589	-2.4132072
PSIP1	-2.1282598	-2.2971473
RAPH1	-3.0795238	-3.4741245
SH3BGRL	-1.557105	-1.7226103
SKAP2	-2.2728949	-2.3051944
SLAMF8	-1.8199296	-1.6651812
SLC12A2	-1.5756764	-3.112134
TBL1XR1	-2.4121609	-2.4426111
TRPS1	-1.9200572	-2.8982197
ZBTB44	-2.2001854	-1.9630974
ZFHX3	-1.7256278	-2.3194134

Table 7-6 251 Overlaying genes between OV-GBM patients and OV-monocyte

Upregulated	OV GBM Log FC	OV Monocyte Log FC
EDN1	1.4694	8.95554473
UTY	2.42759	1.23692083
C4B	4.79599	2.35353971
LMNB1	1.16179	4.34817204
CBX4	0.928646	1.03047509
EMILIN1	1.05703	1.66131506
TSKU	1.34831	1.16199565
MDM2	3.54735	2.22680083
KLF4	2.44845	1.64320857
DDX3Y	2.51135	0.64616785
CANT1	1.09977	0.51254689
CENPJ	1.0331	3.39809609
LBH	1.58416	1.05179759
CHPF	1.38516	3.52153763
CDC42EP4	1.12892	0.79852646
SULF1	1.41987	2.56553514
IER2	1.81911	0.78465545
TXNIP	1.31094	1.20544888
TOR1B	1.0899	2.96289655
CCNL1	1.22957	1.95725806
CDKN1C	1.52705	1.12541173
TSPAN6	1.33912	2.38156479
ITGB7	1.31829	2.14482162
PRAME	4.45481	3.44743792
MAGED2	0.904137	1.04211473
TOP3A	0.918597	1.41146139
COL9A2	1.17508	2.54659541
PSMD3	0.982737	0.55951241
PERP	2.33932	4.08908693
PTGS2	2.35777	5.47869761
CTSD	1.07666	1.66657411
B4GALT6	1.73763	1.4145176
OTUD1	1.06213	1.95508804
PIP4K2C	2.21934	1.32067156
IGFBP4	0.921647	6.52652965
IGSF3	1.19925	2.34797283
OSR2	1.93329	0.65374716
FAM71A	2.9858	5.14136157
PODXL	0.972637	1.55631959
SHISA5	1.21122	0.89150049
RAP1B	3.40272	1.29034685
C17orf96	1.2814	3.11739625
CSRNP1	1.11457	3.82782342
CITED2	1.28121	0.77552848
MESDC1	1.1362	2.50862389
FSIP2	1.37661	0.76492766
NFKBIA	0.83977	2.25119487
LRP3	0.998427	0.76894172
SLC43A3	0.985613	0.66924853
LGALS3BP	1.55178	4.3281251
SPHK1	2.30549	2.45871843
DUSP1	1.87293	1.07310484
IL6	2.22138	1.36900587
METTL1	2.46847	1.06706364
DNAJB5	1.02189	1.63549357
CCDC80	0.989057	3.5989757
JUN	1.75469	1.28089083
SESN2	0.953732	1.65842588
SCML4	2.64337	3.06032645
TMED4	1.04245	0.65965153
BAMBI	2.36771	4.3563653
GABBR1	5.92053	1.8950421
USP11	0.853433	0.8208434
GCNT2	1.59287	1.59734715
RAB9B	1.08647	2.50373246
IL17RD	0.923937	1.74187028
HS3ST3B1	1.45359	4.69244386
CYP27B1	1.99256	5.49065128
TAF7	0.866417	0.80192733
TGM2	1.55475	2.80435485
PLEKHM1	4.9653	1.02721594
VPS18	1.05313	0.55142599
HMGA2	9.2654	3.46132385
LTF	5.71932	2.97913167
MYH7	1.4706	3.42346315
RGMA	1.31099	3.04606143
DDR1	8.01408	1.00732747
HLA-A	2.01104	1.96095803
HLA-B	4.05474	1.91291413
HLA-C	6.78655	1.97493983
LGMN	0.904595	2.39960801
FOS	2.81945	1.47610235
ZFP36	1.36666	0.65069153
POGLUT1	1.33919	1.52396249
GRN	0.84726	1.73185699
CCL3L1	2.6107	5.24435961
SLC35E3	3.90004	0.59432223
ANGPTL4	1.95108	4.78580823
CD70	2.25304	5.30937416
TMTC1	2.18329	2.992312
LPCAT1	1.15259	0.83515105
KLHL9	1.66838	0.56308278

DEGs	OV GBM Log FC	OV Monocyte Log FC
CTDSP2	2.01562	-1.4792477
UNG	1.02526	-1.8934495
PPM1H	2.57553	-1.3642877
FST	2.91753	-1.4340152
PROS1	1.26765	-4.5892007
PIGT	0.941357	-1.0023353
MAGEF1	0.951655	-2.428304
PRMT5	0.890784	-1.5490059
NDRG1	1.21317	-1.4598393
RPUSD2	1.29976	-1.3181224
VMA21	1.13157	-0.9751631
DUS1L	0.958144	-1.2298482
CCT6A	1.91138	-0.6272572
ITGB5	1.15543	-3.4635043
FAM109A	1.27233	-2.4980182
SLC39A14	0.929208	-1.0422239
POU2AF1	-2.93029	1.91028329
DUSP2	1.48878	-2.4878181
SUMF2	1.74702	-1.4241053
MT-ND1	-1.3219	0.64141648
DPH2	1.13088	-0.9714252
FAM3A	1.29987	-1.1427246
AIM2	2.37808	-2.4753896
PYCRL	1.07986	-1.1355231
NDN	2.00774	-2.5013534
HBA2	-1.11238	1.64377362
ERLIN2	1.10367	-1.235707
GNS	1.11425	-0.609752
GEMIN4	1.24691	-1.4155108
RPS4Y1	2.30528	-2.3498155
LFNG	1.18444	-0.7210914
CTSF	0.92504	-4.0553749
GHDC	1.14872	-1.4400772
LILRB3	-6.767	0.80234223
NUP107	4.39089	-0.8388048
BRD2	1.88288	-0.6973966
PFKFB4	1.18437	-0.5619806
EPAS1	0.984702	-0.6412747
SLC16A1	0.987735	-1.4552679
S100P	-3.16564	1.92099078
CXorf24	1.36189	-1.9322471
CHID1	1.02476	-2.3732109
DVL2	0.844624	-0.8022379
DHX40	0.852581	-0.7231418
MCM3	1.09947	-1.1320951
CHST14	1.82309	-1.6227652
CYP2E1	-1.86441	2.06606697
SURF2	2.37632	-0.8959
BCL2L11	1.43764	-1.045039
KIAA0195	0.918755	-1.0617675
GBAS	1.43868	-1.000261
ADAMTS10	2.61639	-5.2072313
TTC30A	1.36651	-1.604773
TRIB3	1.26133	-1.9974059
TMX4	0.93462	-1.242106
PGM5	1.39288	-2.6068963
TIGD3	1.56183	-2.2307422
MKS1	1.08836	-2.3733109
PCOLCE2	2.00363	-3.4586521
SCAP	1.09197	-1.3499316
PIGM	0.983556	-1.6370662
PSPH	1.92411	-1.3249659
C17orf70	1.06409	-1.1639218
SCRN2	1.35265	-2.1650314
TTLL7	-1.31666	1.10057896
MDM1	4.26397	-1.1072537
NUP210	1.202	-2.9410177
FBXO21	1.10617	-1.4711494
TFDP1	1.09587	-0.6405589
TUSC1	1.4977	-1.2444423
ITGA11	1.26583	-2.4472887
AKT1	-1.37838	-0.6685957
MCM6	1.03548	-3.519786
ENC1	1.39364	-1.2794443
SLC25A38	0.941735	-1.4401121
TMEM101	1.13322	-0.9773357
IMPDH2	1.04731	-1.1750239
RANBP6	0.950226	-1.0402325
DDX24	-1.29248	0.59409628
LANCL2	3.90518	-0.9619726
TTC30B	1.3545	-1.443
TPPP3	1.53623	-2.9180145
GPC4	1.92112	-2.768431
SLC2A14	-4.76172	-2.6541404
AMFR	0.994967	-0.7171588

ARSD	1.07086	-2.0160741
TIMELESS	0.971348	-0.6292051
GTF2I	3.17918	-0.7186904
TMEM107	1.56618	-2.178246
HGF	1.8308	-3.9916945
NPDC1	1.13411	-5.8017201
MCM2	1.33958	-1.329685
MCM4	0.98135	-2.2932447
EFNB1	0.956961	-1.7981338
VPS25	0.912817	-1.5510317
KLF2	1.16598	-2.8101212
TMEM106C	1.2143	-0.7165405
VEGFA	1.53883	-1.7511254
MYC	1.2114	-2.325925
SUPT16H	0.771173	-0.6001785
ALKBH5	1.00726	-0.8459492
MPZL2	1.23072	-4.2097819
BCAM	1.15015	-3.4329377
ZNF395	1.16499	-5.227505
IL27RA	1.90635	-1.5587046
CMYA5	-1.52026	2.7220979
SGK1	0.963186	-1.2652894

B3GNT1	0.911413	-5.9248142
TNC	1.48862	-2.859939
ZBTB9	1.24312	-0.7167929
SPINT1	1.10779	-2.875322
NCKIPSD	1.04861	-1.3222219
FSTL3	1.32358	-1.4340152
POFUT1	0.966279	-1.7966649
PAPLN	-1.46268	0.94135247
EGR1	2.37868	-3.3727663
S100A8	-2.2744	-2.9766181
SERPINE1	1.0922	-3.3924654
BTG2	1.53286	-1.3895522
PCMTD2	1.33114	-2.7849438
PRPS2	1.67053	-1.219832
PRKAR1A	1.00339	-0.7298611
AAAS	0.901517	-2.3682264
LMAN2L	1.12034	-1.3052337
INF2	-1.21796	1.40344567
AC018638.1	-2.6185	0.9587601
PBXIP1	0.850798	-1.547971

Downregulated	OV GBM Log FC	OV Monocyte Log FC
ATG2B	-1.41324	-1.5200106
IFI27L2	-1.48127	-1.0744252
FCHO1	-1.17623	-2.8557828
NRG1	-1.93548	-5.6036729
CX3CR1	-1.15904	-6.5172249
VRK1	-2.35807	-1.1581191
POU2F2	-1.27248	-3.2870264
NAIP	-2.07631	-1.4495723
RGS18	-1.46768	-5.6689006
PHOSPHO1	-1.1577	-5.379256

Table 7-7 KEGG enriched pathways for the DEGs regulated by Reo in MO59K single culture

KEGG 983 DEGs in REO	Adjusted P-value	Genes
TNF signaling pathway	6.55E-23	CXCL6;CEBPB;CSF2;CSF1;TNFAIP3;CXCL1;NOD2;CXCL3;PTGS2;TNF;CXCL2;CX3CL1;CXCL5;ICAM1;CASP7;CASP10;CCL5;CCL2;MAP3K8;JUN;EDN1;VCAM1;MLKL;IL15;CCL20;IFNB1;MMP3;LIF;VEGFC;TRAF1;TNFRSF1B;NFKB1;NFKBIA;CXCL10;IL6;IL1B;IRF1;FAS;BIRC2;IL18R1;BIRC3
Cytokine-cytokine receptor interaction	1.23E-20	CXCL6;CSF3;CXCL9;IL20;CSF2;CXCL8;CSF1;IL24;CXCL1;IL1RAP;CXCL3;TNF;CXCL2;CX3CL1;CXCL5;CXCL16;TNFSF13B;TNFSF10;TNFSF11;CCR3;IL15RA;IL11;TNFRSF12A;IL1R1;IL15;TNFRSF19;TNFRSF1B;PRLR;IL1A;IL23A;IL1B;IL3RA;LTB;CXCR4;IFNL2;IFNL1;CCL5;CCL4;CCL2;TNFRSF14;IL12RB1;IFNL3;CCR1;TNFSF18;IL32;IL33;TNFSF14;TNFSF15;CCL20;GDF15;IFNB1;IL34;TNFRSF9;LIF;INHBA;IL22RA1;CXCL10;CXCL11;IL6;FAS;IL7R;IL18R1
NOD-like receptor signaling pathway	1.61E-15	CXCL8;TNFAIP3;CXCL1;NOD2;MEFV;CXCL3;TNF;CXCL2;PANX1;IFI16;CCL5;NAMPT;CASP4;CASP1;NLRP3;CCL2;GBP2;IKBKE;GBP1;GBP4;GBP3;GBP5;JUN;RIPK2;IFNB1;STAT1;STAT2;NFKB1;NFKBIA;IL6;AIM2;OAS1;OAS2;IL1B;OAS3;CARD17;IRF7;RBCK1;MYD88;BIRC2;IRF9;BIRC3
Influenza A	3.96E-14	CXCL8;ADAR;TNF;ICAM1;IFIH1;NXF2;CCL5;TNFSF10;CASP1;TRIM25;NLRP3;CCL2;JAK2;HLA-DOB;IKBKE;IL33;RSAD2;DDX58;IFNB1;STAT1;MX2;STAT2;MX1;EIF2AK2;NFKB1;PML;NFKBIA;CXCL10;IL1A;IL6;OAS1;OAS2;IL1B;OAS3;IRF7;FAS;MYD88;IRF9;TLR3
Viral protein interaction with cytokine and cytokine receptor	1.77E-13	CXCL6;CXCL9;CXCL8;IL20;CSF1;IL24;CXCR4;CXCL1;CXCL3;TNF;CXCL2;CX3CL1;CXCL5;CCL5;CCL4;TNFSF10;CCL2;TNFRSF14;CCR3;CCR1;TNFSF14;CCL20;IL34;TNFRSF1B;IL22RA1;CXCL10;CXCL11;IL6;IL18R1
NF-kappa B signaling pathway	4.61E-13	CXCL8;TNFAIP3;CXCL1;CXCL3;PTGS2;TNF;CXCL2;ICAM1;TNFSF13B;RELB;PLAU;CCL4;TNFSF11;TRIM25;VCAM1;GADD45B;TNFSF14;IL1R1;DDX58;TRAF1;NFKB1;NFKB2;NFKBIA;CYLD;IL1B;LTB;MYD88;BIRC2;BIRC3
Rheumatoid arthritis	8.85E-12	CXCL6;CSF2;CXCL8;CSF1;CXCL1;CXCL3;CXCL2;TNF;CXCL5;ICAM1;TNFSF13B;CCL5;TNFSF11;CCL2;HLA-DOB;IL11;JUN;IL15;CCL20;MMP3;IL1A;IL6;IL23A;IL1B;LTB;TLR2
IL-17 signaling pathway	7.67E-11	CXCL6;CSF3;CEBPB;CSF2;CXCL8;TNFAIP3;CXCL1;CXCL3;PTGS2;CXCL2;TNF;CXCL5;CCL2;IKBKE;JUN;CCL20;MMP3;NFKB1;FOSL1;NFKBIA;CXCL10;IL6;MMP13;IL1B;FOSB
Epstein-Barr virus infection	4.70E-10	CDKN1A;TNFAIP3;TNF;ICAM1;RELB;B2M;IKBKE;HLA-DOB;JUN;GADD45B;IFNB1;STAT1;DDX58;STAT2;HLA-B;TAP2;HLA-C;EIF2AK2;TAP1;ISG15;HLA-F;NFKB1;HLA-E;NFKB2;NFKBIA;CXCL10;IL6;OAS1;OAS2;OAS3;IRF7;FAS;NFKBIE;MYD88;IRF9;TLR2
Coronavirus disease	6.22E-09	CSF3;CSF2;CXCL8;ADAR;TNF;EGFR;IFIH1;C3AR1;CASP1;NLRP3;CCL2;IKBKE;FGA;JUN;IFNB1;STAT1;DDX58;STAT2;MX2;MMP3;MX1;EIF2AK2;ISG15;NFKB1;NFKBIA;CXCL10;IL6;OAS1;OAS2;IL1B;OAS3;CFB;TLR3;MYD88;IRF9;HBEGF;TLR2
Kaposi sarcoma-associated herpesvirus infection	8.34E-09	CDKN1A;CSF2;CXCL8;CXCL1;PTGS2;CXCL3;CXCL2;ICAM1;GNG5;JAK2;IKBKE;CCR3;MICB;CCR1;JUN;IFNB1;STAT1;STAT2;HLA-B;HLA-C;EIF2AK2;HLA-F;NFKB1;HLA-E;NFKBIA;RCAN1;IL6;CLEC2B;GNB4;IRF7;FAS;TLR3;IRF9
JAK-STAT signaling pathway	2.97E-08	CSF3;CDKN1A;CSF2;IL20;IL24;EGFR;IFNL2;SOCS1;IFNL1;PIM1;STAT4;JAK2;IL12RB1;IFNL3;MCL1;IL15RA;IL11;IL15;IFNB1;STAT1;STAT2;LIF;PRLR;IL22RA1;IL6;IL23A;IL3RA;IL7R;IRF9
Lipid and atherosclerosis	3.21E-08	CXCL8;NCF2;CXCL1;CXCL3;TNF;CXCL2;ICAM1;CASP7;CCL5;TNFSF10;CASP1;OLR1;NLRP3;CCL2;JAK2;IKBKE;LDLR;CYP2J2;JUN;XBP1;VCAM1;IFNB1;MMP3;SOD2;NFKB1;ERN1;NFKBIA;IL6;DDIT3;IL1B;IRF7;FAS;MYD88;TLR2

Measles	6.89E-08	TNFAIP3;ADAR;BBC3;IFIH1;IKBKE;JUN;DDX58;IFNB1;STAT1;MX2;STAT2;MX1;EIF2AK2;NFKB1;NFKBIA;IL1A;IL6;OAS1;OAS2;IL1B;OAS3;IRF7;FAS;MYD88;IRF9;TLR2
Legionellosis	1.59E-07	CXCL8;BNIP3;CXCL1;CXCL3;CXCL2;TNF;NFKB1;NFKB2;NFKBIA;BCL2L13;CASP7;IL6;IL1B;CASP1;MYD88;TLR2
Necroptosis	2.66E-07	TNFAIP3;TNF;FTH1;TNFSF10;CASP1;STAT4;NLRP3;JAK2;ZBP1;IL33;MLKL;IFNB1;STAT1;STAT2;EIF2AK2;PLA2G4A;CYLD;IL1A;IL1B;JMJD7-PLA2G4B;FAS;RBCK1;BIRC2;IRF9;TLR3;BIRC3;CHMP5
Toll-like receptor signaling pathway	4.44E-07	JUN;CXCL9;CXCL8;IFNB1;STAT1;TNF;NFKB1;NFKBIA;TLR1;CXCL10;CXCL11;IL6;IL1B;CCL5;CCL4;IRF7;MAP3K8;IKBKE;MYD88;TLR3;TLR2
Cytosolic DNA-sensing pathway	6.34E-07	ZBP1;IL33;DDX58;IFNB1;ADAR;NFKB1;NFKBIA;CXCL10;IL6;AIM2;IL1B;CCL5;CCL4;CASP1;IRF7;IKBKE
C-type lectin receptor signaling pathway	1.98E-06	EGR2;JUN;STAT1;STAT2;PTGS2;TNF;NFKB1;NFKB2;RELB;NFKBIA;CYLD;IL6;IL23A;CLEC7A;IL1B;IRF1;CASP1;NLRP3;IKBKE;IRF9
Hepatitis C	2.62E-06	CDKN1A;IFIT1;CLDN1;TNF;EGFR;IKBKE;LDLR;RSAD2;DDX58;IFNB1;STAT1;MX2;STAT2;MX1;EIF2AK2;NFKB1;NFKBIA;CXCL10;OAS1;OAS2;OAS3;IRF7;FAS;IRF9;TLR3
RIG-I-like receptor signaling pathway	2.66E-06	CXCL8;DDX58;IFNB1;ISG15;TNF;NFKB1;IFIH1;NFKBIA;CXCL10;CYLD;CASP10;DHX58;IRF7;TRIM25;AZI2;IKBKE
Inflammatory bowel disease	5.32E-06	JUN;STAT1;RORA;NOD2;TNF;NFKB1;IL1A;IL6;IL23A;IL1B;STAT4;IL12RB1;HLA-DOB;IL18R1;TLR2
Pertussis	8.04E-06	CXCL6;JUN;CXCL8;TNF;CXCL5;NFKB1;IL1A;CASP7;IL6;IL23A;IL1B;IRF1;CASP1;SERPING1;NLRP3;MYD88
Osteoclast differentiation	1.08E-05	JUN;CSF1;NCF2;IL1R1;IFNB1;STAT1;STAT2;TNF;NFKB1;FOSL2;NFKB2;RELB;FOSL1;NFKBIA;CYLD;IL1A;SOCS1;IL1B;TNFSF11;FOSB;IRF9
Human cytomegalovirus infection	2.20E-05	PTGER4;CDKN1A;CXCL8;CXCR4;PTGS2;TNF;CX3CL1;EGFR;GNG5;CCL5;CCL4;CCL2;B2M;CCR3;CCR1;IL1R1;IFNB1;HLA-B;TAP2;HLA-C;TAP1;HLA-F;NFKB1;HLA-E;NFKBIA;IL6;IL1B;GNB4;FAS
AGE-RAGE signaling pathway in diabetic complications	7.22E-05	JUN;EDN1;VCAM1;CXCL8;STAT1;SERPINE1;VEGFC;TNF;F3;NFKB1;ICAM1;IL1A;IL6;IL1B;PIM1;CCL2;JAK2
Chemokine signaling pathway	8.17E-05	CXCL6;CXCL9;CXCL8;CXCR4;CXCL1;CXCL3;CXCL2;CX3CL1;CXCL5;CXCL16;GNG5;CCL5;CCL4;CCL2;JAK2;CCR3;CCR1;CCL20;STAT1;STAT2;NFKB1;NFKBIA;CXCL10;CXCL11;GNB4
Pathways in cancer	8.17E-05	ALK;CDKN1A;CXCL8;SLC2A1;BBC3;CASP7;EDNRB;PIM1;BDKRB2;BDKRB1;JAK2;NKX3-1;IL15RA;EDN1;IL15;DAPK2;WNT5A;TRAF1;IL23A;IL3RA;KIT;BIRC2;BIRC3;PTGER4;CXCR4;PTGS2;EGFR;RASGRP3;WNT6;GNG5;STAT4;PMAIP1;IL12RB1;JUN;CDKN2B;FZD5;GADD45B;LAMB3;FZD4;STAT1;STAT2;VEGFC;NFKB1;PML;NFKB2;NFKBIA;IL6;GNB4;FAS;IL7R
Hepatitis B	1.38E-04	EGR2;JUN;CDKN1A;CXCL8;DDX58;IFNB1;STAT1;STAT2;TNF;NFKB1;NFKBIA;IFIH1;IL6;CASP10;IRF7;STAT4;FAS;JAK2;IKBKE;MYD88;TLR3;TLR2
MAPK signaling pathway	2.01E-04	PTPRR;CSF1;IL1RAP;AREG;TNF;DUSP16;EGFR;RELB;RASGRP3;CACNA1I;ERBB3;MAP3K8;DUSP5;JUN;GADD45B;IL1R1;DUSP1;VEGFC;PLA2G4A;DUSP8;NFKB1;EREG;NFKB2;EFNA1;IL1A;NR4A1;DDIT3;IL1B;JMJD7-PLA2G4B;KIT;FAS;MYD88
Malaria	2.11E-04	CSF3;IL6;CXCL8;VCAM1;IL1B;PECAM1;CCL2;TNF;MYD88;ICAM1;TLR2
Graft-versus-host disease	2.30E-04	IL1A;IL6;IL1B;HLA-B;HLA-C;FAS;HLA-F;TNF;HLA-DOB;HLA-E
Human immunodeficiency virus 1 infection	3.80E-04	CXCR4;SAMHD1;TNF;GNG5;TRIM5;PAK3;B2M;JUN;APOBEC3F;APOBEC3G;IFNB1;HLA-B;TAP2;HLA-C;TAP1;HLA-F;TNFRSF1B;NFKB1;HLA-E;BST2;NFKBIA;GNB4;FAS;MYD88;TLR2
African trypanosomiasis	4.55E-04	IL6;VCAM1;IL1B;FAS;APOL1;TNF;MYD88;ICAM1;IDO1

Apoptosis	5.26E-04	JUN;GADD45B;TRAF1;TNF;NFKB1;CTSS;BBC3;ERN1;NFKBIA;CASP7;CASP10;DDIT3;IL3RA;TNFSF10;PMAIP1;FAS;BIRC2;MCL1;BIRC3
Tuberculosis	5.71E-04	CEBPB;RIPK2;IFNB1;STAT1;SPHK1;NOD2;TNF;CORO1A;NFKB1;CTSS;TLR1;IL1A;IL6;IL23A;CLEC7A;IRAK2;CASP10;IL1B;JAK2;HLA-DOB;MYD88;TLR2
Human T-cell leukemia virus 1 infection	5.79E-04	CDKN1A;CSF2;SLC2A1;TNF;ETS2;ICAM1;RELB;B2M;HLA-DOB;IL15RA;EGR2;JUN;CDKN2B;MMP7;IL1R1;IL15;HLA-B;HLA-C;HLA-F;NFKB1;HLA-E;NFKB2;FOSL1;NFKBIA;IL6
Leishmaniasis	6.27E-04	JUN;NCF2;STAT1;PTGS2;TNF;NFKB1;NFKBIA;IL1A;IL1B;JAK2;HLA-DOB;MYD88;TLR2
Hematopoietic cell lineage	6.54E-04	IL11;CSF3;CSF2;CSF1;IL1R1;TNF;IL1A;IL6;IL1B;IL3RA;KIT;CD7;IL7R;HLA-DOB;CD34
Chagas disease	9.01E-04	JUN;CXCL8;IFNB1;SERPINE1;TNF;NFKB1;NFKBIA;IL6;IL1B;CCL5;BDKRB2;CCL2;FAS;MYD88;TLR2
Type I diabetes mellitus	0.0013124	IL1A;IL1B;HLA-B;HLA-C;FAS;HLA-F;TNF;HLA-DOB;HLA-E
Complement and coagulation cascades	0.00157667	FGA;SERPINA1;SERPINB2;CFH;SERPINE1;PLAUR;F3;PLAU;BDKRB2;C3AR1;BDKRB1;SERPING1;CFB
Herpes simplex virus 1 infection	0.00157667	SP100;TNF;IFIH1;NXF2;CCL5;ZNF107;CCL2;TNFRSF14;JAK2;IKBKE;HLA-DOB;B2M;ZNF267;TNFSF14;STAT1;IFNB1;DDX58;STAT2;TAP2;HLA-B;EIF2AK2;TAP1;HLA-C;HLA-F;NFKB1;PML;HLA-E;BST2;NFKBIA;IL6;OAS1;OAS2;IL1B;OAS3;IRF7;FAS;MYD88;BIRC2;ZNF850;TLR3;IRF9;BIRC3;TLR2
PD-L1 expression and PD-1 checkpoint pathway in cancer	0.00240566	ALK;BATF2;CD274;BATF3;JUN;STAT1;EGFR;NFKB1;NFKBIA;JAK2;NFKBIE;MYD88;TLR2 CD274 (0.8, 12, 10.6) but down after 48, Dex downregulate JUN (20.7, 55,7, 28.7)
Th17 cell differentiation	0.00447318	JUN;IL1R1;STAT1;RORA;IL1RAP;NFKB1;NFKBIA;IL6;IL23A;IL1B;NFKBIE;JAK2;IL12RB1;HLA-DOB
Human papillomavirus infection	0.00563673	PTGER4;CDKN1A;PTGS2;TNF;EGFR;OASL;WNT6;PARD6A;IKBKE;HES4;FZD5;LAMB3;FZD4;IFNB1;STAT1;STAT2;MX2;WNT5A;MX1;HLA-B;HLA-C;EIF2AK2;ISG15;HLA-F;NFKB1;HLA-E;IRF1;FAS;TLR3;IRF9
Transcriptional misregulation in cancer	0.00724709	CDKN1A;CEBPB;CSF2;CXCL8;GADD45B;LMO2;MMP3;SIX1;PAX3;TRAF1;NFKB1;PML;ETV7;IL6;NR4A3;PLAU;DDIT3;NFKBIZ;BIRC2;BIRC3, GADD45B,MMP3, NR4A3, DDIT3
Salmonella infection	0.0073362	CYFIP2;JUN;CXCL8;MLKL;DYNLT1;RIPK2;AHNAK2;TUBB4A;TNF;NFKB1;PIK3C2B;NFKBIA;IL6;CASP7;IL1B;CASP4;TNFSF10;CASP1;NLRP3;PAK3;MYD88;BIRC2;TLR2;BIRC3
Antigen processing and presentation	0.00795043	HLA-B;TAP2;HLA-C;TAP1;PSME2;HLA-F;TNF;B2M;HLA-DOB;CTSS;HLA-E
Pathogenic Escherichia coli infection	0.0092984	CYFIP2;JUN;CXCL8;IL1R1;CLDN1;TUBB4A;TNF;NFKB1;NFKBIA;IL6;CASP7;MYO1B;IL1B;CASP4;TNFSF10;CASP1;FAS;NLRP3;PAK3;MYD88
Epithelial cell in Helicobacter pylori infection	0.01122109	NFKBIA;JUN;CXCL8;CCL5;CXCL1;CXCL3;CXCL2;EGFR;NFKB1;HBEGF
Allograft rejection	0.01158204	HLA-B;HLA-C;FAS;HLA-F;TNF;HLA-DOB;HLA-E
Inflammatory mediator regulation of TRP channels	0.01555688	CYP2J2;PTGER4;HRH1;TRPA1;IL1R1;IL1B;JMJD7-PLA2G4B;BDKRB2;TRPV3;BDKRB1;PLA2G4A;IL1RAP
Toxoplasmosis	0.01682329	LAMB3;STAT1;TNF;NFKB1;NFKBIA;SOCS1;JAK2;HLA-DOB;LDLR;MYD88;BIRC2;BIRC3;TLR2
Fluid shear stress and atherosclerosis	0.0170558	JUN;EDN1;VCAM1;SDC4;NCF2;IL1R1;DUSP1;TNF;NFKB1;ASS1;ICAM1;IL1A;IL1B;PECAM1;CCL2
Amoebiasis	0.02048975	IL6;CSF2;CXCL8;LAMB3;IL1R1;IL1B;CXCL1;CXCL3;TNF;CXCL2;NFKB1;TLR2
Shigellosis	0.02383351	JUN;CSF2;CXCL8;IL1R1;RIPK2;IFNB1;BNIP3;FOXO6;TNF;EGFR;NFKB1;HK2;NFKBIA;TNIP1;IL1B;CCL5;CASP4;TIFA;CASP1;NLRP3;RBCK1;MYD88
Viral carcinogenesis	0.0252689	EGR2;JUN;CDKN1A;SP100;CDKN2B;HLA-B;HLA-C;EIF2AK2 (PKR);TRAF1;HLA-F;HDAC9;NFKB1;HLA-E;NFKB2;NFKBIA;IRF7;PMAIP1;CCR3;IRF9, JUN, EGR2, PMAIP1

Table 7-8 KEGG enriched pathways for the DEGs regulated by ReoDex in MO59K single culture

KEGG 1523 DEGs in REODEX	Adjusted P-value	Genes
TNF signaling pathway	1.00E-11	CXCL6;CEBPB;CSF2;CSF1;TNFAIP3;CXCL1;NOD2;CXCL3;TNF;CXCL2;CX3CL1;CXCL5;ICAM1;CASP10;CCL5;CCL2;MAP3K8;MAP3K5;EDN1;VCAM1;MLKL;CCL20;IFNB1;TRAF1;CFLAR;TNFRSF1B;NFKB1;NFKBIA;CXCL10;IL6;IL1B;IRF1;FAS;BIRC2;IL18R1;BIRC3
Cytokine-cytokine receptor interaction	7.83E-10	CXCL6;CSF3;CXCL9;CSF2;CXCL8;CSF1;CXCL1;CXCL13;CXCL3;TNF;CXCL2;CX3CL1;CXCL5;CXCL16;TNFSF13B;TNFSF10;IL12A;CCR3;IL15RA;IL4R;IL1R1;IFNGR1;TNFRSF19;IL17RE;OSMR;TNFRSF1B;IL1A;IL23A;IL1B;IL3RA;LTB;CXCR4;IFNL2;ACVR1C;IFNL1;CCL5;CCL4;CCL2;TNFRSF14;IL12RB1;IFNL3;CCR1;TNFSF18;TNFSF14;TSLP;CCL20;IFNB1;IFNLR1;INHBA;IL22RA1;CXCL10;CXCL11;IL6;CXCL12;FAS;ACKR3;LTBR;IL7R;IL18R1
Influenza A	8.09E-10	CIITA;CXCL8;CALCOCO2;ADAR;TNF;ICAM1;IFIH1;CCND3;CCL5;TNFSF10;CASP1;TRIM25;NLRP3;CCL2;IL12A;JAK2;HLA-DOB;IKBKE;RSAD2;DDX58;IFNGR1;IFNB1;STAT1;MX2;STAT2;MX1;EIF2AK2;NFKB1;PML;NFKBIA;CXCL10;IL1A;IL6;OAS1;OAS2;IL1B;OAS3;IRF7;FAS;MYD88;IRF9;TLR3
NOD-like receptor signaling pathway	9.13E-10	CXCL8;TNFAIP3;CXCL1;NOD2;MEFV;CXCL3;TNF;CXCL2;PANX1;IFI16;CCL5;NAMPT;CASP4;CASP1;NLRP3;CCL2;GBP2;IKBKE;GBP1;GBP4;GBP3;GSDMD;GBP5;IFNB1;STAT1;STAT2;TRPV2;NFKB1;NFKBIA;IL6;AIM2;OAS1;OAS2;IL1B;OAS3;CARD17;IRF7;RBCK1;MYD88;BIRC2;IRF9;BCL2L1;BIRC3
Viral protein interaction with cytokine and cytokine receptor	1.93E-09	CXCL6;CXCL9;CXCL8;CSF1;CXCR4;CXCL1;CXCL13;CXCL3;TNF;CXCL2;CX3CL1;CXCL5;CCL5;CCL4;TNFSF10;CCL2;TNFRSF14;CCR3;CCR1;TNFSF14;CCL20;TNFRSF1B;IL22RA1;CXCL10;CXCL11;IL6;CXCL12;ACKR3;LTBR;IL18R1
NF-kappa B signaling pathway	4.76E-09	CXCL8;TNFAIP3;CXCL1;CXCL3;TNF;CXCL2;ICAM1;TNFSF13B;RELB;CCL4;TRIM25;VCAM1;GADD45B;TNFSF14;IL1R1;DDX58;TRAF1;CFLAR;NFKB1;NFKB2;NFKBIA;CXCL12;IL1B;LTB;LTBR;CARD14;MYD88;BIRC2;BCL2L1;BIRC3
JAK-STAT signaling pathway	5.90E-07	CSF3;CDKN1A;CSF2;EGFR;CCND3;IFNL2;SOCS1;IFNL1;MYC;PIM1;STAT4;AOX1;IL12A;JAK2;IL12RB1;IFNL3;MCL1;IL15RA;PDGFRA;IL4R;CISH;TSLP;IFNGR1;IFNB1;STAT1;STAT2;IFNLR1;OSMR;IL22RA1;IL6;IL23A;IL3RA;IL7R;IRF9;BCL2L1
Measles	1.57E-06	TNFAIP3;ADAR;BBC3;IFIH1;CCND3;IL12A;IKBKE;DDX58;IFNB1;STAT1;MX2;STAT2;MX1;EIF2AK2;NFKB1;NFKBIA;IL1A;IL6;OAS1;OAS2;IL1B;OAS3;IRF7;FAS;MYD88;IRF9;HSPA1B;RAB9B;BCL2L1;TLR2;HSPA1A
Rheumatoid arthritis	2.50E-06	CXCL6;CSF2;CXCL8;CSF1;MMP1;CCL20;CXCL1;CXCL3;CXCL2;TNF;CXCL5;ICAM1;TNFSF13B;IL1A;IL6;CXCL12;IL23A;IL1B;CCL5;CCL2;LTB;TEK;HLA-DOB;TLR2
Legionellosis	3.41E-06	CXCL8;BNIP3;CXCL1;CXCL3;CXCL2;TNF;NFKB1;NFKB2;C3;NFKBIA;IL6;IL1B;CASP1;IL12A;HSPA1B;MYD88;TLR2;HSPA1A
Epstein-Barr virus infection	4.51E-06	CDKN1A;TNFAIP3;TNF;ICAM1;RELB;CCND3;MYC;IKBKE;HLA-DOB;GADD45B;IFNB1;STAT1;DDX58;STAT2;HLA-B;TAP2;ENTPD8;HLA-C;EIF2AK2;TAP1;ISG15;HLA-F;NFKB1;HLA-E;SAP30;NFKB2;NFKBIA;CXCL10;IL6;OAS1;OAS2;OAS3;IRF7;FAS;NFKBIE;MYD88;IRF9;TLR2
IL-17 signaling pathway	9.85E-06	CXCL6;CSF3;CEBPB;CSF2;CXCL8;MMP1;CCL20;TNFAIP3;CXCL1;IL17RE;CXCL3;CXCL2;TNF;CXCL5;NFKB1;NFKBIA;CXCL10;IL6;MMP13;IL1B;CCL2;IKBKE;S100A9
Inflammatory bowel disease	2.34E-05	IL4R;IFNGR1;STAT1;RORA;NOD2;TNF;NFKB1;IL1A;IL6;MAF;IL23A;IL1B;STAT4;IL12A;IL12RB1;HLA-DOB;IL18R1;TLR2
Coronavirus disease	1.18E-04	CSF3;CSF2;CXCL8;ADAR;TNF;EGFR;C3;IFIH1;C3AR1;CASP1;NLRP3;CCL2;IL12A;IKBKE;FGA;VWF;IFNB1;STAT1;DDX58;MMP1;STAT2;MX2;MX1;EIF2AK2;ISG15;NFKB1;NFKBIA;CXCL10;IL6;OAS1;OAS2;IL1B;OAS3;CFB;TLR3;MYD88;IRF9;TLR2
Lipid and atherosclerosis	1.18E-04	CXCL8;CXCL1;CXCL3;TNF;CXCL2;ICAM1;CCL5;TNFSF10;CASP1;OLR1;NLRP3;CCL2;IL12A;CD36;JAK2;IKBKE;LDLR;MAP3K5;VAV3;CYP2J2;VCAM1;IFNB1;MMP1;SOD2;NFKB1;ERN1;NFKBIA;IL6;IL1B;IRF7;FAS;HSPA1B;MYD88;TLR2;HSPA1A;BCL2L1

Kaposi sarcoma-associated herpesvirus infection	1.69E-04	CDKN1A;CSF2;CXCL8;LEF1;CXCL1;CXCL3;CXCL2;ICAM1;C3;MYC;JAK2;IKBKE;CCR3;MICB;CCR1;IFNGR1;IFNB1;STAT1;STAT2;HLA-B;HLA-C;EIF2AK2;HLA-F;NFKB1;HLA-E;NFKBIA;RCAN1;IL6;GNB4;IRF7;FAS;TLR3;IRF9
Hepatitis C	3.33E-04	CDKN1A;IFIT1;CLDN1;TNF;EGFR;MYC;IKBKE;LDLR;RSAD2;DDX58;IFNB1;STAT1;MX2;STAT2;MX1;EIF2AK2;CFLAR;NFKB1;NFKBIA;CXCL10;OAS1;OAS2;OAS3;IRF7;CLDN18;FAS;IRF9;TLR3
Pertussis	7.27E-04	CXCL6;CXCL8;TNF;CXCL5;NFKB1;C3;IL1A;IL6;IL23A;IL1B;IRF1;CASP1;SERPING1;NLRP3;IL12A;ITGA5;MYD88
Hematopoietic cell lineage	7.31E-04	CSF3;CSF2;IL4R;CSF1;ITGA4;IL1R1;CD1D;TNF;IL1A;IL6;IL1B;IL3RA;KIT;CD7;CD36;ITGA5;IL7R;HLA-DOB;CD34;CD22
RIG-I-like receptor signaling pathway	8.02E-04	CXCL8;DDX58;IFNB1;ISG15;TNF;NFKB1;IFIH1;NFKBIA;CXCL10;CASP10;DHX58;IRF7;TRIM25;IL12A;AZI2;IKBKE
Cytosolic DNA-sensing pathway	8.02E-04	ZBP1;DDX58;IFNB1;ADAR;NFKB1;NFKBIA;CXCL10;IL6;AIM2;IL1B;CCL5;CCL4;CASP1;IRF7;IKBKE
Malaria	8.90E-04	CSF3;CXCL8;VCAM1;HGF;TNF;ICAM1;IL6;IL1B;CCL2;IL12A;CD36;MYD88;TLR2
Toll-like receptor signaling pathway	0.00124	CXCL9;CXCL8;IFNB1;STAT1;TNF;NFKB1;NFKBIA;CXCL10;CXCL11;IL6;IL1B;CCL5;CCL4;IRF7;IL12A;MAP3K8;IKBKE;MYD88;TLR3;TLR2
Chemokine signaling pathway	0.00156	SHC4;CXCL6;CXCL9;CXCL8;CXCR4;CXCL1;ADCY1;CXCL13;CXCL3;CXCL2;CX3CL1;CXCL5;CXCL16;CCL5;CCL4;CCL2;PTK2B;JAK2;CCR3;CCR1;VAV3;CCL20;STAT1;STAT2;NFKB1;NFKBIA;CXCL10;CXCL11;CXCL12;GNB4
Necroptosis	0.00195	TNFAIP3;TNF;FTH1;TNFSF10;CASP1;STAT4;NLRP3;JAK2;GLUL;ZBP1;MLKL;IFNGR1;IFNB1;STAT1;STAT2;EIF2AK2;CFLAR;IL1A;IL1B;FAS;RBCK1;BIRC2;IRF9;TLR3;BIRC3;CHMP5
Adipocytokine signaling pathway	0.00195	IRS1;ACSL1;SLC2A1;PRKAG2;ACSL5;IRS2;ACSL4;TNFRSF1B;TNF;CPT1B;NFKB1;NFKBIA;CD36;JAK2;NFKBIE
Type I diabetes mellitus	0.00304	IL1A;GAD1;IL1B;HLA-B;HLA-C;FAS;IL12A;HLA-F;TNF;HLA-DOB;HLA-E
African trypanosomiasis	0.00340	IL6;VCAM1;IL1B;FAS;IL12A;APOL1;TNF;MYD88;ICAM1;IDO1
Leishmaniasis	0.00612	ITGA4;IFNGR1;STAT1;TNF;NFKB1;C3;NFKBIA;IL1A;FCGR3B;IL1B;IL12A;JAK2;HLA-DOB;MYD88;TLR2
Chagas disease	0.00622	CXCL8;IFNGR1;IFNB1;SERPINE1;ADCY1;CFLAR;TNF;NFKB1;C3;NFKBIA;IL6;IL1B;CCL5;CCL2;FAS;IL12A;MYD88;TLR2
Transcriptional misregulation in cancer	0.00628	CDKN1A;CEBPB;CSF2;CXCL8;HPGD;SIX1;FOXO1;MYC;NFKBIZ;ELANE;GADD45B;IGFBP3;LMO2;PAX3;PAX5;TRAF1;NFKB1;PML;BAIAP3;ETV7;PER2;IL6;MAF;NR4A3;BCL6;BIRC2;BCL2L1;BIRC3
Toxoplasmosis	0.00692	CIITA;IFNGR1;STAT1;LAMC2;TNF;NFKB1;NFKBIA;SOCS1;IL12A;JAK2;HLA-DOB;LDLR;MYD88;BIRC2;HSPA1B;BCL2L1;BIRC3;TLR2;HSPA1A
C-type lectin receptor signaling pathway	0.00717	PLK3;STAT1;STAT2;TNF;NFKB1;NFKB2;RELB;NFKBIA;IL6;IL23A;CLEC7A;IL1B;IRF1;CASP1;NLRP3;IL12A;IKBKE;IRF9
Graft-versus-host disease	0.00834	IL1A;IL6;IL1B;HLA-B;HLA-C;FAS;HLA-F;TNF;HLA-DOB;HLA-E
Pathways in cancer	0.01112	ALK;CDKN1A;CXCL8;SLC2A1;LAMC2;GLI1;FGF1;BBC3;GLI2;CCND3;MYC;PIM1;IL12A;JAK2;NKX3-1;IL15RA;PDGFRA;EDN1;IL4R;IFNGR1;MMP1;DAPK2;HGF;WNT9A;TRAF1;AXIN2;IL23A;IL3RA;KIT;BIRC2;BIRC3;LEF1;CXCR4;ADCY1;DLL1;EGFR;FOXO1;RASGRP3;WNT6;STAT4;IL12RB1;FZD1;JAG2;FZD5;GADD45B;FZD4;STAT1;STAT2;FN1;NFKB1;PML;NFKB2;NFKBIA;IL6;CXCL12;GSTA4;GNB4;FAS;IL7R;BCL2L1
AGE-RAGE signaling pathway in diabetic	0.01112	EDN1;VCAM1;CXCL8;STAT1;SERPINE1;FN1;TNF;FOXO1;NFKB1;ICAM1;THBD;IL1A;IL6;IL1B;PIM1;CCL2;JAK2

Amoebiasis	0.01352	CSF2;CXCL8;IL1R1;FN1;CXCL1;LAMC2;CD1D;ADCY1;CXCL3;TNF;CXCL2;NFKB1;IL6;IL1B;IL12A;RAB7B;TLR2
Human cytomegalovirus infection	0.01455	CDKN1A;CXCL8;CXCR4;ADCY1;TNF;CX3CL1;EGFR;MYC;CCL5;CCL4;CCL2;PTK2B;CCR3;CCR1;PDGFRA;IL1R1;IFNB1;HLA-B;TAP2;HLA-C;TAP1;HLA-F;NFKB1;HLA-E;NFKBIA;IL6;CXCL12;IL1B;GNB4;FAS
Antigen processing and presentation	0.015568	CIITA;HLA-B;TAP2;HLA-C;TAP1;IFI30;HLA-F;TNF;CTSS;HLA-E;PSME2;HLA-DOB;HSPA1B;HSPA1A
Human papillomavirus infection	0.017770	CDKN1A;MAML2;LAMC2;TNF;EGFR;FOXO1;OASL;WNT6;CCND3;PARD6A;IKBKE;HES4;HES7;FZD1;FZD5;ITGA4;VWF;FZD4;IFNB1;STAT1;STAT2;MX2;MX1;HLA-B;FN1;HLA-C;EIF2AK2;ISG15;WNT9A;AXIN2;HLA-F;NFKB1;HLA-E;MFNG;ITGA10;IRF1;FAS;ITGA5;TLR3;IRF9
Tuberculosis	0.017770	CIITA;CEBPB;NOD2;TNF;CORO1A;CTSS;C3;FCGR3B;CLEC7A;IRAK2;CASP10;IL12A;JAK2;HLA-DOB;PLK3;IFNGR1;IFNB1;STAT1;NFKB1;IL1A;IL6;IL23A;IL1B;MYD88;TLR2
Phagosome	0.018249	COLEC12;DYNC1H1;HLA-B;TAP2;HLA-C;TAP1;HLA-F;CORO1A;TUBB4A;CTSS;HLA-E;C3;FCGR3B;TUBA1A;CLEC7A;OLR1;CD36;ITGA5;RAB7B;HLA-DOB;TUBA8;TLR2
Th1 and Th2 cell differentiation	0.026249	JAG2;IL4R;MAML2;IFNGR1;STAT1;DLL1;NFKB1;NFKBIA;MAF;STAT4;IL12A;JAK2;IL12RB1;NFKBIE;HLA-DOB
FoxO signaling pathway	0.032062	PLK3;CDKN1A;GADD45B;IRS1;PLK2;BNIP3;FOXO6;PRKAG2;IRS2;FBXO32;SOD2;FOXO1;EGFR;IL6;BCL6;TNFSF10;S1PR1;IL7R;RAG1 IRS1 (4.07, 7.09, 21.01) increase GBM viability, BCL6 (5.18, 7.2, 14.1) GBM cell survival, SIPR1 (4.7, 1.59, 0.63) down = increase proliferation GBM
Apoptosis	0.035392	GADD45B;TRAF1;CFLAR;TNF;NFKB1;CTSS;BBC3;ERN1;NFKBIA;TUBA1A;CASP10;IL3RA;TNFSF10;FAS;BIRC2;MAP3K5;MCL1;BCL2L1;TUBA8;BIRC3
Hepatitis B	0.036318	CDKN1A;CXCL8;DDX58;IFNB1;STAT1;STAT2;TNF;NFKB1;NFKBIA;IFIH1;IL6;CASP10;MYC;IRF7;STAT4;PTK2B;FAS;JAK2;IKBKE;MYD88;TLR3;TLR2
Allograft rejection	0.042528	HLA-B;HLA-C;FAS;IL12A;HLA-F;TNF;HLA-DOB;HLA-E
Basal cell carcinoma	0.045158	FZD1;WNT6;CDKN1A;FZD5;GADD45B;FZD4;LEF1;AXIN2;WNT9A;GLI1;GLI2
Osteoclast differentiation	0.045256	CSF1;IL1R1;IFNGR1;IFNB1;STAT1;STAT2;TNF;NFKB1;FOSL2;NFKB2;RELB;NFKBIA;IL1A;SOCS1;FCGR3B;IL1B;FYN;IRF9
Herpes simplex virus 1 infection	0.048407	TNF;IFIH1;ZNF607;ZNF726;IL12A;JAK2;IKBKE;HLA-DOB;IFNGR1;DDX58;TAP2;ZFP69B;HLA-B;TAP1;HLA-C;HLA-F;ZFP90;HLA-E;OAS1;OAS2;IL1B;OAS3;IRF7;ITGA5;ZNF114;BIRC2;TLR3;IRF9;BIRC3;TLR2;SP100;C3;CCL5;CCL2;ZNF624;TNFRSF14;ZNF860;TNFSF14;ZNF184;STAT1;IFNB1;STAT2;EIF2AK2;NFKB1;PML;BST2;NFKBIA;IL6;ZNF30;ZNF74;FAS;MYD88;BCL2L1

Table 7-9 KEGG pathway enrichment for MO59K cells isolated from the coculture model (Veh vs. Reo)

Term of 1722 DEGs between VEH and REO	Adj.p	Genes
Cytokine-cytokine receptor interaction	3.85E-15	ACVRL1;CXCL6;IL1RN;CD40;CSF3;CXCL9;CXCL8;TNFRSF13B;CSF1;CCL4L2;IFNA2;IL24;IL27;CXCL1;FASLG;CXCL13;CXCL3;TNF;CXCL2;CX3CL1;CXCL5;CXCL16;TNFSF13B;IL18RAP;TNFSF10;IL12A;CCR7;AMH;IL15RA;IL15;TNFRSF18;LIFR;OSMR;TNFRSF1B;PRLR;TGFBR1;IL1A;IFNG;IL23A;IL1B;IL3RA;LTA;CCL3L1;EBI3;CXCR5;TNFRSF11B;IL2RG;IFNL2;CCL8;IFNL1;CXCR3;CCL5;CCL4;CCL3;IL36RN;TNFRSF14;IL12RB1;IFNL3;IL12RB2;CCR1;IL32;CCL24;GDF11;IL33;TGFB2;TNFSF14;IFNB1;IL10RA;TNFRSF9;IL36G;IFNLR1;TNFRSF10A;INHBA;IL22RA1;CXCL10;BMP2;CXCL11;IL6;IL7;CLCF1;IL2RB;FAS;IL7R;CCL28;IL18R1
Viral protein interaction with cytokine and cytokine receptor	3.38E-11	CXCL6;CXCL9;CXCL8;CSF1;CCL3L1;CCL4L2;IL24;CXCR5;CXCL1;CXCL13;CXCL3;IL2RG;TNF;CXCL2;CX3CL1;CXCL5;IL18RAP;CCL8;CCL5;CXCR3;CCL4;TNFSF10;CCL3;TNFRSF14;CCR7;CCR1;CCL24;TNFSF14;IL10RA;TNFRSF10A;TNFRSF1B;IL22RA1;CXCL10;CXCL11;IL6;IL2RB;LTA;CCL28;IL18R1
TNF signaling pathway	6.58E-11	CXCL6;CSF1;TRADD;PIK3R3;TNFAIP3;CXCL1;NOD2;CXCL3;PTGS2;TNF;CXCL2;CX3CL1;CXCL5;ICAM1;SOCS3;CASP7;CASP10;CCL5;MAP3K8;JUNB;JAG1;MLKL;RIPK3;IL15;IFNB1;MMP3;DAB2IP;VEGFC;TRAF1;CFLAR;TNFRSF1B;NFKBIA;CXCL10;IL6;MMP14;IL1B;IRF1;LTA;FAS;IL18R1;BIRC3
Influenza A	3.27E-09	CIITA;CXCL8;TRADD;IFNA2;ADAR;FASLG;TNF;ICAM1;PYCARD;IFIH1;TNFSF10;CASP1;TRIM25;IL12A;KPNA5;KPNA2;JAK2;HLA-DOB;IKBKE;RSAD2;DDX58;IL1A;IFNG;OAS1;OAS2;IL1B;OAS3;IRF7;TLR7;IRF9;TLR3;PIK3R3;SOCS3;CCL5;NLRP3;BAK1;IL33;IFNB1;STAT1;MX2;STAT2;MX1;EIF2AK2;TNFRSF10A;PML;NFKBIA;CXCL10;IL6;FAS;MYD88
Epstein-Barr virus infection	4.44E-08	CD40;CDKN1A;TRADD;IFNA2;TNFAIP3;ITGAL;TNF;ICAM1;CCND2;BLNK;B2M;IKBKE;HLA-DOB;DDX58;HLA-B;TAP2;HLA-C;TAP1;HLA-A;HLA-F;HLA-G;RUNX3;HLA-E;CCNA2;CCNA1;OAS1;OAS2;OAS3;IRF7;TP53;IRF9;TLR2;RBPJL;PIK3R3;BCL2L11;PLCG2;E2F2;HES1;BAK1;LYN;IFNB1;STAT1;STAT2;EIF2AK2;ISG15;NFKBIA;CXCL10;IL6;BCL2;FAS;CD247;NFKBIE;MYD88
NOD-like receptor signaling pathway	1.59E-07	CXCL8;IFNA2;ITPR2;TNFAIP3;CXCL1;NOD1;NOD2;ANTXR2;MEFV;CXCL3;TNF;CXCL2;PYCARD;PANX1;PSTPIP1;IFI16;CCL5;NAMPT;CASP1;NLRP3;GBP2;IKBKE;GBP1;GBP4;GBP3;GSDMD;GBP5;GBP7;RIPK3;RIPK2;IFNB1;STAT1;STAT2;CARD6;NFKBIA;P2RX7;IL6;AIM2;OAS1;OAS2;IL1B;OAS3;BCL2;IRF7;TXNIP;MYD88;IRF9;BIRC3
Measles	6.73E-07	TRADD;IFNA2;PIK3R3;TNFAIP3;ADAR;FASLG;IL2RG;BBC3;IFIH1;CCND2;IL12A;BAK1;IKBKE;SLAMF1;STAT5A;DDX58;IFNB1;STAT1;MX2;STAT2;MX1;EIF2AK2;NFKBIA;IL1A;IL6;OAS1;OAS2;IL1B;OAS3;IL2RB;BCL2;CD28;IRF7;FAS;TLR7;TP53;MYD88;IRF9;TLR2
Graft-versus-host disease	6.73E-07	PRF1;HLA-B;GZMB;HLA-C;FASLG;HLA-A;HLA-F;TNF;HLA-G;HLA-E;IL1A;IL6;IFNG;IL1B;CD28;FAS;KLRD1;KLRC1;HLA-DOB
NF-kappa B signaling pathway	1.00E-06	CD40;CXCL8;BCL2A1;CCL4L2;TRADD;TNFAIP3;CXCL1;CXCL3;PTGS2;TNF;CXCL2;ICAM1;TNFSF13B;PLAU;CCL4;PLCG2;BLNK;TRIM25;LYN;EDARADD;TNFSF14;DDX58;TRAF1;CFLAR;NFKBIA;IL1B;BCL2;LTA;PRKCQ;CARD11;MYD88;BIRC3
Kaposi sarcoma-associated herpesvirus infection	2.45E-06	CDKN1A;CXCL8;TRADD;IFNA2;PIK3R3;ITPR2;CXCL1;PTGS2;CXCL3;FGF2;CXCL2;PIK3CG;ICAM1;C3;ZFP36;GNGT2;PPP3CC;PLCG2;E2F2;BAK1;JAK2;IKBKE;CCR1;LYN;ANGPT2;IFNB1;STAT1;STAT2;HLA-B;HLA-C;EIF2AK2;NFATC1;HLA-A;HLA-F;HLA-G;HLA-E;VEGFA;NFKBIA;RCAN1;IL6;CLEC2B;GNB4;IRF7;FAS;TP53;TLR3;IRF9
Inflammatory bowel disease	4.22E-06	TGFB2;STAT1;RORA;NFATC1;GATA3;NOD2;IL2RG;TNF;IL1A;IL6;IL18RAP;IFNG;IL23A;IL1B;TBX21;STAT4;IL12A;STAT6;IL12RB1;HLA-DOB;IL18R1;TLR2;IL12RB2
JAK-STAT signaling pathway	4.24E-06	CSF3;CDKN1A;IFNA2;IL24;PIK3R3;IL2RG;SOCS3;IFNL2;CCND2;SOCS1;IFNL1;STAT4;IL12A;STAT6;JAK2;IL12RB1;IFNL3;MCL1;IL12RB2;STAT5A;IL15RA;PDGFRA;IL15;IFNB1;STAT1;IL10RA;STAT2;LIFR;IFNLR1;OSMR;PRLR;IL22RA1;IL6;IFNG;IL23A;IL7;IL3RA;IL2RB;BCL2;IL7R;IRF9
Type I diabetes mellitus	4.24E-06	PRF1;HLA-B;GZMB;HLA-C;FASLG;HLA-A;HLA-F;TNF;HLA-G;HLA-E;IL1A;IFNG;IL1B;CD28;LTA;FAS;IL12A;HLA-DOB
Th1 and Th2 cell differentiation	5.99E-06	RBPJL;NOTCH1;MAML2;GATA3;IL2RG;DLL1;DLL4;PPP3CC;TBX21;STAT4;IL12A;STAT6;JAK2;IL12RB1;HLA-DOB;IL12RB2;STAT5A;JAG1;STAT1;NFATC1;RUNX3;NFKBIA;IFNG;IL2RB;PRKCQ;MAML3;CD247;NFKBIE
Hepatitis C	6.11E-04	CDKN1A;TRADD;IFNA2;PIK3R3;FASLG;IFIT1;CLDN1;TNF;SOCS3;CLDN23;E2F2;BAK1;IKBKE;RSAD2;DDX58;IFNB1;STAT1;MX2;STAT2;MX1;EIF2AK2;CFLAR;NFKBIA;CXCL10;IFNG;OAS1;OAS2;OAS3;IRF7;FAS;CLDN16;TP53;IRF9;TLR3
Coronavirus disease	7.68E-04	CSF3;CXCL8;C1S;C1R;IFNA2;PIK3R3;CGAS;ADAR;TNF;C4B;C3;IFIH1;C4A;C3AR1;PLCG2;CASP1;NLRP3;IL12A;IKBKE;FGA;IFNB1;STAT1;DDX58;STAT2;MX2;MMP3;MX1;EIF2AK2;ISG15;NFKBIA;SELP;ACE2;CXCL10;IL6;OAS1;OAS2;IL1B;OAS3;TLR7;MASP1;CFB;TLR3;MYD88;IRF9;TLR2

Apoptosis	6.33E-06	BCL2A1;TRADD;PRF1;ITPR2;PIK3R3;CTSW;FASLG;TNF;CTSS;BBC3;SPTA1;CASP7;CTSO;BCL2L11;TUBA3C;CASP10;CTSL;TNFSF10;PMAIP1;BAK1;MCL1;NTRK1;PARP3;DAB2IP;GZMB;TNFRSF10A;TRAF1;CFLAR;TUBA4A;ERN1;NFKBIA;IL3RA;BCL2;BIRC5;FAS;TP53;BIRC3
Natural killer cell mediated cytotoxicity	6.33E-06	IFNA2;ICAM2;PRF1;PIK3R3;FASLG;ITGAL;TNF;ICAM1;FCGR3B;PPP3CC;TNFSF10;PLCG2;RAC3;PTK2B;FYN;KLRC1;KLRC2;IFNB1;SH2D1A;HLA-B;SH2D1B;HLA-C;GZMB;NFATC1;TNFRSF10A;HLA-A;HLA-G;HLA-E;IFNG;RAET1L;FAS;KLRD1;CD48;LCP2;CD247
Rheumatoid arthritis	6.33E-06	CXCL6;CXCL8;CSF1;CCL3L1;CXCL1;CXCL3;ITGAL;CXCL2;TNF;CXCL5;ICAM1;TNFSF13B;CTSL;CCL5;CCL3;ATP6V1E2;HLA-DOB;TGFB2;IL15;MMP3;VEGFA;IL1A;IL6;IFNG;IL23A;IL1B;CD28;TLR2
Allograft rejection	1.34E-05	CD40;PRF1;HLA-B;GZMB;HLA-C;FASLG;HLA-A;HLA-F;TNF;HLA-G;HLA-E;IFNG;CD28;FAS;IL12A;HLA-DOB
Pertussis	1.47E-05	CXCL6;CXCL8;C1S;C1R;NOD1;TNF;CXCL5;C4B;PYCARD;C3;C4A;IL1A;CASP7;IL6;IL23A;IL1B;IRF1;CASP1;IRF8;SERPING1;NLRP3;IL12A;ITGA5;MYD88
Human immunodeficiency virus 1 infection	2.27E-05	TRADD;IFNA2;PIK3R3;ITPR2;CGAS;FASLG;SAMHD1;TNF;CCNB3;CCNB2;CCNB1;GNGT2;PPP3CC;TRIM5;PLCG2;RAC3;PTK2B;BAK1;B2M;AP1M2;APOBEC3F;APOBEC3G;APOBEC3H;IFNB1;LIMK2;HLA-B;TAP2;HLA-C;TAP1;NFATC1;HLA-A;HLA-F;CDC25C;TNFRSF1B;HLA-G;HLA-E;BST2;GNAO1;NFKBIA;BCL2;CDK1;GNB4;FAS;CD247;APOBEC3A;MYD88;TLR2
Toll-like receptor signaling pathway	6.05E-05	CD40;CXCL9;CXCL8;CCL3L1;CCL4L2;IFNA2;PIK3R3;TNF;CCL5;CCL4;CCL3;IL12A;MAP3K8;IKBKE;IFNB1;STAT1;NFKBIA;TLR1;CXCL10;CXCL11;IL6;IL1B;IRF7;IRF5;TLR7;MYD88;TLR3;TLR2
Lipid and atherosclerosis	7.35E-05	CD40;CXCL8;CCL3L1;IFNA2;PIK3R3;CXCL1;FASLG;VLDLR;CXCL3;TNF;CXCL2;ICAM1;PYCARD;CASP7;PPP3CC;CCL5;TNFSF10;CASP1;CCL3;OLR1;NLRP3;IL12A;JAK2;IKBKE;ABCA1;LYN;CYP2J2;HSPA5;IFNB1;MMP3;NFATC1;TNFRSF10A;POU2F2;SOD2;ERN1;NFKBIA;SELP;IL6;IL1B;BCL2;IRF7;FAS;PPARG;TP53;MYD88;TLR2
Antigen processing and presentation	7.53E-05	CD74;CIITA;HSPA5;KLRC2;HLA-B;TAP2;HLA-C;TAP1;HLA-A;HLA-F;TNF;HLA-G;CTSS;HLA-E;IFNG;CTSL;CD8A;PSME2;KLRD1;KLRC1;B2M;HLA-DOB;LGMN
Cytosolic DNA-sensing pathway	8.46E-05	ZBP1;IL33;RIPK3;DDX58;IFNB1;CCL4L2;IFNA2;CGAS;ADAR;PYCARD;NFKBIA;CXCL10;IL6;AIM2;IL1B;CCL5;CCL4;CASP1;IRF7;IKBKE
Complement and coagulation cascades	1.00E-04	FGA;SERPINA1;SERPINB2;C1S;C1R;SERPINE1;F2R;PLAUR;PLAT;F3;SERPINA5;C4B;C3;C4A;THBD;PROCR;PLAU;CR1L;BDKRB2;C3AR1;BDKRB1;SERPING1;MASP1;CFB
Transcriptional misregulation in cancer	2.00E-04	CD40;CDKN1A;CXCL8;BCL2A1;HPGD;SIX1;PLAT;CCND2;PLAU;NFKBIZ;ITGB7;BAK1;SSX2;KDM6A;NTRK1;MEF2C;CDKN2C;BCL11B;IGFBP3;LMO2;MMP3;GZMB;ETV1;PAX5;TRAF1;PBX1;DUSP6;MLF1;PML;CCNA2;ETV7;CCNA1;IL6;NR4A3;SPINT1;BCL6;IL2RB;REL;PPARG;TP53;BIRC3
Cell adhesion molecules	2.00E-04	CD274;CD40;SELPLG;SDC2;ICAM2;NRXN3;ITGAL;CLDN1;ICAM1;CLDN23;ITGB8;ITGAV;ITGB7;ICOS;TIGIT;HLA-DOB;CD34;NEGR1;HLA-B;HLA-C;HLA-A;PDCD1LG2;HLA-F;HLA-G;HLA-E;SELP;VCAN;CD8A;CD28;CDH15;CLDN16;CD22;NECTIN2;NECTIN1
Human cytomegalovirus infection	2.00E-04	PTGER4;CDKN1A;CXCL8;CCL3L1;CCL4L2;TRADD;IFNA2;PIK3R3;ITPR2;CGAS;FASLG;PTGS2;TNF;CX3CL1;GNGT2;PPP3CC;CCL5;CCL4;CCL3;RAC3;E2F2;PTK2B;ITGAV;BAK1;B2M;CCR1;PDGFRA;IFNB1;IL10RA;HLA-B;TAP2;HLA-C;TAP1;NFATC1;HLA-A;HLA-F;HLA-G;HLA-E;VEGFA;GNAO1;NFKBIA;IL6;IL1B;GNB4;FAS;TP53
Legionellosis	2.18E-04	CXCL8;BNIP3;CXCL1;CXCL3;CXCL2;TNF;PYCARD;C3;NFKBIA;CASP7;IL6;CR1L;IL1B;EEF1A2;CASP1;IL12A;MYD88;TLR2
Pathways in cancer	3.90E-04	RET;CDKN1A;CXCL8;IFNA2;FASLG;LAMC2;FGF2;BBC3;CKS1B;FGF5;CASP7;GNGT2;CCND2;RASSF5;BDKRB2;RAC3;BDKRB1;ITGAV;IL12A;JAK2;NKX3-1;IL15RA;PDGFRA;IL15;ITGA2;NCOA3;F2R;TRAF1;TGFBR1;CCNA2;AR;CCNA1;IFNG;IL23A;IL3RA;CKS2;BIRC5;PPARG;TP53;BIRC3;PTGER4;NOTCH1;EPAS1;LAMA1;PIK3R3;TGFA;PTGS2;IL2RG;RASGRP1;DLL1;RASGRP3;DLL4;BCL2L11;PLCG2;STAT4;E2F2;PMAIP1;STAT6;HES1;BAK1;IL12RB1;IL12RB2;NTRK1;STAT5A;TGFB2;JAG1;FZD5;LAMB3;STAT1;FZD7;STAT2;LAMB4;FN1;VEGFC;PML;ESR2;VEGFA;NFKBIA;BMP2;IL6;LPAR5;GSTA4;IL7;IL2RB;BCL2;GNB4;FAS;IL7R
Malaria	4.84E-04	CD40;CSF3;TGFB2;CXCL8;SDC2;ITGAL;TNF;ICAM1;SELP;IL6;IFNG;CR1L;IL1B;IL12A;MYD88;TLR2
Hepatitis B	5.22E-04	CDKN1A;CXCL8;IFNA2;PIK3R3;FASLG;TNF;IFIH1;CASP10;STAT4;E2F2;PTK2B;STAT6;JAK2;IKBKE;STAT5A;TGFB2;EGR3;DDX58;IFNB1;STAT1;STAT2;NFATC1;TGFBR1;NFKBIA;CCNA2;CCNA1;IL6;BCL2;IRF7;BIRC5;FAS;TP53;MYD88;TLR3;TLR2
Chagas disease	0.00175	TGFB2;CXCL8;CCL3L1;IFNB1;SERPINE1;PIK3R3;FASLG;CFLAR;TNF;TGFBR1;C3;GNAO1;NFKBIA;IL6;IFNG;IL1B;CCL5;BDKRB2;CCL3;FAS;IL12A;CD247;MYD88;TLR2
Human papillomavirus infection	0.00266	CDKN1A;MAML2;TRADD;IFNA2;FASLG;LAMC2;TNF;OASL;CCND2;ITGB8;ITGAV;ITGB7;ATP6V1E2;IKBKE;HES7;ITGA2;HLA-B;HLA-C;HLA-A;HLA-F;HLA-G;HLA-E;CCNA2;CCNA1;IRF1;COL6A3;MAML3;ITGA5;TP53;TLR3;IRF9;PTGER4;RBPJL;NOTCH1;LAMA1;PIK3R3;PTGS2;PARD6B;HES1;BAK1;HES4;JAG1;FZD5;LAMB3;IFNB1;STAT1;FZD7;STAT2;MX2;LAMB4;MX1;FN1;EIF2AK2;ISG15;PPP2R3B;VEGFA;FAS

African trypanosomiasis	0.00301	IL6;IFNG;IL1B;FAS;FASLG;IL12A;APOL1;IDO2;TNF;MYD88;ICAM1;IDO1
Human T-cell leukemia virus 1 infection	0.00301	CD40;CDKN1A;PIK3R3;GPS2;BUB1B;ITGAL;IL2RG;TNF;ICAM1;CDC20;CCNB2;ZFP36;PPP3CC;CCND2;PTTG1;E2F2;B2M;HLA-DOB;STAT5A;IL15RA;TGFB2;CDKN2C;IL15;HLA-B;HLA-C;NFATC1;HLA-A;HLA-F;HLA-G;TGFBR1;HLA-E;NFKBIA;CCNA2;CCNA1;IL6;ESPL1;IL2RB;LTA;TLN2;TP53;MAD2L1
Chemokine signaling pathway	0.00311	CXCL6;CXCL9;CXCL8;CCL3L1;CCL4L2;CXCR5;WAS;PIK3R3;CXCL1;CXCL13;CXCL3;CXCL2;CX3CL1;CXCL5;PIK3CG;CXCL16;GNGT2;CCL8;CCL5;CXCR3;CCL4;PLCG2;CCL3;RAC3;PTK2B;CCR7;JAK2;CCR1;LYN;CCL24;STAT1;STAT2;NFKBIA;CXCL10;CXCL11;GNB4;CCL28
Necroptosis	0.00331	TRADD;IFNA2;TNFAIP3;FASLG;TNF;PYCARD;TNFSF10;CASP1;STAT4;NLRP3;STAT6;JAK2;ZBP1;STAT5A;IL33;MLKL;RIPK3;IFNB1;STAT1;STAT2;EIF2AK2;TNFRSF10A;CFLAR;IL1A;IFNG;IL1B;BCL2;FAS;IRF9;TLR3;FTL;BIRC3
Primary immunodeficiency	0.00364	CD79A;CD40;CIITA;TNFRSF13B;CD8A;BLNK;TAP2;TAP1;IL2RG;ICOS;IL7R;RAG1
Cellular senescence	0.00482	CDKN1A;CXCL8;SERPINE1;ITPR2;PIK3R3;FOXM1;ZFP36L2;CCNB3;CCNB2;CCNB1;CCND2;PPP3CC;RASSF5;E2F2;MYBL2;TGFB2;IGFBP3;HLA-B;HLA-C;NFATC1;HLA-A;HLA-F;HLA-G;TGFBR1;HLA-E;CCNA2;CCNA1;IL1A;IL6;CDK1;TP53
C-type lectin receptor signaling pathway	0.00493	PLK3;EGR3;STAT1;STAT2;ITPR2;PIK3R3;NFATC1;LSP1;PTGS2;TNF;PYCARD;NFKBIA;IL6;PPP3CC;IL23A;IL1B;IRF1;PLCG2;CASP1;NLRP3;IL12A;IKBKE;IRF9
Herpes simplex virus 1 infection	0.00674	TRADD;IFNA2;CGAS;FASLG;TNF;IFIH1;ZFP30;ZNF805;ZNF726;IL12A;ZNF600;JAK2;ZNF841;IKBKE;HLA-DOB;B2M;DDX58;ZNF160;TAP2;HLA-B;TAP1;HLA-C;HLA-A;HLA-F;HLA-G;HLA-E;ZNF519;IFNG;OAS1;OAS2;IL1B;OAS3;IRF7;LTA;ITGA5;TP53;ZNF311;TLR3;IRF9;BIRC3;TLR2;ZNF671;ZNF792;SP100;ZNF350;ZNF470;PIK3R3;C3;SOCS3;CCL5;ZNF107;ZNF701;TNFRSF14;BAK1;ZNF267;CD74;ZNF460;TNFSF14;STAT1;IFNB1;STAT2;EIF2AK2;POU2F2;PML;BST2;NFKBIA;IL6;ZNF816;ZNF737;ZNF813;BCL2;FAS;ZNF610;ZNF334;MYD88;NECTIN2;NECTIN1
Th17 cell differentiation	0.00712	STAT5A;STAT1;RORA;NFATC1;GATA3;IL2RG;TGFBR1;NFKBIA;IL6;PPP3CC;IFNG;IL23A;IRF4;IL1B;TBX21;IL2RB;PRKCQ;STAT6;CD247;NFKBIE;JAK2;IL12RB1;HLA-DOB
Osteoclast differentiation	0.00734	CSF1;PIK3R3;TNFRSF11B;TNF;SOCS3;SOCS1;FCGR3B;PPP3CC;PLCG2;BLNK;FYN;JUNB;TGFB2;IFNB1;STAT1;STAT2;NFATC1;TGFBR1;OSCAR;NFKBIA;IL1A;IFNG;IL1B;LCP2;PPARG;IRF9
Autoimmune thyroid disease	0.00820	CD40;IFNA2;PRF1;HLA-B;HLA-C;GZMB;FASLG;HLA-A;HLA-F;HLA-G;HLA-E;CD28;FAS;HLA-DOB
Viral myocarditis	0.01004	CD40;LAMA1;PRF1;HLA-B;HLA-C;HLA-A;ITGAL;HLA-F;HLA-G;ICAM1;HLA-E;CD28;RAC3;FYN;HLA-DOB
Tuberculosis	0.01188	CIITA;TRADD;IFNA2;LSP1;NOD2;TNF;CTSS;C3;CYP27B1;FCGR3B;PPP3CC;IRAK2;CASP10;IL12A;JAK2;HLA-DOB;PLK3;CD74;TGFB2;RIPK2;IFNB1;STAT1;IL10RA;TLR1;IL1A;IL6;IFNG;IL23A;CR1L;IL1B;BCL2;MYD88;TLR2
AGE-RAGE signaling pathway in diabetic complications	0.01405	STAT5A;TGFB2;CXCL8;STAT1;SERPINE1;FN1;PIK3R3;VEGFC;NFATC1;TNF;F3;TGFBR1;ICAM1;VEGFA;THBD;IL1A;IL6;IL1B;PLCG2;BCL2;JAK2
IL-17 signaling pathway	0.01472	CXCL6;USP25;CSF3;CXCL8;TRADD;MMP3;TNFAIP3;CXCL1;CXCL3;PTGS2;CXCL2;TNF;CXCL5;NFKBIA;CXCL10;IL6;MMP13;IFNG;IL1B;IKBKE
RIG-I-like receptor signaling pathway	0.01778	CXCL8;DDX58;IFNB1;TRADD;IFNA2;ISG15;TNF;IFIH1;NFKBIA;CXCL10;CASP10;DHX58;IRF7;TRIM25;IL12A;IKBKE
Leishmaniasis	0.01936	TGFB2;STAT1;PTGS2;TNF;C3;NFKBIA;IL1A;FCGR3B;IFNG;CR1L;IL1B;EEF1A2;IL12A;JAK2;HLA-DOB;MYD88;TLR2
Cell cycle	0.02066	TGFB2;CDKN1A;CDKN2C;PLK1;BUB1B;TTK;CDC25C;PKMYT1;CDC20;CCNB3;CCNA2;CCNB2;CCNA1;CCNB1;CCND2;CDC45;PTTG1;ESPL1;TFDP2;CDK1;E2F2;TP53;BUB1;MAD2L1
Toxoplasmosis	0.02403	TGFB2;CD40;CIITA;LAMB3;LAMA1;STAT1;IL10RA;LAMB4;LAMC2;TNF;PIK3CG;GNAO1;NFKBIA;SOCS1;IFNG;BCL2;IL12A;JAK2;HLA-DOB;MYD88;BIRC3;TLR2
Small cell lung cancer	0.02403	CDKN1A;LAMB3;LAMA1;ITGA2;LAMB4;FN1;PIK3R3;LAMC2;TRAF1;PTGS2;CKS1B;NFKBIA;CKS2;BCL2;E2F2;ITGAV;BAK1;TP53;BIRC3
Hematopoietic cell lineage	0.02467	CSF3;CSF1;ITGA2;TNF;CD1B;IL1A;IL6;CD8A;IL7;CR1L;IL1B;IL3RA;CD7;CD38;CD9;ITGA5;IL7R;HLA-DOB;CD34;CD22
p53 signaling pathway	0.02479	CDKN1A;RRM2;IGFBP3;SERPINE1;TNFRSF10A;BBC3;CCNB2;CCNB1;CCND2;SESN2;BCL2;CDK1;PMAIP1;FAS;GTSE1;TP53
B cell receptor signaling pathway	0.02998	LYN;IFITM1;CD72;DAPP1;PIK3R3;NFATC1;RASGRP3;NFKBIA;CD79A;PPP3CC;BLNK;PLCG2;RAC3;NFKBIE;PIK3AP1;CARD11;CD22
Amoebiasis	0.03314	TGFB2;ARG2;CXCL8;LAMB3;LAMA1;LAMB4;FN1;PIK3R3;CXCL1;LAMC2;SERPINB9;CXCL3;TNF;CD1B;CXCL2;IL6;IFNG;IL1B;IL12A;TLR2
PD-L1 expression and PD-1 checkpoint pathway in cancer	0.03446	BATF2;CD274;BATF3;STAT1;PIK3R3;NFATC1;RASGRP1;BATF;NFKBIA;PPP3CC;IFNG;CD28;PRKCQ;CD247;JAK2;NFKBIE;MYD88;TLR2

Table 7-10 KEGG pathway enrichment for MO59K cells isolated from the coculture model (Veh vs. ReoDex)

Term of 1602 DEGs between VEH and REODEX	Adj.p	Genes
Cytokine-cytokine receptor interaction	4.24E-10	IL1RN;CXCL9;CXCL8;CSF1;CCL4L2;CXCL1;CXCL3;TNF;CXCL2;CXCL16;TNFSF13B;TNFSF10;IL12A;CCR7;AMH;CCR2;IL15RA;IL1R1;IFNGR1;IL15;IL1R2;TNFRSF18;TNFRSF19;TGFBR1;TGFBR2;IL1A;IL23A;IL3RA;LTB;CCL3L1;CXCR4;TNFRSF11B;IL2RG;IFNL2;CCL8;IFNL1;CCL5;CCL4;CCL3;IL12RB1;IFNL3;CCR1;CCL24;GDF11;CCL22;CCL20;IFNB1;TNFRSF9;IFNLR1;TNFRSF10A;INHBA;EPOR;IL22RA1;CXCL10;BMP2;CXCL11;IL6;IL7;FAS;TNFSF8;IL7R;IL18R1
Influenza A	2.37E-08	CXCL8;PIK3R3;ADAR;TNF;ICAM1;IFIH1;CASP8;CCL5;TNFSF10;CASP1;TRIM25;NLRP3;IL12A;JAK2;HLA-DOB;IKBKE;MAPK3;RSAD2;DDX58;IFNGR1;IFNB1;STAT1;MX2;STAT2;MX1;EIF2AK2;PRKCA;TNFRSF10A;PML;NFKBIA;CXCL10;IL1A;IL6;MAVS;OAS1;OAS2;OAS3;IRF7;FAS;MYD88;TLR3
TNF signaling pathway	2.03E-07	CSF1;PIK3R3;TNFAIP3;CXCL1;CXCL3;PTGS2;TNF;CXCL2;ICAM1;CASP7;CASP8;CASP10;CCL5;MAP3K8;MAPK3;MLKL;IL15;CCL20;IFNB1;DAB2IP;VEGFC;TRAF1;CFLAR;NFKBIA;CXCL10;IL6;IRF1;FAS;IL18R1;BIRC3
Viral protein interaction with cytokine and cytokine receptor	2.03E-07	CXCL9;CXCL8;CSF1;CCL3L1;CCL4L2;CXCR4;CXCL1;CXCL3;IL2RG;TNF;CXCL2;CCL8;CCL5;CCL4;TNFSF10;CCL3;CCR7;CCR2;CCR1;CCL24;CCL22;CCL20;TNFRSF10A;IL22RA1;CXCL10;CXCL11;IL6;IL18R1
Epstein-Barr virus infection	1.47E-06	RBPJL;CDKN1A;PIK3R3;TNFAIP3;TNF;ICAM1;BCL2L11;CASP8;MYC;HES1;CD58;B2M;IKBKE;HLA-DOB;GADD45A;IFNB1;STAT1;DDX58;STAT2;HLA-B;TAP2;HLA-C;EIF2AK2;TAP1;ISG15;HLA-A;HLA-F;HLA-E;NFKBIA;CXCL10;CCNA1;IL6;MAVS;OAS1;OAS2;OAS3;IRF7;FAS;NFKBIE;MYD88;TLR2
NOD-like receptor signaling pathway	1.54E-06	CXCL8;TNFAIP3;CXCL1;NOD1;MEFV;CXCL3;TNF;CXCL2;PANX1;CASP8;IFI16;CCL5;NAMPT;CASP1;NLRP3;GBP2;IKBKE;GBP1;GBP4;GBP3;MAPK3;GBP5;GBP7;IFNB1;STAT1;STAT2;CARD6;NFKBIA;IL6;MAVS;AIM2;OAS1;OAS2;OAS3;IRF7;TXNIP;MYD88;BIRC3
Pertussis	2.97E-06	CXCL8;ITGAM;C1S;NOS2;C1R;NOD1;C4BPB;TNF;C4B;C4A;IL1A;CASP7;IL6;IL23A;IRF1;CASP1;SERPING1;NLRP3;IL12A;ITGA5;MYD88;MAPK3
NF-kappa B signaling pathway	1.74E-05	CXCL8;BCL2A1;CCL4L2;TNFAIP3;CXCL1;BCL10;CXCL3;PTGS2;TNF;CXCL2;ICAM1;TNFSF13B;PIDD1;CCL4;TRIM25;EDARADD;IL1R1;GADD45A;DDX58;TRAF1;CFLAR;NFKBIA;LTB;MYD88;BIRC3
Kaposi sarcoma-associated herpesvirus infection	1.74E-05	CDKN1A;CXCL8;PIK3R3;CXCL1;PTGS2;CXCL3;HIF1A;FGF2;CXCL2;ICAM1;ZFP36;CASP8;MYC;GNG7;JAK2;IKBKE;MAPK3;CCR1;ANGPT2;IFNGR1;IFNB1;STAT1;STAT2;HLA-B;HLA-C;EIF2AK2;HLA-A;HLA-F;HLA-E;NFKBIA;RCAN1;IL6;CLEC2B;GNB4;IRF7;FAS;TLR3
Rheumatoid arthritis	2.40E-05	CXCL8;CSF1;CCL3L1;ANGPT1;IL15;CCL20;CXCL1;CXCL3;CXCL2;TNF;ICAM1;TNFSF13B;IL1A;IL6;IL23A;CCL5;CCL3;ACP5;LTB;TEK;ATP6V1E2;HLA-DOB;TLR2
Toll-like receptor signaling pathway	4.86E-05	CXCL9;CXCL8;CCL3L1;IFNB1;STAT1;CCL4L2;PIK3R3;TNF;NFKBIA;CXCL10;CXCL11;IL6;CASP8;CCL5;CCL4;IRF7;CCL3;IL12A;MAP3K8;IKBKE;MYD88;TLR3;TLR2;MAPK3
Hepatitis B	9.05E-05	CDKN1A;CXCL8;PIK3R3;TNF;IFIH1;CASP8;CASP10;MYC;STAT4;PTK2B;JAK2;IKBKE;MAPK3;STAT5A;DDX58;IFNB1;STAT1;STAT2;PRKCA;TGFBR1;TGFBR2;NFKBIA;CCNA1;IL6;MAVS;IRF7;BIRC5;FAS;MYD88;TLR3;TLR2
JAK-STAT signaling pathway	9.05E-05	CDKN1A;PIK3R3;IL2RG;SOCS2;IFNL2;SOCS1;IFNL1;MYC;STAT4;AOX1;IL12A;JAK2;IL12RB1;IFNL3;MCL1;STAT5A;IL15RA;PDGFRA;IFNGR1;IL15;IFNB1;STAT1;STAT2;IFNLR1;EPOR;IL22RA1;IL6;IL23A;IL7;IL3RA;IL7R
Chagas disease	9.05E-05	ACE;CXCL8;CCL3L1;NOS2;IFNGR1;IFNB1;SERPINE1;PIK3R3;CFLAR;TNF;TGFBR1;TGFBR2;GNAO1;NFKBIA;IL6;CASP8;CCL5;CCL3;FAS;IL12A;MYD88;TLR2;MAPK3
Measles	9.05E-05	PIK3R3;TNFAIP3;ADAR;IL2RG;BBC3;IFIH1;CASP8;IL12A;IKBKE;STAT5A;DDX58;IFNB1;STAT1;MX2;STAT2;MX1;EIF2AK2;NFKBIA;IL1A;IL6;MAVS;OAS1;OAS2;OAS3;IRF7;FAS;MYD88;TLR2
Legionellosis	1.22E-04	CXCL8;ITGAM;CR1;CXCL1;CXCL3;CXCL2;TNF;NFKBIA;CASP7;IL6;CASP8;CR1L;CASP1;IL12A;MYD88;TLR2
Coronavirus disease	1.34E-04	CXCL8;C1S;C1R;PIK3R3;ADAR;TNF;C4B;IFIH1;C4A;C3AR1;CASP1;NLRP3;IL12A;IKBKE;MAPK3;FGA;ACE;IFNB1;STAT1;DDX58;STAT2;MX2;MX1;EIF2AK2;PRKCA;ISG15;NFKBIA;ACE2;CXCL10;IL6;MAVS;OAS1;OAS2;OAS3;MASP1;CFB;TLR3;MYD88;TLR2
Apoptosis	3.35E-04	BCL2A1;PRF1;PIK3R3;TNF;CTSS;BBC3;SPTA1;PIDD1;CASP7;BCL2L11;CASP8;CASP10;TNFSF10;PMAIP1;CTSF;MCL1;MAPK3;GADD45A;DAB2IP;TNFRSF10A;TRAF1;CFLAR;NFKBIA;IL3RA;BIRC5;FAS;BIRC3
Chemokine signaling pathway	3.60E-04	CXCL9;CXCL8;CCL3L1;CCL4L2;PIK3R3;CXCR4;ARRB1;CXCL1;CXCL3;CXCL2;CXCL16;CCL8;CCL5;GNG7;CCL4;CCL3;PTK2B;CCR7;PRKACA;JAK2;CCR2;MAPK3;CCR1;VAV3;CCL24;CCL22;CCL20;STAT1;STAT2;NFKBIA;CXCL10;CXCL11;GNB4
Pathways in cancer	3.60E-04	RET;CDKN1A;SPI1;CXCL8;ITGA2B;FGF2;BBC3;CASP7;CASP8;MYC;IL12A;PRKACA;JAK2;NKX3-1;IL15RA;PDGFRA;IFNGR1;IL15;NCOA3;PRKCA;MITF;TRAF1;TGFBR1;TGFBR2;AR;CCNA1;IL23A;IL3RA;BIRC5;BIRC3;PTGER4;LAMA1;PIK3R3;CXCR4;PTGS2;IL2RG;HIF1A;DLL1;FOXO1;RASGRP3;BCL2L11;GNG7;STAT4;PMAIP1;HES1;IL12RB1;MAPK3;JAG2;STAT5A;JUP;NOS2;FZD4;STAT1;GADD45A;FZD7;STAT2;WNT7B;ZBTB16;FN1;VEGFC;PML;EPOR;NFKBIA;BMP2;IL6;IL7;GNB4;FAS;IL7R;FGFR3
Complement and coagulation cascades	4.76E-04	FGA;ITGAM;CR1;C1S;C1R;SERPINE1;PLAT;C4BPB;C4B;C4A;THBD;PROCR;CR1L;C3AR1;ITGAX;SERPING1;MASP1;A2M;CFB
Human cytomegalovirus infection	6.77E-04	PTGER4;CDKN1A;CXCL8;CCL3L1;CCL4L2;PIK3R3;CXCR4;PTGS2;TNF;CASP8;MYC;CCL5;GNG7;CCL4;CCL3;PTK2B;PRKACA;B2M;MAPK3;CCR1;PDGFRA;IL1R1;IFNB1;HLA-

Graft-versus-host disease	9.48E-04	IL1A;IL6;PRF1;HLA-B;HLA-C;FAS;KLRD1;HLA-A;HLA-F;TNF;HLA-DOB;HLA-E
Hematopoietic cell lineage	0.00110	ITGAM;CR1;CSF1;IL1R1;IL1R2;ITGA2B;TNF;CD1B;EPOR;IL1A;IL6;IL7;CR1L;IL3RA;CD7;CD38;ITGA5;IL7R;HLA-DOB;CD34
Leishmaniasis	0.00110	ITGAM;CR1;NOS2;IFNGR1;STAT1;PTGS2;TNF;NFKBIA;IL1A;FCGR3B;CR1L;IL12A;JAK2;HLA-DOB;MYD88;TLR2;MAPK3
Cytosolic DNA-sensing pathway	0.00110	ZBP1;DDX58;IFNB1;CCL4L2;ADAR;NFKBIA;CXCL10;IL6;MAVS;AIM2;CCL5;CCL4;CASP1;IRF7;IKBKE
RIG-I-like receptor signaling pathway	0.00110	CXCL8;DDX58;IFNB1;ISG15;TNF;IFIH1;NFKBIA;CXCL10;MAVS;CASP8;CASP10;DHX58;IRF7;TRIM25;IL12A;IKBKE
Hepatitis C	0.00126	CDKN1A;PIK3R3;IFIT1;CLDN1;TNF;CASP8;MYC;IKBKE;MAPK3;RSAD2;DDX58;IFNB1;STAT1;MX2;STAT2;MX1;EIF2AK2;CFLAR;NFKBIA;CXCL10;MAVS;OAS1;OAS2;OAS3;IRF7;FAS;TLR3
Human immunodeficiency virus 1 infection	0.00171	PIK3R3;CXCR4;SAMHD1;TNF;CCNB3;CCNB2;CCNB1;CASP8;TRIM5;GNG7;PTK2B;B2M;AP1M2;MAPK3;APOBEC3G;IFNB1;HLA-B;TAP2;HLA-C;TAP1;PRKCA;HLA-A;HLA-F;CDC25C;HLA-E;BST2;GNAO1;NFKBIA;GNB4;FAS;MYD88;TLR2;CUL4B
Lipid and atherosclerosis	0.00216	CXCL8;CCL3L1;PIK3R3;CXCL1;CXCL3;TNF;CXCL2;ICAM1;CASP7;CASP8;CCL5;TNFSF10;CASP1;CCL3;OLR1;NLRP3;IL12A;JAK2;IKBKE;MAPK3;VAV3;CYP2J2;XBP1;IFNB1;PRKCA;TNFRSF10A;SOD2;NFKBIA;IL6;IRF7;FAS;MYD88;TLR2
FoxO signaling pathway	0.00259	CDKN1A;GADD45A;HOMER2;PLK2;PLK1;FOXO6;PIK3R3;IRS2;FBXO32;SOD2;FOXO1;TGFBR1;TGFBR2;CCNB3;CCNB2;CCNB1;IL6;BCL2L11;TNFSF10;HOMER3;IL7R;RAG1;MAPK3
Type I diabetes mellitus	0.00395	IL1A;PRF1;HLA-B;HLA-C;FAS;IL12A;HLA-A;HLA-F;TNF;HLA-DOB;HLA-E
African trypanosomiasis	0.00431	IL6;FAS;IL12A;PRKCA;APOL1;IDO2;TNF;MYD88;ICAM1;IDO1
Inflammatory bowel disease	0.00448	IFNGR1;STAT1;RORA;IL2RG;TNF;IL1A;IL6;IL23A;STAT4;IL12A;IL12RB1;HLA-DOB;IL18R1;TLR2
Human papillomavirus infection	0.00499	PTGER4;RBPJL;CDKN1A;LAMA1;ITGA2B;PIK3R3;PTGS2;TNF;FOXO1;OASL;RELN;CASP8;PARD6A;ITGB8;HES1;PRKACA;ATP6V1E2;IKBKE;HES4;MAPK3;HES7;FZD4;IFNB1;STAT1;FZD7;STAT2;WNT7B;MX2;MX1;HLA-B;FN1;HLA-C;EIF2AK2;ISG15;HLA-A;HLA-F;HLA-E;CCNA1;ITGA10;IRF1;FAS;MAML3;ITGA5;TLR3
Allograft rejection	0.00499	PRF1;HLA-B;HLA-C;FAS;IL12A;HLA-A;HLA-F;TNF;HLA-DOB;HLA-E
Cell adhesion molecules	0.00536	NTNG1;CD274;ITGAM;SDC4;NEGR1;ICAM2;HLA-B;HLA-C;HLA-A;PDCD1LG2;F11R;HLA-F;CLDN1;ICAM1;HLA-E;VCAN;ALCAM;SDC1;ITGB8;NRCAM;CD58;HLA-DOB;CD34;NECTIN1
Natural killer cell mediated cytotoxicity	0.00536	VAV3;IFNGR1;IFNB1;ICAM2;PRF1;HLA-B;HLA-C;PIK3R3;PRKCA;TNFRSF10A;HLA-A;TNF;ICAM1;HLA-E;FCGR3B;TNFSF10;RAET1L;PTK2B;FAS;KLRD1;LCP2;MAPK3
AGE-RAGE signaling pathway in diabetic complications	0.00678	STAT5A;CXCL8;STAT1;SERPINE1;FN1;PIK3R3;VEGFC;PRKCA;TNF;FOXO1;TGFBR1;ICAM1;TGFBR2;THBD;IL1A;IL6;JAK2;MAPK3
Amoebiasis	0.00839	CXCL8;ITGAM;NOS2;IL1R1;LAMA1;IL1R2;FN1;PIK3R3;PRKCA;CXCL1;CXCL3;TNF;CD1B;CXCL2;IL6;IL12A;PRKACA;TLR2
Transcriptional misregulation in cancer	0.01026	CDKN1A;SPI1;CXCL8;ITGAM;BCL2A1;SIX1;PLAT;FOXO1;MYC;NFKBIZ;SSX2;KDM6A;CDKN2C;JUP;GADD45A;IL1R2;ZBTB16;MITF;ETV1;TRAF1;PBX1;PML;TGFBR2;ETV7;CCNA1;IL6;NR4A3;BIRC3
Malaria	0.01173	IL6;CXCL8;CR1;LRP1;CR1L;SDC1;IL12A;TNF;MYD88;ICAM1;TLR2
Th1 and Th2 cell differentiation	0.01674	RBPJL;JAG2;STAT5A;IFNGR1;STAT1;IL2RG;DLL1;NFKBIA;STAT4;IL12A;MAML3;JAK2;IL12RB1;NFKBIE;HLA-DOB;MAPK3
Osteoclast differentiation	0.01757	SPI1;CSF1;IL1R1;IFNGR1;IFNB1;STAT1;STAT2;PIK3R3;MITF;TNFRSF11B;TNF;TGFBR1;TGFBR2;NFKBIA;IL1A;SOCS1;FCGR3B;ACP5;LCP2;MAPK3
IL-17 signaling pathway	0.02005	USP25;CXCL8;CCL20;TNFAIP3;CXCL1;CXCL3;PTGS2;CXCL2;TNF;NFKBIA;CXCL10;IL6;CASP8;MMP13;IKBKE;MAPK3
Cellular senescence	0.02021	CDKN1A;CXCL8;GADD45A;SERPINE1;HLA-B;HLA-C;PIK3R3;HLA-A;HLA-F;FOXM1;FOXO1;ZFP36L2;TGFBR1;HLA-E;TGFBR2;CCNB3;CCNB2;CCNA1;IL1A;CCNB1;IL6;MYC;MAPK3
C-type lectin receptor signaling pathway	0.02244	CCL22;STAT1;STAT2;PIK3R3;BCL10;PTGS2;TNF;NFKBIA;IL6;CASP8;IL23A;IRF1;CASP1;NLRP3;IL12A;IKBKE;MAPK3
Necroptosis	0.02468	ZBP1;STAT5A;MLKL;IFNGR1;IFNB1;STAT1;STAT2;EIF2AK2;TNFAIP3;TNFRSF10A;CFLAR;TNF;IL1A;CASP8;TNFSF10;CASP1;STAT4;NLRP3;FAS;JAK2;TLR3;FTL;BIRC3
Th17 cell differentiation	0.02870	STAT5A;IL1R1;IFNGR1;STAT1;RORA;IL2RG;HIF1A;TGFBR1;TGFBR2;NFKBIA;IL6;IL23A;NFKBIE;JAK2;IL12RB1;HLA-DOB;MAPK3
p53 signaling pathway	0.02870	CDKN1A;GADD45A;SERPINE1;TNFRSF10A;BBC3;PIDD1;CCNB2;CCNB1;CASP8;SESN1;PMAIP1;FAS;GTSE1
Herpes simplex virus 1 infection	0.03546	ZNF253;TNF;IFIH1;CASP8;IL12A;JAK2;IKBKE;HLA-DOB;B2M;ZNF484;IFNGR1;DDX58;TAP2;HLA-B;TAP1;HLA-C;HLA-A;HLA-F;HLA-E;OAS1;OAS2;OAS3;IRF7;ZNF799;ITGA5;ZNF114;ZNF311;TLR3;BIRC3;TLR2;ZNF670;SP100;ZNF273;ZNF350;PIK3R3;CCL5;ZNF107;ZNF620;ZNF267;ZNF585A;STAT1;IFNB1;STAT2;EIF2AK2;PML;BST2;NFKBIA;IL6;MAVS;ZNF816;ZNF813;FAS;ZNF699;ZNF257;MYD88;NECTIN1
MAPK signaling pathway	0.03995	CSF1;ARRB1;AREG;FGF2;TNF;RASGRP3;CACNG6;CACNA1I;ERBB3;MYC;RPS6KA2;MAP3K8;PRKACA;MAP4K3;CACNG4;MAPK3;DUSP5;PDGFRA;ANGPT2;ANGPT1;IL1R1;GADD45A;DUSP1;VEGFC;PRKCA;TGFBR1;EREG;MAPK8IP1;CDC25B;TGFBR2;IL1A;FAS;MAPT;TEK;FGFR3;MYD88
Staphylococcus aureus infection	0.04601	ITGAM;C1S;C1R;FPR1;KRT34;FPR2;ICAM1;C4B;C4A;FCGR3B;KRT14;C3AR1;MASP1;HLA-DOB;CFB
Antigen processing and presentation	0.04695	HLA-B;TAP2;HLA-C;TAP1;HLA-A;HLA-F;TNF;CTSS;HLA-E;KLRD1;B2M;HLA-DOB;LGMN
Tuberculosis	0.04984	ITGAM;CR1;NOS2;IFNGR1;IFNB1;STAT1;BCL10;TNF;CTSS;IL1A;IL6;CASP8;FCGR3B;IL23A;IRAK2;CASP10;CR1L;ITGAX;IL12A;JAK2;HLA-DOB;MYD88;TLR2;MAPK3

Table 7-11 KEGG pathway enrichment for MO59K cells isolated from the coculture model (Reo vs. ReoDex)

Term of 339 DEGs between REO and REODEX	P-value	Adj.p	Genes
Cytokine-cytokine receptor interaction	3.20E-06	7.23E-04	IL11;IL33;IL1RN;TGFB2;IFNGR1;IL1R2;TNFRSF18;TNFRSF19;TNFRSF11B;CXCL3;TNFRSF1B;BMP2;IL2RB;XCL1;LTB;CCR5;TNFRSF4;IL12RB2
Rheumatoid arthritis	1.83E-04	0.020659	IL11;TGFB2;MMP3;ACP5;LTB;CXCL3;ICAM1;TLR2
Pathways in cancer	3.10E-04	0.023322	CDKN1A;TGFB2;IFNGR1;WNT7B;PLEKHG5;MGST1;FN1;TGFA;FZD8;LAMC2;ADCY1;FGF5;CCNA2;DLL4;BMP2;IL2RB;CKS2;BDKRB2;BDKRB1;IL12RB2;BIRC3
Complement and coagulation cascades	6.01E-04	0.033972	THBD;SERPINB2;PLAU;BDKRB2;ITGAX;BDKRB1;SERPING1
Salivary secretion	0.001028	0.046497	CST1;DMBT1;CD38;ADCY1;ADRA1B;KCNN4;CST4
Amoebiasis	0.001762	0.066383	TGFB2;IL1R2;FN1;LAMC2;ADCY1;CXCL3;TLR2
Parathyroid hormone synthesis, secretion and action	0.002196	0.070908	NR4A2;CYP27B1;CDKN1A;MMP14;MMP13;PDE4B;ADCY1
Transcriptional misregulation in cancer	0.005609	0.158471	CCNA2;CDKN1A;PLAU;IGFBP3;IL1R2;MMP3;IL2RB;DUSP6;BIRC3
Hippo signaling pathway	0.006746	0.169417	TGFB2;BMP2;RASSF2;WNT7B;FZD8;SNAI2;AREG;BIRC3
NF-kappa B signaling pathway	0.008585	0.194026	PLAU;LTB;CXCL3;CARD11;ICAM1;BIRC3
TNF signaling pathway	0.012108	0.219688	MMP14;MMP3;CXCL3;TNFRSF1B;ICAM1;BIRC3
Toxoplasmosis	0.012108	0.219688	TGFB2;IFNGR1;LAMC2;CCR5;BIRC3;TLR2
Axon guidance	0.012636	0.219688	EFNB2;NTNG2;SEMA7A;ABLIM3;FES;SEMA4B;PLXNB3;SEMA3F
Circadian rhythm	0.015275	0.242685	PER1;PER3;NR1D1
Cell cycle	0.019134	0.242685	CCNA2;TGFB2;CDKN1A;CDC45;CDK1;MAD2L1
Small cell lung cancer	0.020156	0.242685	CDKN1A;CKS2;FN1;LAMC2;BIRC3
JAK-STAT signaling pathway	0.020733	0.242685	IL11;CDKN1A;IFNGR1;FHL1;IL2RB;AOX1;IL12RB2
Nicotinate and nicotinamide metabolism	0.021168	0.242685	NNMT;AOX1;CD38
Basal cell carcinoma	0.022079	0.242685	CDKN1A;BMP2;WNT7B;FZD8
Tyrosine metabolism	0.022809	0.242685	IL4I1;MAOA;AOX1
Inflammatory bowel disease	0.024450	0.242685	TGFB2;IFNGR1;TLR2;IL12RB2
Prostate cancer	0.024691	0.242685	CDKN1A;PLAU;IL1R2;MMP3;TGFA
Hepatocellular carcinoma	0.024698	0.242685	SHC4;TGFB2;CDKN1A;WNT7B;MGST1;TGFA;FZD8
Hematopoietic cell lineage	0.026674	0.245863	IL11;MME;IL1R2;CD38;CD22
Viral protein interaction with cytokine and cytokine receptor	0.027703	0.245863	IL2RB;XCL1;CXCL3;CCR5;TNFRSF1B
Retinol metabolism	0.028285	0.245863	ALDH1A3;CYP26B1;CYP2S1;AOX1
Chagas disease	0.029835	0.249731	TGFB2;IFNGR1;BDKRB2;ADCY1;TLR2
Phenylalanine metabolism	0.032941	0.256629	IL4I1;MAOA
Human T-cell leukemia virus 1 infection	0.033656	0.256629	CCNA2;CDKN1A;TGFB2;IL1R2;IL2RB;ADCY1;ICAM1;MAD2L1
Tryptophan metabolism	0.034065	0.256629	IL4I1;MAOA;AOX1
p53 signaling pathway	0.035429	0.258293	CDKN1A;RRM2;IGFBP3;CDK1
Drug metabolism	0.036839	0.260177	RRM2;MAOA;MGST1;AOX1;FMO3
Breast cancer	0.039446	0.270147	FGF5;SHC4;DLL4;CDKN1A;WNT7B;FZD8
Gastric cancer	0.041679	0.277047	FGF5;SHC4;TGFB2;CDKN1A;WNT7B;FZD8
Steroid biosynthesis	0.044521	0.287479	CYP27B1;TM7SF2

Table 7-12 KEGG pathway enrichment for pre-Dex treated MO59K cells isolated from Veh-PBMC coculture model

Term of 2201 DEGs by pre-DEX	Adj.p	Genes
Cytokine-cytokine receptor interaction	8.28E-14	ACVRL1;CXCL6;IL1RN;CD40;IFNA7;CXCL9;CXCL8;TNFRSF13B;CSF1;CCL4L2;IL27;CXCL1;CXCL3;TNF;CXCL2;CX3CL1;CXCL5;CXCL16;TNFSF13B;TNFSF10;IL12A;CCR7;AMH;CCR2;IL15RA;IL11;IL1R1;IFNGR1;IL15;IL1R2;TNFRSF19;LIFR;TNFRSF1B;TGFBR1;TGFBR2;IL1A;IL23A;IL3RA;LTB;TNFRSF21;CCL13;CSF1R;CCL3L1;EBI3;IL20RB;CXCR4;TNFRSF11B;IL2RG;IFNL2;CCL8;IFNL1;CCL5;CCL4;CCL3;TNFRSF14;IL12RB1;IFNL3;CCR1;TNFSF18;IL32;CCL24;GDF11;CCL22;CCL20;IFNB1;TNFRSF9;IFNLR1;TNFRSF10A;INHBA;BMP7;INHBE;IL22RA1;CXCL10;BMP2;CXCL11;IL6;IL7;FAS;TNFSF8;IL7R;CCL28;IL18R1;PF4
Viral protein interaction with cytokine, cytokine receptor	2.46E-10	CSF1R;CXCL6;CCL13;CXCL9;CXCL8;CSF1;CCL3L1;CCL4L2;IL20RB;CXCR4;CXCL1;CXCL3;IL2RG;TNF;CXCL2;CX3CL1;CXCL5;CCL8;CCL5;CCL4;TNFSF10;CCL3;TNFRSF14;CCR7;CCR2;CCR1;CCL24;CCL22;CCL20;TNFRSF10A;TNFRSF1B;IL22RA1;CXCL10;CXCL11;IL6;CCL28;IL18R1;PF4
TNF signaling pathway	1.99E-09	CXCL6;CEBPB;CSF1;PIK3R3;TNFAIP3;CXCL1;NOD2;CXCL3;PTGS2;TNF;CXCL2;CX3CL1;CXCL5;ICAM1;CASP7;CASP8;CASP10;CCL5;MAP3K8;JUNB;EDN1;JAG1;MLKL;RIPK3;IL15;CCL20;IFNB1;DAB2IP;VEGFC;TRAF1;CFLAR;TNFRSF1B;NFKBIA;CXCL10;IL6;IRF1;FAS;IL18R1;BIRC3
Influenza A	5.23E-07	CIITA;IFNA7;CXCL8;CALCOCO2;PIK3R3;ADAR;TNF;ICAM1;IFIH1;CCND3;CASP8;CCL5;TNFSF10;CASP1;TRIM25;NLRP3;IL12A;BAK1;KPNA2;JAK2;HLA-DOB;IKBKE;RSAD2;DDX58;IFNGR1;IFNB1;STAT1;MX2;STAT2;MX1;EIF2AK2;TNFRSF10A;PML;NFKBIA;CXCL10;IL1A;IL6;MAVS;OAS1;OAS2;OAS3;IRF7;FAS;MYD88;IRF9;TLR3
NOD-like receptor signaling pathway	7.97E-07	IFNA7;CXCL8;ITPR1;TNFAIP3;CXCL1;NOD1;NOD2;MEFV;CXCL3;TNF;CXCL2;PANX1;CASP8;IFI16;CCL5;NAMPT;CASP1;NLRP3;GBP2;IKBKE;GBP1;GBP4;GBP3;GBP5;GBP7;RIPK3;RIPK2;IFNB1;STAT1;STAT2;CARD6;NFKBIA;P2RX7;IL6;MAVS;AIM2;OAS1;OAS2;OAS3;CARD17;BCL2;IRF7;TXNIP;MYD88;IRF9;BCL2L1;BIRC3
Epstein-Barr virus infection	1.27E-06	CD40;CDKN1A;IFNA7;TNFAIP3;TNF;ICAM1;CCND3;CASP8;MYC;B2M;IKBKE;HLA-DOB;DDX58;HLA-B;TAP2;HLA-C;TAP1;HLA-A;HLA-F;HLA-E;CCNA2;CCNA1;OAS1;OAS2;OAS3;IRF7;TP53;IRF9;TLR2;RBPJL;PIK3R3;BCL2L11;PLCG2;HES1;CD58;BAK1;GADD45A;IFNB1;STAT1;STAT2;EIF2AK2;ISG15;NFKBIA;CXCL10;IL6;MAVS;BCL2;FAS;NFKBIE;MYD88
Pertussis	2.83E-06	CXCL6;CXCL8;ITGAM;C1S;C1R;LY96;NOD1;C4BPB;TNF;CXCL5;C4B;C3;C4A;CASP7;CASP1;NLRP3;IL12A;CD14;NOS2;IL1A;IL6;IL23A;IRF1;SERPING1;ITGA5;MYD88
NF-kappa B signaling pathway	1.83E-05	CCL13;CD40;CXCL8;BCL2A1;CCL4L2;LY96;TNFAIP3;CXCL1;CXCL3;PTGS2;TNF;CXCL2;ICAM1;TNFSF13B;CCL4;PLCG2;TRIM25;CD14;EDARADD;IL1R1;GADD45A;DDX58;TRAF1;CFLAR;NFKBIA;BCL2;LTB;MYD88;BCL2L1;BIRC3
Measles	6.59E-05	IFNA7;PIK3R3;TNFAIP3;ADAR;IL2RG;BBC3;IFIH1;CCND3;CASP8;IL12A;BAK1;IKBKE;STAT5A;DDX58;IFNB1;STAT1;MX2;STAT2;MX1;EIF2AK2;NFKBIA;IL1A;IL6;MAVS;OAS1;OAS2;OAS3;BCL2;IRF7;FAS;TP53;MYD88;IRF9;BCL2L1;TLR2
JAK-STAT signaling pathway	1.29E-04	CDKN1A;IFNA7;IL20RB;PIK3R3;IL2RG;SOCS2;CCND3;IFNL2;SOCS1;IFNL1;MYC;STAT4;AOX1;IL12A;JAK2;IL12RB1;IFNL3;MCL1;STAT5A;IL15RA;PDGFRA;IL11;IFNGR1;IL15;IFNB1;STAT1;STAT2;LIFR;IFNLR1;IL22RA1;IL6;IL23A;IL7;IL3RA;BCL2;IL7R;IRF9;BCL2L1
Kaposi sarcoma-associated herpesvirus infection	1.29E-04	CDKN1A;IFNA7;CXCL8;ITPR1;PIK3R3;CXCL1;PTGS2;CXCL3;HIF1A;CXCL2;ICAM1;C3;ZFP36;PPP3CC;CASP8;MYC;PLCG2;BAK1;JAK2;IKBKE;CCR1;ANGPT2;IFNGR1;IFNB1;STAT1;STAT2;HLA-B;HLA-C;EIF2AK2;HLA-A;HLA-F;HLA-E;NFKBIA;HCK;RCAN1;IL6;CLEC2B;GNB4;IRF7;FAS;TP53;TLR3;IRF9
Transcriptional misregulation in cancer	2.28E-04	CSF1R;CD40;CDKN1A;CEBPB;CXCL8;ITGAM;BCL2A1;MAX;SIX1;PLAT;AFF1;MYC;NFKBIZ;CD14;BAK1;SSX2;KDM6A;CDKN2C;JUP;GADD45A;IL1R2;ZBTB16;LMO2;PBX3;MITF;ETV1;TRAF1;PBX1;MLF1;PML;TGFBR2;CCNA2;ETV7;CCNA1;IL6;NR4A3;REL;PPARG;NUPR1;TP53;BCL2L1;BIRC3
Complement and coagulation cascades	2.28E-04	FGA;ITGAM;SERPINA1;C1S;CFH;C1R;SERPINE1;F2R;CFI;PLAT;C4BPB;C4B;C3;C4A;THBD;PROCR;C7;CR1L;C3AR1;SERPING1;MASP1;A2M;CFB;F2RL3
Toll-like receptor signaling pathway	3.33E-04	CD40;CXCL9;IFNA7;CXCL8;CCL3L1;CCL4L2;LY96;PIK3R3;TNF;CASP8;CCL5;CCL4;CCL3;IL12A;MAP3K8;CD14;IKBKE;IFNB1;STAT1;NFKBIA;CXCL10;CXCL11;IL6;IRF7;MYD88;TLR3;TLR2
Rheumatoid arthritis	3.33E-04	CXCL6;CXCL8;CSF1;CCL3L1;CXCL1;CXCL3;CXCL2;TNF;CXCL5;ICAM1;TNFSF13B;CCL5;CCL3;ATP6V0A4;HLA-DOB;IL11;ANGPT1;IL15;CCL20;IL1A;IL6;IL23A;LTB;TEK;TLR2
Legionellosis	4.50E-04	CXCL8;ITGAM;BNIP3;CXCL1;CXCL3;CXCL2;TNF;C3;NFKBIA;CASP7;IL6;CASP8;CR1L;CASP1;IL12A;CD14;MYD88;TLR2
Human T-cell leukemia virus 1 infection	4.58E-04	CD40;CDKN1A;PIK3R3;GPS2;BUB1B;ADCY1;IL2RG;TNF;ETS2;ICAM1;CDC20;CCNB2;CCND3;ZFP36;PPP3CC;PTTG1;MYC;PRKACA;B2M;HLA-DOB;STAT5A;IL15RA;CDKN2B;CDKN2C;SMAD3;MMP7;IL1R1;IL15;IL1R2;HLA-B;HLA-C;HLA-A;HLA-F;TGFBR1;HLA-E;TGFBR2;NFKBIA;CCNA2;CCNA1;IL6;ESPL1;TLN2;TP53;MAD2L1;BCL2L1
Pathways in cancer	5.66E-04	RET;CDKN1A;IFNA7;CXCL8;BBC3;CCND3;CASP7;CASP8;MYC;IL12A;PRKACA;JAK2;NKX3-1;IL15RA;PDGFRA;EDN1;IFNGR1;IL15;ITGA2;NCOA3;F2R;MITF;TRAF1;TGFBR1;TGFBR2;CCNA2;CCNA1;IL23A;COL4A1;IL3RA;BIRC5;PPARG;TP53;BIRC3;PTGER4;CSF1R;MAX;LAMA1;NOTCH4;PTGER2;PIK3R3;TGFA;CXCR4;ADCY1;PTGS2;IL2RG;HIF1A;DLL1;RASGRP3;BCL2L11;PLCG2;STAT4;PMAIP1;HES1;BAK1;IL12RB1;JAG2;STAT5A;CDKN2B;EGLN3;JAG1;SMAD3;FZD5;JUP;NOS2;FZD4;STAT1;GADD45A;FZD7;STAT2;WNT7B;ZBTB16;LAMB4;FN1;VEGFC;PML;NFKBIA;BMP2;IL6;GSTA4;IL7;BCL2;

Chemokine signaling pathway	8.14E-04	CXCL6;CCL13;CXCL9;CXCL8;CCL3L1;CCL4L2;PIK3R3;CXCR4;ARRB1;CXCL1;ADCY1;CXCL3;CXCL2;CX3CL1;CXCL5;CXCL16;CCL8;CCL5;CCL4;PLCG2;CCL3;PTK2B;CCR7;PRKACA;JAK2;CCR2;CCR1;VAV3;CCL24;CCL22;CCL20;STAT1;STAT2;NFKBIA;CXCL10;HCK;CXCL11;GNB4;CCL28;PF4
Apoptosis	8.84E-04	BCL2A1;PRF1;ITPR1;PIK3R3;TNF;CTSS;BBC3;SPTA1;CASP7;BCL2L11;CASP8;TUBA3C;CASP10;TNFSF10;PMAIP1;CTSF;BAK1;MCL1;PARP3;GADD45A;DAB2IP;TNFRSF10A;TRAF1;CFLAR;NFKBIA;IL3RA;BCL2;BIRC5;FAS;TP53;BCL2L1;BIRC3
Lipid and atherosclerosis	0.0021	CD40;IFNA7;CXCL8;CCL3L1;ITPR1;PIK3R3;LY96;CXCL1;CXCL3;TNF;CXCL2;ICAM1;CASP7;PPP3CC;CASP8;CCL5;TNFSF10;CASP1;CCL3;OLR1;NLRP3;IL12A;CD14;JAK2;IKBKE;VAV3;CYP2J2;XBP1;HSPA5;IFNB1;TNFRSF10A;SOD2;NFKBIA;IL6;BCL2;IRF7;FAS;PPARG;TP53;MYD88;TLR2;BCL2L1
Hepatitis B	0.0021	CDKN1A;IFNA7;CXCL8;PIK3R3;TNF;IFIH1;CASP8;CASP10;MYC;STAT4;PTK2B;JAK2;IKBKE;STAT5A;SMAD3;DDX58;IFNB1;STAT1;STAT2;TGFBR1;TGFBR2;NFKBIA;CCNA2;CCNA1;IL6;MAVS;BCL2;IRF7;BIRC5;FAS;TP53;MYD88;TLR3;TLR2
Inflammatory bowel disease	0.0021	SMAD3;IFNGR1;STAT1;RORA;GATA3;NOD2;IL2RG;TNF;IL1A;IL6;IL23A;TBX21;STAT4;IL12A;IL12RB1;HLA-DOB;IL18R1;TLR2
Chagas disease	0.0029	ACE;CXCL8;CCL3L1;NOS2;IFNGR1;IFNB1;SERPINE1;PIK3R3;ADCY1;CFLAR;TNF;TGFBR1;TGFBR2;C3;GNAO1;NFKBIA;IL6;CASP8;CCL5;CCL3;FAS;IL12A;MYD88;TLR2
Osteoclast differentiation	0.0029	CSF1R;CSF1;PIK3R3;TNFRSF11B;LILRA1;TNF;SIRPB1;SOCS1;FCGR3B;PPP3CC;PLCG2;SIRPA;FYN;JUNB;IL1R1;IFNGR1;IFNB1;STAT1;STAT2;MITF;TGFBR1;OSCAR;TGFBR2;NFKBIA;IL1A;LCP2;PPARG;IRF9
Cell adhesion molecules	0.0035	CD274;CD40;ITGAM;SELPLG;SDC4;SDC2;ICAM2;NRXN3;F11R;CLDN1;ICAM1;CLDN23;ITGB8;NRCAM;CD58;HLA-DOB;CD34;NEGR1;HLA-B;HLA-C;HLA-A;PDCD1LG2;HLA-F;HLA-E;VCAN;SELL;SDC1;ESAM;SIGLEC1;NECTIN2;NECTIN1
Cytosolic DNA-sensing pathway	0.0038	ZBP1;IFNA7;RIPK3;DDX58;IFNB1;CCL4L2;ADAR;NFKBIA;CXCL10;IL6;MAVS;AIM2;CCL5;CCL4;CASP1;IRF7;IKBKE
Cellular senescence	0.0039	CDKN1A;CXCL8;SERPINE1;ITPR1;PIK3R3;FOXM1;KIR2DL4;ZFP36L2;ZFP36L1;CCNB3;CCNB2;CCND3;CCNB1;PPP3CC;MYC;CDKN2B;SMAD3;GADD45A;HLA-B;HLA-C;HLA-A;HLA-F;TGFBR1;HIPK3;HLA-E;TGFBR2;CCNA2;CCNA1;IL1A;IL6;CDK1;TP53
Hematopoietic cell lineage	0.0040	CSF1R;IL11;ITGAM;CSF1;IL1R1;IL1R2;ITGA2;CD1C;TNF;CD1B;IL1A;IL6;IL7;CR1L;IL3RA;CD7;CD38;CD14;ITGA5;IL7R;HLA-DOB;CD34;CD33
Human papillomavirus infection	0.0041	CDKN1A;IFNA7;MAML2;TNF;OASL;CCND3;CASP8;ITGB8;ITGB6;PRKACA;IKBKE;HES7;ITGA2;HLA-B;HLA-C;HLA-A;HLA-F;HLA-E;CCNA2;CCNA1;COL4A1;IRF1;MAML3;ITGA5;TP53;TLR3;IRF9;PTGER4;RBPJL;LAMA1;NOTCH4;PIK3R3;PTGS2;RELN;PARD6A;ATP6V0A4;HES1;BAK1;HES4;JAG1;FZD5;FZD4;IFNB1;STAT1;FZD7;STAT2;WNT7B;MX2;LAMB4;MX1;FN1;EIF2AK2;ISG15;PPP2R3B;ITGA10;ITGA11;FAS
Human immunodeficiency virus 1 infection	0.0045	IFNA7;ITPR1;PIK3R3;CXCR4;SAMHD1;TNF;CCNB3;CCNB2;CCNB1;PPP3CC;CASP8;TRIM5;PLCG2;PTK2B;BAK1;B2M;AP1M2;APOBEC3F;APOBEC3G;IFNB1;LIMK2;HLA-B;TAP2;HLA-C;TAP1;HLA-A;HLA-F;CDC25C;TNFRSF1B;HLA-E;BST2;GNAO1;NFKBIA;BCL2;CDK1;GNB4;FAS;MYD88;TLR2;BCL2L1
Amoebiasis	0.0056	CXCL8;ITGAM;NOS2;IL1R1;LAMA1;IL1R2;LAMB4;FN1;PIK3R3;CXCL1;SERPINB9;ADCY1;CD1C;CXCL3;TNF;CD1B;CXCL2;IL6;COL4A1;IL12A;CD14;PRKACA;TLR2
Malaria	0.0067	CD40;CXCL8;GYPC;SDC2;HBB;TNF;ICAM1;IL6;CR1L;SDC1;IL12A;ACKR1;MYD88;TLR2
p53 signaling pathway	0.0067	CDKN1A;GADD45A;SERPINE1;TNFRSF10A;BBC3;CCNB2;CCND3;CCNB1;CASP8;SESN3;SESN2;BCL2;CDK1;PMAIP1;FAS;GTSE1;TP53;BCL2L1
Coronavirus disease	0.0068	IFNA7;CXCL8;C1S;C1R;PIK3R3;ADAR;TNF;C4B;C3;IFIH1;C4A;C7;C3AR1;PLCG2;CASP1;NLRP3;IL12A;IKBKE;FGA;ACE;IFNB1;STAT1;DDX58;STAT2;MX2;MX1;EIF2AK2;ISG15;NFKBIA;ACE2;CXCL10;IL6;MAVS;OAS1;OAS2;OAS3;MASP1;CFB;TLR3;MYD88;IRF9;TLR2
Human cytomegalovirus infection	0.0068	PTGER4;CDKN1A;IFNA7;CXCL8;CCL3L1;PTGER2;CCL4L2;ITPR1;PIK3R3;CXCR4;ADCY1;PTGS2;TNF;CX3CL1;PPP3CC;CASP8;MYC;CCL5;CCL4;CCL3;PTK2B;BAK1;PRKACA;B2M;CCR1;PDGFRA;IL1R1;IFNB1;HLA-B;TAP2;HLA-C;TAP1;HLA-A;HLA-F;HLA-E;GNAO1;NFKBIA;IL6;GNB4;FAS;TP53
Hepatitis C	0.0072	CDKN1A;IFNA7;PIK3R3;IFIT1;CLDN1;TNF;CASP8;MYC;CLDN23;BAK1;IKBKE;RSAD2;DDX58;IFNB1;STAT1;MX2;STAT2;MX1;EIF2AK2;CFLAR;NFKBIA;CXCL10;MAVS;OAS1;OAS2;OAS3;IRF7;FAS;TP53;IRF9;TLR3
RIG-I-like receptor signaling pathway	0.0100	IFNA7;CXCL8;DDX58;IFNB1;ISG15;TNF;IFIH1;NFKBIA;CXCL10;MAVS;CASP8;CASP10;DHX58;IRF7;TRIM25;IL12A;IKBKE
Graft-versus-host disease	0.0112	IL1A;IL6;PRF1;HLA-B;HLA-C;FAS;KLRD1;HLA-A;HLA-F;TNF;HLA-DOB;HLA-E
Allograft rejection	0.0152	CD40;PRF1;HLA-B;HLA-C;FAS;IL12A;HLA-A;HLA-F;TNF;HLA-DOB;HLA-E

Small cell lung cancer	0.0153	CDKN1A;CDKN2B;NOS2;LAMA1;MAX;GADD45A;ITGA2;LAMB4;FN1;PIK3R3;TRAF1;PTGS2;NFKBIA;COL4A1;MYC;BCL2;BAK1;TP53;BIRC3;BCL2L1
Th1 and Th2 cell differentiation	0.0153	RBPJL;JAG2;STAT5A;JAG1;MAML2;IFNGR1;STAT1;GATA3;IL2RG;DLL1;NFKBIA;PPP3CC;TBX21;STAT4;IL12A;MAML3;JAK2;IL12RB1;NFKBIE;HLA-DOB
Tuberculosis	0.0159	CIITA;IFNA7;CEBPB;ITGAM;NOD2;TNF;CTSS;C3;CYP27B1;CASP8;FCGR3B;PPP3CC;IRAK2;CASP10;IL12A;ATP6V0A4;CD14;JAK2;HLA-DOB;PLK3;CD74;NOS2;IFNGR1;RIPK2;IFNB1;STAT1;IL1A;IL6;IL23A;CR1L;BCL2;MYD88;TLR2
FoxO signaling pathway	0.0282	CDKN1A;AGAP2;PIK3R3;IRS2;CCNB3;CCNB2;CCNB1;BCL2L11;TNFSF10;PCK1;RAG1;PLK3;CDKN2B;SMAD3;GADD45A;HOMER2;PLK2;BNIP3;PLK1;FBXO32;SOD2;TGFBR1;TGFBR2;IL6;IL7R
Natural killer cell mediated cytotoxicity	0.0282	IFNA7;ICAM2;PRF1;PIK3R3;TNF;ICAM1;FCGR3B;PPP3CC;TNFSF10;PLCG2;PTK2B;FYN;VAV3;IFNGR1;IFNB1;HLA-B;HLA-C;TNFRSF10A;HLA-A;HLA-E;RAET1L;FAS;KLRD1;CD48;LCP2
Antigen processing and presentation	0.0282	CD74;CIITA;HSPA5;HLA-B;TAP2;HLA-C;TAP1;HLA-A;HLA-F;TNF;CTSS;KIR2DL4;HLA-E;KLRD1;B2M;HLA-DOB;LGMN
African trypanosomiasis	0.0352	IL6;HBB;FAS;IL12A;APOL1;IDO2;TNF;MYD88;ICAM1;IDO1
Type I diabetes mellitus	0.0358	IL1A;PRF1;HLA-B;HLA-C;FAS;IL12A;HLA-A;HLA-F;TNF;HLA-DOB;HLA-E
AGE-RAGE signaling pathway in diabetic complications	0.0358	STAT5A;EDN1;SMAD3;CXCL8;STAT1;SERPINE1;FN1;PIK3R3;VEGFC;TNF;TGFBR1;ICAM1;TGFBR2;THBD;IL1A;IL6;COL4A1;PLCG2;BCL2;JAK2
Th17 cell differentiation	0.0362	STAT5A;SMAD3;IL1R1;IFNGR1;STAT1;RORA;GATA3;IL2RG;HIF1A;TGFBR1;TGFBR2;NFKBIA;IL6;PPP3CC;IL23A;IRF4;TBX21;NFKBIE;JAK2;IL12RB1;HLA-DOB

Table 7-13 KEGG pathway enrichment for pre-Dex treated MO59K cells isolated from the Reo-PBMC coculture model

Term 199 Pre-DEX and REO	P-value	Adjusted P-value	Genes
Cytokine-cytokine receptor interaction	4.00E-05	0.0072381	TNFSF18;IL11;IL33;BMP2;IFNGR1;IL1R2;TNFRSF19;LIF;XCL2;XCL1;TNFRSF11B;TNFRSF21
Pathways in cancer	8.19E-05	0.00741149	IFNGR1;MMP1;WNT7B;ZBTB16;FN1;TGFA;FZD8;LAMC2;ADCY1;FGF5;DLL4;BMP2;BDKRB2;BDKRB1;PIM2;BIRC3
Complement and coagulation cascades	1.99E-04	0.01202969	SERPINB2;PLAU;C5AR1;BDKRB2;BDKRB1;SERPINA5
Rheumatoid arthritis	0.0023233	0.10459578	IL11;MMP1;MMP3;ACP5;TLR2
Transcriptional misregulation in cancer	0.00307607	0.10459578	BCL2A1;PLAU;IL1R2;ZBTB16;MMP3;DUSP6;BIRC3
Amoebiasis	0.00346726	0.10459578	IL1R2;FN1;LAMC2;ADCY1;TLR2
Acute myeloid leukemia	0.00439246	0.10478673	BCL2A1;ZBTB16;PIM2;DUSP6
Retinol metabolism	0.00463146	0.10478673	ALDH1A3;CYP26B1;CYP2S1;AOX1
Hippo signaling pathway	0.00574351	0.11550837	BMP2;WNT7B;FZD8;SNAI2;AREG;BIRC3
Calcium signaling pathway	0.01012293	0.18322501	FGF5;BDKRB2;CACNA1A;BDKRB1;ADCY1;GRPR;SLC8A2
Salivary secretion	0.01372852	0.21379191	CST1;ADCY1;KCNN4;CST4
Prostate cancer	0.01580565	0.21379191	PLAU;IL1R2;MMP3;TGFA
Inflammatory mediator regulation of TRP channels	0.01635406	0.21379191	BDKRB2;TRPV3;BDKRB1;ADCY1
Proteoglycans in cancer	0.01653639	0.21379191	PLAU;WNT7B;FN1;FZD8;TIMP3;TLR2
Chagas disease	0.01866646	0.22524193	IFNGR1;BDKRB2;ADCY1;TLR2
Neuroactive ligand-receptor interaction	0.02061012	0.23043321	KISS1;GABRB1;C5AR1;FPR1;BDKRB2;BDKRB1;FPR2;GRPR
Mineral absorption	0.0216429	0.23043321	MT1X;SLC8A2;MT1E
Basal cell carcinoma	0.02458375	0.24102028	BMP2;WNT7B;FZD8
Toxoplasmosis	0.02530047	0.24102028	IFNGR1;LAMC2;BIRC3;TLR2
MAPK signaling pathway	0.027	0.24856459	FGF5;DUSP1;RASGRF2;TGFA;CACNA1A;AREG;DUSP6
Axon guidance	0.03502591	0.30189	EFNB2;ABLIM2;ABLIM3;SEMA6D;SEMA3A
Circadian rhythm	0.03757537	0.30914278	PER1;NR1D1
Synaptic vesicle cycle	0.04233639	0.33316897	UNC13A;CACNA1A;SLC1A3
Nicotinate and nicotinamide metabolism	0.04686613	0.34777802	NNMT;AOX1